

QG from SymQRG: AdS₃/CFT₂ Correspondence as Topological Symmetry-Preserving Quantum RG Flow

Ning Bao¹, Ling-Yan Hung^{2,3}, Yikun Jiang¹, Zhihan Liu⁴

¹ *Department of Physics, Northeastern University, Boston, MA 02115, USA*

² *Yau Mathematical Sciences Center, Tsinghua University, Beijing 100084, China*

³ *Yanqi Lake Beijing Institute of Mathematical Sciences and Applications (BIMSA), Huairou District, Beijing 101408, China*

⁴ *Department of Physics, Cornell University, Ithaca, New York, USA*

Abstract

By analyzing the non-perturbative RG flows that explicitly preserve given symmetries, we demonstrate that they can be expressed as quantum path integrals of the *SymTFT* in one higher dimension. When the symmetries involved include Virasoro defect lines, such as in the case of $T\bar{T}$ deformations, the RG flow corresponds to the 3D quantum gravitational path integral. For each 2D CFT, we identify a corresponding ground state of the SymTFT, from which the Wheeler-DeWitt equation naturally emerges as a non-perturbative constraint. These observations are summarized in the slogan: **SymQRG = QG**. The recently proposed exact discrete formulation of Liouville theory in [1] allows us to identify a universal SymQRG kernel, constructed from quantum $6j$ symbols associated with $U_q(SL(2, \mathbb{R}))$, which manifests itself as an exact and analytical 3D background-independent MERA-type holographic tensor network. Many aspects of the AdS/CFT correspondence, including the factorization puzzle, admit a natural interpretation within this framework. This provides the first evidence suggesting that there is a universal holographic principle encompassing AdS/CFT and topological holography. We propose that the non-perturbative AdS/CFT correspondence is a *maximal* form of topological holography.

Contents

1	Introduction	4
1.1	AdS/CFT correspondence from generalized symmetries	5
1.2	Outline of the paper	7
1.3	Summary of framework	11
2	From Wilson-Kadanoff RG to SymQRG	12
2.1	Wilson-Kadanoff RG	12
2.2	Quantum RG	14
2.3	SymQRG: Topological Symmetry-Preserving Quantum RG	14
3	$T\bar{T}$ deformation for 2D CFTs as SymQRG	20
3.1	3D phase space gravitational path integral from iterative $T\bar{T}$ deformation	21
3.2	$T\bar{T}$ deformation from 3D gravitational path integral	24
3.3	Wheeler-DeWitt equation from $T\bar{T}$ deformation	27
4	SymQRG for exact tensor network state sum representation of 2D CFTs	32
4.1	Turaev-Viro TQFT, Levin-Wen string-net model and topological order	32
4.2	SymQRG for tensor network state sum representation of 2D CFT path integrals	35
4.3	Wheeler-DeWitt equation and Callan-Symanzik equation from tensor networks	45
4.4	Roles of tensor networks	49
5	3D Quantum Gravity as SymTFT	52
5.1	3D gravity and Chern-Simons theory	53
5.2	Virasoro TQFT	54
5.3	Discrete realization of the Virasoro RG operator	57
5.4	Remarks on the lattice Liouville theory from quantum Teichmuller theory	63
5.5	Exact bulk dual at finite N and universal semi-classical gravity dual at large N	65
6	Quantum Gravity from Algebra	67
6.1	Topological holographic principle	67
6.2	Looking for $ \Psi\rangle_\Lambda$: From crossing symmetry to anyon condensation/gauging	69
6.2.1	Crossing symmetry and emergence of 3D bulk	69
6.2.2	Modular invariance and anyon condensation/gauging	71
6.3	Dynamics vs. kinematics – where is the information encoded?	73
6.4	Implications for Quantum Gravity	76
6.4.1	Wormholes, null states, and factorization	76
6.4.2	Chaos from (topological) Order	79

7	Discussions	82
A	Review of Turaev-Viro TQFT and fusion category	86
A.1	Turaev-Viro TQFT from Chern-Simons theory	86
A.2	Turaev-Viro TQFT from fusion category	93
B	Tensor network state sum representation of 2D CFT path integrals	96
C	Tensor network SymQRG	100
D	Tensor network for CFT wavefunctions from Euclidean path integrals, perfect tensors and random tensors	106
E	Quantum Teichmuller theory and its connection to $U_q(SL(2, \mathbb{R}))$ $6j$ symbols	112
E.1	Reviewing quantum Teichmuller theory and Teichmuller TQFT	112
E.2	$U_q(SL(2, \mathbb{R}))$ $6j$ -symbols and quantum Teichmuller theory	119

1 Introduction

The quest for a complete non-perturbative theory of quantum gravity remains one of the most profound challenges in modern theoretical physics. Among the most promising frameworks is the AdS/CFT correspondence [2–4], which establishes a duality between a conformal field theory (CFT) in D -dimensions and a $(D + 1)$ -dimensional gravitational theory with asymptotically Anti-de Sitter (AdS) spacetime. This duality not only provides a powerful tool for studying strongly coupled quantum field theories but also offers deep insights into the nature of spacetime itself.

A very important aspect of the AdS/CFT correspondence is that global symmetries of the field theory exhibit themselves as gauge symmetries in the bulk. In particular, conformal transformations of the field theory are connected to a subset of diffeomorphisms in the asymptotically AdS $_{D+1}$ spacetime. Other global symmetries in the field theory also manifest as gauge symmetries in the holographic dual. This structure bears striking resemblance to the “topological holographic principle” [5–14], proposed in the study of generalized symmetries [15],¹ where the path integral of a quantum field theory (QFT) with symmetries on a D -manifold Σ_D is produced from the path integral of a topological field theory (often called SymTFT) in $(D + 1)$ dimensions on a manifold of the form $\Sigma_D \times I$, with I being an interval. This is often called “sandwich construction” [5–8]. The SymTFT is chosen so that a given global symmetry of the QFT is gauged in the TQFT [7, 16]. This strongly suggests that the two holographic principles are closely related.

On the other hand, the renormalization group (RG) flow also plays an important role in the AdS/CFT correspondence. It has been proposed that the flow of field theory couplings is encoded in the AdS bulk [17–19]. If the topological holographic principle is indeed related to AdS/CFT correspondence, then it is important to recover data of the RG flow in the SymTFT bulk.

Can the combination of topological symmetries and RG, the two most important non-perturbative aspects of strongly interacting QFTs, reveal new insights into quantum gravity? In this paper, we demonstrate that a “topological symmetry-preserving quantum RG” process, referred to as “SymQRG”, can be translated to the path integral of the SymTFT, which probes deeper into the bulk of asymptotically AdS $_{D+1}$ spacetimes. In particular in 2D, RG processes preserving an irrational collection of topological lines related to Virasoro representations produce a precise 3D *quantum* gravitational path integral that is given by two copies of the Virasoro/Teichmuller TQFT [1, 20–22]. i.e. When the symmetry concerned contains an irrational collection of topological line operators [15, 20] related to Virasoro representations, the SymTFT is a long-range entangled topological order [23–26] that contains 3D quantum gravity.

We summarize this principle as

$$\text{SymQRG}(\text{Virasoro lines}) = \text{QG} .$$

¹The modern approach to symmetries involves studying topological operators within the theory; hence, we will also refer to this as topological symmetries.

A class of RG flows driven by $T\bar{T}$ deformation [27,28] is proposed to be related to bulk gravitational path integral. We demonstrate that in 2D this is indeed a special case of symmetry-preserving RG flows that can be expressed as a quantum gravitational path integral.

The second example we consider arises from a discrete formalism: the exact tensor network state sum representation of 2D CFTs, in particular the Liouville theory [1,29–31]. This method produces for us a well-defined gravitational *quantum path integral, non-perturbative in G_N* from a quantum RG flow. While we considered the Liouville theory explicitly in [1], the symmetry-preserving RG operator \hat{U}_{RG} extracted from coarse-graining the triangulation of the CFT path integral is universal – after all, they follow only from crossing kernels of correlation functions between Virasoro representations, and is shared by all theories preserving Virasoro symmetries. We note that such a discrete yet exact formulation of the quantum path integral is naturally a holographic tensor network. Many well established tensor network methods could then be applied to continuum field theories.

1.1 AdS/CFT correspondence from generalized symmetries

By incorporating this well-established class of examples into our framework and understanding it in light of the SymTFT, we gain new insights into several aspects of the AdS/CFT correspondence.

First, it sheds light on the role that individual CFT plays in the gravitational path integral. While different CFTs serve as fixed points of the quantum RG process preserving the same collection of symmetries, they still exhibit *distinct* modular invariant spectra. Within the sandwich construction, this information is encoded in the “topological boundary condition” of the SymTFT. When the bulk path integral includes a topological boundary condition \mathcal{B} , it prepares a state $|\Psi(\mathcal{B})\rangle_{\Sigma_D}$ on the surface Σ_D . The non-topological boundary condition at the other end of the sandwich can then be specified by a bra state $\langle\Omega|$ on Σ_D , which can be viewed as a basis vector in one dimension higher. The D dimensional QFT *partition function* is a $(D + 1)$ dimensional *wavefunction*, which can be written as an overlap

$$Z_{\text{QFT}}(\Sigma_D) = \langle\Omega|\Psi(\mathcal{B})\rangle_{\Sigma_D} . \tag{1.1}$$

Translated to the AdS/CFT correspondence, on the CFT side, the ket state -or the topological boundary condition \mathcal{B} together with the bulk-encodes all the sewing rules or operator product expansion (OPE) data of the 2D CFT [32]. This state is inherently 3D. When the CFT contains a large number of degrees of freedom, the bulk thus emerging has semi-classical geometrical meanings. In the AdS context, instead of treating this as an explicit boundary condition, we can view it as a complete specification of the quantum measure for the bulk path integral, which is often obscured in the semi-classical limit. This precise choice of measure guarantees the exact correspondence between 2D CFT and 3D gravity, and ensures factorization in the bulk. In general, the bulk theory coming from a given CFT does not sum over all geometries. One of the main observations of this paper is the importance of an underlying 3D quantum state that underlies any 2D CFT, and it determines the geometries to be summed in the bulk. On the other hand, the bra state—or the physical boundary

condition—defines theories at different scales along the symmetry-preserving RG trajectory. These states can also be interpreted as basis states at different finite cutoffs in the bulk. Together, the ket and bra states form the basis of SymQRG and bridge the AdS/CFT correspondence (QG).

Second, the Wheeler-DeWitt equation plays a pivotal role in the AdS/CFT correspondence by enforcing diffeomorphism invariance along the radial direction of the AdS geometry. Its significance in the emergence of 3D spacetime and its deep connection to the Ward identities in CFT_2 were proposed in the beautiful works of [28, 33, 34]. Within the SymTFT sandwich construction, this equation corresponds to the “vanishing flux condition”, a constraint naturally satisfied by the ground state of the SymTFT.² This condition, inherently fulfilled by the state $|\Psi(\mathcal{B})\rangle$ by construction, enables the formulation of a topological symmetry-preserving RG flow. The corresponding Callan-Symanzik equation aligns directly with the Wheeler-DeWitt equation, establishing SymQRG as a direct probe into the bulk and realizing the UV/IR correspondence. In our lattice construction, the vanishing flux condition emerges as crossing symmetry in the CFT, which underpins a topological symmetry-preserving block-spin transformation. This, in turn, results in an exact and analytic multiscale entanglement renormalization ansatz (MERA)-like [35] tensor network representation that captures field theory across multiple scales. The analogy between the AdS/CFT correspondence and the MERA tensor network was, in fact, the original motivation to relate them [36]. Here, we elevate this analogy to a precise statement.

Many questions about the intrinsic non-perturbative properties of quantum gravity find natural answers within our framework — for example, the factorization puzzle related to wormhole contributions, and the quantum chaos associated with scattering in black hole backgrounds.

Meanwhile, it is well known that SymTFT is supposed to be a topological theory and that $\langle\Omega|$, the non-topological boundary condition of the sandwich, carries most of the dynamical information of the QFT. At first glance, this appears to contradict the AdS/CFT correspondence, where the bulk is expected to capture the dynamical information of the boundary CFT. However, explicit constructions of the sandwich for 2D rational CFTs and Liouville theory [1, 29, 30] reveal that the complexity of the bulk depends crucially on the amount of symmetry encoded within it. As the bulk encodes a larger share of boundary theory symmetries, the complexity of $\langle\Omega|$ decreases. When the bulk fully captures all the topological symmetries of the CFT, the boundary condition descends into a collection of conformal blocks that are purely kinematical, determined by representation theory.

In the examples we study explicitly in this paper, ranging from rational CFT and the Liouville theory, the corresponding holographic duals preserving the symmetries are topological. However, in more general cases where the symmetries involve an infinite and perhaps even continuous spectrum

²To be more precise, the physical states of the Turaev-Viro TQFT, which is the SymTFT for 2D CFTs, are equivalent to ground states of the Levin-Wen string-net model as we explain in Sec. 4.1, and we will use these terms interchangeably throughout the paper.

of charges, the bulk “SymTFT” may no longer remain *topological*. See for example [37].³ Perhaps SymTFT is more generally “SymFT”.

In this paper, we believe we have presented strong evidence supporting a universal holographic principle that unites the non-perturbative AdS/CFT correspondence and “topological” holography. **AdS/CFT probably follows from the *maximal* Sym(T)FT that makes explicit *all* the symmetries, non-invertible and otherwise, of the CFT.**

1.2 Outline of the paper

The structure of the paper is as follows: In Sec. 2, we review the Wilsonian and Kadanoff RG frameworks, emphasizing their distinctions from holographic RG. To reconcile these differences, we introduce a framework termed “quantum RG” [38, 39], which we further extend into SymQRG. This section explains in detail the underlying concepts and procedures of SymQRG.

To concretize this framework, we present two examples of SymQRG:

- In Sec. 3, we explore the $TT\bar{T}$ deformation for continuum field theories [27, 28], demonstrating its natural fit within the SymQRG framework. Specifically, we show that $TT\bar{T}$ -deformed theories are connected through an integral kernel corresponding to the 3D gravitational path integral. We then reformulate this in operator formalism, verifying that it satisfies the Wheeler-DeWitt equation. Written in operator formalism, it is clear that there is an underlying 3D long-range entangled ground state that fulfills the no-flux condition, underlying any 2D CFTs.
- In Sec. 4, we extend the tensor network state sum representation of 2D CFTs, as introduced in [1, 29–31], to establish a discrete formalism for SymQRG. This section begins with a review of the Turaev-Viro TQFT and the Levin-Wen string-net model, coming from the Moore-Seiberg data of 2D CFTs, which serve as the SymTFT for 2D CFTs. Following this, we revisit the construction of exact tensor networks for 2D CFTs, framing them as overlaps in the Hilbert space of the underlying string-net model, explicitly realizing the sandwich construction using intrinsic CFT data. The two quantum states in (1.1) are expressed separately in terms of conformal blocks and BCFT structure coefficients. Using these “BCFT Legos”, we simultaneously build up both the CFT and the bulk AdS spacetime [31]. We then elaborate on the SymQRG procedure inherent in this construction, showing how it yields an analytic MERA-like tensor network. Additionally, we analyze deformations away from the CFT fixed points and their implications. We conclude this section by emphasizing the pivotal role tensor networks play in the exact construction of both the CFT and its bulk dual.

Recognizing that this example might be unfamiliar to many readers yet crucial for advancing the study of the non-perturbative and background independent dictionary for the AdS/CFT

³As we will see, our construction of the bulk and the topological boundary comes from the OPE coefficients of the theory, which captures *all* the dynamical information when we use the whole chiral algebra of the CFT. Thus, we think it is unlikely that it only captures a topological subsector of the theory

correspondence, we include Fig. 1 as a preview of the entire procedure, and Fig. 2 for a logical map behind tensor network SymQRG.

The formalism above applies to CFT with any topological symmetries. In Sec. 5, we investigate the conditions under which the SymTFT is related to 3D Einstein gravity. We first focus on the case of 3D pure Einstein gravity. We elaborate on the connection between the Virasoro TQFT [22] and the discrete RG operator discovered during the discretization of the Liouville theory [1], constructed from representations of $U_q(SL(2, \mathbb{R}))$. We also briefly comment on the connection to quantum Teichmüller theory and the lattice Liouville theory [21, 40]. Geometric notions like geodesic lengths and volume in 3D arise when considering symmetries associated with these Virasoro lines, and the anyons in these theories are related to BTZ black holes [41]. Finally, we illustrate how 3D gravity universally emerges in the semi-classical limit from any microscopic large N holographic 2D CFTs, with a discrete and dense spectrum, through coarse-graining, while emphasizing its distinction from the non-perturbatively exact holographic correspondence.

In Sec. 6, we explore how the algebraic consistency conditions, or the bootstrap constraints of 2D CFTs are encoded in the topological boundary condition attached to the 3D bulk, or the state $|\Psi(\mathcal{B})\rangle$, and their fundamental role in the emergence of a 3D bulk. These algebraic properties are intrinsically tied to the topological symmetries encoded in the bulk SymTFT. These conditions fall into two categories:

- **The no-flux condition and crossing symmetry:** These conditions enable the SymQRG process, facilitating deeper exploration into the bulk and ensuring consistency across scales. They manifest as the Wheeler-DeWitt equation in gravity.
- **Gauging/anyon condensation and modular invariance:** These conditions guarantee a modular invariant spectrum for the 2D theory, allowing the 3D bulk to collapse into an intrinsically defined 2D theory. This can be understood as specifying a precise quantum measure for the 3D theory, a critical component in achieving a genuine 2D/3D correspondence.

Next, we elucidate how the decomposition of CFT information into $\langle \Omega |$ and $|\Psi(\mathcal{B})\rangle$ is related to the symmetry we extract into the SymTFT. We then explore the implications of these findings for quantum gravity. Specifically, we analyze the role of null states and wormholes, and demonstrate how the topological boundary helps address the factorization puzzle. Furthermore, we show that quantum chaos arises naturally from symmetry principles. In particular, we emphasize how Lorentzian correlators — including out-of-time-ordered correlation functions — are determined by the Moore-Seiberg data of 2D CFTs.

We conclude our paper with some discussions on future directions.

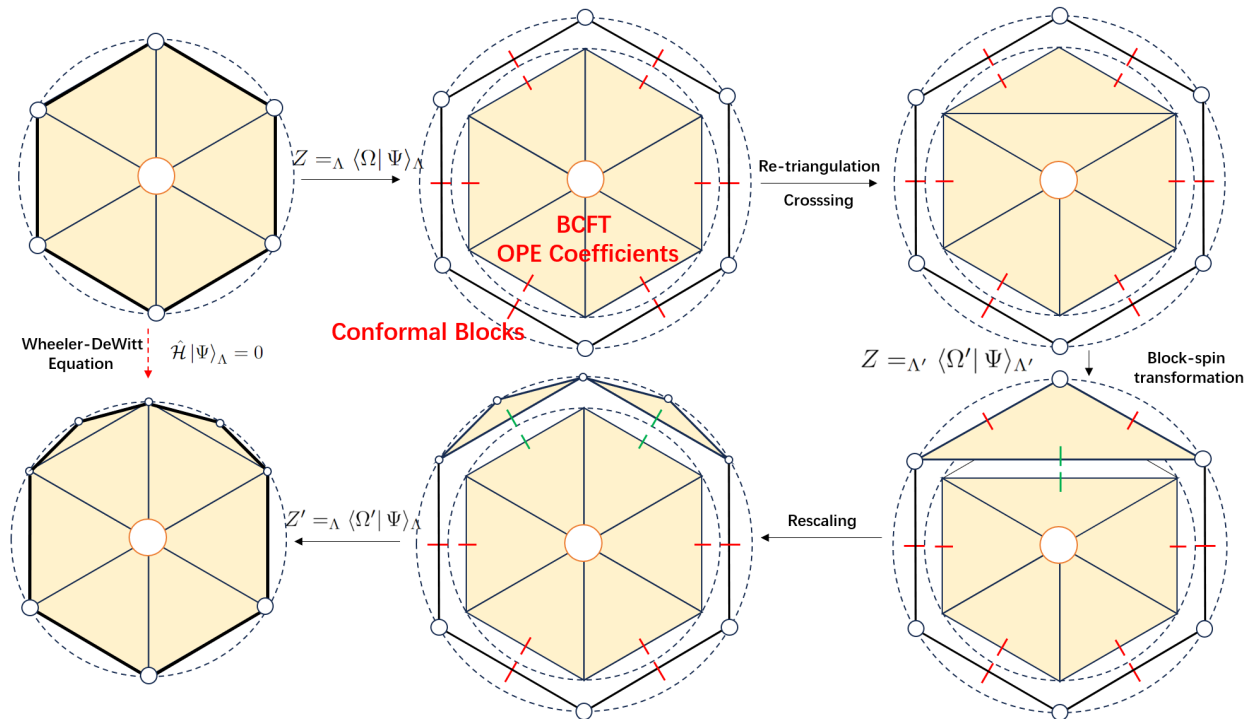


Figure 1: An illustration of the SymQRG coarse-graining procedure for the tensor network state sum representation of field theories in Sec. 4. The orange circle in the middle of the bulk indicates the topological boundary. The second step is the crucial step where we use the topological invariance of the bulk path integral (corresponding to 2D CFT crossing) to perform re-triangulation on $|\Psi\rangle_\Lambda$. In the third step, we contract the state ${}_\Lambda \langle \Omega |$ defined on the red edges with the triangle to turn it into the state ${}_{\Lambda'} \langle \Omega' |$ defined on the longer green edge, realizing a symmetry-preserving block-spin transformation. Before the rescaling procedure, we land on the bottom right diagram where the field theory lattice gets coarse-grained and we probe deeper into the UV direction of the bulk. After the rescaling procedure, the overlap corresponds to a deformed path integral, and is equivalent to imposing another finite-cutoff boundary condition further towards the IR direction in the bulk. In the CFT, the fact that we move towards the IR is represented by the smaller holes after rescaling.

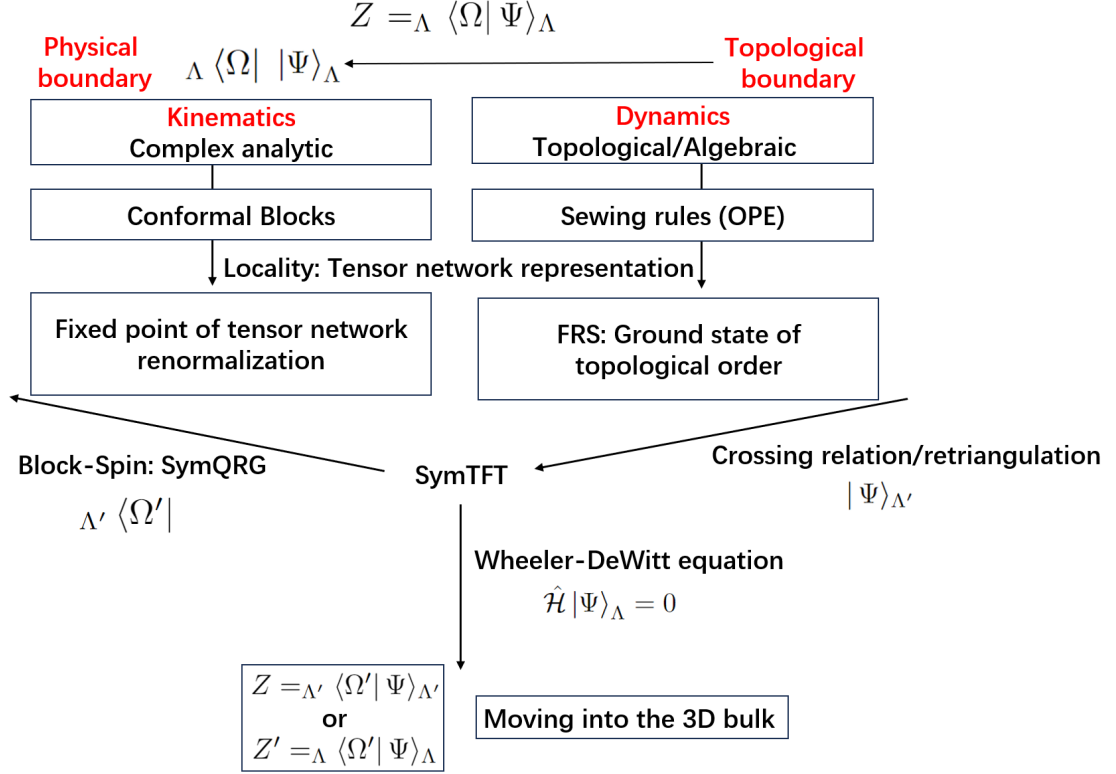


Figure 2: A logical map of the tensor network SymQRG. The sandwich construction in the study of generalized symmetries allow us to express the CFT path integral as an overlap of 3D states, where the bra state corresponds to a “physical boundary condition” that controls the kinematics (conformal blocks) in the 2D CFT; the ket state is a ground state of the SymTFT, which corresponds to a “topological boundary condition” attached to the 3D bulk, and governs the dynamics (OPE coefficients) of the 2D CFT. Both states admit tensor network representations due to the *locality* inherent in field theories. The underlying Hilbert space is provided by the Levin-Wen string net model based on the Moore-Seiberg data of the 2D CFT. Using the crossing symmetry or re-triangulation invariance of the $|\Psi\rangle_{\Lambda}$ state, we can naturally obtain a topological symmetry-preserving RG procedure that progresses into the bulk of the SymTFT. The crossing symmetry ensures that the “Wheeler-DeWitt” equation, or the no-flux constraint, is satisfied.

1.3 Summary of framework

Since this paper is rather long and includes many technical details, let us summarize the overall framework below.

- 1) Given a 2D CFT, we first have a chiral algebra V (we mainly focus on Virasoro in this paper). The representations of V form the (irrational generalization of the) Moore-Seiberg category $\mathcal{C} = \text{Rep}(V)$ [42].
- 2) Using \mathcal{C} , we can construct the 3D SymTFT of this theory using the Turaev-Viro/Levin-Wen string-net type construction [23, 24].
- 3) V can be understood as specifying a physical boundary condition, or a quantum state $\langle \Omega |$ in the Levin-Wen string-net theory Hilbert space, which can be constructed explicitly using conformal blocks.
- 4) All the dynamical information of the CFT is encoded in the topological boundary condition of the SymTFT, which uniquely corresponds to a solution of certain algebraic equations, and can be translated into CFT bootstrap consistency conditions. Each individual CFT is identified with a ground state $|\Psi\rangle$ of the SymTFT, and can be constructed explicitly using BCFT OPE coefficients of the CFT.
- 5) The sandwich construction identifies a 3D wavefunction $\langle \Omega | \Psi \rangle$ with the 2D CFT partition function. Explicitly written on the string-net Hilbert space, this gives an exact and analytic background-independent MERA-type holographic tensor network [1, 29–31, 35], discretizing the CFT path integral.
- 6) Probing deeper into the bulk SymTFT corresponds to a symmetry-preserving RG flow. In practice, it corresponds to finding different physical boundary conditions $\langle \Omega |$, which are related by gluing additional 3D SymTFT path integral. The Wheeler-DeWitt equation and the Callan-Symanzik equation get mapped to the no-flux constraint on the ground state $|\Psi\rangle$.
- 7) The bulk SymTFT is related to 3D gravity in either an exact or a coarse-grained sense, when the SymTFT contains a large number of Virasoro defect lines, corresponding to heavy operators in the CFT. Summing over certain quantum geometries in the bulk emerges from the algebraic data of the CFT.

This paper includes five appendices. Appendix A provides details on the Turaev-Viro TQFT. Appendices B and C offer a detailed explanation of the tensor network construction of 2D CFTs and the explicit procedure for the associated SymQRG. Appendix D discusses the exact tensor network construction of CFT wavefunctions from the Euclidean path integral, and the connection to perfect tensors and random tensors. Appendix E provides a brief review of quantum Teichmüller theory and the Teichmüller TQFT, and their connection to the $U_q(SL(2, \mathbb{R}))$ $6j$ symbols.

		Wilson-Kadanoff RG	Quantum RG	SymQRG
Operators	Classification	No special organization	Simple and composite operators	Simple and composite operators, based on symmetry charges
	Kept in RG	All	Simple	Simple
Couplings	Simple operators	Classical, Non-dynamical	Quantum, Dynamical	Quantum, Dynamical Controlled by SymTFT
	Composite operators	Classical, Non-dynamical	Implicit	Implicit

Figure 3: Comparison between three different RG procedures. Wilson-Kadanoff RG keeps all the couplings during each RG step, and the couplings are classical and non-dynamical. Quantum RG projects onto a subset of simple operators during each RG step, which makes the corresponding couplings quantum and dynamical in the emergent bulk. SymQRG projects onto simple operators classified based on symmetry charges, and the bulk generated is the symmetry-preserving SymTFT.

2 From Wilson-Kadanoff RG to SymQRG

The AdS/CFT correspondence has been famously argued to be related to RG flows from its very inception [2–4, 17]. However, there are notable differences between holographic RG flows and the conventional Wilson-Kadanoff RG flow. In this section, we begin by briefly reviewing the Wilson-Kadanoff RG flow and then demonstrate the need to upgrade it to “Quantum RG” [38, 39]. We further extend this framework to SymQRG, where the dynamical bulk generated by the RG procedure is the SymTFT, preserving the topological symmetries. The comparison between these concepts is summarized in Fig. 3.

2.1 Wilson-Kadanoff RG

Let us briefly recall the procedure for the Wilson-Kadanoff RG flow [43, 44]. In Wilson-Kadanoff RG, we begin with a theory with a momentum cutoff Λ_{RG} . In the path integral formulation of the partition function, this corresponds to integrating over field configurations with momenta below the

cutoff,⁴

$$Z = \int \mathcal{D}\phi_{|k| < \Lambda_{\text{RG}}} e^{-S(\phi)}. \quad (2.1)$$

The first step of Wilson-Kadanoff RG is coarse-graining, where we integrate out some high-energy degrees of freedom, resulting in a theory with a lower momentum cutoff $\Lambda'_{\text{RG}} < \Lambda_{\text{RG}}$. In terms of the partition function, this corresponds to a partial integration over the momentum shell $\Lambda'_{\text{RG}} < |k| < \Lambda_{\text{RG}}$:

$$\begin{aligned} Z &= \int \mathcal{D}\phi_{|k| < \Lambda'_{\text{RG}}} \mathcal{D}\phi_{\Lambda'_{\text{RG}} < |k| < \Lambda_{\text{RG}}} e^{-S(\phi)} \\ &= \int \mathcal{D}\phi_{|k| < \Lambda'_{\text{RG}}} e^{-S'(\phi)}, \end{aligned} \quad (2.2)$$

where $S'(\phi)$ is the effective action on the lower cut-off scale Λ'_{RG} , and should not be confused with derivatives. Importantly, coarse-graining does *not* alter the underlying partition function, and we are merely viewing the theory at a different scale.⁵

The second step is to “zoom out”, where we rescale $|k|$ so that the upper limit of integration is restored to Λ_{RG} . Additionally, for operators with nontrivial anomalous dimensions, we rescale the field ϕ to obtain a new field ϕ' , ensuring that the kinetic term remains canonically normalized. The partition function, now expressed in terms of the new fields, is given by:

$$Z' = \int \mathcal{D}\phi'_{|k| < \Lambda_{\text{RG}}} e^{-S''(\phi')}. \quad (2.3)$$

As a result of this whole process, the couplings in the effective field theory change, leading to a deformation of the theory and generating an RG flow in the space of theories.

To illustrate as an example, consider a term in the effective action of the form:

$$\int d^d x g_i O_i, \quad (2.4)$$

where g_i is the scale-dependent coupling associated with the operator O_i . Operators are classified as “relevant, marginal, or irrelevant” based on how their couplings evolve under RG flow. For example, operators whose $|g_i|$ decreases and eventually approaches zero under RG flow are termed irrelevant operators. After the two-step RG procedure, the theory can be seen as deformed by an additional term $\int d^d x, \delta g_i O_i$ in the action, leading to a new effective theory where the coupling satisfies $|g_i + \delta g_i| < |g_i|$.

Different theories are said to lie on the same RG trajectory if they are related by the Callan-

⁴Notice that the cutoff Λ_{RG} can be implemented in various ways, such as a smooth momentum cutoff [45] or a real-space cutoff on a lattice [44]. Likewise, there are different RG schemes for performing the RG transformation. For the sake of illustration, we adopt a hard momentum cutoff [43], and implement the RG transformation through a momentum shell integral.

⁵In practical computations, we usually perform some approximation or truncation in couplings in this step, which leads to a different answer after coarse-graining. In this paper, we always take the exact RG perspective.

Symanzik equation, which implies that the effect of deformation can be compensated by a rescaling of the system.

2.2 Quantum RG

Since the discovery of the AdS/CFT correspondence, it has been proposed that the change of scale, or RG flow, in the D -dimensional boundary theory is closely tied to the emergence of the extra radial direction in $D + 1$ -dimensional asymptotically AdS spacetime [2–4, 17]. This connection has been studied systematically under the framework of “holographic RG flow” [18, 19]. However, as noted in [46, 47] and emphasized in [38], there is a notable distinction between holographic RG and conventional Wilson-Kadanoff RG. In traditional RG procedures, the couplings in the boundary theory evolve according to first-order differential equations dictated by the beta functions, and they remain *classical/non-dynamical*. In contrast, in holography, these couplings correspond to fields in the gravitational bulk, where they are inherently *quantum/dynamical*. Most importantly, in the AdS/CFT correspondence, the boundary metric tensor h_{ij} serves as a classical background source for the stress energy tensor T_{ij} of the boundary CFT. This fixed metric defines the geometric 2D background on which the CFT is placed, and the CFT stress tensor encodes the response of the theory to variations in this background. In contrast, bulk theory is a theory of quantum gravity, where the bulk metric tensor $g_{\mu\nu}$ is a dynamical field that evolves according to gravitational dynamics and is capable of quantum fluctuations.

To resolve this tension, Lee proposed a manipulation in [38, 39] that converts the sources into dynamical and quantum degrees of freedom in the bulk. This is achieved by retaining only a subset of operators that forms a basis of simple operators in the operator space during RG flows. Specifically, in large N holographic theories, double-trace operators are inevitably generated from single-trace operators during RG transformations [46], and we re-express these double-trace operators in terms of single-trace operators and keep only the single-traces at each step of the RG. We will adopt this perspective in the context of the $T\bar{T}$ deformation in Sec. 3, explicitly demonstrating how this procedure transforms the boundary metric h_{ij} into the dynamical and quantum metric fields g_{ij} in the bulk. This approach, known as *Quantum RG*, has been shown to reproduce key aspects of the quantum holographic correspondence in specific settings.

2.3 SymQRG: Topological Symmetry-Preserving Quantum RG

In this paper, we take a step further to explain the meaning of this projection into simple operators from a symmetry principle that extends beyond the large N limit, highlighting its crucial role in the context of the AdS₃/CFT₂ correspondence. The key insight is that holography can be understood as an RG transformation that *explicitly* preserves certain *topological symmetries* of the 2D theories. This collection of symmetries includes generically non-invertible symmetries, and they follow from the representation of the chiral algebra inherent in any 2D CFTs, as first discovered by Moore and

Seiberg [42, 48]. These topological symmetries manifest themselves as topological line operators in the CFT [20, 49, 50]. The connection between this symmetry and the complete set of CFT gluing rules was elucidated in a series of seminal works collectively referred to the FRS construction in the literature, named after Fuchs, Runkel and Schweigert, as well as Fröhlich and Fjelstad [32]. The emergence of a 3D hyperbolic geometry from 2D CFTs is precisely captured by this “Virasoro modular geometry” for irrational CFTs [33, 51–54]. More details on the emergence of the quantum group/non-commutative geometry $U_q(SL(2, \mathbb{R}))$ and its connection to 3D gravity are the focus of Sec. 5.

In general, for a given set of symmetries in a 2D theory, it is associated with a 3D (topological) theory that follows from gauging the set of symmetries. For conventional discrete group symmetries with symmetry group G , the 3D theory corresponds to a topological gauge theory with gauge group G . More generally, for a rational collection of non-invertible symmetries, the “gauged” theory is a 3D TQFT [11, 55], which is the SymTFT. The Hilbert space of the SymTFT defined on a given 2D manifold Σ provides a symmetry-preserving basis for the construction of symmetry-preserving 2D theories. In this light, the 3D background gravitational theory itself functions as the “SymTFT” for irrational 2D CFTs. This SymTFT can be further used to carry out an RG flow that explicitly preserves topological symmetries [1, 29–31]. Therefore, the holographic *duality* can be understood as a manifestation of the non-perturbative *symmetries* for theories at different scales along a topological symmetry preserving RG trajectory. We refer to this framework as “topological symmetry-preserving quantum RG” or “SymQRG”.

Let us briefly summarize the idea and explicit procedure behind SymQRG. Two concrete realizations of this framework are presented in Sec. 3 for the continuum $T\bar{T}$ deformation, and in Sec. 4 for the exact discrete real-space tensor network representation of 2D field theories.

The idea is that we can always express the 2D QFT partition functions as an overlap between two 3D quantum states,

$$Z = {}_{\Lambda} \langle \Omega^{\lambda}(\gamma_{ij}) | \Psi \rangle_{\Lambda} , \quad (2.5)$$

where the subscript Λ denotes some reference scale (which we will make precise in explicit constructions), γ_{ij} is the metric on which the theory is defined and λ labels the dimensionful couplings of the theory. In Sec. 3, λ refers to the coupling for the $T\bar{T}$ deformation, which has mass dimension -2 . This is in turn related to the size of the holes we introduce on the lattice in Sec. 4. In the language of generalized symmetries [15], this overlap realizes the “sandwich construction” [5–8], as shown in Fig. 4, where ${}_{\Lambda} \langle \Omega^{\lambda}(\gamma_{ij}) |$ corresponds to a *physical* boundary condition that captures geometrical notions such as distances and positions in a 2D QFT. For instance, in our $T\bar{T}$ example in Sec. 3.3, this state can be interpreted as the finite cutoff “position space” basis states [56] in 3D quantum gravity; In Sec. 4, we use the Hilbert space of the Levin-Wen string-net model [24] underlying the tensor network construction to write down a continuous family of states, labelled by the size of the

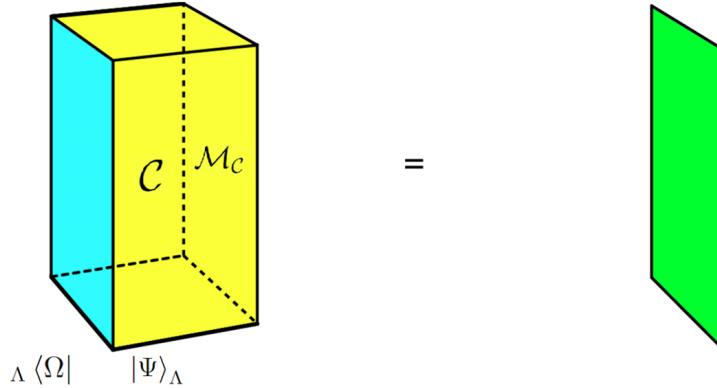


Figure 4: An illustration of the sandwich construction, where any D -dimensional field theory is equivalent to collapsing the two boundaries of a $D + 1$ -dimensional SymTFT, which governs the topological symmetries of the original theory. A topological boundary condition and a physical boundary condition are specified on the two boundaries. The precise meaning of \mathcal{C} and $\mathcal{M}_\mathcal{C}$ in the context of 2D CFTs will be explained in 6.2.

holes. In both of these cases, $\lambda = 0$ corresponds to an RG fixed point (CFT). We also want to emphasize that these states describes the *kinematical* aspects of the 2D theory. *Dynamics* are encoded in the ket state $|\Psi\rangle_\Lambda$, which corresponds to the state obtained from a 3D path integral associated with a *topological* boundary condition⁶. The state contains the algebraic information of 2D CFT, such as its sewing rules, i.e. *all* the OPE coefficients. [32]. The holographic principle thus equates this 3D wavefunction with 2D partition functions, and we will elaborate more on this in Sec. 6.

In terms of the 3D bulk theory that captures the non-invertible symmetries of the 2D CFT, the state $|\Psi\rangle_\Lambda$ is a topological ground state satisfying the no-flux constraint

$$\hat{\mathcal{H}}|\Psi\rangle_\Lambda = 0 . \tag{2.6}$$

For the $T\bar{T}$ deformation, this constraint equation manifests itself as the Wheeler-DeWitt equation. In the example of the real-space tensor network, this condition implies that this state is a ground state of the underlying topological order, describing the long-range entanglement in 2D CFTs from the consistency conditions of the sewing/crossing relation. We emphasize that it is this state $|\Psi\rangle_\Lambda$ that underlies the emergence of the third radial direction, and *non-perturbatively exact* nature of the $\text{AdS}_3/\text{CFT}_2$ correspondence.

SymQRG is the statement that there exist different physical boundary conditions, corresponding to different states $|\Omega\rangle_\Lambda$, whose overlap with a fixed topological ground state $|\Psi\rangle_\Lambda$ gives different theories along an RG trajectory. These theories are interconnected through the inclusion of an integral kernel corresponding to additional path integrals in the bulk SymTFT. The presence of a

⁶This combination is referred to as a “quiche” in [6].

no-flux ground state guarantees that the Callan-Symanzik equation naturally implies the Wheeler-DeWitt equation. We can find the ${}_{\Lambda} \langle \Omega |$ states using the following procedure inspired by our tensor network construction on the lattice [1, 29–31].

We first change a realization of the original overlap using:

$${}_{\Lambda} \langle \Omega^{\lambda}(\gamma_{ij}) | \Psi \rangle_{\Lambda} = {}_{\Lambda} \langle \Omega^{\lambda}(\gamma_{ij}) | \hat{U}_{\text{RG}}^{\Lambda, \Lambda'} | \Psi \rangle_{\Lambda'} , \quad (2.7)$$

where $|\Psi\rangle_{\Lambda'}$ is a different realization of the topological ground state on a different probe scale. Since this is a topological ground state, the RG operator $\hat{U}_{\text{RG}}^{\Lambda, \Lambda'}$ that changes the representation at different scales for $|\Psi\rangle$ in this context is precisely given by the 3D bulk TQFT path integral⁷, which in this case is the 3D quantum gravity path integral.

We now define the new bra state as:

$${}_{\Lambda'} \langle \Omega'^{\lambda}(\gamma_{ij}) | \equiv {}_{\Lambda} \langle \Omega^{\lambda}(\gamma_{ij}) | \hat{U}_{\text{RG}}^{\Lambda, \Lambda'} . \quad (2.8)$$

This process precisely matches the notion of coarse-graining/spin-blocking, since we get two different representations of the same partition function at two different scales,

$${}_{\Lambda} \langle \Omega^{\lambda}(\gamma_{ij}) | \Psi \rangle_{\Lambda} = {}_{\Lambda'} \langle \Omega'^{\lambda}(\gamma_{ij}) | \Psi \rangle_{\Lambda'} . \quad (2.9)$$

After rescaling, we get a deformed state,

$${}_{\Lambda'} \langle \Omega'^{\lambda}(\gamma_{ij}) | \rightarrow {}_{\Lambda} \langle \Omega'^{\lambda}(\gamma_{ij}) | . \quad (2.10)$$

From the Callan-Symanzik equation, we know that the effect of this deformation is the same as directly deforming the coupling, so we can equate

$${}_{\Lambda} \langle \Omega^{\lambda(\frac{\Lambda}{\Lambda'})^2}(\gamma_{ij}) | = {}_{\Lambda} \langle \Omega'^{\lambda}(\gamma_{ij}) | . \quad (2.11)$$

Thus, the deformed partition function with a different coupling can be written in terms of the

⁷Since this is a topological ground state of a TQFT, the representation of this state at different scales might sound unfamiliar. In any explicit realization of the theory in the form of field theory or lattice model, the expression of the path integral in the presence of a boundary (i.e. the ground state wave function) would depend on the choice of extra structures on the boundary surface not intrinsic to the theory, e.g. a boundary metric, or a triangulation in a discrete model as discussed in Sec. 4.

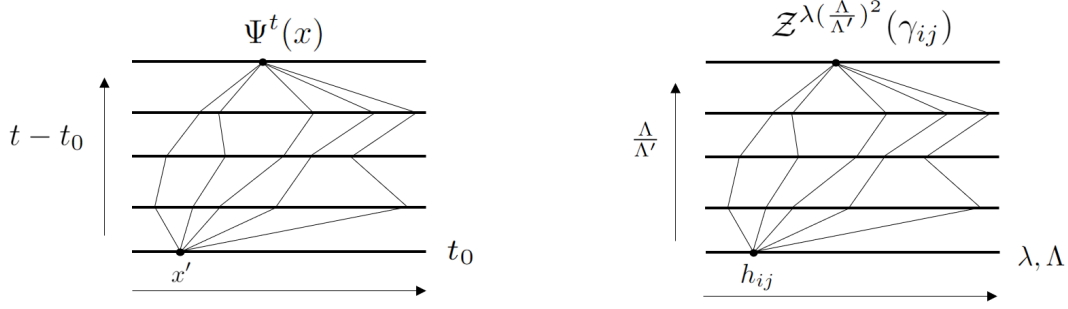


Figure 5: Comparison between Feynman’s path integral (2.13) in quantum mechanics on the left and the topological symmetry-preserving quantum RG (2.12) for quantum field theories. They both take a form of path integral in an extra dimension that sums over all possible paths connecting x at different time and source J at different RG time. The “bulk” in (2.12) is a space of 2D field theories with symmetries.

original partition function as

$$\begin{aligned}
\mathcal{Z}^{\lambda(\frac{\Lambda}{\Lambda'})^2}(\gamma_{ij}) &= {}_{\Lambda} \langle \Omega^{\lambda(\frac{\Lambda}{\Lambda'})^2}(\gamma_{ij}) | \Psi \rangle_{\Lambda} \\
&= \int \mathcal{D}h_{ij\Lambda} \langle \Omega^{\lambda(\frac{\Lambda}{\Lambda'})^2}(\gamma_{ij}) | \Omega^{\lambda}(h_{ij}) \rangle_{\Lambda} {}_{\Lambda} \langle \Omega^{\lambda}(h_{ij}) | \Psi \rangle_{\Lambda} \\
&= \int \mathcal{D}h_{ij\Lambda} \langle \Omega^{\lambda}(\gamma_{ij}) | e^{-\int_{\lambda}^{\lambda(\frac{\Lambda}{\Lambda'})^2} \hat{H}_{\text{grav}}} | \Omega^{\lambda}(h_{ij}) \rangle_{\Lambda} {}_{\Lambda} \langle \Omega^{\lambda}(h_{ij}) | \Psi \rangle_{\Lambda} \\
&= \int \mathcal{D}h_{ij} K_{\text{grav}}(\gamma_{ij}, h_{ij}, \lambda(\frac{\Lambda}{\Lambda'})^2, \lambda) \mathcal{Z}^{\lambda}(h_{ij}) ,
\end{aligned} \tag{2.12}$$

where in the second line, we insert a complete basis labelled by the metric, and the kernel $K_{\text{grav}}(\gamma_{ij}, h_{ij}, \lambda(\frac{\Lambda}{\Lambda'})^2, \lambda)$ relating different deformed partition functions is a gravitational path integral. The coupling λ appears to play the role of a “radial time” (more precise connection is in (3.27)), such that this equation takes the same form as the conventional Feynman path integral representation of the evolution of a wave function in quantum mechanics in the Heisenberg picture, i.e.⁸

$$\begin{aligned}
\Psi^t(x) &= \langle x(t) | \Psi \rangle \\
&= \int dx' \langle x(t) | x' \rangle \langle x' | \Psi \rangle \\
&= \int dx' \langle x | e^{-i \int_{t_0}^t \hat{H}} | x' \rangle \langle x' | \Psi \rangle \\
&= \int dx' K(x, x', t, t_0) \Psi^{t_0}(x') ,
\end{aligned} \tag{2.13}$$

where we keep the time dependence explicit to make the relation to (2.12) manifest. The third

⁸Recall that basis states have time dependence in Heisenberg picture, because they are eigenstates of time dependent operators.

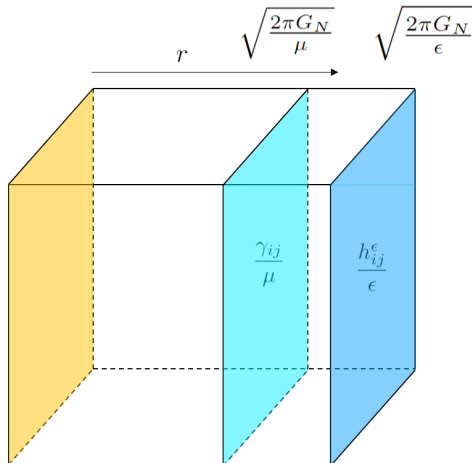


Figure 6: The SymQRG deformation changes the bra state ${}_{\Lambda} \langle \Omega^\lambda(h_{ij}) |$ by gluing extra path integral of the bulk SymTFT onto it. This can equivalently be interpreted as imposing a different boundary condition, corresponding to a different cutoff.

equality returns to the basis defined at $t = t_0$, which also coincides with the basis state in the Schrödinger picture, using the Hamiltonian \hat{H} . The kernel $K(x, x', t, t_0)$ in the fourth line is the transition amplitude, which can be expressed explicitly using Feynman’s path integral. We will see in Sec. 3.1, the quantum RG procedure [38, 39] is exactly analogous to time evolution in quantum mechanics. The position x is the fixed argument of our wavefunction $\Psi(x)$, similar to the role played by the source J or h in $Z(J)$ or $Z(h)$ in QFTs. In fact, solution to the $T\bar{T}$ deformation exactly takes the form of (2.12), and this deformed partition function is nothing but the Wheeler-DeWitt wave functional in the Heisenberg picture. This comparison with usual quantum mechanical treatment makes manifest the existence of an underlying quantum state $|\Psi\rangle_{\Lambda}$, which we will show to be a long-range entangled ground state of the topological order in the bulk, associated to the underlying Moore-Seiberg data. The ${}_{\Lambda} \langle \Omega^\lambda(\gamma_{ij}) |$ states correspond to finite cutoff Dirichlet boundary conditions in the AdS/CFT correspondence. Alternatively, these states can be understood as the implementation of mixed boundary conditions at asymptotic infinity⁹, arising from double-trace deformations [57–61]. Interestingly, when interpreted as boundary conditions, this suggests that these boundary conditions all generate the same Virasoro algebra in a nontrivial way [60].

We note that in quantum mechanics, the “bulk” generated by Hamiltonian evolution connecting time slices is determined by *one* theory. On the other hand, in holography, the “bulk” generated by RG time evolution is connecting *different* theories i.e. at each slice a given state determines

⁹Naively, the bulk is a TQFT, so the notion of radial distances in the bulk does not seem to make sense. However, this becomes possible because the boundary conditions break topological invariance, and there is a scale λ within these boundary conditions. The relative scale between the parameters of different boundary conditions can then be interpreted as the parameterization of a radial distance

the Hamiltonian of a lower-dimensional theory. This is dynamically evolved by the bulk to other theories living on a different r slice¹⁰. The Hilbert space of the 3D gravitational bulk on a 2D slice is thus the *space of 2D theories with symmetries* [39, 62]. Different 2D theories are labeled by different boundary conditions corresponding to different ${}_{\Lambda} \langle \Omega^{\lambda}(h_{ij}) |$ and $|\Psi\rangle_{\Lambda}$. Note that this is not the complete theory space for 2D QFTs. Rather, the 3D gravitational bulk restricts the space of theories to those preserving the same topological symmetries (with at most spontaneous symmetry breaking). In a non-perturbative setting, the symmetry provides an exact basis labelling different quantum theories.

This entire procedure is deeply inspired by the formalism introduced by Lee and formalized in [39], with a crucial addition: since 3D bulk gravity is essentially a topological order with long-range entanglement, quantum RG should incorporate generalized symmetries. This turns out to follow naturally from the long-range entangled topological ground state $|\Psi\rangle_{\Lambda}$ in the sandwich construction, which is crucial to obtaining the *exact* holographic dual, and captures the essence of the Wheeler-DeWitt equation. In our lattice construction, this also allows us to connect the symmetric RG to the crossing symmetry of the 2D CFT. Finally, the topological boundary in $|\Psi\rangle_{\Lambda}$ implies that the bulk path integral spans a sandwich that can be compressed into an intrinsically 2D theory, encapsulating the fact that the constructed 2D theory is indeed anomaly free. Thus, $|\Psi\rangle_{\Lambda}$ carries the necessary ingredients of a 3D/2D duality (i.e. *equivalence*).

3 $T\bar{T}$ deformation for 2D CFTs as SymQRG

We begin by elaborating on the framework in the context of the $T\bar{T}$ deformation [27, 28]. Recent studies have shown that 2D QFTs can undergo an integrable deformation called $T\bar{T}$ deformations [27, 63]. Furthermore, it was proposed in [28] that these deformed theories can be interpreted as dual to theories of “finite cutoff holography”, satisfying the Wheeler-DeWitt equation [28, 34]. In these discussions, the absolute value of the $T\bar{T}$ coupling $|\mu|$ increases under deformation. Since $|\mu|$ decreases under a coarse-grain RG flow, reflecting the irrelevant nature of the $T\bar{T}$ operator, and because the deformed theories satisfy the Callan-Symanzik equation, the $T\bar{T}$ deformation can be understood as an “inverse RG flow”, fine-graining towards the UV.

In this section, we emphasize two complementary aspects of the $T\bar{T}$ deformation. First, in Sec. 3.1, we apply iterative quantum RG to 2D $T\bar{T}$ deformations, deriving an integral transform formula that relates $\mathcal{Z}^{\mu}(\gamma_{ij})$ at different couplings. The kernel of this transform is identified with the 3D gravitational path integral. Second, in Sec. 3.2, we demonstrate how the 3D bulk gravitational phase-space path integral can be used to deform 2D theories, naturally giving rise to the $T\bar{T}$ deformation. In Sec. 3.3, we rewrite these results in the operator formalism, highlighting the connection between the Wheeler-DeWitt equation and an underlying long-range entangled ground

¹⁰We should emphasize that the Hamiltonians of the lower dimensional theories resulting from different boundary conditions on a radial slice of the bulk should not be confused with the radial Hamiltonian of the bulk quantum gravity.

state that satisfies the no-flux condition (2.6). Many of the manipulations in this section are formal, especially regarding subtleties in defining Hilbert spaces and path-integral measures in continuum field theories. The ideas presented in this section are not entirely new; similar concepts have been explored in [38, 64–68]¹¹. The primary goal of this section is to illustrate the SymQRG framework through the concrete example of $T\bar{T}$ deformation on curved spacetimes. This discussion also serves as a natural transition to the subsequent exploration of a more precisely defined lattice construction.

3.1 3D phase space gravitational path integral from iterative $T\bar{T}$ deformation

In this subsection, we first focus on the simpler case where the deformation parameter λ is constant. The generalization to spatially varying deformations $\lambda(x)$ and their physical implications will be addressed later.

We start with the CFT partition function defined on a 2D Euclidean metric γ_{ij} , denoted as $\mathcal{Z}_{\text{CFT}}[\gamma_{ij}]$. The $T\bar{T}$ deformation on 2D curved spacetimes generates a family of deformed theories parameterized by λ , which satisfy the flow equation [28, 64–66]¹²,

$$\frac{d}{d\lambda} \mathcal{Z}^\lambda[\gamma_{ij}] = - \int d^2x \left[\frac{c}{48\pi\lambda} \sqrt{\gamma} R(\gamma_{ij}) + \frac{12\pi}{c\sqrt{\gamma}} \left(\frac{1}{2} (\gamma_{ik}\gamma_{jl} + \gamma_{il}\gamma_{jk}) - \gamma_{ij}\gamma_{kl} \right) \frac{\delta}{\delta\gamma_{ij}} \frac{\delta}{\delta\gamma_{kl}} \right] \mathcal{Z}^\lambda[\gamma_{ij}]. \quad (3.1)$$

Introducing μ as a reference scale with mass dimension -2 , the interpretation of which in the context of AdS_3 and CFT_2 will be clarified below, we define a dimensionless parameter z as:

$$\lambda(z) = \mu e^z. \quad (3.2)$$

The flow equation can then be solved for small δz as follows:

$$\mathcal{Z}^{\lambda(\delta z)}[\gamma_{ij}] = e^{\delta S(\mu, \delta z, -i\frac{\delta}{\delta\gamma_{ij}}, \gamma_{ij})} \mathcal{Z}^{\lambda(0)}[\gamma_{ij}], \quad (3.3)$$

where the deformation action functional is:

$$\delta S(\mu, \delta z, -i\frac{\delta}{\delta\gamma_{ij}}, \gamma_{ij}) = -\mu\delta z \int d^2x \left[\frac{c}{48\pi\mu} \sqrt{\gamma} R(\gamma_{ij}) + \frac{12\pi}{c\sqrt{\gamma}} \left(\frac{1}{2} (\gamma_{ik}\gamma_{jl} + \gamma_{il}\gamma_{jk}) - \gamma_{ij}\gamma_{kl} \right) \frac{\delta}{\delta\gamma_{ij}} \frac{\delta}{\delta\gamma_{kl}} \right]. \quad (3.4)$$

Alternatively we can write,

$$\mathcal{Z}^{\lambda+\delta\lambda}[\gamma_{ij}] = e^{\delta S'(\lambda, \delta\lambda, -i\frac{\delta}{\delta\gamma_{ij}}, \gamma_{ij})} \mathcal{Z}^\lambda[\gamma_{ij}], \quad (3.5)$$

¹¹Especially in [64], the $T\bar{T}$ -deformed partition functions were proposed to be viewed as wavefunctions in 3D gravity in the Schroedinger picture. However, as we will see, it is the Heisenberg picture—where the physical state remains unchanged while the basis states evolve with time—that fits more naturally into our framework. This perspective makes the connection between the SymTFT, the Wheeler-DeWitt equation and the no-flux condition of the state manifest.

¹²We use a different convention from [28, 66], where $\gamma_{ij}^{\text{ours}} = \frac{1}{8} \gamma_{ij}^{\text{theirs}}$.

where

$$\delta S'(\lambda, \delta\lambda, -i\frac{\delta}{\delta\gamma_{ij}}, \gamma_{ij}) = -\delta\lambda \int d^2x \left[\frac{c}{48\pi\lambda} \sqrt{\gamma} R(\gamma_{ij}) + \frac{12\pi}{c\sqrt{\gamma}} \left(\frac{1}{2}(\gamma_{ik}\gamma_{jl} + \gamma_{il}\gamma_{jk}) - \gamma_{ij}\gamma_{kl} \right) \frac{\delta}{\delta\gamma_{ij}} \frac{\delta}{\delta\gamma_{kl}} \right]. \quad (3.6)$$

Expanding equation (3.3) or (3.5) to leading order in small δz readily reproduces the flow equation (3.1). The term

$$\frac{c}{48\pi\lambda} \sqrt{\gamma} R(\gamma_{ij}) \quad (3.7)$$

originates from the change in Casimir energy and is tied to the Wess-Zumino consistency condition. Its inclusion ensures that the RG flow is scheme-independent and is related to diffeomorphism invariance in the emergent 3D bulk [47, 66, 69].

The other term

$$\frac{12\pi}{c\sqrt{\gamma}} \left(\frac{1}{2}(\gamma_{ik}\gamma_{jl} + \gamma_{il}\gamma_{jk}) - \gamma_{ij}\gamma_{kl} \right) \frac{\delta}{\delta\gamma_{ij}} \frac{\delta}{\delta\gamma_{kl}} \quad (3.8)$$

is the double-trace operator $T\bar{T}$ that deforms the theory. Reversing the direction of the flow corresponds to the generation of double-trace operators by the RG flow.

We now adopt the approach proposed in [38], aiming to reformulate the double-trace deformation in terms of the single-trace operator T . To achieve this, we introduce an auxiliary pair of 2D fields and rewrite (3.3) as:

$$\begin{aligned} \mathcal{Z}^{\lambda+\delta\lambda}[\gamma_{ij}] &= e^{\delta S'(\lambda, \delta\lambda, -i\frac{\delta}{\delta\gamma_{ij}}, \gamma_{ij})} \mathcal{Z}^{\lambda}[\gamma_{ij}] \\ &= \int \mathcal{D}h_{ij}^{(1)} \mathcal{D}\pi^{(1),ij} e^{\int d^2x i\pi^{(1),ij}(\gamma_{ij} - h_{ij}^{(1)}) + \delta S'(\lambda, \delta\lambda, \pi^{(1),ij}, \gamma_{ij})} \mathcal{Z}^{\lambda}[h_{ij}^{(1)}]. \end{aligned} \quad (3.9)$$

The intuition behind this rewriting is to introduce Lagrange multipliers to encode the fact that the metric serves as the source for the stress tensor T or the momentum π in the action. This can be explicitly verified as follows. We rewrite the above equation as:

$$\mathcal{Z}^{\lambda+\delta\lambda}[\gamma_{ij}] = \int \mathcal{D}h_{ij}^{(1)} \mathcal{D}\pi^{(1),ij} e^{\int d^2x [-\delta\lambda\pi \cdot \Gamma \cdot \pi + \delta\lambda S_1 \cdot \pi - \delta\lambda R(\gamma, \lambda)]} \mathcal{Z}^{\lambda}[h_{ij}^{(1)}], \quad (3.10)$$

where

$$\begin{aligned} \Gamma &= -\delta(x-y) \frac{12\pi}{c\sqrt{\gamma}} \left(\frac{1}{2}(\gamma_{ik}\gamma_{jl} + \gamma_{il}\gamma_{jk}) - \gamma_{ij}\gamma_{kl} \right), \\ S_1 &= i \frac{\gamma_{ij} - h_{ij}^{(1)}}{\delta\lambda}, \\ R(\gamma, \lambda) &= \frac{c}{48\pi\lambda} \sqrt{\gamma} R(\gamma_{ij}). \end{aligned} \quad (3.11)$$

By performing the Gaussian integral for π , we obtain

$$\int \mathcal{D}h_{ij}^{(1)} e^{\int d^2x [\frac{\delta\lambda}{4} S_1 \cdot \Gamma^{-1} \cdot S_1 - \delta\lambda R(\gamma, \lambda)]} \mathcal{Z}^{\lambda}[h_{ij}^{(1)}], \quad (3.12)$$

where

$$\Gamma^{-1} = -c \frac{\delta(x-y)\sqrt{\gamma}}{12\pi} \left(\frac{1}{2}(\gamma^{ik}\gamma^{jl} + \gamma^{il}\gamma^{jk}) - \gamma^{ij}\gamma^{kl} \right). \quad (3.13)$$

Thus the result reads

$$\mathcal{Z}^{\lambda+\delta\lambda}[\gamma_{ij}] = \int \mathcal{D}h_{ij}^{(1)} e^{\int d^2x \left[\frac{c\sqrt{\gamma}}{48\pi\delta\lambda} (h_{ij}^{(1)} - \gamma_{ij}) \left(\frac{1}{2}(\gamma^{ik}\gamma^{jl} + \gamma^{il}\gamma^{jk}) - \gamma^{ij}\gamma^{kl} \right) (h_{kl}^{(1)} - \gamma_{kl}) - \frac{c\delta\lambda}{48\pi\lambda} \sqrt{\gamma} R(\gamma_{ij}) \right]} \mathcal{Z}^\lambda[h_{ij}^{(1)}]. \quad (3.14)$$

Next we perform the change of variables via

$$h_{ij}'^{(1)} = h_{ij}^{(1)} - \gamma_{ij}, \quad (3.15)$$

then we get

$$\mathcal{Z}^{\lambda+\delta\lambda}[\gamma_{ij}] = \int \mathcal{D}h_{ij}'^{(1)} e^{\int d^2x \left[\frac{c\sqrt{\gamma}}{48\pi\delta\lambda} h_{ij}'^{(1)} \left(\frac{1}{2}(\gamma^{ik}\gamma^{jl} + \gamma^{il}\gamma^{jk}) - \gamma^{ij}\gamma^{kl} \right) h_{kl}'^{(1)} - \frac{c\delta\lambda}{48\pi\lambda} \sqrt{\gamma} R(\gamma_{ij}) \right]} \mathcal{Z}^\lambda[h_{ij}'^{(1)} + \gamma_{ij}], \quad (3.16)$$

which is precisely the solution of (3.1) in terms of the Hubbard-Stratonovich transformation, and can be interpreted as coupling the original theory to 2D random geometry [28, 70].

Since we aim to perform the deformation iteratively and ultimately relate Z^μ to Z^ϵ —where the regulated CFT is defined at $\epsilon < \mu$ —we rewrite equation (3.9) as

$$\begin{aligned} \mathcal{Z}^\mu[\gamma_{ij}] &= e^{\int d^2x \delta S(\mu e^{-\delta z}, \delta z, -i \frac{\delta}{\delta \gamma_{ij}}, \gamma_{ij})} \mathcal{Z}^{\mu e^{-\delta z}}[\gamma_{ij}] \\ &= \int \mathcal{D}h_{ij}^{(1)} \mathcal{D}\pi^{(1),ij} e^{\int d^2x i\pi^{(1),ij}(\gamma_{ij} - h_{ij}^{(1)}) + \delta S(\mu e^{-\delta z}, \delta z, \pi^{(1),ij}, \gamma_{ij})} \mathcal{Z}^{\mu e^{-\delta z}}[h_{ij}^{(1)}]. \end{aligned} \quad (3.17)$$

In the above equation, we introduce

$$\lambda = \mu e^{-z}, \quad z = m\delta z, \quad (3.18)$$

Here, m represents the number of steps performed in the iterative quantum RG. Note that $\delta\lambda = -\lambda\delta z$ is now negative. We iterate this procedure in (3.17) and take the limit $\delta z \rightarrow 0$, ultimately expressing the result as a 3D path integral [38]. The 2D auxiliary fields $h_{ij}^m(x)$ and $\pi_{ij}^m(x)$ are promoted to 3D fields $h_{ij}(x, \lambda)$ and $\pi_{ij}(x, \lambda)$. As anticipated, this process transforms the metric h_{ij} - originally the source of the single-trace 2D boundary stress tensor - into a dynamical 3D metric field, thereby realizing *quantum gravity*.

Furthermore, by writing

$$i\pi^{(m+1),ij}(h_{ij}^{(m)} - h_{ij}^{(m+1)}) = -i(\lambda^{(m+1)} - \lambda^{(m)})\pi^{(m+1),ij} \frac{h_{ij}^{(m+1)} - h_{ij}^{(m)}}{\lambda^{(m+1)} - \lambda^{(m)}}, \quad (3.19)$$

we observe that this expression, in the limit $\delta z \rightarrow 0$, becomes a derivative term:

$$-id\lambda\pi(\lambda)^{ij}\partial_\lambda h(\lambda)_{ij} . \quad (3.20)$$

The initial condition for the path integral is imposed using a delta function:

$$\mathcal{Z}^\mu[\gamma_{ij}] = \int \mathcal{D}h_{ij}^{(0)} \mathcal{D}\pi^{(0),ij} e^{i \int d^2x \pi^{(0),ij} (\gamma_{ij} - h_{ij}^{(0)})} \mathcal{Z}^\mu[h_{ij}^{(0)}] = \int \mathcal{D}h_{ij}^{(0)} \delta(h_{ij}^{(0)} - \gamma_{ij}) \mathcal{Z}^\mu[h_{ij}^{(0)}] . \quad (3.21)$$

The integration limits for our 3D path integral are:

$$\begin{aligned} \lambda_{\text{ini}} &= \mu, & h_{ij}(\mu) &= \gamma_{ij} ; \\ \lambda_{\text{fin}} &= \epsilon, & h_{ij}(\epsilon) &= h_{ij}^\epsilon . \end{aligned} \quad (3.22)$$

In the end, we obtain:

$$\begin{aligned} \mathcal{Z}^\mu[\gamma_{ij}] &= \int \mathcal{D}h_{ij}^\epsilon \int_{\substack{h_{ij}(\mu)=\gamma_{ij} \\ h_{ij}(\epsilon)=h_{ij}^\epsilon}} \mathcal{D}h_{ij} \mathcal{D}\pi^{ij} \exp \left[\int_\mu^\epsilon d\lambda \int d^2x \left(-i\pi^{ij} \partial_\lambda h_{ij} - \frac{1}{2\lambda} \left(\frac{24\pi\lambda}{c\sqrt{h}} (\pi^{ij} \pi_{ij} - \pi^2) \right. \right. \right. \\ &\quad \left. \left. \left. - \frac{c\sqrt{h}}{24\pi} R(h_{ij}) \right) \right) \right] \mathcal{Z}^\epsilon[h_{ij}^\epsilon] . \end{aligned} \quad (3.23)$$

This result is a 3D path integral that closely resembles the phase-space path integral of 3D gravity. As we will demonstrate, by addressing certain subtleties involving counterterms, it becomes evident that this is indeed the 3D gravity path integral between two slices. Furthermore, the relationship between $\mathcal{Z}^\epsilon[h_{ij}^\epsilon]$ at the endpoint of the deformation and $\mathcal{Z}_{\text{CFT}}[h_{ij}^\epsilon]$ will be clarified in the subsequent discussion.

3.2 $T\bar{T}$ deformation from 3D gravitational path integral

It was further proposed in [28], building upon earlier results in [34], that a Wheeler-DeWitt wavefunction $\Psi(g)$ in 3D quantum gravity can be obtained from the deformed partition functions $Z^{(\mu)}(\gamma)$ via¹³:

$$\Psi(\gamma/\mu) = e^{\frac{1}{8\pi G_N \mu} \int d^2x \sqrt{\gamma}} \mathcal{Z}^{(\mu)}[\gamma_{ij}] . \quad (3.24)$$

where the induced metric on a constant μ cutoff surface is related to the field theory metric by $g_{ij} = \frac{\gamma_{ij}}{\mu}$, mirroring the standard relation in holography as $\mu \rightarrow 0$. The additional term in the exponent represents a 2D cosmological constant and is associated with the holographic counterterm. In Sec. 3.3, we will show that this manipulation turns the flow equation (3.1) into the Wheeler-

¹³We choose the same sign as in [28, 71] for the $T\bar{T}$ deformation and counter term, which corresponds to the opposite sign leading to the Nambu-Goto string action [72]. This choice of sign gives the correct conformal anomaly equation in the Euclidean signature as in (3.53).

DeWitt equation [28].

We now demonstrate that equation (3.24) is precisely equivalent to deforming the 2D CFT partition function using the 3D gravitational path integral, expressed as follows¹⁴:

$$\begin{aligned} \Psi(\gamma/\mu) = \int \mathcal{D}h_{ij}^\epsilon \int_{g_{ij}(\mu)=\frac{\gamma_{ij}}{\mu}}^{g_{ij}(\epsilon)=\frac{h_{ij}^\epsilon}{\epsilon}} \mathcal{D}g_{ij} \mathcal{D}\Pi^{ij} \exp \left[\int_\mu^\epsilon d\lambda \int d^2x \left(-i\Pi^{ij} \partial_\lambda g_{ij} - \frac{1}{2\lambda} \left(\frac{16\pi G_N}{\sqrt{g}} (\Pi^{ij} \Pi_{ij} - \Pi^2) \right. \right. \right. \\ \left. \left. \left. - \frac{\sqrt{g}}{16\pi G_N} (R(g_{ij}) + 2) \right) \right) \right] e^{\frac{1}{8\pi G_N \epsilon} \int d^2x \sqrt{h^\epsilon} \mathcal{Z}^\epsilon[h_{ij}^\epsilon]} . \end{aligned} \quad (3.25)$$

Here, the kernel is the 3D bulk gravitational path integral in the gauge of the following form¹⁵:

$$ds^2 = \frac{d\lambda^2}{4\lambda^2} + g_{ij} dx^i dx^j = \frac{d\lambda^2}{4\lambda^2} + \frac{h_{ij}}{\lambda} dx^i dx^j . \quad (3.26)$$

where the indices are raised and lowered using the bulk metric g . We have gauge-fixed the lapse function to $N = \frac{1}{2\lambda}$ and the shift vector to $N^i = 0$. A more general lapse function would correspond to a non-uniform RG deformation, $\lambda(x)$; while introducing a non-zero shift vector would represent performing a diffeomorphism on each step of the RG procedure for each 2D radial slice. For simplicity, we will not delve into these generalizations, but they can be incorporated using methods outlined in [38, 66].

If we identify

$$\lambda = \frac{2\pi G_N}{r^2} , \quad (3.27)$$

the metric takes the conventional Fefferman-Graham form [28]:

$$ds^2 = \frac{dr^2}{r^2} + \frac{h_{ij}}{2\pi G_N r^2} dx^i dx^j , \quad (3.28)$$

with r being the radial direction in the asymptotically AdS spacetime. The combination:

$$e^{\frac{1}{8\pi G_N \epsilon} \int d^2x \sqrt{h^\epsilon} \mathcal{Z}^\epsilon[h_{ij}^\epsilon]} \quad (3.29)$$

is the total divergent “bare partition function”, related to the finite CFT partition function $\mathcal{Z}_{\text{CFT}}[h_{ij}^\epsilon]$, which is defined with a regulator at the small scale ϵ [66]. The partition function $\mathcal{Z}^\epsilon[h_{ij}^\epsilon]$ includes a logarithmic divergence associated with the conformal anomaly. We deliberately separate out the boundary cosmological constant counterterm $e^{\frac{1}{8\pi G_N \epsilon} \int d^2x \sqrt{h^\epsilon}}$ in holographic renormalization [74]. This separation establishes connections between the rescaling in (3.30), the shift reparametrization in (3.33), the cancellation of the bulk cosmological constant in (3.36), and the inclusion of a linear Weyl transformation generator term that compensates for the rescaling in (3.37). Together, these

¹⁴Subtleties related to the flat measure in the phase-space path integral of gravity are analyzed in detail in [66, 73].

¹⁵Strictly speaking, this foliation of metric only needs to cover the region between $\lambda = \epsilon$ and $\lambda = \mu$.

elements interact in a well-balanced and harmonious manner [28, 75].

We can now relate this to the 2D RG framework by introducing new variables through the following transformation:

$$\Pi^{ij} = \lambda \pi^{ij}, g_{ij} = \frac{h_{ij}}{\lambda}. \quad (3.30)$$

We also define

$$\frac{\pi_{ij}}{\lambda} = \Pi_{ij} = \Pi^{mn} g_{im} g_{jn} = \frac{\pi^{mn} h_{im} h_{jn}}{\lambda}. \quad (3.31)$$

Thus, we can use h to raise and lower the indices for π , preserving the inner products as those for Π . The relationship between Π/π and g/h encapsulates the rescaling process in the RG.

With this transformation, we rewrite equation (3.25) as

$$\begin{aligned} \Psi(\gamma/\mu) = & \int \mathcal{D}h_{ij}^\epsilon \int_{\substack{h_{ij}(\mu)=\gamma_{ij} \\ h_{ij}(\epsilon)=h_{ij}^\epsilon}} \mathcal{D}h_{ij} \mathcal{D}\pi^{ij} \exp \left[\int_\mu^\epsilon d\lambda \int d^2x \left(-i\lambda \pi^{ij} \partial_\lambda \left(\frac{h_{ij}}{\lambda} \right) \right. \right. \\ & \left. \left. - \frac{1}{2\lambda} \left(\frac{16\pi G_N \lambda}{\sqrt{h}} (\pi^{ij} \pi_{ij} - \pi^2) - \frac{\sqrt{h}}{16\pi G_N \lambda} (R(\frac{h_{ij}}{\lambda}) + 2) \right) \right) \right] e^{\frac{1}{8\pi G_N \epsilon} \int d^2x \sqrt{h^\epsilon} \mathcal{Z}^\epsilon[h_{ij}^\epsilon]}. \end{aligned} \quad (3.32)$$

Next, we perform the change of variables:

$$\pi^{ij} = \pi'^{ij} - \frac{i}{16\pi G_N \lambda} \sqrt{h} h^{ij}, \quad (3.33)$$

and for simplicity, we will continue to denote the new variable π'^{ij} as π^{ij} to facilitate comparison, as it serves as a dummy variable. This procedure does not alter the total path integral but instead reorganizes the terms within it. It renders (3.25) manifestly equivalent to (3.24).

First, we have the change in the first term of (3.25) as,

$$\delta \left(-i\lambda \pi^{ij} \partial_\lambda \left(\frac{h_{ij}}{\lambda} \right) \right) = -\frac{\sqrt{h}}{16\pi G_N} h^{ij} \partial_\lambda \left(\frac{h_{ij}}{\lambda} \right) = -\frac{1}{16\pi G_N} \left(\frac{\sqrt{h} h^{ij} \partial_\lambda h_{ij}}{\lambda} - \frac{2\sqrt{h}}{\lambda^2} \right) = -\frac{1}{8\pi G_N} \partial_\lambda \left(\frac{\sqrt{h}}{\lambda} \right), \quad (3.34)$$

This term is a total derivative with respect to λ , and thus the change of variables introduces two boundary terms:

$$\int_\mu^\epsilon d\lambda d^2x \delta \left(-i\lambda \pi^{ij} \partial_\lambda \left(\frac{h_{ij}}{\lambda} \right) \right) = \int d^2x \left(\frac{1}{8\pi G_N \mu} \sqrt{\gamma} - \frac{1}{8\pi G_N \epsilon} \sqrt{h^\epsilon} \right), \quad (3.35)$$

The second term precisely cancels the boundary cosmological counterterm at ϵ , while the first term corresponds to the boundary term at μ in (3.24).

Next, we consider:

$$\begin{aligned} \frac{16\pi G_N \lambda}{\sqrt{h}} \delta(\pi^{ij} \pi_{ij} - \pi^2) &= \frac{16\pi G_N \lambda}{\sqrt{h}} \left(\frac{i\sqrt{h}}{8\pi G_N \lambda} \pi_i^i + \frac{|h|}{(128\pi G_N \lambda)^2} \right) \\ &= 2i\pi_i^i + \frac{\sqrt{h}}{8\pi G_N \lambda} . \end{aligned} \quad (3.36)$$

The second term cancels precisely with the bulk cosmological constant term in (3.25). The first term, which is linear in momentum, represents the Weyl transformation generator. Notably, it can be combined with the term $-i\lambda\pi^{ij}\partial_\lambda\left(\frac{h_{ij}}{\lambda}\right)$ as follows:

$$\begin{aligned} &-i\lambda\pi^{ij}\partial_\lambda\left(\frac{h_{ij}}{\lambda}\right) - \frac{1}{2\lambda}(2i\pi_i^i) \\ &= -i\pi^{ij}\partial_\lambda h_{ij} + i\frac{\pi_i^i}{\lambda} - i\frac{\pi_i^i}{\lambda} = -i\pi^{ij}\partial_\lambda h_{ij} . \end{aligned} \quad (3.37)$$

Collecting all the pieces, we get:

$$\begin{aligned} \Psi(\gamma/\mu) &= e^{\frac{1}{8\pi G_N \mu} \int d^2x \sqrt{\gamma}} \int \mathcal{D}h_{ij}^\epsilon \int_{\substack{h_{ij}(\mu)=\gamma_{ij} \\ h_{ij}(\epsilon)=h_{ij}^\epsilon}} \mathcal{D}h_{ij} \mathcal{D}\pi^{ij} \exp \left[\int_\mu^\epsilon d\lambda \int d^2x (-i\pi^{ij}\partial_\lambda h_{ij} \right. \\ &\quad \left. - \frac{1}{2\lambda} \left(\frac{16\pi G_N \lambda}{\sqrt{h}} (\pi^{ij} \pi_{ij} - \pi^2) - \frac{\sqrt{h}}{16\pi G_N \lambda} R\left(\frac{h_{ij}}{\lambda}\right) \right) \right] \mathcal{Z}^\epsilon[h_{ij}^\epsilon] . \end{aligned} \quad (3.38)$$

Using the fact that for constant λ , we have:

$$R\left(\frac{h_{ij}}{\lambda}\right) = \lambda R(h_{ij}) . \quad (3.39)$$

Finally, employing the Brown-Henneaux central charge relation [76],

$$c = \frac{3}{2G_N} , \quad (3.40)$$

equation (3.38) matches exactly with (3.24). Thus, the $T\bar{T}$ deformation is obtained from the 3D gravitational path integral with minimal effort. Similar ideas could potentially provide a simpler approach to derive analogous deformations in higher dimensions and other theories, as explored in [68, 71].

3.3 Wheeler-DeWitt equation from $T\bar{T}$ deformation

Since the deformation arises from the gluing of the 3D gravity path integral to a 2D CFT partition function, it is plausible that the partition function of the deformed theory satisfies the Wheeler-DeWitt equation. By expressing this in operator formalism, we will explicitly uncover the precise

meaning of this condition and an underlying quantum state behind 2D CFTs in this section.

We begin by rewriting (3.25) in terms of the unscaled variables:

$$\begin{aligned} \Psi(\gamma/\mu) &= \int \mathcal{D}h_{ij}^\epsilon \int_{\substack{g_{ij}(\mu)=\frac{\gamma_{ij}}{\mu} \\ g_{ij}(\epsilon)=\frac{h_{ij}^\epsilon}{\epsilon}}} \mathcal{D}g_{ij} \mathcal{D}\Pi^{ij} \exp \left[\int_\epsilon^\mu d\lambda \int d^2x \left(i\Pi^{ij} \partial_\lambda g_{ij} \right. \right. \\ &\left. \left. + \frac{1}{2\lambda} \left(\frac{16\pi G_N}{\sqrt{g}} (\Pi^{ij} \Pi_{ij} - \Pi^2) - \frac{\sqrt{g}}{16\pi G_N} (R(g_{ij}) + 2) \right) \right) \right] e^{\frac{1}{8\pi G_N \epsilon} \int d^2x \sqrt{h^\epsilon} \mathcal{Z}^\epsilon[h_{ij}^\epsilon]} , \end{aligned} \quad (3.41)$$

with the integration limit switched to characterise evolution *into* the bulk. Then we introduce a collection of states $\langle g_{ij} = \frac{\gamma_{ij}}{\lambda}, \lambda |$, in analogous to the “position basis” in quantum mechanics, to be metric eigenstates in the Heisenberg picture, which plays the role of ${}_\Lambda \langle \Omega^\lambda(\gamma_{ij}) |$ discussed in the earlier section. Then the Schrödinger picture metric eigenstates are defined at reference “time” $\lambda = \epsilon$ satisfying [56]:

$$\hat{g}_{ij} |g_{ij}\rangle_{dx^i} = g_{ij} |g_{ij}\rangle_{dx^i} , \quad (3.42)$$

where dx^i represents the chosen coordinate system used to describe the metric and serves the same role as Λ in Sec. 2.3 and Sec. 4. For simplicity, we will omit this subscript dx^i in the following discussion.

Next, we define a state $|Z_{\text{CFT}}\rangle$ via:

$$\langle g_{ij}, \lambda | Z_{\text{CFT}} \rangle = e^{\frac{1}{8\pi G_N} \int d^2x \sqrt{g} \mathcal{Z}^\lambda[\lambda g_{ij}]} . \quad (3.43)$$

Expanding out the path integral (3.41) as evolution of $|Z_{\text{CFT}}\rangle$ in the basis $\langle g_{ij} = \frac{h_{ij}}{\lambda}, \lambda |$, we obtain

$$\begin{aligned} \Psi(\gamma/\mu) &\equiv \langle g_{ij} = \frac{\gamma_{ij}}{\mu}, \mu | Z_{\text{CFT}} \rangle \\ &= \int \mathcal{D}h_{ij}^\epsilon \langle g_{ij} = \frac{\gamma_{ij}}{\mu}, \mu | g_{ij} = \frac{h_{ij}^\epsilon}{\epsilon}, \epsilon \rangle \langle g_{ij} = \frac{h_{ij}^\epsilon}{\epsilon}, \epsilon | Z_{\text{CFT}} \rangle , \end{aligned} \quad (3.44)$$

where we insert the “momentum basis” $|\Pi^{ij}\rangle$ between each small “radial” interval, satisfying

$$\langle g_{ij} | \Pi^{ij} \rangle = e^{i\Pi^{ij} g_{ij}} , \quad (3.45)$$

and integrate out the Π^{ij} fields, as we did above.

Introducing the Hamiltonian density

$$\hat{\mathcal{H}} = -\frac{16\pi G_N}{\sqrt{\hat{g}}} (\hat{\Pi}^{ij} \hat{\Pi}_{ij} - \hat{\Pi}^2) + \frac{\sqrt{\hat{g}}}{16\pi G_N} (R(\hat{g}_{ij}) + 2) , \quad (3.46)$$

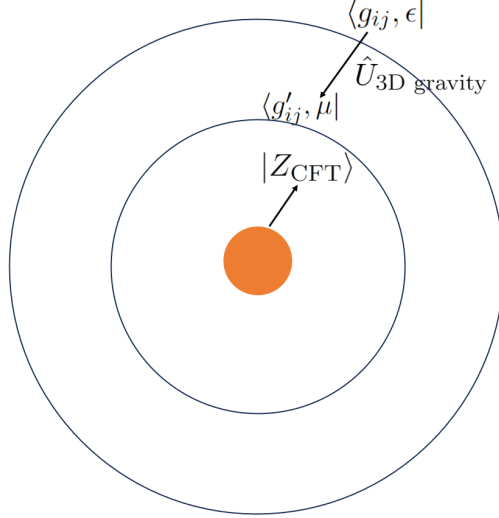


Figure 7: The Wheeler DeWitt wavefunction is an overlap between an underlying 3D quantum state $|Z_{\text{CFT}}\rangle$ and another metric eigenstate $\langle g_{ij}, \lambda |$ in the Heisenberg picture. The metric eigenstates at different radial time are related by the kernel $\hat{U}_{\text{3D gravity}}$.

then (3.44) can be written as

$$\begin{aligned} \Psi(\gamma/\mu) &= \int \mathcal{D}h_{ij}^\epsilon \langle g_{ij} = \frac{\gamma_{ij}}{\mu}, \epsilon | e^{-\int_\epsilon^\mu \frac{d\lambda}{2\lambda} \int d^2x \hat{\mathcal{H}}} |g_{ij} = \frac{h_{ij}^\epsilon}{\epsilon}, \epsilon\rangle \langle g_{ij} = \frac{h_{ij}^\epsilon}{\epsilon}, \epsilon | Z_{\text{CFT}}\rangle \\ &= \langle g_{ij} = \frac{\gamma_{ij}}{\mu}, \epsilon | \hat{U}_{\text{3D gravity}} | Z_{\text{CFT}}\rangle, \end{aligned} \quad (3.47)$$

where $\hat{U}_{\text{3D gravity}}$ represents the radial evolution operator in 3D gravity, and this equation resembles (2.12). Moreover, we see $|Z_{\text{CFT}}\rangle$ is exactly the $|\Psi\rangle_\Lambda$ state underlying 2D CFTs. See Fig. 7 for an illustration.

Acting on wavefunctions in the metric basis for general states $|\varphi\rangle$, $\hat{\mathcal{H}}$ becomes a differential operator:

$$\begin{aligned} &\langle g_{ij} = \frac{h_{ij}}{\lambda} | \hat{\mathcal{H}} | \varphi \rangle \\ &= \left[\frac{16\pi G_N \lambda}{\sqrt{\hbar}} \left(\frac{1}{2} (h_{ik} h_{jl} + h_{il} h_{jk}) - h_{ij} h_{kl} \right) \frac{\delta}{\delta h_{ij}} \frac{\delta}{\delta h_{kl}} + \frac{\sqrt{\hbar}}{16\pi G_N \lambda} (R(\frac{h_{ij}}{\lambda}) + 2) \right] \langle g_{ij} = \frac{h_{ij}}{\lambda} | \varphi \rangle \\ &= \mathcal{H}(\lambda, h_{ij}, \frac{\delta}{\delta h_{ij}}) \langle g_{ij} = \frac{h_{ij}}{\lambda} | \varphi \rangle, \end{aligned} \quad (3.48)$$

where we scaled the metric by the lapse.

Thus, we have the Wheeler-DeWitt equation,

$$\begin{aligned}
\mathcal{H}(\mu, \gamma_{ij}, \frac{\delta}{\delta\gamma_{ij}})\Psi(\gamma/\mu) &= \mathcal{H}(\mu, \gamma_{ij}, \frac{\delta}{\delta\gamma_{ij}}) \langle g_{ij} = \frac{\gamma_{ij}}{\mu}, \epsilon | \hat{U}_{\text{3D gravity}} | Z_{\text{CFT}} \rangle \\
&= \langle g_{ij} = \frac{\gamma_{ij}}{\mu}, \epsilon | \hat{\mathcal{H}} \hat{U}_{\text{3D gravity}} | Z_{\text{CFT}} \rangle \\
&= \langle g_{ij} = \frac{\gamma_{ij}}{\mu}, \epsilon | \hat{U}_{\text{3D gravity}} \hat{\mathcal{H}} | Z_{\text{CFT}} \rangle .
\end{aligned} \tag{3.49}$$

In the second equation, we apply the Baker-Campbell-Hausdorff formula and use the fact that the terms arising from the commutator of the Hamiltonian constraints vanish due to the momentum constraint (2D diffeomorphism) [38, 68].

Now we show that this is equal to zero, which comes from:

$$\hat{\mathcal{H}} | Z_{\text{CFT}} \rangle = 0 . \tag{3.50}$$

Explicitly, in metric basis, we have:

$$\begin{aligned}
&\langle g_{ij} = \frac{\gamma_{ij}}{\mu}, \epsilon | \hat{U}_{\text{3D gravity}} \hat{\mathcal{H}} | Z_{\text{CFT}} \rangle \\
&= \int \mathcal{D}h_{ij}^\epsilon \langle g_{ij} = \frac{\gamma_{ij}}{\mu}, \epsilon | \hat{U}_{\text{3D gravity}} | g_{ij} = \frac{h_{ij}^\epsilon}{\epsilon}, \epsilon \rangle \langle g_{ij} = \frac{h_{ij}^\epsilon}{\epsilon}, \epsilon | \hat{\mathcal{H}} | Z_{\text{CFT}} \rangle .
\end{aligned} \tag{3.51}$$

Now we can evaluate¹⁶:

$$\begin{aligned}
\langle g_{ij} = \frac{h_{ij}^\epsilon}{\epsilon}, \epsilon | \hat{\mathcal{H}} | Z_{\text{CFT}} \rangle &= \mathcal{H}(\epsilon, h_{ij}^\epsilon, \frac{\delta}{\delta h_{ij}^\epsilon}) \langle g_{ij} = \frac{h_{ij}^\epsilon}{\epsilon}, \epsilon | Z_{\text{CFT}} \rangle \\
&= \left[\frac{16\pi G_N \epsilon}{\sqrt{h^\epsilon}} \left(\frac{1}{2} (h_{ik}^\epsilon h_{jl}^\epsilon + h_{il}^\epsilon h_{jk}^\epsilon) - h_{ij}^\epsilon h_{kl}^\epsilon \right) \frac{\delta}{\delta h_{ij}^\epsilon} \frac{\delta}{\delta h_{kl}^\epsilon} + \frac{\sqrt{h^\epsilon}}{16\pi G_N \epsilon} \left(R(\frac{h_{ij}^\epsilon}{\epsilon}) + 2 \right) \right] \left(e^{\frac{1}{8\pi G_N \epsilon} \int d^2x \sqrt{h^\epsilon} \mathcal{Z}^\epsilon[h_{ij}^\epsilon]} \right) \\
&= e^{\frac{1}{8\pi G_N \epsilon} \int d^2x \sqrt{h^\epsilon}} \left[\frac{16\pi G_N \epsilon}{\sqrt{h^\epsilon}} \left(\frac{1}{2} (h_{ik}^\epsilon h_{jl}^\epsilon + h_{il}^\epsilon h_{jk}^\epsilon) - h_{ij}^\epsilon h_{kl}^\epsilon \right) \frac{\delta}{\delta h_{ij}^\epsilon} \frac{\delta}{\delta h_{kl}^\epsilon} - 2h_{ij}^\epsilon \frac{\delta}{\delta h_{ij}^\epsilon} + \frac{\sqrt{h^\epsilon}}{16\pi G_N \epsilon} R(\frac{h_{ij}^\epsilon}{\epsilon}) \right] \mathcal{Z}^\epsilon[h_{ij}^\epsilon] ,
\end{aligned} \tag{3.52}$$

Similarly to (3.38), when the Hamiltonian is passed through the boundary cosmological constant counter term, the bulk cosmological constant term is cancelled, and the linear term absent in the Hamiltonian is generated. The first term of (3.52) approaches zero as $\epsilon \rightarrow 0$, reflecting the irrelevance of $T\bar{T}$ deformation under RG flow. Together, they lead to the 2D conformal anomaly equation:

$$\left(-2h_{ij}^\epsilon \frac{\delta}{\delta h_{ij}^\epsilon} + \frac{\sqrt{h^\epsilon}}{16\pi G_N \epsilon} R(\frac{h_{ij}^\epsilon}{\epsilon}) \right) \mathcal{Z}^\epsilon[h_{ij}^\epsilon] = \left(-2h_{ij}^\epsilon \frac{\delta}{\delta h_{ij}^\epsilon} + \frac{\sqrt{h^\epsilon}}{16\pi G_N} R(h_{ij}^\epsilon) \right) \mathcal{Z}^\epsilon[h_{ij}^\epsilon] = 0 . \tag{3.53}$$

¹⁶Some formally infinite constants are dropped, and we can think of this as a normal-ordering prescription common in $T\bar{T}$ literature.

The remarkable connection between the Wheeler-DeWitt equation and the conformal anomaly equation was first highlighted by Freidel in [34], based on earlier observations made by Verlinde in [33]. In the context of the $T\bar{T}$ deformation [28], the deformed partition function, which satisfies the Wheeler-DeWitt equation, is proposed to be the quantum gravity wavefunction at a finite cutoff surface $r_c = \sqrt{2\pi G_N/\mu}$.

The state $\langle g_{ij} = \frac{\gamma_{ij}}{\mu}, \mu |$ corresponds to the standard Dirichlet boundary conditions imposed on finite-cutoff surfaces in the AdS/CFT correspondence. These conditions can equivalently be described as mixed boundary conditions at asymptotic infinity, linked to double-trace deformations [59, 60, 77]. Given that $T\bar{T}$ -deformed theories have been demonstrated to preserve the Virasoro algebra in a highly nontrivial manner [60], it implies that these boundary conditions also lead to the same Virasoro symmetry.

Notably, the reformulation of these results in the operator formalism demonstrates that the Wheeler-DeWitt equation is an operator equation, independent of the basis chosen. Exploring Wheeler-DeWitt states in alternative bases would be a very interesting direction for future research.

Finally, as shown in [68], using techniques similar to (3.49), we can demonstrate that the deformed partition function $\mathcal{Z}^\mu(\gamma_{ij})$ in (3.23), which does not include the boundary cosmological counterterm present in the Wheeler-DeWitt wavefunction (3.24), satisfies the Callan-Symanzik equation,

$$\left(\int d^2x \pi_i^i - i\mu \frac{\partial}{\partial \mu} \right) \mathcal{Z}^\mu(\gamma_{ij}) = 0 . \quad (3.54)$$

This implies that the $T\bar{T}$ deformed theories lie on a single RG trajectory.

In fact, it also means that the overlap in (3.43) and the Wheeler-DeWitt wavefunction is “time-independent”, as

$$\langle g_{ij}, \lambda | Z_{\text{CFT}} \rangle = e^{\frac{1}{8\pi G_N} \int d^2x \sqrt{g}} \mathcal{Z}^\lambda[\lambda g_{ij}] = e^{\frac{1}{8\pi G_N} \int d^2x \sqrt{g}} \mathcal{Z}^{\lambda'}[\lambda' g_{ij}] = \langle g_{ij}, \lambda' | Z_{\text{CFT}} \rangle \quad (3.55)$$

or

$$\hat{U}_{\text{3D gravity}} |Z_{\text{CFT}} \rangle = |Z_{\text{CFT}} \rangle , \quad (3.56)$$

being consistent with (3.50).

This example perfectly illustrates the SymQRG paradigm introduced in Sec. 2.3, rooted in the fact that the original CFT defines a 3D quantum state, satisfying (3.50). This no-flux condition indicates that this state corresponds to a ground state of a 3D TQFT. At first glance, the connection to topological symmetries may seem obscure. The quick answer lies in the following observation: the $T\bar{T}$ deformation is a deformation that preserves all the topological symmetries, as the topological defect lines \hat{X}_i commute with the stress tensor at any points on the 2D surface by definition,

$$[\hat{T}(z), \hat{X}_i] = [\hat{T}(\bar{z}), \hat{X}_i] = 0 \quad (3.57)$$

In the next section, we introduce a discrete framework for SymQRG, utilizing the exact tensor network state sum representation of 2D CFTs, which will make the connection to topological symmetries more explicit. We will return to the question of when this bulk SymTFT describes 3D gravity in Sec. 5.

4 SymQRG for exact tensor network state sum representation of 2D CFTs

In this section, we illustrate the SymQRG framework using the exact tensor network state sum representation of 2D CFTs developed in [1, 29–31] as a second example. We demonstrate how the $|\Psi\rangle_\Lambda$ state is constructed from the BCFT structure coefficients, while the ${}_\Lambda\langle\Omega|$ state arises from conformal blocks, discretizing the CFT. The interplay between these states, through the crossing symmetry of the CFT, enables SymQRG and facilitates the construction of an exact MERA-like tensor network [35] with an emergent RG direction in the bulk.

In Sec. 4.1, we begin with a brief review of the discrete Turaev-Viro TQFT [23], which is the SymTFT of the 2D CFTs, and then explain its connection to the Levin-Wen string-net model [24]. Following this, in Sec. 4.2, we revisit the tensor network state sum representation of 2D CFTs, and show how it is related to SymQRG. Finally, in Sec. 4.4, we summarize the pivotal role tensor networks play in describing both 2D field theories and their corresponding 3D bulk theories.

Additional details on the Turaev-Viro TQFT can be found in appendix A. For more information on the tensor network construction of 2D CFTs and the explicit procedure for SymQRG, see appendix B and appendix C. Readers interested in the exact tensor network construction of CFT wavefunctions from the Euclidean path integral can refer to appendix D.

4.1 Turaev-Viro TQFT, Levin-Wen string-net model and topological order

In the seminar work of Moore and Seiberg [42], it was found that for a rational CFT with a given chiral symmetry, its chiral modules form a modular tensor category \mathcal{C} . Each primary corresponds to an object in the category. The collection of topological symmetry operators is also determined by this modular tensor category, and also the associated SymTFT. This connection is precisely embodied in the higher-dimensional bulk appearing in the sandwich construction, as explained in Sec. 2.3. In fact, this SymTFT can be constructed explicitly within a discrete formalism using the Moore-Seiberg category \mathcal{C} , corresponding to the Turaev-Viro TQFT [23]. For readers unfamiliar with the discrete formulation of this TQFT, appendix A provides an introduction and explains its connection to the continuum Chern-Simons gauge theory [78, 79].

Briefly speaking, to define the Turaev-Viro TQFT on a 3D manifold, the process begins by triangulating the 3D manifold with tetrahedra, followed by coloring the edges with representations j . Then each tetrahedron is assigned a quantum $6j$ in the fusion category \mathcal{C} corresponding to the

six edges of the tetrahedron. Additionally, for every edge labelled j that lies in the interior of the 3D manifold and is shared by multiple tetrahedra, we include a factor of the quantum dimension d_j . The $6j$ symbol and quantum dimension d_j associated with a fusion category are reviewed in appendix A. Finally, we sum over the coloring of all edges. i.e. ¹⁷

$$Z(\mathcal{M}) = \sum_{\{j_e\}} \prod_{v \in \mathcal{M}} D^{-2} \prod_{e' \in \partial \mathcal{M}} \sqrt{d_{j_{e'}}} \prod_{e \notin \partial \mathcal{M}} d_{j_e} \prod_{\Delta_3} \Gamma_3(\{j_{e \in \Delta_3}\}), \quad (4.1)$$

where Γ_3 are $6j$ symbols as defined in (A.6).

The normalization convention in the literature attaches a factor of D^{-2} to every vertex. This normalization ensures $Z(S^2 \times S^1) = 1$.

The Turaev-Viro theories turn out to be equivalent to quantum systems known as the Levin-Wen string-net model [24]. More precisely, the latter is essentially a Hamiltonian formulation of the Turaev-Viro TQFT [80]. They describe quantum phases of matter known as topological orders in 2+1 D.

The Hamiltonian of each Levin-Wen model is constructed from the same fusion category \mathcal{C} . The Hilbert space of the model on a 2d spatial surface Σ is defined on a three-valent graph (i.e. each vertex is connected to 3 edges). The dual graph is actually simply a triangulation of the surface Σ . See Fig. 8 for an illustration. The Hilbert space is a tensor product of the vector space \mathcal{H}_e on each edge e , and \mathcal{H}_e is spanned by simple objects in the input fusion category \mathcal{C} as basis vectors.

The Hamiltonian is a generalization of lattice gauge theories (in the case of Z_2 , this is the famous toric code model of Kitaev [81]). It contains a sum over projectors on the vertices and plaquettes, which may appear to take a complicated form [24], but it has a very simple origin. First, at every 3-valent vertex of the graph, it imposes that the three objects meeting at the vertex must admit a fusion channel to the 0 object. This is essentially the ‘‘Gauss’s law’’ or ‘‘gauge invariance’’ in the Chern-Simons theory. There are also ‘‘plaquette projectors’’ defined for each plaquette on the graph. That is precisely equivalent to applying the operator ω defined in (A.16) to the state (or its generalization thereof for a general input fusion category \mathcal{C} not related to a group G). It projects the ground-state wavefunction to have vanishing flux across every closed loop on the surface Σ .

The ground states of the Levin-Wen model are the same as the physical states in the Turaev-Viro TQFT. Ground-state wavefunctions of the Levin-Wen model on a non-trivial 2d surface Σ can be obtained by the Turaev-Viro path integral over a 3d manifold \mathcal{M} such that Σ is on the boundary $\partial \mathcal{M}$, and that the surface triangulation matches with the choice chosen for the Levin-Wen model in question. This fact will play an important role in the next subsection.

Topological orders in 2+1 D are gapped phases of matter that exhibit long-range entanglement in their ground states. The low-energy excitations are characterized by anyonic excitations that can

¹⁷A square root is assigned to the quantum dimensions of the boundary edges.

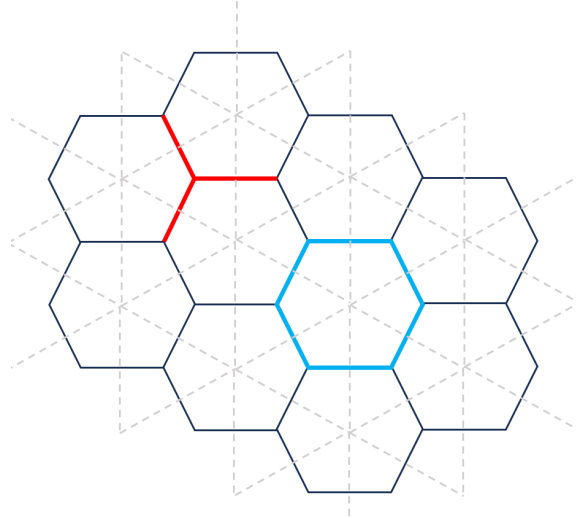


Figure 8: The Levin-Wen string-net model is defined on a 3-valent graph dual to a triangulation (depicted as the shaded grey lattice). The Hamiltonian of this model consists of a sum of projectors acting on the vertices and plaquettes of the graph. Vertex projectors illustrated in red enforce the “Gauss’s law”, while plaquette projectors depicted in blue impose the “no flux condition”. The ground state of this model corresponds to physical states of the Turaev-Viro TQFT.

carry nontrivial braiding statistics.

That the Turaev-Viro model/Levin-Wen model supplies the low energy effective description of topological order can be understood intuitively. First, as a gapped model in the low-energy limit, it is a fixed point under renormalization group flow with zero correlation length. Given the Pentagon relation and the relation (A.15), the wavefunction constructed from the Turaev-Viro path integral can be freely re-triangulated. It is thus a fixed-point wavefunction by construction [24, 82]. Secondly, it exhibits *long-range entanglement*, which can be understood as the lack of local order parameters, or any order parameter must be non-local. In the Turaev-Viro/Levin-Wen models, one can naturally construct line operators that commute with the Hamiltonian. They correspond precisely to Wilson lines in the language of Chern-Simons theory. One can also understand such long-range entanglement as a result of the Gauss’s law or gauge invariance constraint, and the vanishing flux constraint. Both conditions lead to global constraints on the wave function, which lies at the heart of long-range entanglement. One main result of this paper is that this long-range entanglement property is also the crux of the Wheeler-DeWitt equation in 3D gravity.

Anyon excitations correspond to open-Wilson lines, which exhibit non-trivial braiding relation. We note that even if the input category \mathcal{C} does not come with a braiding structure, the line operators that one can construct out of it acquire a braided structure. The collection of anyon line operators that can be constructed from the Turaev-Viro / Levin-Wen model forms a *braided fusion category* called the *Drinfeld center* $D(\mathcal{C})$ of \mathcal{C} . For the case where \mathcal{C} is a modular tensor category as is the case for rational CFTs, $D(\mathcal{C}) = \mathcal{C} \boxtimes \bar{\mathcal{C}}$, which essentially corresponds to chiral and antichiral halves of the

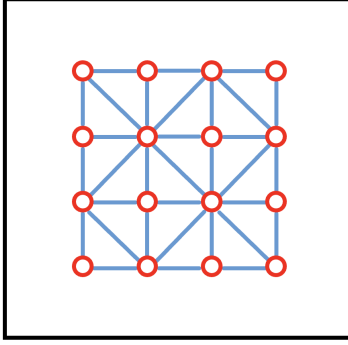


Figure 9: A tiling of 2D manifold using chipped triangles. We specify boundary conditions on the holes colored red.

CFT. These operators are also called “ribbon operators” due to framing anomaly [78]. The lattice constructions of these line operators in Dijkgraaf-Witten/Kitaev topological lattice gauge models are given in [81]. The construction in the more generalized Turaev-Viro/ Levin-Wen topological lattice models is given in [24] and later extended in [83] to include charge excitations.

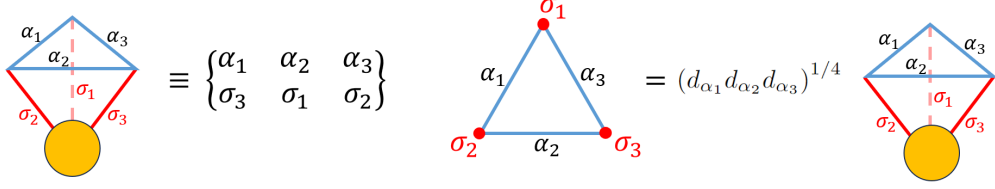
4.2 SymQRG for tensor network state sum representation of 2D CFT path integrals

The observation made in [1, 29–31], motivated by [13, 14, 84] and the foundational works of FRS [32], and also independently in [85], is that 2D CFTs admit a discrete tensor network state sum representation arising from a novel perspective on cutting and gluing their path integrals. The result can be explicitly written as an overlap (2.5) in the Hilbert space of the Levin-Wen string net models.

We cut open the 2D manifold into chipped triangles, as illustrated in Fig. 9. The tiny holes in the figure have radius R , and are introduced in [1, 29–31] for regularization purposes. They are taken to zero at the end of the computation to recover the original CFT. However, in this paper, we demonstrate that these holes serve a more significant role: by allowing R to vary, they introduce a continuous family of topological symmetry-preserving deformations away from the original CFT. These deformations are analogous to the $T\bar{T}$ deformations discussed in Sec. 3, and similarly arise from gluing 3D gravitational path integrals -represented here by quantum $6j$ symbols - onto the 2D theories.

We first fix some conformal boundary conditions σ_a on these tiny circles, and each chipped triangle is an open pair of pants, with states labeled by the primaries α_i and descendants I_i running on the edges. The CFT path integral on each chipped triangle gives,

$$\mathcal{T}_{(\alpha_1, I_1)(\alpha_2, I_2)(\alpha_3, I_3)}^{\sigma_1 \sigma_2 \sigma_3}(\Delta, R) = \tilde{C}_{\alpha_1 \alpha_2 \alpha_3}^{\sigma_3 \sigma_1 \sigma_2} \tilde{\gamma}_{I_1 I_2 I_3}^{\alpha_1 \alpha_2 \alpha_3}(R), \quad (4.2)$$



The tilde indicates a special choice of normalization that we explain in (B.3). We introduce the diagrammatic notation, where we denote $\tilde{\gamma}_{I_1 I_2 I_3}^{\alpha_1 \alpha_2 \alpha_3}(R)$ using black dashed lines, and $\tilde{C}_{\alpha_1 \alpha_2 \alpha_3}^{\sigma_3 \sigma_1 \sigma_2}$ using blue solid lines and red circles, as shown in Fig. 10.

For general (non-diagonal) CFTs, there is a remarkable formula first discovered by Runkel, relating the BCFT OPE coefficients to the (generalized) $6j$ symbols [32, 86] as,

$$\tilde{C}_{\alpha_1 \alpha_2 \alpha_3}^{\sigma_3 \sigma_1 \sigma_2} = (d_{\alpha_1} d_{\alpha_2} d_{\alpha_3})^{1/4} \left\{ \begin{array}{ccc} \alpha_1 & \alpha_2 & \alpha_3 \\ \sigma_3 & \sigma_1 & \sigma_2 \end{array} \right\}, \quad (4.3)$$

where d_{α_i} is the quantum dimension associated with α_i . In general, the label set for the primaries and boundary conditions are different, and the curly brackets denote the generalized $6j$ symbols with mixed indices. These generalized symbols can also be expressed in terms of the standard $6j$ symbols where all indices are in the same label set of primaries, multiplying some additional factors [32, 87]. The standard $6j$ symbols have the interpretation of a 3D path integral configuration associated to a tetrahedron, as we reviewed above and in appendix A, and the additional factors correspond to a topological boundary condition in the 3D Turaev-Viro TQFT [32, 87]. Therefore, we see some emergent 3D object from these BCFT OPE coefficients! We introduce the following diagrammatic representation.

After summing over all intermediate primaries and descendants, we get a partition function that depends on the fixed boundary conditions $\{\sigma_a\}$ ¹⁸

$$\mathcal{Z}(\{\sigma_a\}, R) = \sum_{\{\alpha_i\}} \sum_{\{I_i\}} \prod_{\Delta} \mathcal{T}_{(\alpha_i, I_i)(\alpha_j, I_j)(\alpha_k, I_k)}^{\sigma_a \sigma_b \sigma_c}(\Delta, R), \quad (4.4)$$

where a represents the set of all vertices, and i denotes the set of all edges. Contributions from all chipped triangles are multiplied together, with each triangle Δ defined by its corresponding vertices (a, b, c) and edges (i, j, k) , although their dependencies are omitted for simplicity of notation. Finally, we sum up all possible values α_i and I_i values assigned to each edge. Notice that the sum over descendants corresponds to the definition of conformal blocks.

As pointed out in [85], inserting more and more tiny holes with fixed boundary conditions corre-

¹⁸Here we are writing the insertion of complete basis of states with a sum. In a theory with a continuous family of primary operators such as the Liouville theory, this will be replaced by an integral [1, 31]. Subtleties related to convergence are also discussed in those papers.

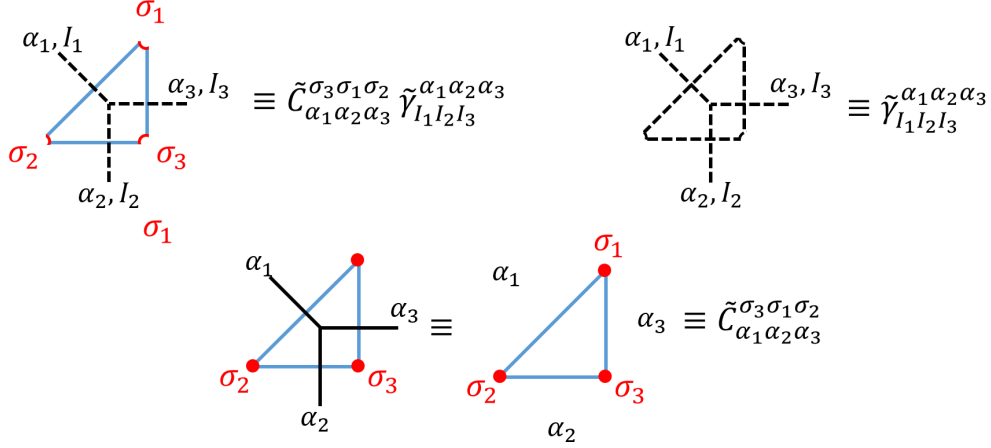


Figure 10: Diagrammatic notation for $\tilde{C}_{\alpha_1 \alpha_2 \alpha_3}^{\sigma_3 \sigma_1 \sigma_2}$ and $\tilde{\gamma}_{I_1 I_2 I_3}^{\alpha_1 \alpha_2 \alpha_3}(R)$.

sponds to operator insertions that deform the theory away from the original CFT, and, in general, turns on a relevant deformation that does not recover the CFT in the IR limit. The resolution proposed in [1, 29–31], building on earlier work [88], and also independently by [85], is to sum over boundary conditions. This approach also reveals a nice connection to topological symmetry and $T\bar{T}$ deformation.

It was proposed that we sum over the boundary conditions with a specific weight, proportional to the quantum dimension $\omega_{\sigma_a} \propto d_{\sigma_a}$ associated with the boundary conditions σ_a ¹⁹, for each vertex a :

$$\mathcal{Z}(R) = \sum_{\{\sigma_a\}} \prod_v \omega_{\sigma_a} \sum_{\{\alpha_i\}} \sum_{\{\{I_i\}\}} \prod_{\Delta} \mathcal{T}_{(\alpha_i, I_i)(\alpha_j, I_j)(\alpha_k, I_k)}^{\sigma_a \sigma_b \sigma_c}(\Delta, R). \quad (4.5)$$

This sum over boundary conditions was referred to “entanglement brane boundary condition” in [88], the “cloaking boundary condition” in [85], and “shrinkable boundary condition” in [1, 29–31], highlighting the different roles played by this sum. This summation exhibits two closely related magical effects. First, we can go to the dual closed channel where, instead of boundary conditions, we view the tiny holes as defining some “conformal boundary states” [89]. The weighted sum of the boundary states results in the “vacuum Ishibashi state” [1, 29–31, 85, 88],

$$|0\rangle\rangle = |0\rangle + \frac{2}{c} L_{-2} \bar{L}_{-2} |0\rangle + \dots \quad (4.6)$$

In the space of boundary states, this vacuum Ishibashi state is as close as we can get to the vacuum state, and the deformation away from the original CFT partition function is given by $\frac{2}{c} L_{-2} \bar{L}_{-2} |0\rangle$. From the state-operator correspondence, this corresponds to the $T\bar{T}$ operator [85]. In other words,

¹⁹The proportionality constant is chosen for normalization consideration

at leading order in small R , we have,

$$R^4 \frac{2}{c} \sum_v \langle T\bar{T}(v) \rangle + \dots \quad (4.7)$$

As we introduce increasingly tiny holes into our system, the underlying CFT will be deformed. However, because the $T\bar{T}$ operator is irrelevant, the theory flows back to the original CFT in the infrared. This irrelevance of $T\bar{T}$ is crucial, as it guarantees that we can achieve an exact fixed point in a controlled and analytic manner. Notably, $T\bar{T}$ commutes with all topological defect lines. In fact, this holds beyond the small R limit, *all* topological defects in the CFT can freely traverse the holes equipped with the “cloaking boundary condition”, behaving as if the holes transparent. This property can be explicitly demonstrated [1, 85]:

$$\left. \begin{array}{c} a \\ | \\ \bigcirc R \\ | \\ \bigcirc R \\ | \\ a \end{array} \right\} = \left. \begin{array}{c} a \\ | \\ \bigcirc R \\ | \\ \bigcirc R \\ | \\ a \end{array} \right\} , \quad (4.8)$$

in the path integral, where the circle R labels the hole, and a labels any topological defect line in the theory. The connection between criticality and topological symmetry was suggested in [13, 14, 84].

Next, the introduction of the weighted sum also brings the SymTFT—specifically, the Turaev-Viro TQFT we reviewed above—into the discussion. To make this connection explicit, we first introduce a Hilbert space defined on the edges, which is the Hilbert space of the Levin-Wen string-net models [24]²⁰, as illustrated in Fig. 11. The Hilbert space is given by $\mathcal{H}_\Lambda = \text{Span}\{ |\{\alpha_i\}\rangle_\Lambda \equiv |\alpha_1, \alpha_2, \dots, \alpha_{|e|}\rangle_\Lambda \}$, where the primary labels α_i are assigned to all the edges, and Λ denotes the lattice on which these basis states are defined. These basis states are orthonormal by definition.

Now we can rewrite the partition function (4.5) as an overlap of states in this Hilbert space,

$$\mathcal{Z}(R) = {}_\Lambda \langle \Omega^R | \Psi \rangle_\Lambda . \quad (4.9)$$

²⁰Recall that the lattice of the conventional Levin-Wen model is on the dual graph of triangulation. A proper definition of this Hilbert space also involves introducing degrees of freedom at the junctions to label the multiplicity of the vector space associated with the fusion of topological defects. For simplicity, in this paper, we always assume multiplicity one and suppress this degree of freedom. We thank Greg Moore and Sahand Seifnashri for discussions on this point

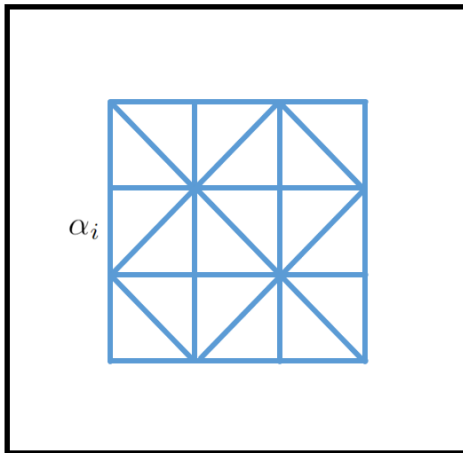


Figure 11: The 2D lattice on which we define our Hilbert space.

where

$$|\Psi\rangle_\Lambda = \sum_{\{\sigma_a\}} \prod_v \omega_{\sigma_a} \sum_{\{\alpha_i\}} \prod_\Delta \tilde{C}_{\alpha_i \alpha_j \alpha_k}^{\sigma_c \sigma_a \sigma_b} |\{\alpha_i\}\rangle_\Lambda, \quad (4.10)$$

and

$${}_\Lambda \langle \Omega^R | = \sum_{\{\alpha_i\}} {}_\Lambda \langle \{\alpha_i\} | \sum_{\{I_i\}} \prod_\Delta \tilde{\gamma}_{I_i I_j I_k}^{\alpha_i \alpha_j \alpha_k}(R). \quad (4.11)$$

The state ${}_\Lambda \langle \Omega^R |$ encodes all position-dependent contributions, with the wavefunctions being chiral conformal blocks, thus embodying the local Virasoro algebra V . The primary labels α_i correspond to the objects in the representation category \mathcal{C} of V , where $\mathcal{C} = \text{Rep}(V)$.

On the other hand, the state $|\Psi\rangle_\Lambda$ captures all BCFT OPE coefficients. Remarkably, this state is precisely a ground state of the Levin-Wen string-net model, or equivalently, the Turaev-Viro theory constructed from \mathcal{C} . Especially, it satisfies the no-flux constraint (2.6).

For an illustration, see Fig. 12, which depicts a ground state of the Turaev-Viro TQFT defined on the sphere. This state is obtained by performing the path integral from the topological boundary, shown in orange, to the outer boundary of a 3D ball. As constructed, both states defined on the discrete lattice are projected entangled pair state (PEPS) tensor network states²¹ defined on a two-dimensional lattice [91], as illustrated in Fig. 13. The dangling physical legs, shown in red, correspond to the primary labels α_i . The hidden layer of the auxiliary legs represents the internal degrees of freedom, and they take values in the set of boundary conditions σ_a for $|\Psi\rangle_\Lambda$ and in the set of integer-valued descendant labels I_i for ${}_\Lambda \langle \Omega^R |$. For ${}_\Lambda \langle \Omega^R |$, the presence of infinitely many descendants results in a bond dimension that is *infinite*. This *infinite* bond dimension is what allows

²¹For readers unfamiliar with PEPS tensor networks, they can be understood as a two-dimensional generalization of the more familiar one-dimensional matrix product states (MPS) [90].

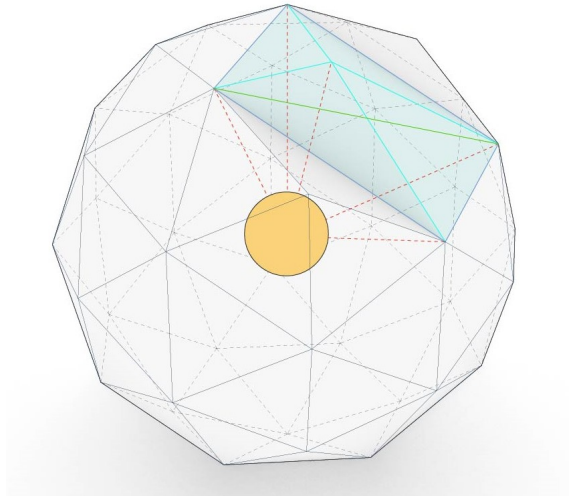


Figure 12: The ground state $|\Psi\rangle_\Lambda$ on a 2D sphere is obtained from a Turaev-Viro path integral in a 3D ball. The orange blob at the center of the ball represents the topological boundary, which will be explained in Sec. 6.2. Two different representations of this ground state, on the cyan edges and green edges, are connected by an additional layer of the tetrahedra, shaded in grey. This connection can be explicitly verified using the properties of the (generalized) $6j$ symbols, leading to (14). We glue this extra layer of tetrahedron to ${}_\Lambda\langle\Omega^R|$, performing the “block-spin” coarse-graining on the boundary while simultaneously moving into the bulk.

for an exact representation of the fixed-point tensor network of the *gapless* boundary condition associated with a *continuum field theory*.

To recover the CFT partition function, we simply take

$$\mathcal{Z}_{\text{CFT}} = \lim_{R \rightarrow 0} (\Pi_\nu e^{-\frac{\epsilon}{6} \ln(R)})_\Lambda \langle \Omega^R | \Psi \rangle_\Lambda . \quad (4.12)$$

The meaning of this factor will be explained after we discuss the SymQRG procedure that relates the family of theories labeled by different R 's. Note that while our construction has been illustrated using CFT partition functions as an example, it can be readily generalized to the computation of correlation functions with operator insertions, as outlined in [1] and Sec. 6.2. More results along this direction will be reported in the future.

The idea of rewriting a 2D field theory partition function as a “strange correlator”(2.5) in the topologically ordered string-net Hilbert space, to capture the topological symmetry of the theory, was inspired by the proposal in [13]. This approach was initially applied to certain 2D integrable lattice models, generalizing similar observations made for symmetry protected topological (SPT) phases in [92]. A key insight from [13] is that this formulation naturally provides an analytic real-space tensor network RG algorithm, taking advantage of the fact that $|\Psi\rangle_\Lambda$ is a ground state of the topological order [93, 94].

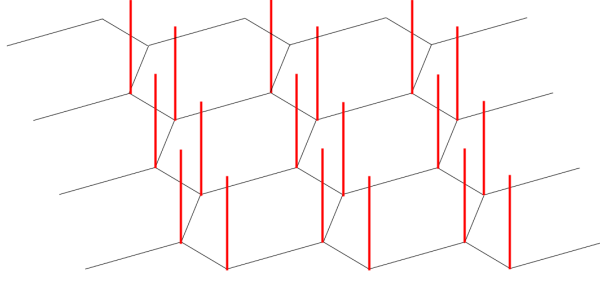


Figure 13: The projected entangled pair state (PEPS) tensor network states have dangling physical legs colored in red and contracted auxiliary legs colored in black. They are the two-dimensional analogues of the one-dimensional matrix product states.

We begin by outlining the general RG procedure for arbitrary ${}_{\Lambda}\langle\Omega|$ states and then demonstrate its application to the specific state ${}_{\Lambda}\langle\Omega^R|$ in (4.11) we constructed above. The procedure parallels the $T\bar{T}$ deformation, but is now enhanced with techniques from the lattice TQFT framework reviewed in appendix A.

The RG map is constructed from the equation summarized in Fig. 14 about Levin-Wen ground states $|\Psi\rangle_{\Lambda}$ that we show in detail in appendix C. In deriving this formula, we are essentially using the crossing symmetry of the CFT. Therefore, we get the transformation rule that relates a ground state at scale Λ and another larger scale $\Lambda' = \sqrt{2}\Lambda$,

$$|\Psi\rangle_{\Lambda} = \hat{U}_{\text{RG}}^{\Lambda,\Lambda'} |\Psi\rangle_{\Lambda'} . \quad (4.13)$$

Under this RG transformation, four BCFT structure coefficients are reduced to two, by gluing an additional layer of tetrahedra, corresponding to the Turaev-Viro TQFT path integral, as illustrated in Fig. 12. The Levin-Wen ground states serve as exact fixed points of this block-spin RG map [82]. This can be easily understood, since the two states in Fig. 12 both correspond to a Turaev-Viro path integral, producing a ground state.

As outlined in Sec. 2.3, this procedure can also be used to define the coarse-graining map for ${}_{\Lambda}\langle\Omega^R|$, as follows:

$${}_{\Lambda'}\langle\Omega'^R| = {}_{\Lambda}\langle\Omega^R|\hat{U}_{\text{RG}}^{\Lambda,\Lambda'} . \quad (4.14)$$

This ensures that the overlap remains invariant across different scales. Now contracted with the ${}_{\Lambda}\langle\Omega^R|$ state, the extra layers of tetrahedra progressively move into the bulk with each RG step, realizing the UV/IR correspondence in the AdS/CFT correspondence [17].

We emphasize that the RG operator is constructed from the $6j$ symbols carrying only indices α_i in \mathcal{C} (which specifies the SymTFT), and not the theory-specific boundary conditions σ_a (which corresponds to a specific choice of topological boundary condition). Therefore, it is universal for all $|\Psi\rangle_{\Lambda}$ states that share the same SymTFT and topological symmetries. The ribbon operators in the

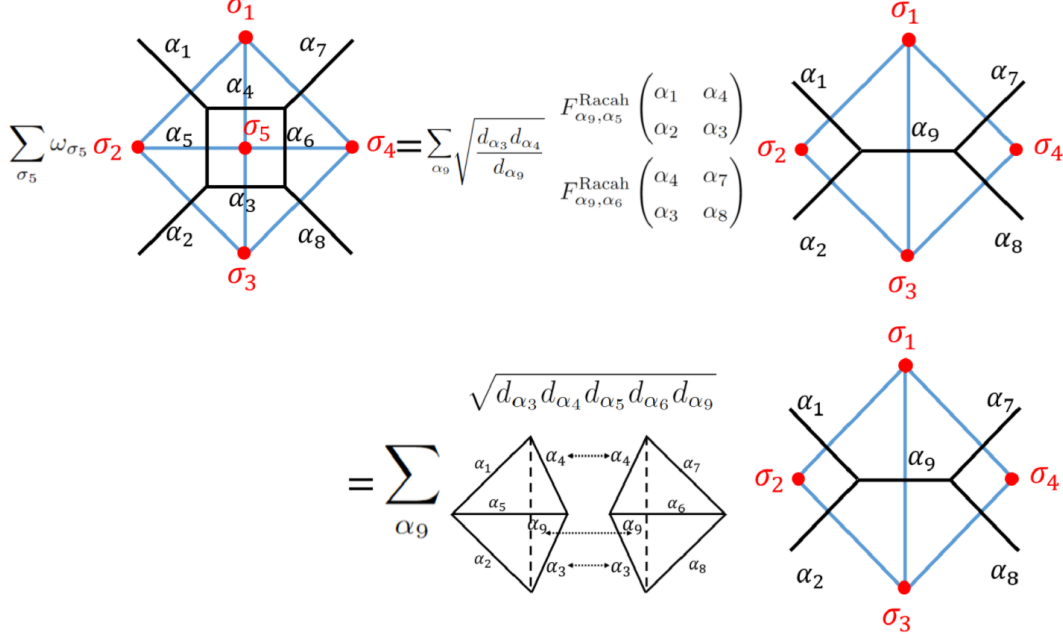


Figure 14: Coarse-graining equation of the Levin-Wen ground state $|\Psi\rangle_\Lambda$.

SymTFT is naturally inherited as the topological operators of the CFT.

By repeatedly applying this coarse-graining procedure, we obtain a multilayer quantum circuit that carries a structure resembling the MERA tensor network [35], as illustrated in Fig. 15. (For clarity and simplicity, we flatten the boundary and suppress one spatial dimension in the drawing.) This tensor network effectively probes the same theory at different scales Λ , with the bulk generated being the SymTFT. In essence, we are employing “BCFT Legos” to simultaneously construct the CFT path integral and the bulk quantum spacetime through the tensor network [31]! This is conceptually aligned with the “BC-bit” proposal suggested in [95], with two differences: First, we provide a method to glue different BCFT components together in the end, removing the tiny holes in the boundary CFT and bulk AdS, thereby recovering the entire boundary and bulk path integral; second, the correspondence is exact, encompassing a sum over quantum geometries, rather than being restricted to a single semi-classical saddle geometry.

At the current stage, this entire procedure establishes a form of a “pregeometry”, as no geometric notions of the 3D spacetime have emerged [96]. The precise connection to 3D gravity and the emergence of metric structures will be the focus of the next section.

Incorporating the rescaling step, the entire procedure can be illustrated using Fig. 1, or the fine-grained version in Fig. 16²², which closely resembles the $T\bar{T}$ deformation discussed in earlier

²²These 2D diagrams in fact correspond precisely to tensor networks related to 2D JT gravity and will be presented in [97].

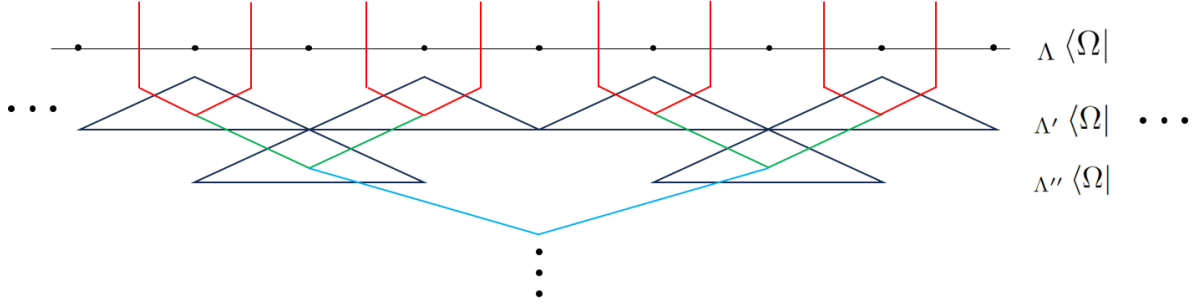


Figure 15: Applying the coarse-graining procedure multiple times, we get the familiar multi-layer quantum circuit, widely used in tensor network renormalization literature.

sections. The logical map behind the tensor network SymQRG is summarized in Fig. 2.

As demonstrated in [1, 29–31], the state ${}_{\Lambda} \langle \Omega^R |$, constructed using conformal blocks, is a fixed point of this RG procedure in the limit $R \rightarrow 0$. Now, let us explore its behavior for the more general case of $R > 0$. The general coarse-graining procedure for an arbitrary seed state ${}_{\Lambda} \langle \Omega |$ involving singular value decomposition is review in appendix C.

For the family of theories proposed in (4.9), we can achieve some analytical insights, particularly near the fixed point, by using the properties of conformal blocks. Considering the ${}_{\Lambda} \langle \Omega |$ state constructed from conformal blocks $\tilde{\gamma}$, locally, the coarse-grained wavefunction is given by:

$$\begin{aligned} \Omega'^{\Lambda'}(\alpha_{i=1,2,7,8,9}) = & \sum_{\alpha_{i=3,4,5,6}} \sqrt{\frac{d_{\alpha_3} d_{\alpha_4}}{d_{\alpha_9}}} F_{\alpha_9, \alpha_5}^{\text{Racah}} \begin{pmatrix} \alpha_1 & \alpha_4 \\ \alpha_2 & \alpha_3 \end{pmatrix} F_{\alpha_9, \alpha_6}^{\text{Racah}} \begin{pmatrix} \alpha_4 & \alpha_7 \\ \alpha_3 & \alpha_8 \end{pmatrix} \\ & \sum_{I_3, I_4, I_5, I_6} \tilde{\gamma}_{I_1 I_5 I_4}^{\alpha_1 \alpha_5 \alpha_4} \tilde{\gamma}_{I_2 I_3 I_5}^{\alpha_2 \alpha_3 \alpha_5} \tilde{\gamma}_{I_8 I_6 I_3}^{\alpha_8 \alpha_6 \alpha_3} \tilde{\gamma}_{I_7 I_4 I_6}^{\alpha_7 \alpha_4 \alpha_6} . \end{aligned} \quad (4.15)$$

Diagrammatically we have,

$$\sum_{\alpha_{i=3,4,5,6}} \sum_{I_3, I_4, I_5, I_6} \sqrt{\frac{d_{\alpha_3} d_{\alpha_4}}{d_{\alpha_9}}} F_{\alpha_9, \alpha_5}^{\text{Racah}} \begin{pmatrix} \alpha_1 & \alpha_4 \\ \alpha_2 & \alpha_3 \end{pmatrix} F_{\alpha_9, \alpha_6}^{\text{Racah}} \begin{pmatrix} \alpha_4 & \alpha_7 \\ \alpha_3 & \alpha_8 \end{pmatrix} \quad (4.16)$$

Using the properties of the conformal blocks and crossing kernels shown in appendix C, we turn it into

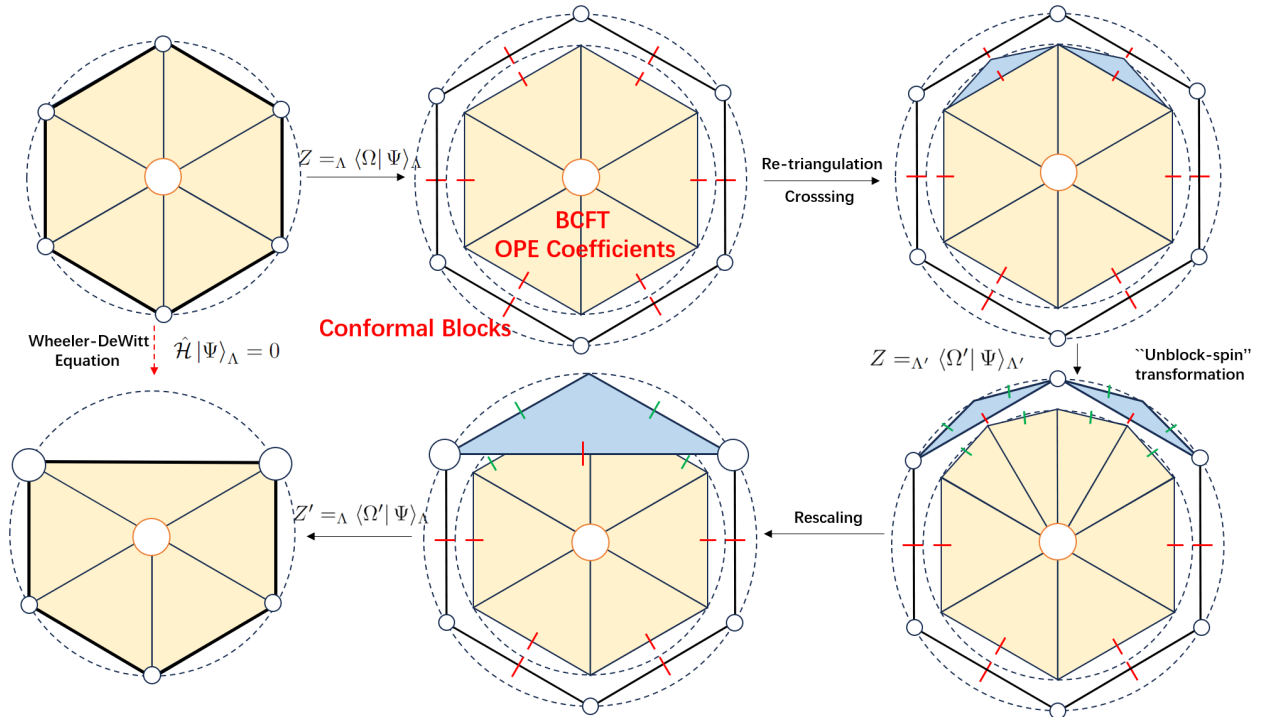


Figure 16: An illustration of the SymQRG fine-graining procedure for the tensor network state sum representation of field theories. In the second step above, we use the topological invariance (crossing symmetry in CFT) and the orthogonality condition to express the bulk path integral as the larger region evolving backwards into the bulk. Similar to the coarse-grained example in Fig. 1, the bottom right diagram gives the fine-grained version of same partition function. The bottom left gives the deformed partition function after rescaling, corresponding to the previous $T\bar{T}$ deformed partition function in Sec. 3.

$$\sum_{I'_3, I'_4, I_9, I'_9}$$

(4.17)

In the limit where $R \rightarrow 0$, the contribution of the tiny bubble factorizes from the remaining degrees of freedom, and we have “disentangled” these degrees of freedom. The bubble provides the universal Casimir energy contribution of $e^{\frac{c}{6} \ln(R)}$, and for the rest we obtain precisely the contribution from two larger triangles:

$$e^{\frac{c}{6} \ln(R)} \sum_{I_9}$$

This shows that the hole is shrinkable, and the state we constructed becomes a fixed point in the limit $R \rightarrow 0$.

When we rescale back to the original lattice size, we obtain a triangulation with smaller holes. On the other hand, reversing the entire procedure results in a triangulation with larger holes, (4.7) indicates that this performed the $T\bar{T}$ deformation to the original theory. These are illustrated in Fig. 17.

4.3 Wheeler-DeWitt equation and Callan-Symanzik equation from tensor networks

The tensor network enables a discrete realization of the Wheeler-DeWitt equation. When the deviation of the boundary state $\langle \Omega |$ from the CFT fixed point corresponds to $T\bar{T}$ deformation, we expect it should recover flows described by (3.52) and thus (3.1).

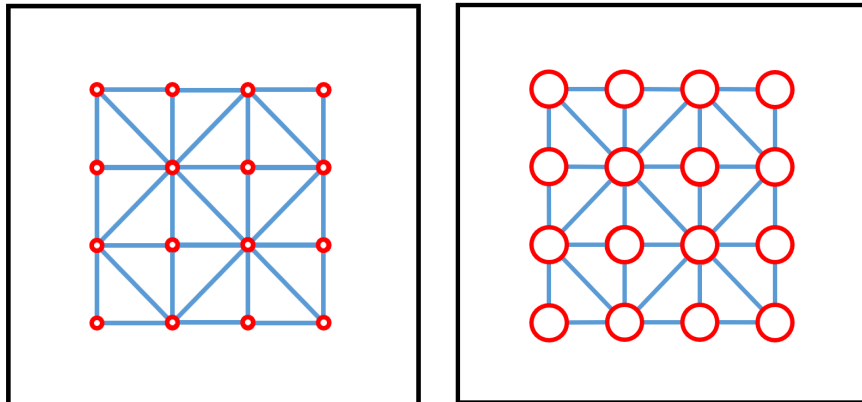


Figure 17: After the rescaling, the RG procedure near the conformal fixed point leads to the theory with smaller holes, and the inverse RG procedure leads to the theory with larger holes.

The line of logic has been outlined in section 2.3 and 3.3 for the continuous formulation, and we will make various ingredients explicit in the discrete formulation here too.

The key ingredient is that in the partition function expressed as in (4.9), the wave-function $|\Psi\rangle_\Lambda$ as shown in (4.10) is a ground state of the Levin-Wen model satisfying

$$\hat{\mathcal{H}}_\Lambda |\Psi\rangle_\Lambda = 0, \quad (4.18)$$

where $\hat{\mathcal{H}}_\Lambda$ is the Hamiltonian of the Levin-Wen model defined on the same lattice Λ [24], and it imposes the analogue of the no-flux condition as in the continuous Chern-Simons theory²³. Equation (4.18) is the explicit discrete version of (3.50), anticipated in (2.6) which is essentially the Wheeler-DeWitt equation.

This may look a bit formal and we will consider more explicit RG flows to show that it reproduces our familiar Callan-Symanzik equation. In particular to make comparison with the discussion in Sec. 3, we again consider a theory deformed perturbatively away from a CFT fixed point, this was shown to be by given by the $T\bar{T}$ deformation. As explained in (4.6) and (4.7), the small radius R of each hole is equivalent to introducing a finite coupling to $T\bar{T}$ in the hole, at least to the first leading contribution from the small R expansion. Comparing with (3.1), we have, to linear order in the $T\bar{T}$ perturbation coupling λ

$$\frac{2R^4}{c} \approx \frac{12\pi R^2 \lambda}{c} \implies \lambda \approx \frac{R^2}{6\pi}, \quad (4.19)$$

where we have approximated $\int d^2x \sqrt{\gamma} T\bar{T}$ by

$$\int d^2x \sqrt{\gamma} T\bar{T} \approx R^2 \sum_v T\bar{T}(v). \quad (4.20)$$

²³It is convenient for us to shift the ground state energy to 0, which can always be arranged

As expected, the hole size R is related to the $T\bar{T}$ coupling λ . The precise constant of proportionality is not important. We can thus use ${}_{\Lambda}\langle\Omega^R|\Psi\rangle_{\Lambda}$ interchangeably with ${}_{\Lambda}\langle\Omega^{\lambda}|\Psi\rangle_{\Lambda}$ at least for small R given the conversion (4.19). The scale Λ that appeared in (2.5) now takes a precise meaning of the lattice scale chosen in the surface triangulation of the path-integral. Since this triangulation scale is arbitrarily chosen in representing the continuum field theory, one can consider it as a renormalization scale or a metric scale. Now as explained in (2.8), the bulk SymTFT produces a symmetry-preserving RG operator $U_{\text{RG}}^{\Lambda,\Lambda'}$ that changes the scale Λ . This operator is constructed explicitly using quantum $6j$ symbols in (4.13).

Equation (4.18) ensures the relation (4.13) relating the ground state at different scales. This in turn implies the equality.

$${}_{\Lambda}\langle\Omega^{\lambda}|\Psi\rangle_{\Lambda} = {}_{\Lambda}\langle\Omega^{\lambda}|\hat{U}_{\text{RG}}^{\Lambda,\Lambda'}|\Psi\rangle_{\Lambda'}. \quad (4.21)$$

Now a lot of the discussion in section 2.3 takes definite shape in the discrete formulation. As in (2.8) the RG operator here can be absorbed in ${}_{\Lambda}\langle\Omega^{\lambda}|\Psi\rangle_{\Lambda}$ as in (4.14) to produce

$${}_{\Lambda'}\langle\Omega^{\lambda}|\Psi\rangle_{\Lambda'} \equiv {}_{\Lambda}\langle\Omega^{\lambda}|\hat{U}_{\text{RG}}^{\Lambda,\Lambda'}|\Psi\rangle_{\Lambda}. \quad (4.22)$$

Now we want to define a *new* state by relabelling the lattice scale back to Λ as advocated in (2.10) and (2.11). i.e.

$${}_{\Lambda}\langle\Omega^{\lambda'}|\Psi\rangle_{\Lambda} \equiv {}_{\Lambda'}\langle\Omega^{\lambda}|\mathcal{P}^{\Lambda,\Lambda'}|\Psi\rangle_{\Lambda'} = {}_{\Lambda}\langle\Omega^{\lambda'}|\Psi\rangle_{\Lambda}, \quad \lambda' \approx \lambda(\Lambda/\Lambda')^2, \quad (4.23)$$

where $\mathcal{P}^{\Lambda,\Lambda'}$ is simply a relabelling operator. The new state to leading order in R is nothing but the original boundary condition with the holes rescaled after the RG step that say combines four triangles into two, as illustrated in Fig. 17. i.e. $R' = R\Lambda/\Lambda'$, explaining the approximate equality above, confirming equation (2.11). R needs to be small because the finite size of the hole contains more perturbation than the $T\bar{T}$ deformation alone, and the RG process would generally generate flow in couplings of higher powers of the stress tensor too. To leading order in R however the RG process is only shifting the $T\bar{T}$ coupling. The act of RG and rescaling lattice size equivalent to the conformal transformation $h_{ij}\partial_{h_{ij}}$. We show that such a transformation is equivalent to shifting the $T\bar{T}$ coupling and now we are ready to write down the Callan-Symanzik equation. We can arrange the re-triangulation that defines the RG operator such that Λ' is arbitrarily close to Λ . Therefore we can obtain an infinitesimal form of the flow equation

$${}_{\Lambda}\langle\Omega^{\lambda'}|\Psi\rangle_{\Lambda} - {}_{\Lambda}\langle\Omega^{\lambda}|\Psi\rangle_{\Lambda} \approx \delta\lambda \frac{d{}_{\Lambda}\langle\Omega^{\lambda}|\Psi\rangle_{\Lambda}}{d\lambda} \approx \delta\lambda \left(\sum_v \left(\frac{c}{12\lambda} \right) + \frac{12\pi}{c} \int d^2x \sqrt{\gamma} T\bar{T} \right) {}_{\Lambda}\langle\Omega^{\lambda}|\Psi\rangle_{\Lambda}, \quad (4.24)$$

where we have made use of the conversion in (4.19) and (4.20). The term proportional to c follows from the fact that there is a universal factor in the small R limit at every hole proportional to $\exp(c/6 \ln R)$, as explained below (4.17).

The expression ${}_{\Lambda}\langle\Omega^{\lambda}|\Psi\rangle_{\Lambda}$ diverges as $R \rightarrow 0$, and regularization was introduced in (4.12).

Therefore we could consider the flow equation of the regularized path-integral. Instead of expressing it as (4.12) where a factor is included for each vertex, we could consider distributing these factors to individual triangles. The reason for that is that we are defining a tensor network representation of the path-integral, and supposedly one should reproduce the path-integral given the local expression of individual triangle. Consider for simplicity triangulation of the surface so that the triangles are equilateral triangles – this has the virtue that the three vertices of the triangle would be on equal footing, and each vertex is shared by 6 triangles. In that case the natural assignment of regularization factor to each triangle is that each vertex of the triangle acquires a factor of $\exp(-c \ln R/36)$. i.e. We have

$$\Lambda \langle \Omega^\lambda | \Psi \rangle_{\Lambda, \text{Reg}} \equiv e^{-\frac{c \ln R}{36} \sum_v \chi(v)} \Lambda \langle \Omega^\lambda | \Psi \rangle_\Lambda, \quad (4.25)$$

where $\chi(v)$ is the number of triangles sharing this vertex v . Then the flow equation of the regulated partition function is given by

$$\lambda \frac{d_\Lambda \langle \Omega^\lambda | \Psi \rangle_{\Lambda, \text{Reg}}}{d\lambda} \approx \left(\frac{c}{48\pi} \int_M d^2x \sqrt{\gamma} \text{Ri} + \frac{12\pi}{c} \int d^2x \sqrt{\gamma} T\bar{T} \right) \Lambda \langle \Omega^\lambda | \Psi \rangle_{\Lambda, \text{Reg}}, \quad (4.26)$$

where we have made use of

$$\sum_{v \in G} (6 - \chi(v)) = 6\chi_M = \frac{6}{4\pi} \int_M d^2x \sqrt{\gamma} \text{Ri}, \quad (4.27)$$

for some 2D manifold M triangulated by a graph G , and χ_M the Euler characteristic of the manifold M . Ri is used to denote the Ricci scalar to avoid confusing it with the hole radius R . Contrasting with the flow equation (3.1), we observe an overall minus sign on the right-hand side. This is consistent with the $T\bar{T}$ deformation parameter having a relative minus sign in (4.7) compared to the scenario considered in Sec. 3. With a different starting point for the deformation away from a CFT, further deformation always increases the magnitude $|\lambda|$ of the $T\bar{T}$ coupling. So far the sign considered in this section conforms with other lattice construction of $T\bar{T}$ deformation such as those involving inhomogeneous transfer matrix. (For a review please see [98].) It is currently not known how to construct lattice models that reproduce the $T\bar{T}$ deformation corresponding to simple finite r cutoff in the AdS space discussed in [28] and also our (3.1). We also note that the regularization of the path-integral of the lattice model is different, which is crucial to the sign of the second term.

$T\bar{T}$ deformation is only one very specific choice of symmetry preserving deformations away from the CFT fixed point. One can describe more general quantum RG flows with more generic $\Lambda \langle \Omega |$ that introduces other deformations away from the CFT fixed point. In a general quantum RG flow, the discrete form of the Wheeler-DeWitt equation is generically following from

$$\Lambda \langle \Omega^{\lambda'} | \hat{\mathcal{H}}_\Lambda \hat{U}_{\text{RG}}^{\lambda', \lambda} | \Psi \rangle_\Lambda = \Lambda \langle \Omega^{\lambda'} | \hat{U}_{\text{RG}}^{\lambda', \lambda} \hat{\mathcal{H}}_\Lambda | \Psi \rangle_\Lambda = 0, \quad (4.28)$$

where we have defined

$$\hat{U}_{\text{RG}}^{\lambda, \Lambda} \equiv \hat{U}_{\text{RG}}^{\Lambda, \Lambda} \mathcal{P}_{\Lambda \Lambda}. \quad (4.29)$$

As discussed above, this property enables us to perform the SymQRG, and moves us into the SymTFT bulk. This shows the connection between crossing/re-triangulation invariance and the Wheeler-DeWitt equation, which is responsible for the emergence of a 3D bulk.

In the upcoming section, we will explore the application of this formalism when the bulk SymTFT contains 3D gravity. Translated into gravitational language, the no-flux condition is the statement that torsion vanishes and the curvature is constant. In the study of spin foam models, particularly those for spacetimes with positive cosmological constants, it has been shown that semi-classically, the Hamiltonian constraint corresponds to flat holonomy. In the quantum domain, this constraint is capturing re-triangulation invariance, enforced by the Pentagon identity [99]. Understanding how to achieve parallel results directly for spacetimes with negative cosmological constants, and understand 3D gravity directly in terms of $U_q(SL(2, \mathbb{R}))$ Levin-Wen model (especially issues regarding convergence) are interesting future directions.

4.4 Roles of tensor networks

Tensor networks play an important role in elucidating the connection between any 2D CFTs and their corresponding 3D Turaev-Viro TQFT/string-net model, which encodes the topological symmetries of the CFT. Through a non-perturbative approach, tensor networks reveal hidden structures in CFTs, providing us with a versatile framework to study such relationships in depth. Before we delve into the realm of gravity, it is worthwhile to address a fundamental question: why are tensor networks relevant here, and what unique advantages do they offer for an explicit non-perturbative realization of the boundary-to-bulk map?

Tensor Network as Manifestations of Locality

At the heart of using tensor networks in this setting is the non-perturbative manifestation of *locality*, which means that we can construct the path integral over an extended region by recursively gluing smaller, simpler regions together. This means that we can build up the path integral of a theory by locally assembling pieces, each of which encapsulates partial data of the system. Each subregion is equipped with indices that label the local path integrals, and the “gluing” operation is captured by summing over intermediate states, essentially represented by tensor contractions. In this sense, the tensor network seems to be the correct language encoding local physics.

The FRS theorem can be understood as providing a local tensor network representation of our $|\Psi\rangle_{\Lambda}$ [32], responsible for the topological/algebraic information of sewing rules encoded in the CFT path integral. On the other hand, our complementary construction of the state ${}_{\Lambda}\langle\Omega|$ [1, 29–31] provides the other half of the geometrical/complex analytical path integral information, ensuring

a balanced and coherent picture of the complete structure of the system, as summarized in Fig. 2. In retrospect, the validity of this approach is underpinned by the inherent locality of 2D CFTs themselves.

Moreover, by using this exact tensor network structure and the associated RG transformation, the locality of the boundary-to-bulk map is also made explicit. This locality is the essence of the Ryu-Takayanagi (RT) formula [100] and bulk reconstruction [101–104]. In our framework, tensor networks offer a non-perturbative realization of these ideas, with locality of the map manifest at every scale. We note however that the RT formula is *more* than locality. In fact, the tensor network was first invoked due to the similarity between the MERA network and the RT formula [36]. At the end however, our exact tensor network turns out graph independent. One might wonder if the structure of MERA thus plays no role after all. It turns out specific choice of graphs still plays a role in our discussion. This is because when we do a particular computation (such as the entanglement entropy of a given sub-region A), certain graph would lead to tremendous simplification. In the case of entanglement entropy, it turns out that if we arrange a triangulation that carries a MERA-like structure, as discussed in [1] and reviewed in Appendix D, the computation of the entanglement entropy *simplifies*. The location of the RT surface precisely determines the entanglement spectrum, thanks to the “quasi-perfect” property of the CFT tensors. The entanglement cut behaves almost exactly as in simple models based on perfect tensors [105], and many insights from the existing holographic tensor network literature still apply to our construction. This shows that rather than giving up on the graph, our tensor network does remember these structures. The graph independence is a way to incorporate an *infinite* number of graphs, which can be invoked depending on the precise computation that makes use of a particular structure. This is of course a necessary ingredient because our tensor network is an *exact discrete representation of continuum field theory*.

Gauge/global symmetry for bulk/boundary and topological error-correcting-code

A natural question arises within the tensor network framework: What indices, or basis, should be used to encode the tensors? The answer lies within the intrinsic topological symmetries of the CFT. In non-perturbative strongly interacting models, symmetries remain some of the most robust and intrinsic features of a theory. In the current context, the Hilbert space that characterizes the strange correlators, is defined by the Levin-Wen string-net model, which naturally captures the CFT’s topological symmetries: topological symmetries of the CFT exhibit themselves as ribbon operators in the Levin-Wen model.

Within the SymQRG procedure, a projection onto bases at various lattice scales is performed, where these bases, fixed by the symmetry of the theory, consistently reduce to the same set of labels defined by the topological symmetry (i.e. coarse-graining does not introduce new labels). This step mirrors the projection onto single-trace operators in the “quantum RG” transformations. To preserve the topological symmetry on the lattice, the transformation itself is governed by quantum

$6j$ symbols. Correspondingly, the part of the tensor network responsible for the bulk theory is provided by the quantum $6j$ symbols. This approach also gives rise to a unique structure: in the bulk, it induces *gauge symmetry*²⁴, while on the boundary, it preserves *global symmetry*. Gauge invariance essentially projects the tensor product of the boundary degrees of freedom onto an overall group singlet. Group transformation at the boundary is not part of the gauge symmetry, and they become global symmetry of the boundary degrees of freedom. This is realized in the usual WZW/Chern-Simons relation, and also in the AdS/CFT correspondence. Similarly, in the tensor network literature, geometrically higher dimensional tensor networks with gauge symmetry are used to construct global symmetric wave function in one lower dimension [108].

In addition, the bulk-to-boundary map and holographic tensor networks are proposed to have error-correcting code properties [104, 105, 109]. Since our tensor network construction involves the topological order, it suggests that the holographic error correcting code in the AdS₃/CFT₂ correspondence is in fact a fault-tolerant topological error correcting code, as explained in Kitaev’s seminal work [81]²⁵. Quantum information can be stored through long-range entanglement of the topological order [110], which is a gravitational theory here. The relationship between the anyons and BTZ black holes will be briefly explained in Sec. 5.

Bulk reconstruction and background independence

The problem of reconstructing physics in the gravitational bulk from boundary CFT data falls under the program of bulk reconstruction. As emphasized in [111], this is a two-step procedure in conventional methods on “states dual to a single geometry” in the large N limit. We first use a connection between CFT quantities and bulk geometrical objects to reconstruct a single background metric in the large N limit. Next, we reconstruct low-energy operators on the fixed pre-existing background, utilizing the entanglement generated by matter fields superimposed on the geometrical configurations, using a variety of interesting techniques from quantum information theory. By construction, these methods cannot work for states dual to “superposition of geometries”, or beyond the large N limit where we have a good notion of semi-classical spacetimes.

In this section, we demonstrate a method for reconstructing the exact bulk dual from the CFT algebra at any finite N . In the next section, we will see that quantum geometries naturally emerge from the CFT data, and the resulting bulk always involves a sum over these emergent quantum geometries. This framework is inherently background independent: no pre-existing geometries are assumed, and bulk operators are inherently defined within the CFT itself [112], emerging alongside the geometries. The large N semi-classical results can be recovered at the saddle points. However, working backward, starting from these saddle points, makes it inherently challenging to understand the emergence of spacetime once it has already emerged in the semi-classical approximation. One

²⁴Tensor network toy models for holography involving gauge symmetry in the bulk have been explored in [106, 107].

²⁵The Levin-Wen model for topological orders based on fusion categories [24] are generalizations of Kitaev’s toric code model based on groups.

interesting thing we want to point out is that the sum over geometries in the bulk, in general, does not seem to include all the geometries as we usually think. The information on which geometries we need to sum in the bulk to recover a CFT is encoded in the OPE coefficients, as we will elaborate in Sec. 6.

To emphasize the background independence, let us ask the following question: How can we construct a gravity theory on a lattice while preserving diffeomorphism invariant and background independence? The answer is that, while our theory is always defined on a fixed bulk/boundary lattice, this lattice has nothing to do with the target space geometries [1, 31, 107]. The length of the lattice sites also have nothing to do with the geodesic lengths in bulk geometry. The emergence of geometry arises from the fact that the algebraic data in the CFT admit emergent target-space geometrical interpretations.

5 3D Quantum Gravity as SymTFT

In Sec. 3, we discussed the connection between an RG flow driven by $T\bar{T}$ deformations and the gravitational path integral. Specifically, we demonstrated that coarse-graining the $T\bar{T}$ -deformed CFT is equivalent to treating the background metric as a dynamical variable and evolving it according to Einstein’s gravitational evolution. This highlights one of the central themes of the current paper: $QRG = QG$. In Sec. 4, we have illustrated how to construct the SymQRG evolution on a lattice that explicitly preserves topological symmetries.

However, it is perhaps not yet obvious how the RG flow driven by $T\bar{T}$ deformation and the SymQRG are related, and what makes the emergent bulk theory *Einsteinian*? We have alluded to the fact that the choice of $T\bar{T}$ deformation is special because it preserves topological symmetries, and an RG process that preserves topological symmetries should only change couplings of symmetry-preserving operators. In the case of 2D CFTs, this 3D bulk being Einsteinian is by no means an accident. The 3D bulk theory can be shown, in a very precise manner, to be the SymTFT for the collection of topological defect lines [20] that are being preserved by the RG process, as discussed in the last section. In this section, we identify the topological defect lines associated with 3D gravity. We begin with the case of 3D pure gravity, and then explore the connection to general irrational large N holographic CFTs, where 3D Einstein gravity serves as the universal approximate SymTFT.

The discussion of the SymTFT has so far been mostly restricted to symmetries that are rational – i.e. there is a finite and discrete set of conserved charge operators, and the corresponding holographic bulk – the SymTFT alluded to – is a rational topological theory²⁶.

When the RG process preserves irrational symmetries, the corresponding SymTFT is expected to be an irrational theory. As is well known, 3D Einstein gravity with a negative cosmological constant can be related, at least classically, to Chern-Simons theory with gauge group $SL(2, \mathbb{R}) \times SL(2, \mathbb{R})$,

²⁶See [37, 113–115] for some recent works to generalize the SymTFT to describe some simple continuous symmetries.

which is non-compact [77, 116]. This is very suggestive that 3D gravity is indeed a SymTFT in a way analogous to the rational cases. The difficulty is that the RG we discussed so far is a *quantum* RG process, and the corresponding bulk theory is a quantum gravitational theory. The quantum path integral that emerges in the quantum RG process needs extra care when we take the emergent bulk theory as a gravitational quantum path integral. To clearly see the topological symmetries, the Chern-Simons formulation of gravity is very useful, but it needs to be upgraded to a *quantum version*.

It has been proposed that the quantum version of the bulk theory is given by a TQFT related to the quantum Teichmüller theory [21, 33, 52]. Recent development of the Virasoro TQFT [22] and subsequently the discovery of a discrete formulation of the Liouville theory [1, 31] produces an explicit construction of this quantum bulk theory that reduces to Einstein gravity in the semi-classical limit. The anyons in this theory are related to BTZ black holes! In the following, we first give a brief review of the connection of the Chern-Simons theory and Einstein theory and the quantum upgrade to Virasoro TQFT. An explicit expression of the quantum RG process would then be obtained using the discrete formulation for two copies of the Virasoro TQFT [1]. Then we comment on the connection to quantum Teichmüller theory and the lattice Liouville theory. In the end, we will explain how the consideration of pure gravity is related to any generic large N 2D holographic CFTs, clarifying the differences and connections between exact duality at finite N and the universal bulk dual upon coarse-graining.

5.1 3D gravity and Chern-Simons theory

It is well known that 2+1-dimensional Einstein-Hilbert action with a negative cosmological constant can be rewritten as a Chern-Simons theory, at least at the level of the action [77, 116].

Let us briefly review the formulation here. The action of 2+1 dimensional Einstein-Hilbert action in Lorentzian signature with a negative cosmological constant reads²⁷:

$$I_G[g] = \frac{1}{16\pi G_N} \int d^3x \sqrt{-g} [R + 2] , \quad (5.1)$$

Given a metric

$$ds^2 = g_{\mu\nu} dx^\mu dx^\nu , \quad (5.2)$$

we can define a vielbein e_μ^a satisfying

$$g_{\mu\nu} = e_\mu^a e_\nu^b \eta_{ab} , \quad (5.3)$$

where a, b are tangent space indices and e_μ^a are tangent vectors. The tangent space indices are raised and lowered by the Minkowski metric η . The choice of e_μ^a is not unique.

²⁷We work in Lorentzian signature here to avoid discussing various subtleties regarding analytic continuation into Euclidean signature. A careful analysis of this problem in AdS₃ is done in the recent work [117].

We note that for a spin-connection compatible with the vielbein, it is defined as

$$\mathcal{D}_\mu e_\nu^a = \partial_\mu e_\nu^a - \Gamma_{\mu\nu}^\rho e_\rho^a + \omega_\mu^a{}_b e_\nu^b \equiv 0, \quad (5.4)$$

where $\Gamma_{\mu\nu}^\rho$ is the metric connection, i.e. the Christoffel symbols. In this case, it is well known that the Riemann tensor is given by

$$R_{\mu\nu\rho\sigma} dx^\rho \wedge dx^\sigma = R^{ab} e_a{}_\mu e_b{}_\nu, \quad R^{ab} = d\omega^{ab} + \omega_c^a \wedge \omega^{cb}, \quad (5.5)$$

where ω_μ^{ab} is the spin connection.

Now, at the level of the action, (5.1) can be written as

$$I_G = \frac{1}{8\pi G_N} \int e^a \wedge (d\omega_a + \frac{1}{2} \epsilon_{abc} \omega^b \wedge \omega^c) + \frac{1}{6} \epsilon_{abc} e^a \wedge e^b \wedge e^c = \frac{k_+}{4\pi} I_{CS}(A^{(+)}) - \frac{k_-}{4\pi} I_{CS}(A^{(-)}), \quad (5.6)$$

where we defined

$$A^{(\pm)} = \omega^a \pm e^a, \quad \omega^a = \frac{1}{2} \epsilon^{abc} \omega_{bc}, \quad (5.7)$$

with repeated indices are summed. The $I_{CS}(A)$ is the Chern-Simons action,

$$I_{CS}(A) = \int \text{Tr}(A \wedge dA + \frac{2}{3} A \wedge A \wedge A), \quad k_\pm = \frac{1}{4G_N}. \quad (5.8)$$

Here $A = A^a T_a$, where T^a form the fundamental representation of the $sl(2, \mathbb{R})$ Lie algebra, with $[T_a, T_b] = T_a T_b - T_b T_a = \epsilon_{abc} T^c$, and satisfies $\text{Tr}(T_a T_b) = \frac{1}{2} \eta_{ab}$.

Thus I_G takes precisely the form discussed in (A.1), except that the gauge group $G = SL(2, \mathbb{R})$ here is non-compact. This is basically a first-order formulation of relativity. Note that by varying e^a and ω^a independently, the former is equivalent to the Einstein equation and the latter gives the torsion-free condition, imposing compatibility of ω^a with e^a . These conditions are equivalent to the vanishing of field strength as in (A.3), and the Wheeler-DeWitt equation [33, 34].

5.2 Virasoro TQFT

As reviewed in the previous section, the connection between gravity and Chern-Simons theory is made originally at the classical level. It has been noted that 3D quantum gravity cannot possibly be a simple quantization of the Chern-Simons theory, since the path integral would include those connections that do not appear to have a sensible geometric interpretation from the perspective of gravity [118].

Since 3D gravity does not contain dynamical degrees of freedom, the appropriate quantum theory of gravity is expected to remain a TQFT. However, as is already hinted by the classical relation, the TQFT follows from a non-compact group, and it would not be expected to be a rational TQFT. Quantization of irrational TQFT in general is not very well understood. The mathematical and

physical understanding of irrational theories has far from reached the same level of rigor as their rational counterparts. When the TQFT is irrational, one has to grapple with issues with defining an appropriate measure in the quantum phase space and also convergence of the path integral. This is a generally unsolved problem.

Virasoro TQFT [22] is a proposed quantized version of the $SL(2, \mathbb{R})$ Chern-Simons theory that eventually leads to a relatively well-defined TQFT, importantly non-perturbatively at the level k and thus the Newton constant G_N from (5.8). It makes an essential restriction of the space of connections that is appropriate for a quantum gravitational interpretation. The restriction excludes connections that correspond to degenerate metrics of the physical phase space. Considering canonical quantization on a Cauchy surface Σ , the classical phase space of 2D metrics on the surface Σ turns out to be two copies of the Teichmuller space. The Teichmuller space is also the universal covering of the moduli space of the Riemann surface Σ . The quantum gravity theory is proposed to follow from quantizing this space.

Quantization of one copy of the Teichmuller space has been considered in [33], and a TQFT was suggested to be associated to it, which descends from one copy of the $SL(2, \mathbb{R})$ Chern-Simons theory. The Hilbert space of the purported TQFT is shown to be furnished by the space of (holomorphic) Virasoro conformal blocks. This is analogous to usual Chern-Simons theories whose Hilbert spaces are given by the space of Kac-Moody conformal blocks. Importantly, it is shown that the Gauss's law constraint satisfied by the ground state wavefunctions $\Psi[\phi, \mu]$ is equivalent to the Virasoro Ward identities,

$$\left((\bar{\partial} - \mu\partial - 2\partial\mu) \frac{\delta}{\delta\mu} + \frac{ic}{24\pi} \partial^3 \mu \right) \Psi[\phi, \mu] = 0 , \quad (5.9)$$

where the zweibein (e^+, e^-) is related to ϕ, μ by

$$e^+ = e^\phi (dz + \mu d\bar{z}) , \quad e^- = e^{\bar{\phi}} (d\bar{z} + \bar{\mu} dz) . \quad (5.10)$$

This is consistent with the expectation of the AdS/CFT correspondence, in which the Virasoro (or more generally conformal) Ward identity is shown to be related to the Wheeler-DeWitt equation in the bulk gravitational theory when both chiral sectors are included. As we argued in previous sections, this is a special case of the wider connection between symmetry-preserving RG flows and constraints in the bulk dual of the CFT.

There is a rigorous mathematical and discrete formulation of the Teichmuller TQFT [21] based on the construction of representations of the mapping class group. For a long time, it was unclear how the gravitational theory/Chern Simons theory can be directly compared to the construction there.

The Virasoro TQFT proposed in [22] further upgrades the discussion of [33], by supplying an explicit inner product of states, which was only formally defined.

As discussed above, the Teichmuller/ Virasoro TQFT corresponds only to one copy of the $SL(2, \mathbb{R})$

Chern-Simons theory, and the ground states discussed above correspond only to the holomorphic conformal blocks.

A very important observation is that when the Virasoro TQFT is evaluated on a manifold of the form $\Sigma \times I$, for some Riemann surface Σ and an interval I , the path integral gives the following operator

$$Z_{\text{Vir}}(\Sigma \times I) = \int d^{3g-3+n} \vec{P} \rho_{g,n}^C(\vec{P}) |\mathcal{F}_{g,n}^C(\vec{P})\rangle \otimes \langle \mathcal{F}_{g,n}^C(\vec{P})|, \quad (5.11)$$

where $|\mathcal{F}_{g,n}^C(\vec{P})\rangle$ is a basis of chiral Virasoro conformal blocks in a given channel C on the Riemann surface $\Sigma_{g,n}$ of genus g with n punctures, and $\rho_{g,n}^C(\vec{P})$ is the OPE density of the Liouville theory on $\Sigma_{g,n}$ [22]. This observation will allow us to identify a discrete formulation of the RG flow as the quantum evolution in 3D quantum gravity later in the section.

As is already apparent from the classical description, gravity should contain two copies of $\text{SL}(2, \mathbb{R})$ corresponding to the holomorphic and anti-holomorphic sectors of the dual CFT. Therefore, it is proposed that the proper quantum version of 3D gravity with a negative cosmological constant should be given by two copies of the Virasoro TQFT.

In particular, it is proposed that the gravitational path integral on a (hyperbolic) manifold M with fixed topology is basically related to the square of the Virasoro TQFT path integral. More precisely, taking into account of subtleties with gauge equivalence/redundancies under the action of the mapping class groups, the relation (for quantization related to 3D on shell solutions) is proposed to be [22]:

$$Z_{\text{grav}}(M) = \frac{1}{|\text{Map}_0(M, \partial M)|} \sum_{\gamma \in \text{Map}/\text{Map}(M, \partial M)} |Z_{\text{Vir}}(M^\gamma)|^2, \quad (5.12)$$

where M^γ is related to M by a modular transformation at ∂M , and $\text{Map}(M, \partial M)$ is the relative mapping class group equivalent to $\text{Diff}(M, \partial M)/\text{Diff}_0(M, \partial M)$, for $\text{Diff}(M, \partial M)$ denoting bulk diffeomorphisms that maps the boundary to itself. $\text{Map}_0(M, \partial M)$ is part of the bulk mapping class group acting trivially on the boundary ∂M . As this answer is a sum over the modular images, it provides a manifestly modular invariant answer. However, in Sec. 6.2, we will show that this is not the only way to achieve modular invariance; there is an alternative approach related to gauging or, more precisely, anyon condensation, that yields an answer dual to a true CFT. This perspective was also emphasized in [119].

If the ‘‘squared’’ Virasoro TQFT is the correct non-perturbative quantized version of 3D Einstein gravity, then the RG operator derived in (3.47) should be re-expressed clearly as an evolution in two copies of the Virasoro TQFTs, giving a mathematically clean and precise expression of the path integral over geometries.

However, this is somewhat tricky, since the Virasoro descendants do not show up explicitly in the formulation of the Virasoro TQFT. It is not clear as of now how to introduce deformation to the CFT and discuss RG flows within the current formulation of the Virasoro TQFT.

To make a connection with the Virasoro TQFT more explicitly, we need an alternative way of computing the evolution in the Virasoro TQFT. This is explained in the next subsection, where we identify the correct evolution, which can be expressed in a discrete formalism in terms of quantum $6j$ symbols (and their analytic continuation thereof) of the quantum group $U_q(SL(2, \mathbb{R}))$.

5.3 Discrete realization of the Virasoro RG operator

To find an alternative quantum formulation of the evolution operator in (3.47), we seek inspiration from the recent work of deriving the holographic bulk dual of the Liouville theory [1, 31]. The final answer we get will be universal for theories sharing the same topological symmetries, not restricted to the Liouville theory we start with.

In [1, 31], it is observed that the Liouville CFT admits a discretization as described in the previous section, leading to (4.12), despite the fact that the Liouville CFT is an irrational theory.

In the case of Liouville theory, the related BCFT structure coefficients have been explicitly solved [120–122]. The conformal boundary conditions are labeled σ , and the boundary-changing operators span representations of the Virasoro algebra, each belonging to a Virasoro primary family labeled by α . These representations have conformal dimensions $h_\alpha = \alpha(Q - \alpha)$, where

$$Q \equiv b + b^{-1} . \tag{5.13}$$

Q is related to the central charge of the CFT by

$$c = 1 + 6Q^2 . \tag{5.14}$$

Both σ and α take values in $Q/2 + i\mathbb{R}_{>0}$. Let us parametrize them as

$$\alpha = \frac{Q}{2} + iP_\alpha , \quad \sigma = \frac{Q}{2} + iP_\sigma . \tag{5.15}$$

Then the conformal dimension is

$$h_\alpha = \frac{c-1}{24} + P_\alpha^2 , \quad P_\alpha > 0. \tag{5.16}$$

The structure coefficients in a specific choice of normalization ²⁸ are given by quantum b - $6j$ symbols of certain special representations of the quantum group $U_q(SL(2, \mathbb{R}))$, with $q = \exp(i\pi b^2)$ as follows

²⁸We normalize all the closed and open Liouville operators by dividing the square root of the Liouville reflection coefficients, compared to [122]. This normalization has the advantage that operators and all expressions are invariant under reflection $P \rightarrow -P$. We also normalize the open Liouville operators by a square root of the bulk OPE coefficient. The details can be found in the appendix of [1].

[1]²⁹,

$$C_{\alpha_1, \alpha_2, \alpha_3}^{\sigma_3, \sigma_1, \sigma_2} = (\mu(P_{\alpha_1})\mu(P_{\alpha_2})\mu(P_{\alpha_3}))^{1/4} \left\{ \begin{array}{ccc} \alpha_1 & \alpha_2 & \alpha_3 \\ \sigma_3 & \sigma_1 & \sigma_2 \end{array} \right\}_b . \quad (5.17)$$

For later convenience, we also include the Virasoro crossing kernel in this normalization, which is

$$F_{\alpha_6, \alpha_5}^{\text{Racah}} \left(\begin{array}{cc} \alpha_1 & \alpha_4 \\ \alpha_2 & \alpha_3 \end{array} \right) = \frac{1}{\sqrt{2}} \sqrt{\mu(P_{\alpha_5})\mu(P_{\alpha_6})} \left\{ \begin{array}{ccc} \alpha_1 & \alpha_4 & \alpha_5 \\ \alpha_3 & \alpha_2 & \alpha_6 \end{array} \right\}_b . \quad (5.18)$$

The properties of the b - $6j$ symbols with this particular normalization and the connection to quantum hyperbolic geometry are analyzed in detail in [124]. It is remarkable that a carefully chosen normalization for Liouville operators makes the BCFT structure constants and the crossing kernels directly proportional to these $6j$ symbols, taking *exactly* the same form as in rational CFTs in (4.3) and (C.6).

These representations are special, as they are representations of the “modular double” introduced by Faddeev, which means that they are simultaneously representations of the dual quantum group $U_{\tilde{q}}(SL(2, \mathbb{R}))$, $\tilde{q} = \exp(i\pi/b^2)$ [125, 126], and it was anticipated that they would play an important role in irrational CFTs.

Given the parallel of these formulas with rational theories, it allows the Liouville CFT path integral $Z_{\text{Liouville}}(\Sigma)$ on a Riemann surface Σ to also be expressed as a strange correlator analogous to (4.9). i.e.

$${}_{\Lambda} \langle \Omega^R | \Psi_{\text{Liouville}} \rangle_{\Lambda} , \quad (5.19)$$

where $|\Psi_{\text{Liouville}}\rangle_{\Lambda}$ is given by

$$|\Psi_{\text{Liouville}}\rangle_{\Lambda} = \prod_v \int_0^{\infty} dP_{\sigma_a} \mu(P_{\sigma_a}) \prod_e \int_0^{\infty} dP_{\alpha_i} \sqrt{\mu(P_{\alpha_i})} \prod_{\Delta} \left\{ \begin{array}{ccc} \alpha_i & \alpha_j & \alpha_k \\ \sigma_c & \sigma_a & \sigma_b \end{array} \right\}_b |\{\alpha_i\}\rangle_{\Lambda} , \quad (5.20)$$

where the Plancherel measure $\mu(P_{\alpha})$ is given by

$$\mu(P_{\alpha}) = S_{0\alpha} = 4\sqrt{2} \sinh(2\pi P_{\alpha} b) \sinh\left(\frac{2\pi P_{\alpha}}{b}\right) , \quad (5.21)$$

and R parametrizes the hole size as explained in section 4.2. Similarly, ${}_{\Lambda} \langle \Omega^R |$ is again given by

$${}_{\Lambda} \langle \Omega^R | = \prod_i \int_0^{\infty} dP_{\alpha_i} \langle \{\alpha_i\} | \sum_{\{I_i\}} \prod_{\Delta} \left(\tilde{\gamma}_{I_i I_j I_k}^{\alpha_i \alpha_j \alpha_k}(R) \right) , \quad (5.22)$$

which are constructed from Virasoro conformal blocks as discussed in the previous section. Note

²⁹The connection between representations of the Virasoro algebra for general central charge c and representations of quantum groups $U_q(SL(2, \mathbb{R}))$ serves as an irrational analog of the Kazhdan-Lusztig equivalence [123].

that, similar to the discussion in the previous section, the vector space in which $|\Psi\rangle_\Lambda$ and ${}_\Lambda\langle\Omega|$ reside is spanned by the tensor products of the edge Hilbert space, in the chosen triangulation of the Riemann surface Σ , and each edge is colored by the Virasoro primary labels α .

These quantum $6j$ symbols of $U_q(SL(2, \mathbb{R}))$ also satisfy a Pentagon relation given by

$$\frac{1}{\sqrt{2}} \int_0^\infty dP_{\delta_1} \mu(P_{\delta_1}) \begin{Bmatrix} \alpha_1 & \alpha_2 & \beta_1 \\ \alpha_3 & \beta_2 & \delta_1 \end{Bmatrix}_b \begin{Bmatrix} \alpha_1 & \delta_1 & \beta_2 \\ \alpha_4 & \alpha_5 & \gamma_2 \end{Bmatrix}_b \begin{Bmatrix} \alpha_2 & \alpha_3 & \delta_1 \\ \alpha_4 & \gamma_2 & \gamma_1 \end{Bmatrix}_b = \begin{Bmatrix} \beta_1 & \alpha_3 & \beta_2 \\ \alpha_4 & \alpha_5 & \gamma_1 \end{Bmatrix}_b \begin{Bmatrix} \alpha_1 & \alpha_2 & \beta_1 \\ \gamma_1 & \alpha_5 & \gamma_2 \end{Bmatrix}_b . \quad (5.23)$$

Therefore, like in (4.13) and Fig. 14, one can construct a QRG operator $\hat{U}_{\text{RG}}^{\Lambda, \Lambda'}$, which amounts to gluing tetrahedra, now using these quantum $6j$ symbols of $U_q(SL(2, \mathbb{R}))$. Let us denote that by $\hat{U}_{\text{RG}}^{\Lambda, \Lambda'}(U_q(SL(2, \mathbb{R})))$. When we use this operator to perform the QRG, it manifestly preserve the topological defect lines associated to (5.16). Now we would like to argue that this is the discrete and non-perturbative version of the gravitational evolution effecting the RG flow operator $\hat{U}_{\text{3D gravity}}$ obtained in (3.47), i.e

$$\hat{U}_{\text{3D gravity}} \underset{\text{Continuum}}{=} \hat{U}_{\text{Virasoro TQFT}^2} \underset{\text{Discrete}}{=} \hat{U}_{\text{RG}}^{\Lambda, \Lambda'}(U_q(SL(2, \mathbb{R}))) \quad (5.24)$$

An initial evidence lies in the large c semi-classical limit of the quantum $6j$ symbols of $U_q(SL(2, \mathbb{R}))$. As shown in [1], in the limit $b \rightarrow 0$,

$$\left\{ \begin{array}{ccc} \frac{Q}{2} + i \frac{l_4}{2\pi b} & \frac{Q}{2} + i \frac{l_5}{2\pi b} & \frac{Q}{2} + i \frac{l_6}{2\pi b} \\ \frac{Q}{2} + i \frac{l_1}{2\pi b} & \frac{Q}{2} + i \frac{l_2}{2\pi b} & \frac{Q}{2} + i \frac{l_3}{2\pi b} \end{array} \right\}_b \xrightarrow{b \rightarrow 0} \exp \left(- \frac{\text{Vol}(T\{l_i\}) + \sum_i l_i \theta_i / 2}{\pi b^2} \right) ,$$

where $\text{Vol}(T\{l_i\})$ is the volume of a hyperbolic tetrahedron with edges labeled $\{i\}$ and geodesic lengths given by $\{l_i\}$ ³⁰, and θ_i is the dihedral angle sandwiched between the faces in the tetrahedron sharing the edge i . Thus, geometrical notions such as geodesic length naturally emerge in the large N limit of $U_q(SL(2, \mathbb{R}))$, assigning a clear bulk geometrical interpretation to the primary label P .

The Plancherel measure that shows up at every internal label that is integrated over, contributes in the small b limit,

$$\ln \mu(P(l)) \approx \frac{l}{4G_N} , \quad P = \frac{l}{2\pi b} . \quad (5.25)$$

As the generalization of quantum ‘‘dimension’’, this is indeed related to the Cardy formula for the density of states [127] and the entropy of the BTZ black hole [128], a connection on which we will elaborate shortly.

Collecting the quantum $6j$ symbols and the Plancherel measure in $\hat{U}_{\text{RG}}^{\Lambda, \Lambda'}$, it gives in the $b \rightarrow 0$ limit

$$\exp(-S_{EH} + \frac{\sum_e (2\pi - \Theta_e) l_e}{8\pi G_N}) , \quad (5.26)$$

³⁰The usual connection between $6j$ symbols and hyperbolic volume is in terms of the dihedral angles. We have used an identity to turn this into a relation in terms of geodesic lengths; see [1].

where

$$S_{EH} = -\frac{1}{16\pi G_N} \int_H d^3x \sqrt{g}(R+2) , \quad (5.27)$$

and we plugged in $R = -6$. $\Theta_e = \sum_i \theta_i$ is the sum over dihedral angles of tetrahedra sharing this internal edge e , and can be identified with the Gibbons-Hawking-York term in the presence of codimension-two corner singularities, which is also called the Hayward term [129, 130]. They do not contribute when one considers saddles with smooth geometries. The gravitational constant is related to the central charge by the standard Brown-Henneaux relation (3.40), $c \approx 6/b^2 = 3/2G_N$.

This means that $\hat{U}_{\text{RG}}^{\Lambda, \Lambda'}(U_q(SL(2, \mathbb{R})))$ reduces to the semi-classical gravitational integral in the AdS spacetime at the limit $b \rightarrow 0$ or $c \rightarrow \infty$. At finite c , the theory involves a summation over all possible *quantum geometries* corresponding to each RG step, which are constructed from the complete set of quantized geodesic configurations building up the quantum spacetimes.

To show that $\hat{U}_{\text{RG}}^{\Lambda, \Lambda'}(U_q(SL(2, \mathbb{R})))$ is also the desired flow operator non-perturbatively in b , we wish to show that this is the correct discrete version of two copies of the Virasoro TQFT evaluated on the same manifold of the form $\Sigma \times I$. To do so, we use (5.11). Consider folding the path integral of the Virasoro TQFT on $\Sigma \times I$ in the middle of I . This produces a state $|\Psi\rangle$

$$|\Psi\rangle = \int d\vec{P} \rho_{g,n}^C(\vec{P}) |\mathcal{F}_{g,n}^C(\vec{P})\rangle \otimes |\overline{\mathcal{F}_{g,n}^C}(\vec{P})\rangle , \quad (5.28)$$

where the “folded bra” becomes $|\overline{\mathcal{F}_{g,n}^C}(\vec{P})\rangle$ which now denotes the anti-holomorphic basis for conformal blocks. The state $|\Psi\rangle$ is thus a sum over basis holomorphic and antiholomorphic conformal blocks in exactly the linear combination that coincides with the Liouville theory. Our state $|\Psi_{\text{Liouville}}\rangle$ is indeed the same state by construction (despite being expressed in a basis that breaks up the closed conformal blocks into open ones tiling the same surface). Therefore, our discrete representation of $|\Psi_{\text{Liouville}}\rangle$ should be equivalent to the folded Virasoro TQFT evaluated on $\Sigma \times I$. In particular, the RG operator $\hat{U}_{\text{RG}}^{\Lambda, \Lambda'}(U_q(SL(2, \mathbb{R})))$, which essentially grows the I direction of $\Sigma \times I$ in $|\Psi_{\text{Liouville}}\rangle$, using tetrahedra associated to the $U_q(SL(2, \mathbb{R}))$ $6j$ symbols, should also be a discrete realization of two copies of the Virasoro TQFT on $\Sigma \times I$, as illustrated in Fig. 18. In other words, the quantum $6j$ symbols indeed reproduce two copies of the Virasoro TQFT, as expected of the quantized theory of gravity. This relation is reminiscent of the connection between rational Turaev-Viro TQFT and two copies of Chern-Simons theories we reviewed in Appendix A³¹.

This provides a rare example of an irrational theory, expressed in a discrete form, analogous to the Turaev-Viro TQFT reviewed in the previous section. In general, the mathematical structure underlying irrational theories is not fully understood. However, this well-defined example of Liouville theory suggests that a lot of the results for rational CFTs can indeed be generalized to irrational ones, and these underlying structures are responsible for the universal holographic correspondence.

³¹The CFT in that case is the non-chiral Wess-Zumino-Witten model [78, 79].

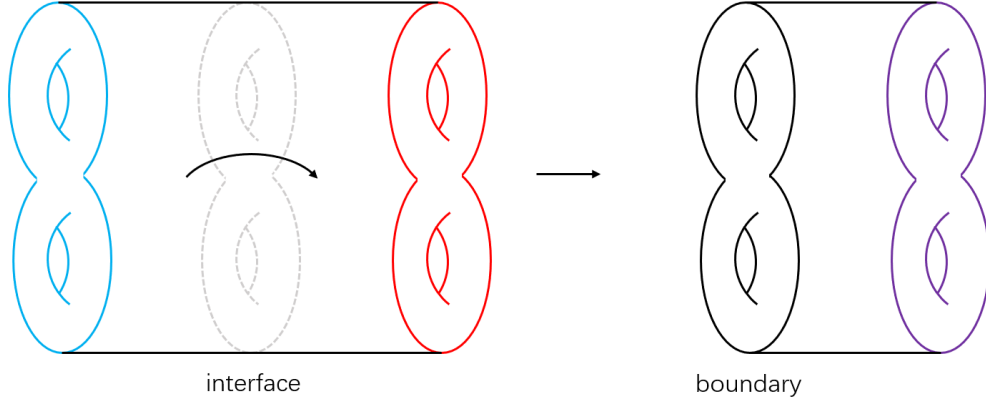


Figure 18: The Virasoro TQFT computation on $\Sigma \times I$ is shown on the left. On the right, we fold the diagram along the interface in the middle, making it a boundary. Two copies of Virasoro TQFT are on the right, and produce exactly the state $|\Psi_{\text{Liouville}}\rangle$ representing Liouville theory.

We also note that the $6j$ symbols are diffeomorphism-invariant objects. This is evident already in the classical limit, where they are related to the volume of hyperbolic tetrahedra and dihedral angles and geodesic lengths, which are expressible as the Einstein-Hilbert action and the Gibbons-Hawking-York term/Hayward term. Therefore, the theory is explicitly independent of the choice of coordinates. As explained in appendix A, with the Pentagon relation, triangulations on any boundary surface can be changed to any other. The Pentagon relation guarantees the so-called “3-2 Pachner move”. To be completely independent of triangulation in the bulk, one also needs the “4-1 Pachner move” that converts between four tetrahedra and one tetrahedron. This could not be achieved in the current case due to divergence [22, 31]. Therefore, triangulation in the bulk is not completely arbitrary, but by reconstructing the CFT partition function, it suggests a canonical triangulation that is depicted in Fig. 12 and adopted in $|\Psi_{\text{Liouville}}\rangle$. In the tensor network SymQRG procedure, the block-spin transformation modifies the boundary triangulations solely through the 3-2 move. The gluing of tetrahedra in the bulk avoids introducing new bulk vertices, which could lead to divergences if the 4-1 move were required. Consequently, the procedure remains well-defined and finite, even without resorting to the full Turaev-Viro construction.

This approach aligns with the spirit of the Regge-Ponzano model [131] for quantum gravity, now extended to spacetimes with a negative cosmological constant. However, we stress that analyzing bulk gravity alone is insufficient; incorporating an asymptotic boundary that realizes the $\langle \Omega |$ state is crucial to obtaining a finite, well-defined answer, dual to a CFT. This is the key insight of the AdS/CFT correspondence [2–4].

This gives the strongest yet evidence that the quantum non-perturbative version of gravity adopts a Turaev-Viro-type construction associated with representations of $U_q(SL(2, \mathbb{R}))$. Since the q -deformed algebra has interpretations as non-commutative geometries (or quantum groups), this strongly suggests that at finite Newton’s constant the precise geometrical framework of Quantum

Gravity also involves non-commutative geometries.

Having expressed the QRG operator explicitly in terms of $\hat{U}_{\text{RG}}^{\Lambda, \Lambda'}(U_q(SL(2, \mathbb{R})))$, we return to the question of symmetries preserved by the RG evolution. The virtue of a Chern-Simons formulation of gravity is to make the symmetry preserved in the RG process explicit. This benefit is inherited in the current formulation. There are continuous spectra of topological line operators in the bulk theory [1]. They correspond to Verlinde lines in the Liouville CFT which we reproduce here:

$$\hat{X} = \int_{\frac{\mathbb{Q}}{2} + i\mathbb{R}^+} d\alpha \frac{S_{P_x, P_\alpha}[\mathbf{1}]}{\mu(P_\alpha)} \mathcal{P}^\alpha, \quad (5.29)$$

where \mathcal{P}^α is a projection operator given by $\sum_{j,k} |\alpha, j, k\rangle \langle \alpha, j, k|$ with the j and k label the sum over descendants on the chiral/anti-chiral halves, and

$$S_{P_1, P_2}[\mathbf{1}] = 2\sqrt{2} \cos(4\pi P_1 P_2). \quad (5.30)$$

These are the counter-parts of Wilson lines in the Chern-Simons theory.

The anyons in this theory are, in fact, related to BTZ black holes [41, 128]. This can be seen by first noting that the conformal dimensions of the dual field theory operators are given by (5.16), corresponding to hyperbolic holonomies of $SL(2, \mathbb{R})$. Taking a chiral and anti-chiral pair with h_α and $h_{\bar{\alpha}}$, this gives all rotating BTZ black hole states with energy $h_\alpha + h_{\bar{\alpha}}$ and angular momentum $h_\alpha - h_{\bar{\alpha}}$. In addition, the product of the quantum dimension $\mu(P_\alpha)\mu(P_{\bar{\alpha}})$, as given in (5.21), matches precisely the Cardy density of states [127]. In the semi-classical limit, the logarithm of the product of quantum dimensions, as shown in (5.25), corresponds to the horizon area of the corresponding BTZ black hole over $4G_N$, which is just the black hole entropy, as noted in [128]. We can also use the $6j$ symbol associated with these anyons to study scattering in 3D black holes [51].

The ω loop projector (A.16) in this context is,

$$\hat{\omega} = \int_{\frac{\mathbb{Q}}{2} + i\mathbb{R}^+} d\alpha \mu(P_\alpha) \mathcal{P}^\alpha. \quad (5.31)$$

In gravity, the insertion of this operator ensures the contractibility of the dual cycle [132]. For the Hartle-Hawking state of two-sided eternal BTZ black holes, this operator insertion applies the topological restrictions of contractibility in Euclidean signature and modifies the definition of the trace. It gives an additional $\langle \ln \hat{\omega} \rangle$ contribution in the calculation of the entanglement entropy. In the semi-classical limit, the eigenvalues $\ln(\mu(P_\alpha))$ are the areas, so this is the expectation value of the “quantum area operator”, which gives the correct answer we expect for the generalized entropies [132, 133]³². The interpretation of these line operators and their state counterparts (FZZT state [120, 121] and ZZ state [136]) as wormholes and black holes in 3D gravity are also discussed in [132].

³²The necessity of similar “defect operator” imposing a topological constraint, in the factorization map and calculation of entanglement entropy, is pointed out in JT gravity in [134], and the topological string theory in [135].

In fact, the $T\bar{T}$ deformation preserves these Verlinde lines associated with Virasoro primaries as topological symmetries. Therefore, flows driven by $T\bar{T}$ deformations admit an interpretation as RG flow generated by these symmetry-preserving RG operators which, as we have shown, admit an interpretation as a gravitational evolution. In cases where the CFT preserves *more* or *fewer* symmetries, such as topological lines associated with more general (rational) quantum group representations in the presence of a chiral algebra that is bigger than the Virasoro algebra, then the bulk evolution could be expanded (or diminished) to make those symmetries explicit. The discussion of RG operators descending from rational TQFTs in the previous section essentially makes other rational symmetries explicit. When the RG flow does preserve these Virasoro lines, it could *always* be expressed in terms of $\hat{U}_{\text{RG}}^{\Lambda, \Lambda'}(U_q(SL(2, \mathbb{R})))$. Although we obtained this operator by studying $|\Psi_{\text{Liouville}}\rangle$, we land on something that goes way beyond the Liouville theory. The quantum RG operator plays a universal role, since all it does is to make the symmetries preserved in the RG process explicit, the former of which determines what the latter looks like from the mathematics of representation theory. The Liouville theory, which is one example that preserves the symmetry, serves as a vehicle for us to derive the general RG operator. In other words, $|\Psi_{\text{Liouville}}\rangle$ is one solution to (4.13), but *every* modular invariant CFT (which we do not yet know other than Liouville theory) preserving at least the same collection of symmetries would supply an independent solution to (4.13). The take-home message is – symmetries help us identify a *universal* QRG operator $\hat{U}_{\text{RG}}^{\Lambda, \Lambda'}(U_q(SL(2, \mathbb{R})))$ that admits an interpretation as a *quantum gravitational path integral*. In other words,

$$\text{SymQRG}(\text{Virasoro lines}) = \text{QG} \tag{5.32}$$

which is the central result of the current paper.

This completes our journey connecting Virasoro lines, symmetry preserving RG flows and quantum gravitational evolution.

5.4 Remarks on the lattice Liouville theory from quantum Teichmuller theory

In the literature, it is known that there is a lattice integrable model that also recovers the Liouville CFT in the thermodynamic limit [40].

The transfer matrix of the lattice model is constructed using operators in the quantum Teichmuller theory of Kashaev [52, 137]. In appendix E, we review the construction of these operators and explain the connection to the $U_q(SL(2, \mathbb{R}))$ $6j$ -symbols.

The Hilbert space of the discrete Liouville theory on a circle is constructed as follows. First, consider an annulus, where each side of the annulus represents a chiral/anti-chiral half of the theory. Discretize the annulus into one single row of squares, and for each square draw a diagonal say from the top left corner to the bottom right corner. This produces a simple triangulation of the annulus. Mark a corner in each triangle. Then attach a pair of Kashaev’s canonical variable (q_v, p_v) as in (E.9) to each triangle labeled Δ_v .

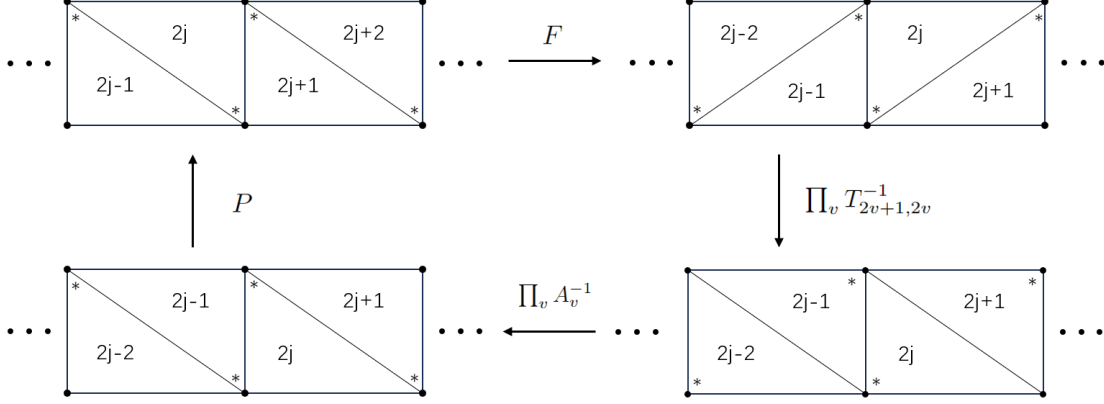


Figure 19: The transform matrix F can be constructed from the product of T , A and P operators.

These canonical variables are related to the discretized quantum Liouville field r_j as follows [138],

$$\kappa(r_v) = \begin{cases} p_v + p_{v-1} & \text{if } v = 0 \bmod 2, \\ q_v + q_{v-1} & \text{otherwise} \end{cases} \quad (5.33)$$

where κ denotes the fact that this is a reducible representation of the operator algebra satisfied by r_j , where $\exp(2\pi b r_j) \rightarrow \exp(-\phi(x))$ in the semi-classical limit $b \rightarrow 0$, and the continuum limit. The transfer matrix acts as follows. It is basically implementing the mapping class transformation on the annulus, shearing one boundary of the annulus one lattice site forward relative to the other boundary. After the shear the lattice would look different. This is illustrated in Fig. 19. One can convert the sheared lattice back into its original shape using the “crossing transformation” as in Fig. 59, with the T operator in (E.13) and also the A operator introduced in (E.16) that moves the marked point.

The transfer matrix, denoted F is then given by

$$F = \mathcal{N} P \prod_v A_v \prod_v T_{2v+1,2v}, \quad (5.34)$$

for some appropriate overall normalization factor \mathcal{N} , and P denotes the cyclic permutation of the vertex on one boundary of the annulus.

The important observation is that the collection of T_{vw} operators are the building blocks of the (chiral) quantum Teichmüller theory, each being geometrically a tetrahedron. The repeated application of the transfer matrix F is thus a path integral of the Teichmüller theory over a 3-dimensional manifold that takes the form of $A_2 \times I$, where A_2 is the annulus and I is an interval corresponding to the time direction in which the transfer matrix is generating an evolution, as illustrated in Fig. 20.

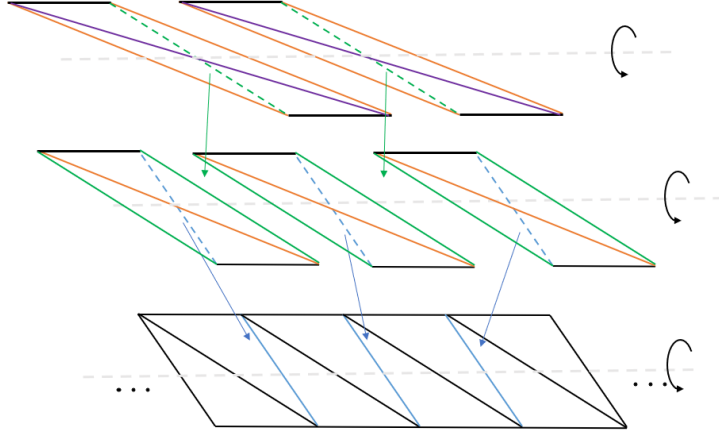


Figure 20: The path integral of the lattice Liouville theory is coming from gluing the tetrahedron operators in quantum Teichmüller theory. When we fold the diagram in the middle, this becomes the sandwich construction, with a seed state not at its RG fixed point.

This path integral in fact conforms with the construction of the Liouville CFT as a strange correlator (5.19). The slab is a chiral path integral of the Teichmüller TQFT with two boundaries, corresponding to the chiral/anti-chiral parts. It is related to the non-chiral sandwich by folding in the middle, similar to Fig. 18. Of course in our exact lattice construction realizing Liouville theory (5.19), the physical boundary condition corresponding to $\langle \Omega |$ is constructed from conformal blocks and represents an RG fixed point. Meanwhile, the discrete quantum Liouville theory construction outlined in this section supplies another seed state $\langle \Omega |$, similar to the case of the product state for the lattice Ising model [13, 84]. By applying the RG procedure outlined in Sec. 4.2 and appendix C to this seed state, we expect to recover the fixed-point tensor described in (5.19).

5.5 Exact bulk dual at finite N and universal semi-classical gravity dual at large N

In this section, we focus on the continuous spectrum (5.16), which describes theories related to pure gravity, for example the Liouville theory [1, 31]. What is the connection with general holographic CFTs? The answer to this question was first proposed in [51], and recently also emphasized in the discussion for the role played by ensemble averages in holography in terms of coarse-graining and the eigenstate thermalization hypothesis (ETH) [139–144].

Before addressing this question, let us first revisit the concept of “Quantum Gravity”. Quantum gravity is defined as a theory that is non-perturbatively complete and reduces to Einstein gravity in the semi-classical limit.

General irrational large N holographic CFTs are expected to have a discrete spectrum instead of

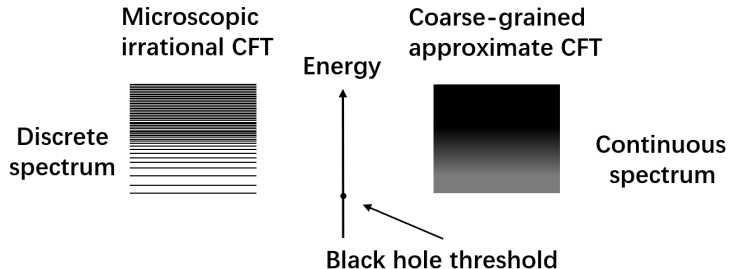


Figure 21: The comparison of spectrum between individual irrational large N holographic CFTs and the theory after coarse-graining. Since the discrete spectrum on the left is dense, we can approximate it with the continuous spectrum on the right.

a continuous one that we studied in this section, and similarly for the associated topological defect lines. However, the general large N holographic CFTs have a large gap and a dense spectrum for heavy states above the black hole threshold that is approximately continuous; see Fig. 21. The idea is that for individual 2D holographic CFTs, the heavy state dynamics of these theories can be universally approximated by the results outlined in this section. The coarse-grained result has a continuous spectrum (5.16) with Cardy density of states [127], and the heavy-state matrix elements are given by random matrices, from a generalized version of the ETH [51, 139, 144]. These coarse-grained matrix elements involving heavy states can be obtained by studying the bootstrap equations involving identity in certain dual channels [145–147], and then applying an argument similar to [148] to the OPE coefficients, to extend the regime of validity in the large N limit. The final result is universally captured by the quantum group $U_q(SL(2, \mathbb{R}))$, where quantum Teichmüller theory and geometries emerge. More details on the average over open structure coefficients in a CFT and its connection to the emergence of gravity will be presented in a forthcoming publication [149].

In other words, even with the presence of additional fields and fine structures in a 2D CFT, the universality of heavy-state statistics at large N ensures the universal emergence of a thermodynamic description with a 3D Einsteinian gravity sector in the bulk. States below the threshold will contribute to extra fields coupled to the gravity sector. For example, we can have worldline actions coupled to the Einstein-Hilbert action as in [150]. In this sense, gravity serves as a universal long-range entangled phase of matter, when there are infinitely many degrees of freedom. Building on this discussion, we emphasize the two distinct roles that Liouville theory plays. On one hand, it serves as an exact dual to pure gravity in a precise sense [1, 22, 132, 151]. On the other hand, it functions as a universal approximation for generic 2D holographic theories when viewed through a coarse-grained lens [51, 142–145].

The above line of logic on coarse-graining explains why the bulk dual theory universally behaves as semi-classical gravity at large N . In terms of the RG operator and 3D quantum states, this is the

statement that³³:

$$\begin{aligned}
\hat{U}_{\text{RG}} &\overset{\text{Large } N}{\underset{\text{Coarse-graining}}{\approx}} \hat{U}_{\text{RG,3D gravity}} \\
|\Psi\rangle &\overset{\text{Large } N}{\underset{\text{Coarse-graining}}{\approx}} |\Psi\rangle_{\text{3D gravity}}
\end{aligned}
\tag{5.35}$$

However, equipped with our machinery, especially the exact tensor network construction of the boundary CFT and bulk dual, we believe that we can always have an *exact, non-perturbative* quantum gravitational dual at finite N using the construction. The sandwich construction is generically true due to symmetry considerations; the RG map moving us into the bulk only relies on the exact crossing symmetry. Therefore, as long as we have a self-consistent 2D CFT, we will be able to get a quantum bulk dual theory. With a discrete spectrum, the bulk dual will deviate from a purely geometrical Einstein theory, and we get light matter fields and also stringy fields with fine-tuned couplings to exactly satisfy the non-perturbative bootstrap equations [51]. However, after we construct the exact bulk theory using the tensor network for holographic CFTs, it will approximate the geometrical bulk we described in this section in the semi-classical limit. The AdS/CFT correspondence offers a framework for addressing the question of quantum gravity. It is not merely an approximate correspondence valid only after coarse-graining or at the large N semi-classical level. While coarse-grained results can provide excellent approximations for certain questions, the true power of the correspondence lies in its unique ability to define non-perturbative completions of Einstein gravity through the CFTs.

6 Quantum Gravity from Algebra

6.1 Topological holographic principle

The topological holographic principle was proposed in [5–14]. Practically, it states that the path integral of a D dimensional theory with symmetry on a manifold Σ_D can be expressed in terms of the path integral of a $D + 1$ dimensional TQFT over a manifold $\Sigma_D \times I$, where I is an interval. This manifold $\Sigma_D \times I$ is often referred to as a “sandwich”. The two boundaries of the sandwich are assigned different boundary conditions: one is the physical boundary condition, and the other is the topological boundary condition. In this paper, we associate the quantum state ${}_{\Lambda}\langle\Omega|$ with the physical boundary and the SymTFT ground state $|\Psi\rangle_{\Lambda}$ with the topological boundary combined with the bulk.

In the context of 2D CFTs, the connection with a 3D TQFT is well-established. The 3D Chern-Simons theory path integral evaluated on a 3D manifold M_3 with boundary ∂M_3 famously reduces to the WZW model on the 2D boundary [78,79]. It is also well known that the 2D boundary theory is anomalous and can only exist as boundaries of a 3D theory. The anomaly is canceled by the

³³This is to be compared with an intrinsic ensemble of CFTs, which correspond to $|\Psi\rangle = \sum_i p_i |\Psi\rangle_i$, where p_i is a chosen weight for the ensemble average.

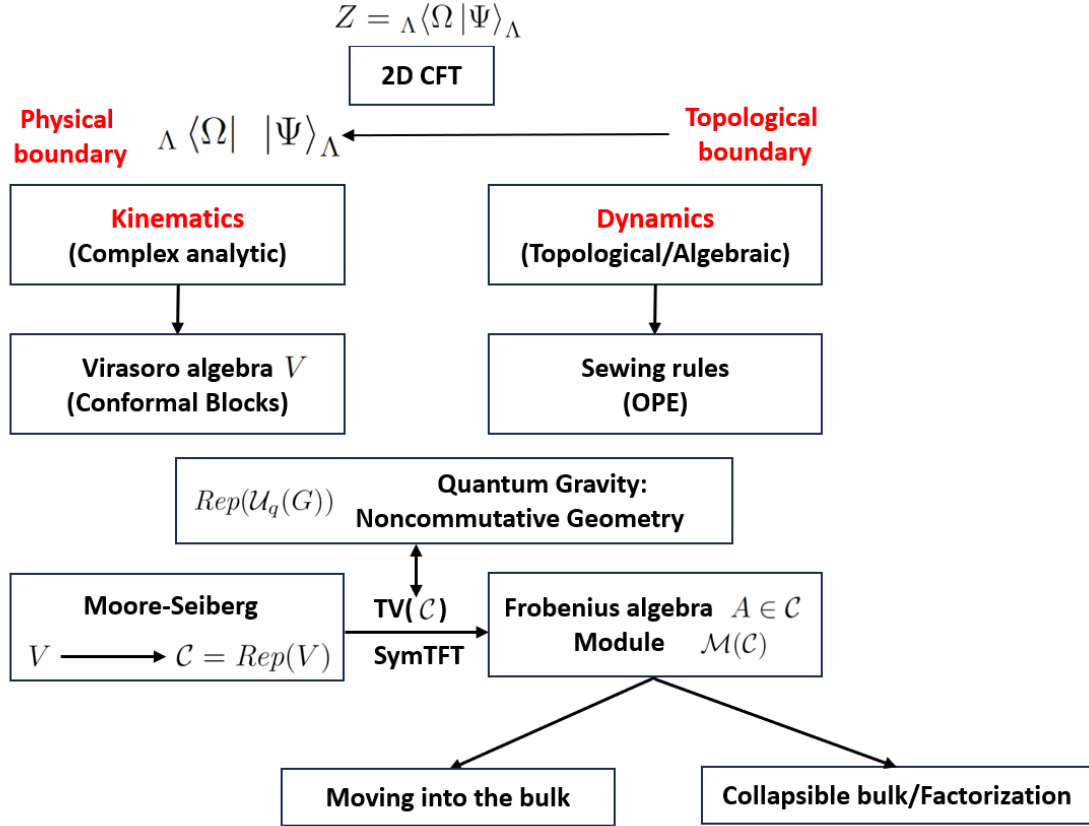


Figure 22: Summary of the logic behind FRS construction and Sec. 6.2, as well as its connection to the bulk SymTFT and quantum gravity.

3D bulk via the anomaly inflow mechanism. In the sandwich construction, the resulting 2D theory is anomaly-free and thus exists as a consistent stand-alone theory. The anomaly-free condition is encoded in the topological boundary of the sandwich.

In the previous sections, we have focused primarily on the physical boundary, represented by the state ${}_{\Lambda} \langle \Omega |$, and its connection to the RG flow via the bulk SymTFT. In doing so, we have assumed the existence of a CFT, corresponding to a well-defined state $|\Psi\rangle_{\Lambda}$ that encodes the topological boundary. One of the key observations in this paper is that each individual 2D CFT corresponds to a specific state $|\Psi\rangle_{\Lambda}$. In this section, we reverse the logic and focus on constructing the topological boundary condition. The key questions to consider are the following. How can we determine a topological boundary condition for a given SymTFT? What are the algebraic conditions, and how do they relate to CFT consistency relations? To begin, we provide a brief overview of the FRS construction [32]. As explained earlier, given a chiral algebra V (Virasoro in this context), Moore and Seiberg identified an associated fusion category $\mathcal{C} = \text{Rep}(V)$ arising from the representations of V (labeled by primaries) [42]. The chiral algebra V is encoded in the $\langle \Omega |$ part of the overlap, appearing

as conformal blocks. Using the Turaev-Viro construction [23], a 3D TQFT can be constructed using \mathcal{C} , which serves as the SymTFT associated with the symmetries of the theory. To obtain an intrinsic 2D CFT, it suffices to determine a suitable topological boundary condition, enabling the sandwich construction to function. In the language of the overlap (2.5), this corresponds to identifying *which* topological ground state matches each individual CFT.

FRS provided an answer to this question [32]. In fact, we have already encountered this answer when working backwards from a CFT. These answers are encoded in the BCFT structure coefficients used to construct the state $|\Psi\rangle_\Lambda$. In Sec.6.2, we briefly outline the algebraic conditions that the topological boundary condition must satisfy and explain how these conditions relate to the CFT consistency requirements. From these algebraic properties, quantum gravity in the bulk emerges naturally. In Sec.6.4, we discuss the implications of these algebraic properties for quantum gravity. Specifically, we address the factorization puzzle concerning wormhole contributions in the gravitational path integral and explain how the out-of-time-ordered correlator is inherently encoded within the symmetry framework.

This section is rather technical, so we include a logical map in Fig. 22 before we start.

6.2 Looking for $|\Psi\rangle_\Lambda$: From crossing symmetry to anyon condensation/gauging

6.2.1 Crossing symmetry and emergence of 3D bulk

The CFT path integral was found to be related to a wavefunction $|\Psi\rangle_\Lambda$ introduced in (4.10). This is supposed to be a ground state of the Turaev-Viro (or Levin-Wen) model.

On a general 2D manifold Σ with noncontractible cycles, there is generically ground-state degeneracies. For example, on a torus, the number of degenerate ground states of the Turaev-Viro model with input fusion category \mathcal{C} is equal to the number of simple objects in $D(\mathcal{C})$. The basis of ground states on the torus can be constructed by inserting Wilson lines/ribbon operators along the non-contractible cycle in the path integral over a solid torus.

Which of the ground states is selected in (4.10)? The information lies in the labels σ in (4.10). In the CFT, σ labels the conformal boundary conditions where in the collection at least one of them preserves one copy of the chiral algebra³⁴. The set of labels correspond to objects of a *module category* $\mathcal{M}_{\mathcal{C}}$ of \mathcal{C} . Each $\mathcal{M}_{\mathcal{C}}$ corresponds to a topological boundary condition of the Turaev-Viro TQFT [11, 32, 152, 153].

As a module (or representation) of \mathcal{C} , it means that objects in \mathcal{C} can act on the objects of $\mathcal{M}_{\mathcal{C}}$. i.e. the action is a *functor* that maps $\mathcal{C} \otimes \mathcal{M}_{\mathcal{C}} \rightarrow \mathcal{M}_{\mathcal{C}}$. The functor at the level of the objects maps the objects in $\mathcal{C} \otimes \mathcal{M}_{\mathcal{C}}$ to the objects in $\mathcal{M}_{\mathcal{C}}$. One can understand this map physically. This means that excitations in the bulk TQFT (which are objects in the bulk category) can move to the gapped boundary and fuse with boundary excitations (which are objects in the module category), producing

³⁴As it is noted in [32], the framework does not require maximally extending the chiral algebra and allows one to include boundary conditions that break part of the chiral symmetries

other excitations in the boundary [154–156]. We denote this fusion map by $W_{cm}^{m'}$, where $c \in \mathcal{C}$ and $m, m' \in \mathcal{M}_{\mathcal{C}}$.

This map should satisfy a number of associativity constraints [32, 157]. In particular, one can imagine taking two objects in $c_{1,2} \in \mathcal{C}$ and fusing them with an object $m \in \mathcal{M}_{\mathcal{C}}$. We can first fuse them together to get c_k before fusing with m to get $n \in \mathcal{M}_{\mathcal{C}}$. Alternatively, c_i can be fused with m to get $m' \in \mathcal{M}_{\mathcal{C}}$ which is then subsequently fused with c_j to get $n \in \mathcal{M}_{\mathcal{C}}$.

These two fusion processes are related by

$$W_{c_1 m}^{m'} W_{c_2 m'}^n = \sum_{c_3 \in \mathcal{C}} \tilde{C}_{c_1 c_2 c_3}^{n m m'} V_{c_1 c_2}^{c_3} W_{c_3 m}^n, \quad (6.1)$$

where $V_{c_1 c_2}^{c_3}$ is the fusion map of \mathcal{C} introduced above equation (A.21). This associativity relation above is similar to (A.21), except that two types of fusion maps are involved. The associativity coefficients $\tilde{C}_{c_1 c_2 c_3}^{n m m'}$ play a similar role as the quantum $6j$ symbols involved previously, but now it contains indices in both \mathcal{C} and $\mathcal{M}_{\mathcal{C}}$. As a result, we can expect these coefficients to also satisfy a version of the Pentagon equation. It is given by

$$\tilde{C}_{c_1 c_5 c_4}^{m_4 m_1 m_2} \tilde{C}_{c_3 c_5 c_2}^{m_2 m_3 m_4} = \sum_{c_6} \tilde{C}_{c_1 c_2 c_6}^{m_3 m_1 m_2} \tilde{C}_{c_3 c_4 c_6}^{m_1 m_3 m_4} F_{c_6, c_5}^{\text{Racah}} \begin{pmatrix} c_1 & c_4 \\ c_2 & c_3 \end{pmatrix}. \quad (6.2)$$

This is nothing but the crossing invariance of BCFT four-point functions in (C.5), which was instrumental in establishing the re-triangulation invariance of the tensor network representation of the CFT partition functions. Furthermore, we demonstrate how this property facilitates a symmetry-preserving spin-blocking RG procedure. In the bulk, this corresponds to adding an additional layer of tetrahedra and probing deeper into the bulk, as reflected by the emergence of the $6j$ symbol $F_{\alpha_6, \alpha_5}^{\text{Racah}} \begin{pmatrix} \alpha_1 & \alpha_4 \\ \alpha_2 & \alpha_3 \end{pmatrix}$ of the SymTFT.

The ground states of the Levin-Wen and Turaev-Viro models satisfy the no-flux constraint, and it has been shown in [24, 82] that this constraint ensures crossing symmetry and re-triangulation invariance, as expressed in (6.2). Conversely, wavefunctions derived from (6.2) inherently satisfy the no-flux condition, identifying them as ground states. Intuitively, this connection arises because the plaquette projection operator in the Levin-Wen model is constructed by effectively gluing a tetrahedron onto the wavefunctions. The work of FRS [32] demonstrates an equivalence between the associativity coefficients $\tilde{C}_{c_1 c_2 c_3}^{n m m'}$ and the BCFT OPE coefficients, translating them into the crossing relation in the CFT. This identification is a direct manifestation of locality in the boundary-to-bulk map.

This is precisely the statement that *crossing symmetry* of the 2D CFT is responsible for the emergence of a 3D bulk. This was first proposed in the large N limit in higher dimensions [158]. Here we see an exact quantum statement in the context of the AdS₃/CFT₂ correspondence. Under

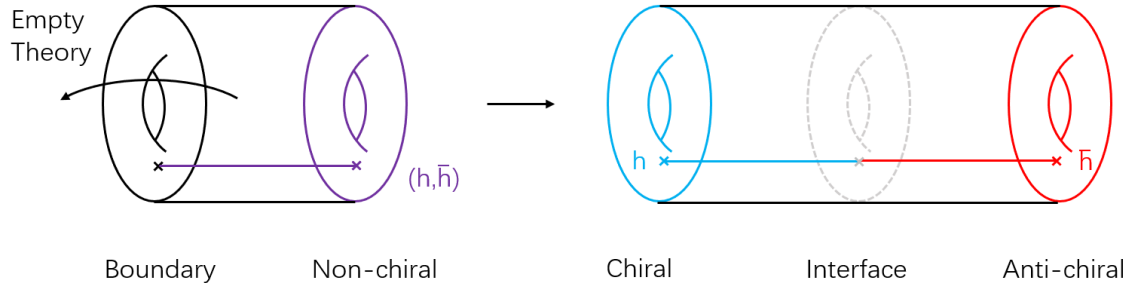


Figure 23: We can unfold the boundary to be an interface or a surface operator. This operator pairs the left moves and right movers into a modular invariant theory.

SymQRG, they manifest themselves as the Wheeler-DeWitt equation.

Four-point crossing symmetry alone is insufficient to define self-consistently the CFT defined on arbitrary 2D manifolds. The additional constraints on the topological boundary are related to *modular invariance* in the CFT. More specifically, as already mentioned above, the CFT boundary conditions are also classified by the objects of $\mathcal{M}_{\mathcal{C}}$. This piece of data is closely related to the modular invariant *spectrum* of the full CFT.

6.2.2 Modular invariance and anyon condensation/gauging

Now let's explain the remaining conditions. As shown in FRS [32], to get a self-consistent CFT which is crossing symmetric and modular-invariant on arbitrary Riemann surfaces, we need to find a so-called symmetric special Frobenius algebra $\mathcal{A} \subset \mathcal{C}$, for \mathcal{C} the Moore-Seiberg category which is a modular tensor category. A Frobenius algebra is a collection of objects in \mathcal{C} , together with a product structure that maps $\mathcal{A} \otimes \mathcal{A} \rightarrow \mathcal{A}$. The algebra admits modules/representations too, and they also form a fusion category $\mathcal{M}(\mathcal{A})$. Each representation $X \in \mathcal{M}(\mathcal{A})$ is also a collection of objects in \mathcal{C} . They are characterized by the action of the algebra on them. i.e. $\rho_X : \mathcal{A} \otimes X \rightarrow X$. ρ_X is the counter-part of representation matrices of a group G while \mathcal{A} plays the role of the group G .

In the left-right CFT with SymTFT given by $\mathcal{C} \boxtimes \bar{\mathcal{C}}$, the Frobenius algebra $\mathcal{A} \subset \mathcal{C}$ defines a topological boundary condition for $\mathcal{C} \boxtimes \bar{\mathcal{C}}$ [32], or in other words, an interface with the trivial empty theory. We will not enumerate all the algebraic conditions on \mathcal{A} , which can be readily found in [32]. (A concise review can be found in [159]). One important implication however, is that this topological boundary condition $\mathcal{B}_{\mathcal{A}}$ can be understood as the location across which certain “anyon condensation” [160–163] occurs, which convert the topological theory $\mathcal{C} \boxtimes \bar{\mathcal{C}}$ to the trivial theory. The collection of anyons in $\mathcal{C} \boxtimes \bar{\mathcal{C}}$ that condense across the topological boundary $\mathcal{B}_{\mathcal{A}}$ is also an algebraic object called the Lagrangian algebra $\mathcal{L}_{\mathcal{A}} \subset \mathcal{C} \boxtimes \bar{\mathcal{C}}$. $\mathcal{L}_{\mathcal{A}}$ is related to \mathcal{A} by taking the “center” of the latter. Their precise relation can also be found in [32]. Anyon condensation means that certain collections of topological lines “condense” in the trivial phase, and are no longer conserved

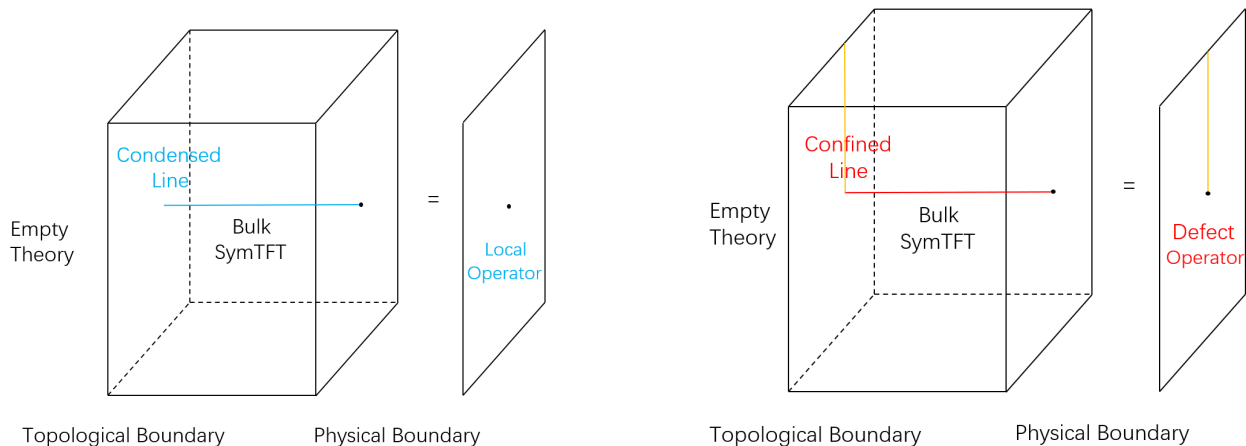


Figure 24: Left: local operators in 2D comes from condensed line operators in the 3D bulk; Right: defect operators in 2D comes from confined line operators in the 3D bulk. In both pictures, there is only an empty theory to the left of the topological boundary after anyon condensation.

quantities. The topological boundary as an interface between the TQFT and the condensed phase is where these condensed lines could enter and disappear into the condensate. The collection of condensed lines carry precisely the topological charge of “local operators” of the D dimensional theory. The topological defect lines of the D dimensional theory correspond to lines that could not pass through the boundary, and are called “confined”. They are restricted to the boundary because of the non-trivial statistics with the condensate. This is nicely explained in [55, 164] in the case of 2D rational CFT and is illustrated in Fig. 24. The condition of symmetric special Frobenius algebra makes sure that the topological defect lines in the bulk are either condensed or confined, and no lines can leak through it, thus leaving the other side of the topological boundary an empty theory.

The condensed collection of lines, which forms a Lagrangian algebra $\mathcal{L}_{\mathcal{A}}$ is known to be in 1-1 correspondence with modular invariants [165]. Therefore, each topological boundary $\mathcal{B}_{\mathcal{A}}$ controls the spectrum of local operators in the CFT in turn ensures that this spectrum is modular invariant. The condensation of lines can also be understood as the “gauging” of higher-form symmetries, and it has been proposed that the holographic duals of rational CFTs can be understood as taking the path integral of a pair of Chern-Simons theories and gauging the corresponding higher-form symmetries [119]. Before gauging, the ground states of the TQFT are on equal footing, and each produces some combination of CFT conformal blocks [78] that generically cannot exist independently in 2D (i.e. not modular invariant). After gauging, however, it singles out a unique ground state of the TQFT, so that the 3D bulk can be effectively collapsed, allowing the 2D theory to stand on its own, suggesting that the latter has an anomaly free spectrum. As an example, consider the theory defined on the torus. This gauging produces a unique choice of spectrum for the sum over the left and right moving sectors, ensuring modular invariance and intrinsic consistency as a 2D CFT. This

pairing of left and right movers can also be visualised by unfolding the doubled Chern-Simons theory at the boundary, and turning the latter into an interface or surface operator inside a single copy of Chern-Simons theory [152, 153, 166], as shown in Fig. 23. In fact, this unfolded picture lies at the heart of the FRS construction [32].

For example, diagonal RCFT corresponds to condensation of diagonal pairs of lines $i \otimes \bar{i}$, $\forall i \in \mathcal{C}$. This corresponds to taking $\mathcal{M}_{\mathcal{C}} = \mathcal{C}$, or equivalently, $\mathcal{A} = 1$. This module category/Frobenius algebra exists in all fusion categories \mathcal{C} . Liouville theory corresponds to this diagonal gauging for two copies of the Virasoro TQFT, as explained in [1, 22], and illustrated in (5.28). Other choices of condensation can provide theories with states of non-zero integer spin³⁵. We note that for more general irrational CFTs one would have to look for more non-trivial \mathcal{A} , which is certainly a highly non-trivial problem for irrational \mathcal{C} ³⁶.

The bottom line is that each such Frobenius algebra \mathcal{A} determines a *modular invariant* full CFT associated with the Moore-Seiberg data \mathcal{C} , and at the same time, the $\mathcal{M}(\mathcal{A})$ for given \mathcal{A} can be identified with $\mathcal{M}_{\mathcal{C}}$ [32]. In other words, the Frobenius algebra \mathcal{A} determines both the full modular invariant CFT spectrum, and also its boundary conditions and boundary changing operators.

We are now ready to address the question of the precise state $|\Psi\rangle_{\Lambda}$ selected by a given CFT. This state arises directly from the bulk path integral combined with the topological boundary. Specifically, the state resides on one of the boundaries of $\Sigma_2 \times I$, while the other boundary is labeled by $\mathcal{M}_{\mathcal{C}}$, as depicted in Fig. 4³⁷. The topological holographic principle implies that the topological boundary conditions of the Turaev-Viro TQFT associated with $\mathcal{M}_{\mathcal{C}}$, or equivalently $\mathcal{M}(\mathcal{A})$, provide the complete data required to determine the full CFT. We can explicitly express the corresponding state for any 2D CFT on the string-net Hilbert space using the BCFT OPE coefficients, as shown in (4.10)³⁸.

6.3 Dynamics vs. kinematics – where is the information encoded?

We have discussed in detail the roles played by the state $|\Psi\rangle$, which encodes information about the topological boundary of the sandwich; and the state $\langle\Omega|$, which governs the physical boundary. In [5], it is observed that the physical boundary contains the dynamics of the theory, while the SymTFT and the topological boundary are responsible solely for the symmetries, when the symmetries form a

³⁵A nontrivial Frobenius algebra \mathcal{A} will provide a theory other than Liouville theory, whose bulk SymTFT is two copies of the Virasoro TQFT, potentially with non-zero spinning states.

³⁶Strictly speaking, since there are now infinitely many objects, this is no longer a fusion category. However, the success in Liouville theory suggests the existence of a generalized mathematical framework that extends to the irrational case.

³⁷There is an alternative way to understand this state. Instead of directly using the generalized $6j$ symbols as in (4.10), one can also consider coloring the topological boundary by the coefficients μ defining the product morphism of the corresponding Frobenius algebra \mathcal{A} , as illustrated in [29, 32].

³⁸This state for which the labels $\sigma \in \mathcal{M}_{\mathcal{C}}$ has appeared and been discussed in the tensor network literature exploring different Levin-Wen ground states [32, 87]. In some cases, different $\mathcal{M}_{\mathcal{C}}$ can provide different representations of the same ground state.

discrete group. This result appears to contradict our discussion and the AdS/CFT correspondence, where $\langle\Omega|$ seems to be merely kinematical, constructed from conformal blocks, while the state $|\Psi\rangle$ which associates to a topological boundary, carries the structure coefficients of the CFT, which are typically associated with the theory's dynamics.

In fact, for each individual theory, there can be multiple ways to realize it as a sandwich. As noted in the Introduction, the location where dynamics is encoded depends on the extent to which the theory's symmetries are explicitly realized in the SymTFT. When the SymTFT captures only a limited subset of the CFT symmetries, the physical boundary state $\langle\Omega|$ retains a larger portion of the dynamical data. Conversely, as more symmetries are made explicit within the SymTFT, the physical boundary state simplifies accordingly. If *all* the symmetries are made explicit in the SymTFT, the physical boundary becomes purely kinematical, and the bulk together with the topological boundary, determines the theory's dynamics.

This reasoning can be illustrated using the paradigmatic example of the Ising CFT. The Ising CFT has a \mathbb{Z}_2 global symmetry, and its path integral can be expressed as a sandwich where the SymTFT bulk is the \mathbb{Z}_2 toric code in 2+1 dimensions. In this case, the boundary condition $\langle\Omega|$ is more nontrivial: different conformal primaries with the same \mathbb{Z}_2 charges are nontrivially packaged within $\langle\Omega|$. If, however, we extract the complete set of symmetries, including all non-invertible ones, the bulk SymTFT becomes the 2+1D Turaev-Viro TQFT/Levin-Wen model based on the Ising category. In this scenario, as in other rational theories, the topological boundary and the bulk contain the CFT's structure coefficients, making the physical boundary purely kinematical. Therefore, the AdS/CFT correspondence can be understood as the *maximal* SymFT sandwich reconstruction of the CFT!

The advantage of the sandwich construction thus lies in its ability to cleanly separate the kinematical part of a lower-dimensional QFT as a boundary condition, while the dynamical part is captured by the bulk (together with the topological boundary, even if this is not always explicit), as what we believe the AdS/CFT correspondence is doing.

We emphasize that in the conventional study of the AdS/CFT correspondence, we only specify the asymptotic boundary condition. This precisely corresponds to our ${}_{\Lambda}\langle\Omega|$ state, which is constructed from conformal blocks and represents the conformal symmetry at the boundary. The conventional approach then involves summing over all the smooth bulk saddles compatible with these boundary conditions. For example, with a torus boundary, we include a sum over $SL(2, \mathbb{Z})$ modular images, corresponding to different contractible cycles in the solid torus, and this ensures the modular invariance of a potential 2D dual [167, 168]. However, this approach generally does not yield a *bona fide* unitary 2D quantum mechanical theory. In 2D CFTs, modular invariance typically arises from a carefully organized spectrum of states that transform into each other under $SL(2, \mathbb{Z})$, rather than from summing over modular images of individual sectors. This latter perspective allows us to interpret the topological boundary condition together with the 3D bulk, or $|\Psi\rangle_{\Lambda}$ as determining the

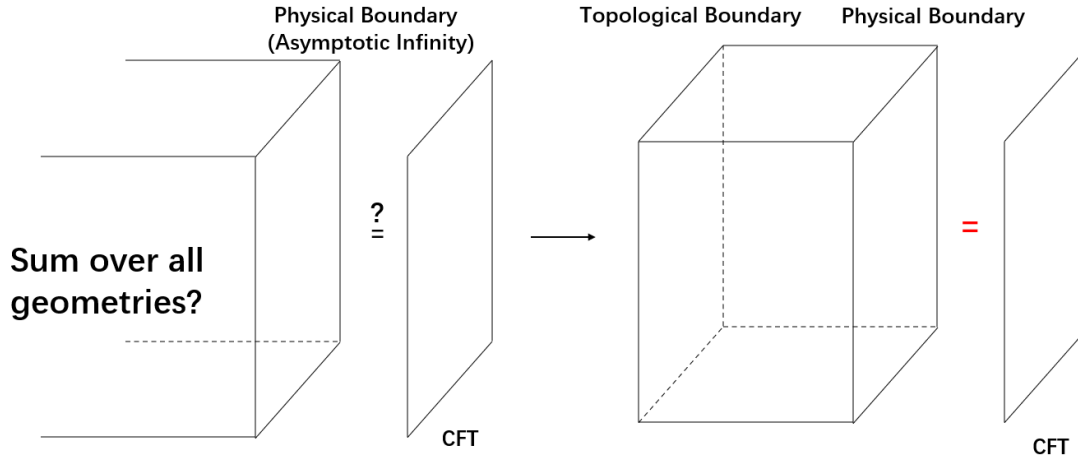


Figure 25: On the left, we have the conventional AdS/CFT dictionary, where the bulk path integral involves summing over geometries compatible with a given boundary condition. In general, this sum does not match the partition function of a CFT. On the right, the sandwich construction introduces a topological boundary that can be interpreted as a choice of measure for the bulk path integral. This choice ensures that the bulk path integral precisely reproduces the partition function of a CFT.

quantum measure of the 3D gravity path integral, effectively selecting which bulk geometries (and also non-geometrical solutions) to include in order to construct a dual to 2D CFTs by design. Notice that even in the semi-classical limit, the choice of quantum measure determines which saddles are included in the saddle point approximation when the integration contour is deformed³⁹. Different choices of $|\Psi\rangle_\Lambda$ would give us different UV completions for the bulk quantum gravity theory, and the dictionary is not complete before we specify this information⁴⁰. See Fig. 25 for an illustration of these two dictionaries. We will argue below that this is related to a solution of the factorization puzzle. If we view the CFT as providing a self-consistent UV completion of AdS quantum gravity, then we probably shall not sum over all possible geometries for a consistent UV completion, and the question of which geometries should be included in the gravitational path integral is inherently answered by the structure of the CFT.

Here, let us pause to emphasize a different perspective compared to the discussion of holographic duals constructed from gauging [119], as briefly mentioned above. It was suggested there that the corresponding bulk is trivial. This is equivalent to squeezing the sandwich flat, and focusing on the empty theory beyond the topological boundary. However, from our perspective, the holographic bulk dual is actually *not* trivial when one focuses on $|\Psi\rangle_\Lambda$ and retains the non-trivial bulk region

³⁹A simple example is the Stokes phenomena, see for example [169, 170].

⁴⁰Unless there are some other reasons for there to be a unique choice of $|\Psi\rangle_\Lambda$ [171], so we can leave this choice implicit.

between the physical boundary and the topological boundary.

Finally, let us comment on the observation that flows driven by $T\bar{T}$ in *any* CFT appear to always produce an emergent gravity bulk, referred to as a “fake bulk” in [66]. In light of the discussion in this paper, it becomes clear that the bulk described in [66] corresponds to $\hat{U}_{\text{RG}}^{\Lambda, \Lambda'}$ in (4.13). As we have demonstrated, the $T\bar{T}$ deformation preserves all topological symmetries, and the RG flow it generates can be expressed through an RG kernel, effectively represented by a gravitational path integral over quantum geometries. However, the complete integral of the bulk path is governed by the state $|\Psi\rangle_{\Lambda}$, with the complete quantum measure determined by the infrared topological boundary condition. This boundary condition specifies which quantum geometries are included in the path integral. In the context of [66], this crucial aspect is implicitly embedded within the initial CFT path integral.

We have demonstrated that the exact correspondence between a 2D boundary and a 3D bulk theory arises from the full set of CFT self-consistency relations, which can be succinctly summarized by *crossing symmetry* and *modular invariance* [32, 42, 48, 53]. These self-consistency relations of 2D CFTs can also be elegantly encapsulated into algebraic equations connected to the 3D bulk SymTFT.

In summary, the *crossing symmetry* ensures the existence of a topological ground state $|\Psi\rangle$ that satisfies the no-flux condition. This property allows a symmetry-preserving RG flow to probe deeper into the bulk, relating the RG Callan-Symanzik equation into the Wheeler-DeWitt equation. On the other hand, *modular invariance* provides the framework to end this procedure by specifying the quantum measure in 3D. This measure is encoded in the choice of a specific ground state $|\Psi\rangle$, which allows the termination and collapse of the 3D bulk into an intrinsically well-defined 2D theory.

6.4 Implications for Quantum Gravity

We have explored the algebraic constraints on the topological boundary and their physical significance. In this subsection, we will examine the implications of these algebraic properties within the symmetry framework for Quantum Gravity. Specifically, we will first demonstrate how the topological boundary addresses the factorization puzzle. Following this, we will show that the Lorentzian-signature out-of-time-ordered correlation function is entirely encoded in the Moore-Seiberg data of 2D CFTs, revealing Chaos from (topological) Order.

6.4.1 Wormholes, null states, and factorization

Recently, there has been growing interest in spacetime wormholes due to the remarkable observation made in [172, 173] that in some models, the inclusion of certain wormhole saddles in the Euclidean gravitational path integral can reproduce the Page curve at leading order in G_N , a result that has been proposed as a key feature for ensuring unitary black hole evaporation, resolving the information paradox [174]. Although these calculations involve large N approximations and do not offer a dynamical mechanism explaining how information escapes from black holes, they represent the first

successful reproduction of the Page curve through a gravity computation. This is particularly notable because the problem has long been considered sensitive to UV dynamics, and an answer was not anticipated within the framework of semi-classical approximations. On the other hand, the inclusion of new wormhole saddles not only led to the factorization puzzle [175], but also calls into question the precise interpretation of the holographic correspondence. Should a given bulk describes a unique CFT, or an ensemble average of them [171, 176]? The modern perspective is that, in general, *semi-classical* gravity is a coarse-grained description of the dual chaotic CFT [140, 150, 176], in the sense of the ETH [139], as we explained above.

In fact, in the spirit of [173, 177], we might formulate the information paradox as the following problem: we have a matrix (reduced density matrix for radiation) with a large dimension, which is approximately diagonal (thermal density matrix [174]), and this seems to contradict the rank of this matrix, bounded by the entropy e^S [178]. One resolution to this problem lies in the off-diagonal elements of the matrix, which reduces the rank of the matrix. The observation made in [172, 173] is that in certain computations such as the higher moments of the reduced density matrix of radiation, we can use the Euclidean spacetime wormhole saddles to reduce the rank, at leading orders in G_N . In similar settings, it is also shown that we can also reduce the rank of the Gram matrix of certain overcomplete black hole microstates constructed from dust particles, using wormhole saddles, to the black hole entropy $e^{A/4}$, at leading order in G_N [179].

Is there a more microscopic and non-perturbative explanation for this reduction in rank? An answer to this question was proposed in [177], which highlighted that the reduction of rank in a matrix corresponds to the existence of kernel or *null states* in the theory, inherently tied to constraints and gauge equivalence in quantum gravity. In the current context, this gauge equivalence is suggested to arise from an equivalence relation imposed on geometries with different topologies, a perspective emphasized in [180]⁴¹.

In our framework, there are two types of constraints in the CFT and its dual gravity, as explained in Sec. 6.2. The first is the Wheeler-DeWitt equation, which ensures that $|\Psi\rangle_\Lambda$ is a ground state of the Turaev-Viro model and satisfies the no-flux condition, allowing us to re-triangulate the 2D radial slice. In the language of the CFT, this corresponds to the crossing invariance condition (C.5). The second constraint is the gauging constraint in the bulk SymTFT, associated with modular invariance on the boundary. This constraint seems to be the one encoding the gauge equivalence of different topologies, a perspective also suggested in [119].

Let us illustrate this with the factorization puzzle for partition functions [175]. Consider computing two copies of the CFT partition functions, $Z_1(m_1)Z_2(m_2)$, where m_1 and m_2 are the moduli of the 2D CFTs. According to the conventional semi-classical holographic dictionary, this corresponds to fixing boundary conditions with two asymptotic boundaries and finding all bulk solutions compatible with these boundary conditions. The two dominant saddles in this setup are the disconnected

⁴¹See also earlier works pointing out that the number of connected components of space cannot serve as a non-perturbative diffeomorphism-invariant operator in quantum gravity [181].

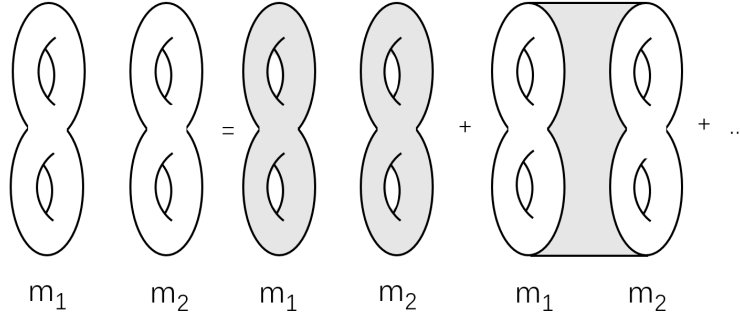


Figure 26: The computation of $Z_1(m_1)Z_2(m_2)$ with the conventional semi-classical holographic dictionary. This approach fixes two distinct boundary conditions corresponding to m_1 and m_2 , then identifies all geometrical saddles consistent with these asymptotic boundaries. The two leading saddles in this setup are a disconnected configuration and a wormhole saddle that connects the two boundaries, as illustrated on the right-hand side of the equation. Notably, this result does not factorize, in contrast to the original factorized result in the CFT.

configuration and the connected wormhole configuration, as illustrated in Fig. 26⁴². This leads to the factorization puzzle. However, in sandwich construction, the way to recover the original factorized answer is straightforward: we simply insert two topological boundaries into the “connected bulk”, effectively splitting it into two “disconnected” pieces separated by the empty theory. This factorization arises because anyons in the bulk are either condensed (they are gauged and disappear) or confined (they are stuck on the topological boundary), preventing them from leaking into the intermediate empty region. See Fig. 27 for an illustration. The sandwich construction thus seems to elegantly provide a solution to the factorization puzzle through the algebraic properties of the CFT and SymTFT! We emphasize that it is not necessary to stick to this language of topological boundary conditions to observe factorization. Instead, we can interpret it as defining the quantum measure for the bulk 3D gravity path integral as we explained above. From this perspective, the factorization of 3D quantum gravity arises from a precise definition of the measure for the bulk theory (which might include non-geometrical contributions).

Each choice of topological boundary condition appears to correspond to a choice of an “ α state” in the language of [177, 183], where the partition functions factorize, as suggested by [119]. In our formalism, this is encoded in our state $|\Psi\rangle_\Lambda$. However, as explained above, our perspective differs slightly from [119]. Specifically, we do not collapse the entire bulk and place the topological structure directly on top the physical boundaries, nor do we view the bulk as entirely trivial (which is the region beyond the topological boundary where anyon condensation occurred). The bulk remains non-

⁴²We deliberately use the genus two Riemann surfaces as our 2D boundary manifolds to get a connected wormhole saddle in 3D. In the case of torus boundaries in pure gravity, it is known that there are no such saddles. However, we can perform an exact computation for these off-shell configurations using some assumptions [117, 143, 176]. However, subtleties with respect to the bulk mapping class group in 3D gravity and the connection to random matrix spectral statistics in 2D [117, 182] are still not completely understood. Our exact formulation might give hints on this problem.

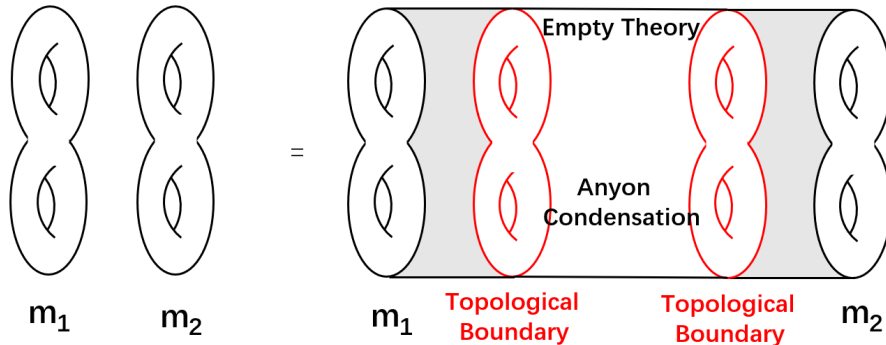


Figure 27: The computation of $Z_1(m_1)Z_2(m_2)$ using the sandwich construction factorizes into product of $Z_1(m_1)$ and $Z_2(m_2)$ by construction. The topological boundaries ensure that anyons in the bulk are either condensed or confined on the topological boundaries, so the “connected” bulk we draw above is in fact two “disconnected” pieces.

trivial within the sandwich, and in this light, the factorization puzzle can be resolved by identifying the quantum measure for the gravitational path integral over the non-trivial bulk which is encoded in the topological boundary condition, or the state $|\Psi\rangle_\Lambda$.

The AdS/CFT correspondence supposedly identifies given CFT to a particular quantum theory of gravity. From the SymTFT perspective, the non-perturbative completion contains UV-sensitive data such as the quantum measure that is specified by the dual CFT. Generic choices or assumptions about such data specifying the bulk path-integral most likely do not have a quantum CFT dual. We believe that translating these insights back into the semi-classical picture can guide us toward a deeper understanding of quantum gravity.

For example, translating Fig. 27 back into the semi-classical picture shown in Fig. 26, understanding the additional elements required for factorization in semi-classical gravity, and exploring connections to earlier proposals in other gravitational or string-theoretic models, such as those in [177, 184–186]—are important directions for future investigation. Recently, it has also been proposed that an underlying symmetry principle, related to a gauge constraint, could eliminate worm-hole contributions in the gravitational path integral, producing a unitary quantum theory. It is also worth understanding the precise relation between the Hopf algebra described in [187]⁴³, the “baby universe category” proposed in [188], and the Moore-Seiberg symmetry category \mathcal{C} for 2D CFTs.

6.4.2 Chaos from (topological) Order

Recent studies have revealed the fascinating connection between quantum gravity and quantum chaos [189, 190]. It is natural to ask, where is quantum chaos in our formalism based on topological symmetries? Naively, the study of symmetry provides an organizing framework and defines the

⁴³Quantum groups are Hopf algebras by definition. In the case of rational CFTs, recovering a quantum group from the modular tensor category associated with the CFT can be done by the Tannaka duality.

superselection sectors of a theory, positioning it in seemingly direct contrast to the disordered nature of chaos, making them, at best, tangential properties of the theory. However, we will see that at least in the context of 2d CFTs, the most common diagnostic of quantum chaos, out-of-time-ordered correlator(OTOC) in *Lorentzian signature* [191], are completely determined by the Moore Seiberg data of the SymTFT.

Consider any two CFT primary operators W and V , the OTOC is defined as the normalized four point function

$$C(t) = \frac{\langle W(t)VW(t)V \rangle_\beta}{\langle W(t)W(t) \rangle_\beta \langle VV \rangle_\beta}, \quad (6.3)$$

in the thermal state with inverse temperature β . It is crucial that the four operators are in *Lorentzian* out-of-time ordering. In fact, if the four operators are all in Euclidean signature, the ordering of the operators does not matter at all, and we can even use this single-valuedness as one of the bootstrap equations. The Lorentzian correlators are all analytical continuation of Euclidean ones, and each choice of the ordering in Lorentzian signature correlators correspond to a specific $i\epsilon$ prescription [189, 192, 193]⁴⁴. More specifically, the CFT four point functions in Euclidean signature can be expanded in terms of the conformal blocks as:

$$\sum_{h_i, \bar{h}_i} C_{VVO_{h_i, \bar{h}_i}} C_{WWO_{h_i, \bar{h}_i}} \mathcal{F}_{WW}^{VV}(h_i, z) \bar{\mathcal{F}}_{WW}^{VV}(\bar{h}_i, \bar{z}), \quad (6.4)$$

where we inserted a basis of states labeled by conformal families h_i, \bar{h}_i . The $C_{VVO_{h_i, \bar{h}_i}}$ and $C_{WWO_{h_i, \bar{h}_i}}$ are OPE coefficients, and $\mathcal{F}_{WW}^{VV}(h_i, z)$ is the holomorphic conformal block with cross ratios z (with $\bar{\mathcal{F}}_{WW}^{VV}(\bar{h}_i, \bar{z})$ the anti-holomorphic counterpart). The analytical structure of the conformal blocks is shown in Fig. 28.

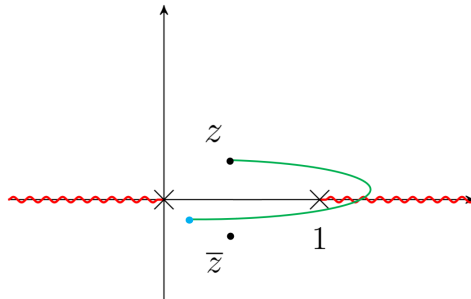


Figure 28: The kinematical regime related to the computation of the OTOC is a Lorentzian kinematics that lies on the “second sheet”, meaning we need to traverse the branch cut on $(1, \infty)$ and pick up a monodromy for the chiral conformal blocks.

In Euclidean signature, the cross ratios z and \bar{z} are complex conjugates of each other, shown

⁴⁴Study of Lorentzian CFT in the analytical conformal bootstrap program in recent years have lead to fruitful new results, see [194].

as the black dots. In Lorentzian signature, z and \bar{z} are independent, and also, when we carefully follow the $i\epsilon$ prescription in Lorentzian signature, we see that the cross ratio z in the OTOC crosses the branch cut at $z = 1$, which is usually said to “go to the second sheet”, and then land on the blue dot on the second sheet. Notice that \bar{z} however does not cross any branch cuts, so there is an asymmetry between z and \bar{z} , which is important to get a different full correlator in Lorentzian signature. The branch cut in the cross ratio space for the conformal blocks also has an interpretation in real space [195, 196], as coming from the W operator entering the lightcone of the V operator, and the difference in the choice of branch cuts is what gives the non-vanishing commutator for timelike separated operators, and is intrinsic to causality and Lorentzian signature. The “Lyapunov regime” common in the study of chaos further corresponds to taking $z, \bar{z} \rightarrow 0$, and this kinematical regime is usually called the CFT Regge limit [193, 197]. Assuming Virasoro identity block dominance and using the explicit expression for the identity block in the heavy-heavy-light-light limit, we can get the maximal Lyapunov exponent behavior expected for 2D holographic CFTs [198, 199].

In fact, there is an exact answer for the OTOC, without using any assumptions, using the fact that the winding around branch point $z = 1$ is picking up a monodromy of the conformal blocks, and there is a monodromy matrix M implementing it exactly [42], such that

$$\mathcal{F}_{WW}^{VV}(h_i, z) \xrightarrow{(1-z) \rightarrow e^{-2\pi i}(1-z)} \sum_{h_j} M_{ij} \mathcal{F}_{WW}^{VV}(h_j, z). \quad (6.5)$$

In addition, the monodromy matrix can be just expressed in terms of the $6j$ symbols, as ⁴⁵

$$M_{ij} = \sum_{h_k} e^{-2\pi i(h_k - h_W - h_V)} F_{h_i, h_k} \begin{pmatrix} h_V & h_V \\ h_W & h_W \end{pmatrix} F_{h_k, h_j} \begin{pmatrix} h_V & h_W \\ h_V & h_W \end{pmatrix}. \quad (6.6)$$

The fact that we can write the OTOC in terms of the topological data is certainly not just a coincidence. It is the fact that the monodromy is just a combination of braid moves, as shown in Fig. 29⁴⁶. From the bulk-boundary correspondence [78], or unfolding the sandwich construction, we can also see the monodromy explicitly as anyons nontrivially linking themselves in the bulk, as shown in [200].

This point of view of understanding quantum chaos and OTOC from the exchange algebra was emphasized in the context of 2D CFT in [51, 201, 202]. In the context of holography, this is the dual of the bulk exchange algebra found in [203], responsible for the exponential blueshift coming from the Dray and ’t Hooft shockwave effect [204]. As noted in [51], the goal of conformal bootstrap is

⁴⁵We use a slightly different convention from above sections, where now the chiral primaries are labeled by their conformal dimensions h instead of the previously used α .

⁴⁶Here, we are employing a reversed logic compared to [42, 48]: Suppose we already possess the Moore-Seiberg data of the CFT. We can use this data to determine the conformal blocks on the second sheet. Notably, this data was originally derived by first analyzing the monodromies of the conformal blocks.

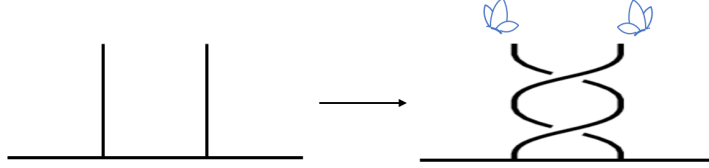


Figure 29: The monodromy of conformal blocks is determined by the braid matrix of the underlying Moore-Seiberg tensor category. This controls the Lyapunov behavior and the butterfly effect, encapsulating the idea of “Chaos from Order”.

to ensure that correlation functions remain single-valued in Euclidean signature. In other words, quantum statistics are invisible or “confined” in Euclidean, non-chiral, full CFTs. However, after we solve the bootstrap equations which are topological in nature as we explained, and manage to hide the quantum statistics, these topological data will get “deconfined” in Lorentzian signature, controlling the Lorentzian dynamics, causality(commutator), and information scrambling of the theory, which gives “*Chaos from Order*”.

Finally, we want to point out an interesting fact. Rational CFTs, whose SymTFTs are governed by modular tensor categories, which are finite in nature, are *not* chaotic. Quantum chaos only appears when we have irrational CFTs, or infinitely many degrees of freedom. This suggests “infinitely more is more different” [205], and we will discuss the quest for some new infinite-dimensional mathematical structure in the discussion section.

7 Discussions

In this paper, we demonstrated how a holographic bulk emerges naturally from considerations of a topological symmetry-preserving quantum RG flow. When the symmetry preserved is the infinite collection of Virasoro lines in a 2D theory, then a 3D gravitational bulk emerges. The full bulk path-integral however sensitively depends on the complete non-perturbative definition of the CFT – the latter essentially determines a 3D state $|\Psi\rangle$ that gives the precise quantum measure of the bulk path-integral, and this information is theory dependent even for theories preserving the same collection of symmetries.

So far the explicit examples we have considered, where non-perturbative structure coefficients have been solved completely, are restricted to rational CFTs, and also the Liouville theory, which despite being irrational, is very special. The lack of a vacuum state in the normalizable physical spectrum of Virasoro TQFT [22] and thus its diagonal gauging⁴⁷, leads to a density of states that deviate from the Cardy’s universal result, makes it a rather atypical example.

⁴⁷The normalizable physical states, forming a complete basis in the Hilbert space of the Virasoro TQFT, are given by Liouville conformal blocks corresponding to hyperbolic monodromies. This set includes all states above the black hole threshold but excludes the vacuum state [22]. The vacuum state has been argued to arise from a path integral that does not produce normalizable states within the TQFT.

While certain choice of measure of the bulk path-integral may lead to ensemble averages of CFTs, we hope that we have shown, at least with certain examples that in principle an appropriate measure can be chosen to recover a precise CFT. How such quantum measure can be constructed for more general irrational CFT, perhaps through the search of *Frobenius algebra* of the “category” of Virasoro lines, is certainly worth further exploration.

It would be extremely important to find examples that are more typically holographic although we expect to have presented evidence that the framework of SymQRG/QG would continue to hold more generally. Nevertheless, our construction appears to suggest that a non-perturbative understanding of the CFT offers the ultimate guidance to constructing the corresponding bulk Quantum Gravity.

We conclude this paper with a discussion of some interesting future directions.

von Neumann algebra and 2D CFT

As discussed above, the bulk dual of the CFT is represented by a sum over quantum geometries, providing an exact description at finite N . In the large N limit, certain quantum geometries emerge as dominant saddles in this sum, allowing for a semi-classical, low-energy geometrical description. To better understand this emergence, recent studies have proposed algebraic quantum field theory (AQFT), specifically von Neumann algebras, as a suitable framework, noting the appearance of emergent Type III von Neumann algebra structures in the large N limit [206].

A natural question arises: how are these two distinct algebraic approaches for field theories and emergence of geometry related, and how are categorical structures, such as the $6j$ symbols, encoded within von Neumann algebras? In 2D CFT, there appears to be a dictionary connecting these approaches. AQFT in 2D is rigorously constructed using “conformal nets”, and its connection to the functorial formalism is discussed in [207]. A key element in this framework is the role of superselection sectors and “subfactor theory” [208]⁴⁸. This approach might provide a new understanding of the Type II algebra structures observed in the context of higher-dimensional gravity [209], which plays a role in black holes and cosmology [210,211]. Applied to 3D gravity, this Type II algebra is analogous to the JT gravity case studied in [212]. In the current situation, we even achieve its UV completion, since we start from a 2D CFT. We will report further results on these ideas in future work.

Infinitely more is more different

New structures are known to emerge in the study of quantum many-body problems, often encapsulated by the slogan “more is different” [213]. In Sec. 4, we saw an example of this principle, where an *infinite* bond dimension for the $\langle \Omega |$ state allows us to place a gapless field theory on a lattice in an exact fashion. Here, it is probably more appropriate to say that ‘infinitely more is more different’ [205]. This infinity stems from the infinite spacetime entanglement inherent in field theories, analogous to the Type III algebra structure in quantum field theories [214].

⁴⁸We thank Keiichiro Furuya for discussions on this topic and collaboration on related project.

In the case of irrational CFTs, an additional layer of infinity appears due to the infinite number of primary fields in $|\Psi\rangle$. This infinity drives the large N limit of a CFT and enables chaotic behavior, in contrast to rational CFTs. It mirrors the emergence of Type III factors in the large N limit as discussed above [206]. For the SymTFT description, this implies that an infinite number of anyons are required to describe the bulk theory of gravity. Consequently, for irrational CFTs, we do not have a fusion category, which by definition requires finitely many objects. This fact also limits our Turaev-Viro construction for $U_q(SL(2, \mathbb{R}))$, as it lacks the 4-1 move invariance. However, when we consider these three-dimensional manifolds with boundaries, combined with boundary conformal blocks, the construction does make sense and yields a convergent result consistent with the Virasoro/Teichmüller TQFT, at least for the diagonal Liouville CFT, as explicitly shown in [1, 31]. This suggests the existence of a novel mathematical structure, essential for the study of *quantum gravity*.

This resonates with an analogy from quantum mechanics: the commutation relation

$$[\hat{x}, \hat{p}] = i\hbar . \tag{7.1}$$

cannot hold in a finite-dimensional Hilbert space, as taking the trace on both sides leads to a contradiction. A precise understanding of these new categorical structures, which require infinitely many objects, remains an open and important question.

Stringy dual

In this paper, we focus primarily on the topological symmetries associated only with the Virasoro algebra, which is related to pure gravity as demonstrated in Sec. 5. To explore theories with stringy duals, which include non-geometrical components (such as higher spin fields), we will consider a broader set of topological symmetries within the theory. For instance, the bulk dual of symmetric orbifolds of certain CFTs has been shown to correspond to tensionless strings in AdS₃ [215]. It would be interesting to examine the topological symmetries of these theories in greater detail, to understand how the bulk AdS₃ × S³ × T⁴ emerging from our construction, and to see how they relate to the worldsheet perspective. In that case, we might still construct the bulk dual using tetrahedra; however, the physical meaning associated with the charges will differ from that of the Virasoro case, where they correspond to geodesic distances. Some of the charges might have the interpretation of extra compact dimensions in the bulk.

Higher dimensional AdS/CFT correspondence

Our tensor network formalism depends significantly on the unique properties of 3D gravity, particularly its topological nature. Extending this line of reasoning may provide insight into constructing a non-perturbative bulk dual in higher dimensions. However, since gravitons are dynamical in higher dimensions, we want to explore several possibilities to address this tension. One possibility, as noted

in [37], is that the bulk theory may lose its topological character due to the irrational nature of the symmetry. Another possibility is that the bulk topological invariance could be spontaneously broken, even if it initially exhibits a topological structure. Alternatively, it is possible that the bulk theory remains genuinely topological in the non-perturbative regime.

An important lesson from the study of string theory, and recent studies on generalized symmetries is that understanding the non-perturbative aspects of quantum field theories or their gravitational duals benefits greatly from a categorical approach, which involves examining structures across various dimensions and their interactions. Consequently, in higher-dimensional CFTs and holographic correspondences, the analysis of local correlation functions alone seems to be insufficient to capture all non-perturbative information, and a comprehensive understanding of the theory requires examining the roles of defects and boundaries within it. Finally, we note that the higher-dimensional analogue of the $T\bar{T}$ deformation currently only applies in the semi-classical large N limit [68, 71]. Away from the large N limit, does this SymTFT perspective provide a non-perturbative understanding?

Holographic complexity

The volume/action of the bulk theory is proposed to be connected to the notion of complexity in the CFT [216]. There is a large volume of work exploring this connection, and it has been shown that perhaps more generally there are an infinite class of bulk quantities that could be understood as complexity [217]. However, precise definitions of complexity on both sides have been tricky to identify. Our discrete formulation of the path-integral could be used to define notions of complexity in field theories that can be directly translated between the bulk and the boundary. For example, since each $6j$ symbol for the Virasoro lines can be interpreted as the volume of hyperbolic tetrahedra, we can assign definite complexity to individual “gate” corresponding to the $6j$ symbols that builds up the path-integral. Our $U_q(SL(2, \mathbb{R}))$ $6j$ symbols seem to be particularly promising, since Liouville theory has been proposed to capture path integral complexity for 2D CFTs [218].

Acknowledgement

We thank Nathan Benjamin, Christian Ferko, Keiichiro Furuya, Hao Geng, Sarah Harrison, Daniel Jafferis, Hong Liu, Juan Maldacena, Shinsei Ryu, Sahand Seifnashri, Shu-Heng Shao, Herman Verlinde and Frank Verstraete for helpful discussions. We thank Wei Bu, Wan Zhen Chua, Christian Ferko, Hao Geng, Ziming Ji, Chen-Te Ma, Yixu Wang, Zixia Wei and Chen Yang for comments and discussions on the draft. We thank Lin Chen, Gong Cheng, Keiichiro Furuya, Hao Geng, Zheng-Cheng Gu, Bing-Xin Lao for collaboration on related projects. We thank Zhenhao Zhou for plotting the 3D diagrams in this paper. YJ thanks Juan Maldacena for the invitation and hospitality during a visit to the Institute for Advanced Study, where the idea of this paper originated from discussions with people there. YJ and NB acknowledge the support by the U.S Department of Energy

ASCR EXPRESS grant, Novel Quantum Algorithms from Fast Classical Transforms, and Northeastern University. LYH acknowledges the support of NSFC (Grant No. 11922502, 11875111). ZL is supported by NSF grant PHY-2110463.

A Review of Turaev-Viro TQFT and fusion category

In this appendix, we provide a review of the Turaev-Viro TQFT [23]. We start from the Turaev-Viro TQFT associated to two copies of the continuum Chern-Simons field theory, and explain its connection to the Roberts invariants [219] defined using handle decomposition. For the Roberts invariant, the ω projection operator plays an important role, which we also use in the main text. Then we provide a review on fusion category theory and discuss the Turaev-Viro TQFT based on fusion categories.

A.1 Turaev-Viro TQFT from Chern-Simons theory

The Turaev-Viro TQFT was originally constructed to produce path integrals over 3D manifolds and recover topological invariants. While the Turaev-Viro TQFT is a discrete TQFT [23], it has been shown that a subclass of it is equivalent to two copies of Chern-Simons (CS) theory with a generic compact (non-) Abelian gauge group G [78], which is easier to understand for field theorists. Here we give an introduction first through the lens of CS theory, before giving the general formulation based on fusion categories.

Consider taking a pair of Chern-Simons gauge theories with the same compact gauge group G (such as $SU(2)$) but opposite chirality. i.e. The action is given by

$$S = \frac{k}{4\pi} \left(\int \text{tr}(A_L \wedge dA_L + \frac{2}{3} A_L \wedge A_L \wedge A_L) \right) - \frac{k}{4\pi} \left(\int \text{tr}(A_R \wedge dA_R + \frac{2}{3} A_R \wedge A_R \wedge A_R) \right), \quad (\text{A.1})$$

for independent gauge fields A_L, A_R , which are Lie algebra valued one forms in the same gauge group G . More explicitly,

$$A_{L,R} = (A_{L,R}^a)_\mu T^a dx^\mu, \quad (\text{A.2})$$

where T^a are generators of the Lie algebra.

It was proven that these classes of theories admit an equivalent discrete Turaev-Viro formulation [23]. We note that the equations of motion for the Lagrange multipliers $A_{L,R;0}$ impose the constraint that the field strengths vanish

$$F_{L,R} \equiv dA_{L,R} - i[A_{L,R}, A_{L,R}] = 0. \quad (\text{A.3})$$

The idea of the discrete formulation of the 3D TQFT is to construct the phase space of the fields on a simplex (i.e. a tetrahedron Δ_3), and then assign the to each field configuration $\{A\}_{\Delta_3}$

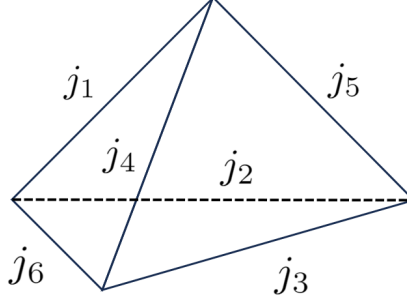


Figure 30: Wilson line network on a tetrahedron.

defined on a simplex a value, which can be understood as $e^{-S(\Delta_3)(\{A\})}$. The path integral $Z(\mathcal{M})$ on an arbitrary manifold \mathcal{M} would be given by triangulating the manifold, coloring the simplices by different field configurations, and finally obtaining

$$Z(\mathcal{M}) = \sum_{\{A\}} \prod_{\Delta_3} e^{-S(\Delta_3)(\{A\})} . \quad (\text{A.4})$$

In the context of Chern-Simons gauge theories, field configurations can be described by the eigenvalues of Wilson line operators. In fact, one can consider networks of open Wilson lines that meet at vertices. Open Wilson lines between two points take the form

$$W_{m_1 m_2}^j(x_1, x_2) = \mathcal{P} \left(\exp \left(\int_{x_1}^{x_2} dx^\mu A_\mu^a T^a(j) \right) \right)_{m_1 m_2} , \quad (\text{A.5})$$

where \mathcal{P} denotes path-ordering, and $T^a(j)$ are generators of the Lie algebra in representation j . The indices m_1, m_2 correspond to the indices of the representation j .

To designate a field configuration to a 3-simplex, it is natural to consider inserting a Wilson line along each edge of a tetrahedron. These Wilson lines meet at a vertex. To ensure gauge invariance, the three representations carried by the three Wilson lines meeting at a vertex should be projected to the gauge-invariant sub-space. The vertex is thus a vector in the “intertwining space”. In a single chiral copy of the Chern-Simons theory, the expectation value of Wilson lines forming a tetrahedron embedded in S^3 takes a simple result.

It is given by the quantum $6j$ symbol

$$\left\langle \prod_{e \in \Delta_3} W^{j_e}(e) \right\rangle_{S^3} = \left\{ \begin{array}{ccc} j_1 & j_2 & j_5 \\ j_3 & j_4 & j_6 \end{array} \right\}_{G_k} \equiv \Gamma_3(\{j_{e \in \Delta_3}\}) , \quad (\text{A.6})$$

where j_i is the label of the representation a Wilson line operator took in the edge i , and e is an edge of the tetrahedron Δ_3 . This configuration of Wilson lines is illustrated in Fig. 30.

This result can be heuristically understood as follows in the classical limit $k \rightarrow \infty$. At every vertex V where the Wilson lines meet, by gauge invariance it should produce an intertwiner, which is the usual *Clebsch Gordon coefficient* for group G in the $k \rightarrow \infty$ limit

$$V_{m_1 m_2 m_3}^{j_1 j_2 j_3} = \begin{bmatrix} j_1 & j_2 & j_3 \\ m_1 & m_2 & m_3 \end{bmatrix}, \quad (\text{A.7})$$

where m_i corresponds to the indices in the representation j_i that the Wilson line carries. Since there are four vertices, it would produce four such intertwiners. Using the extra fact that the local magnetic flux is constrained to be vanishing (A.3), each face of the tetrahedron produces delta functions connecting the indices m_i from different Wilson lines. Finally one makes use of

$$\left\{ \begin{array}{ccc} j_1 & j_2 & j_3 \\ j_3 & j_4 & j_6 \end{array} \right\}_G = \sum_{m_i} \begin{bmatrix} j_1 & j_2 & j_3 \\ m_1 & m_2 & m_3 \end{bmatrix} \begin{bmatrix} j_2 & j_3 & j_6 \\ m_2 & m_3 & m_6 \end{bmatrix} \begin{bmatrix} j_3 & j_4 & j_5 \\ m_3 & m_4 & m_5 \end{bmatrix} \begin{bmatrix} j_4 & j_1 & j_6 \\ m_4 & m_1 & m_6 \end{bmatrix} \quad (\text{A.8})$$

to recover the final result of the $6j$ symbol in (A.6) in the leading $k \rightarrow \infty$ limit.

Equation (A.6) is the non-perturbative result at finite k . At finite k , distinct representations j can be identified. As is well known, the CS action on a manifold with a 2-dimensional boundary leads to boundary terms corresponding to the Wess-Zumino-Witten (WZW) model. The quantized model carries a symmetry given by a Kac-Moody algebra. Each remaining sector j is in one-to-one correspondence with integrable highest weight representations of the Kac-Moody algebra at level k . For example, where $G = SU(2)$, $j \sim k/2 - j$ [78], and we are left with the set of distinct representations $0 \leq j \leq k/2$ for given k .

Each representation j is associated to a “quantum dimension” d_j . In the classical case, d_j is simply the actual dimension of the representation j . At finite k it is an “effective dimension” of the representation in the following sense. Consider a number of Wilson lines ending at punctures of a 2d surface. In the quantized theory, one can obtain the dimension of the Hilbert space on the 2d surface with these punctures. The result is equal to the dimension of fusion space of the representations of the Wilson lines to the trivial representation. In the limit where there is a large number N of the same representation j , the dimension of the fusion space approaches d_j^N , as if this d_j is indeed the internal dimension of the representation j , which is precisely the case in the classical case. This can be readily proved using the Verlinde formula that connects the modular matrix and the fusion coefficient $N_{j_1 j_2}^{j_3} \in \mathbb{Z}_{\geq 0}$ that gives the number of fusion channels between j_1, j_2 and j_3 [20].

It can be extracted from the expectation value of a single j Wilson loop [78].

$$\langle W^j(C) \rangle_{S^3} \equiv d_j = \frac{S_{0j}}{S_{00}}, \quad (\text{A.9})$$

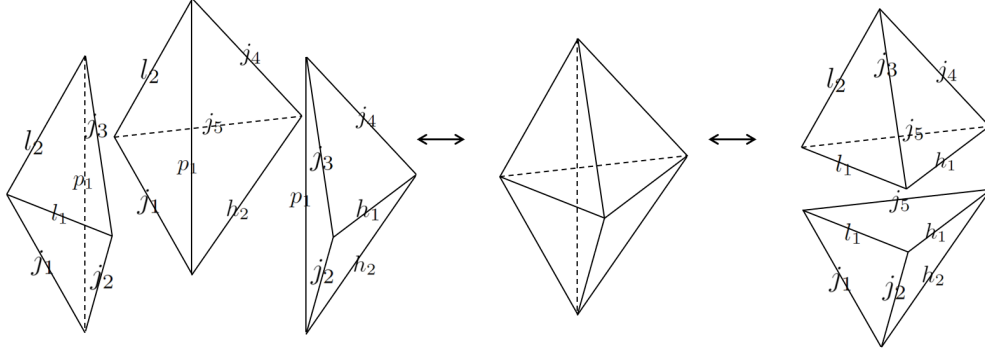


Figure 31: The Pentagon identity (A.11) is equivalent to the 3-2 Pachner move for tetrahedra in 3D.

where C is any closed loop embedded in S^3 , and S_{ij} is the modular matrix associated with the character χ_j of the chiral Kac-Moody representation corresponding to the Wilson line representation j . We note that the above result can also be extracted directly from $\chi_j(\tau)$,

$$d_j = \lim_{\tau \rightarrow 0} \frac{\chi_j(\tau)}{\chi_0(\tau)}, \quad \chi_j(\tau) = \text{tr}_i(e^{-\tau L_0}), \quad (\text{A.10})$$

where the trace above is taken over the Kac-Moody primary i and its descendant states following from quantizing the WZW model on a circle.

The quantum $6j$ symbols satisfy the Pentagon relation given by

$$\sum_{p_1} d_{p_1} \left\{ \begin{matrix} j_1 & j_2 & l_1 \\ j_3 & l_2 & p_1 \end{matrix} \right\}_{G_k} \left\{ \begin{matrix} j_1 & p_1 & l_2 \\ j_4 & j_5 & h_2 \end{matrix} \right\}_{G_k} \left\{ \begin{matrix} j_2 & j_3 & p_1 \\ j_4 & h_2 & h_1 \end{matrix} \right\}_{G_k} = \left\{ \begin{matrix} l_1 & j_3 & l_2 \\ j_4 & j_5 & h_1 \end{matrix} \right\}_{G_k} \left\{ \begin{matrix} j_1 & j_2 & l_1 \\ h_1 & j_5 & h_2 \end{matrix} \right\}_{G_k}. \quad (\text{A.11})$$

The Pentagon identity can be represented graphically in 3D as Fig. 31.

Now, this expectation value can be interpreted as that of the doubled theory (A.1) on a tetrahedron. The intuitive way to see this is that a tetrahedron embedded in S^3 essentially divides it into two tetrahedra glued together at the edges. (For a lower-dimensional case, imagine drawing a triangle in S^2 . The triangle divides S^2 into two triangles glued together at the edges.) Suppose one folds the external tetrahedron into the internal one, this leads to the doubled theory (A.1) filling up one tetrahedron. Before folding, the gauge field is taken continuous across the boundary of the tetrahedron. i.e.

$$(A_{\text{inside}} - A_{\text{outside}})|_{\text{surface of } \Delta_3} = 0. \quad (\text{A.12})$$

Since the path integral outside is folded in, it corresponds to the following boundary conditions of the doubled theory

$$(A_L + A_R)|_{\text{surface of } \Delta_3} = 0, \quad (\text{A.13})$$

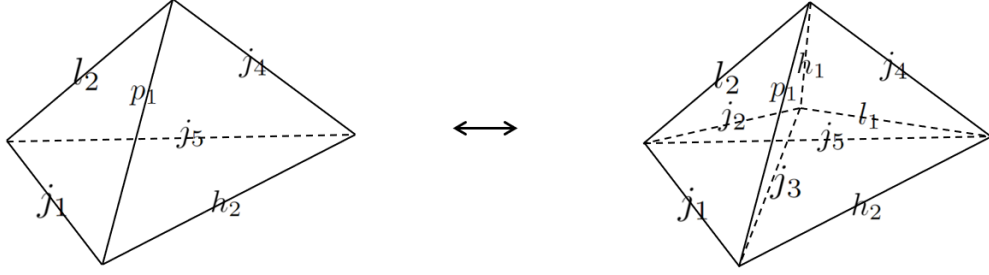


Figure 32: Equation (A.15) corresponds to the Pachner 4-1 move for 3D tetrahedra.

where A_R inside the tetrahedron is defined as the value of A_{outside} through a reflection, and the interface becomes the boundary after folding.

We can now construct the Turaev-Viro topological invariant over an arbitrary 3D manifold using the tetrahedra as building blocks [23]. The process begins by triangulating the 3D manifold with tetrahedra, followed by coloring the edges with representations j . Then each tetrahedron is assigned a $6j$ corresponding to the six edges of the tetrahedron. Furthermore, for every edge labeled j that lies in the interior of the 3D manifold and is shared by multiple tetrahedra, we include a factor of d_j . Finally, we sum over the coloring of all edges, i.e.⁴⁹

$$Z(\mathcal{M}) = \sum_{\{j_e\}} \prod_{v \in \mathcal{M}} D^{-2} \prod_{e' \in \partial \mathcal{M}} \sqrt{d_{j_{e'}}} \prod_{e \notin \partial \mathcal{M}} d_{j_e} \prod_{\Delta_3} \Gamma_3(\{j_{e \in \Delta_3}\}), \quad (\text{A.14})$$

where Γ_3 are $6j$ symbols as defined in (A.6).

The normalization convention in the literature attaches a factor of D^{-2} to every vertex. This normalization ensures $Z(S^2 \times S^1) = 1$.

Notice that a single tetrahedron can be subdivided into 4 tetrahedra. The path integral over 4 tetrahedra indeed recovers the result of 1 tetrahedron. i.e.

$$\left\{ \begin{matrix} j_1 & p_1 & l_2 \\ j_4 & j_5 & h_2 \end{matrix} \right\}_{G_k} = \sum_{h_1, j_2, j_3, l_1} \frac{d_{h_1} d_{j_2} d_{j_3} d_{l_1}}{D^2} \left\{ \begin{matrix} j_1 & p_1 & l_2 \\ h_1 & j_2 & j_3 \end{matrix} \right\}_{G_k} \left\{ \begin{matrix} j_1 & j_3 & j_2 \\ l_1 & j_5 & h_2 \end{matrix} \right\}_{G_k} \left\{ \begin{matrix} j_3 & p_1 & h_1 \\ j_4 & l_1 & h_2 \end{matrix} \right\}_{G_k} \left\{ \begin{matrix} j_2 & h_1 & l_2 \\ j_4 & j_5 & l_1 \end{matrix} \right\}_{G_k}. \quad (\text{A.15})$$

This is depicted in Fig. 32.

The Pentagon relation (A.11), together with (A.15), which correspond to the Pachner 3-2 move and the Pachner 4-1 move, are the crucial identities ensuring that $Z(\mathcal{M})$ is independent of triangulation [23, 220]. This also explains the factor d_i assigned to the gluing of edges. In the context of 3D gravity, this re-triangulating invariance is closely related to 3D diffeomorphism invariance.

To make a further connection of the path integral (A.14) with that of two copies of Chern-Simons

⁴⁹A square root is assigned to the quantum dimensions of the boundary edges.

theory, we make use of the “Chain-Mail” construction introduced by Roberts in [219].

Consider a very special linear combination of the Wilson loops ω given by [219]⁵⁰:

$$\omega(C) = \mathcal{N} \sum_j^{k/2} d_j W^j(C) . \quad (\text{A.16})$$

This linear combination is special in that $\omega(C)$ is essentially a projector, constraining the flux across the loop C to vanish, this operator plays an important role in the definition of the Levin-Wen string-net model [24] to be reviewed below, and it also has a nice physical interpretation in gravity language [132], as we explain in Sec. 5. Classically, the Wilson loop operator in representation j on a closed loop C would give the character of j evaluated on the group element $g = \exp(\oint_C A)$. Characters satisfy the following identity:

$$\sum_j d_j \text{tr}(R(g)) = \delta(g) , \quad (\text{A.17})$$

indeed leads to a projection to trivial flux through the loop C .

At finite k , this remains a projection operator. Normalization in a rational theory (where k is finite and G is compact) is usually chosen as

$$\mathcal{N}^{-2} = D^2 \equiv \sum_j d_j^2 . \quad (\text{A.18})$$

We note that D is finite for finite k , but diverges as $k \rightarrow \infty$. This is one subtlety that forbids naive generalization of rational Turaev-Viro theories to irrational ones.

These lines satisfy interesting properties, illustrated in Fig. 33. It suggests that these Wilson line configurations of ω loops can be assembled by matching the Wilson lines meeting at two vertices, and that can be interpreted as joined lines. Consequently, a continuum path integral of intertwining ω loops can be reduced to disconnected Wilson lines joined at the vertices. This is the idea behind the Chain-Mail construction. Starting with a triangulation T of a 3D manifold, we consider the thickening of its dual complex T^* , which provides a handle decomposition D of the original 3D manifold. The vertices of T^* correspond to 0-handles, the edges of T^* correspond to 1-handles, the faces of T^* correspond to 2-handles, and the 3-cells correspond to 3-handles. Next, we insert ω loops on all components of the handle decomposition. This process is illustrated for each tetrahedron in Fig. 34.

By considering the dual graph corresponding to the network of Wilson lines, and recursively

⁵⁰This collection of Wilson loops is often denoted as Ω in literature. However, since Ω is already used in this paper to represent the state corresponding to the physical boundary conditions, we instead denote this loop operator by ω .

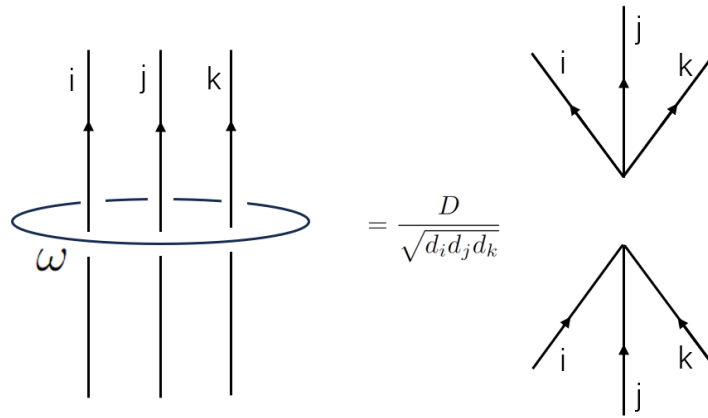


Figure 33: Property of the ω loop. This property can be used to relate the topological invariant defined by Roberts on the handle decomposition of 3D manifolds to the Turaev-Viro invariant defined using triangulation via tetrahedra.

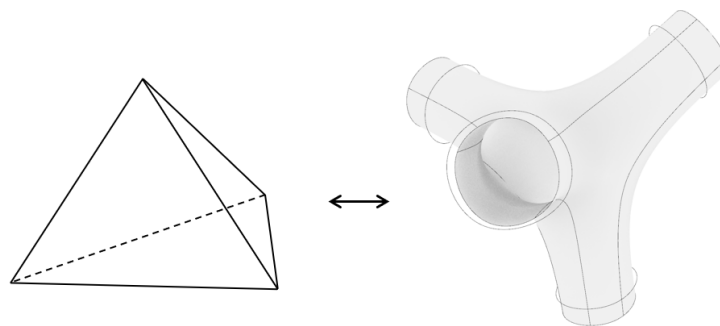


Figure 34: The tetrahedron and associated handle decomposition coming from thickening the dual. We insert the ω loops in the handle decomposition to get the Roberts invariant.

using the relation in Fig. 33, it recovers the path integral with the insertion of ω loops, which serves only to project every loop back to vanishing flux [221]. The resultant network is called the “Chain-Mail” [219]. The corresponding expectation value of closed Wilson loops is denoted as $C(\mathcal{M}, D)$. Roberts invariants can be defined as:

$$R(\mathcal{M}) = D^{-d_3-d_0} C(\mathcal{M}, D) , \quad (\text{A.19})$$

where d_3 and d_0 represent the number of 3-handles and 0-handles in D , respectively. As defined, this invariant is independent of the specific handle decomposition and serves as a topological invariant of D . Using Fig. 33, it can also be shown that this Roberts invariant matches precisely with the Turaev-Viro invariant, $R(\mathcal{M}) = Z(\mathcal{M})$ [219]. Finally, the expectation value of ω loops on \mathcal{M} can be computed using surgery, and gives a product of two copies of the chiral Reshetikhin-Turaev-Witten invariants [78, 219, 222], consistent with our expectation.

A.2 Turaev-Viro TQFT from fusion category

In the above, we attempt to give an introduction to the Turaev-Viro theory to emphasize that it can be understood in field-theoretic terms as Chern-Simons theories. However, the Turaev-Viro TQFT can also be defined independently of the Chern-Simons theory.

As we have seen above, the basic building block of the Turaev-Viro TQFT is given by the so-called quantum $6j$ symbol in (A.6). While it arises in the context of Chern-Simons gauge theory, the mathematical structure it belongs to can be defined independently of a field-theoretic realization. The mathematical structure concerned is the *fusion category* \mathcal{C} . There are many comprehensive reviews on the subject. (For reviews for physicists, one can consult, for example, [11, 14, 164, 223]. More mathematical treatment can be found, for example, in [224].) Here, we provide a basic skeleton to make it easier for our readers to follow more sophisticated expositions.

A fusion category \mathcal{C} contains the following ingredients.

1. A collection of *objects* $\{a, b, c, d \dots\}$. Strictly speaking, the number of objects should be finite.
2. A collection of maps between objects $\{f, g, \dots\}$, called *morphisms*.
3. The category \mathcal{C} is equipped with a tensor product \otimes :

$$a \otimes b = \bigoplus_c N_{ab}^c c , \quad (\text{A.20})$$

where $N_{ab}^c \in \mathbb{Z}_{\geq 0}$ is the dimension of the fusion space mapping $a \otimes b$ to c .

We also impose a few extra properties:

- The objects are *simple*, namely the space of morphism $\text{Hom}(a, a)$ mapping the object to itself is one-dimensional.

$$\begin{array}{c}
 a \quad b \quad c \\
 \diagdown \quad \diagup \quad / \\
 \quad e \quad \quad \quad \backslash \\
 \quad \quad \quad \quad \quad d
 \end{array}
 = \sum_{f \in \mathcal{C}} \sqrt{d_e d_f} \left\{ \begin{array}{ccc} a & b & e \\ c & d & f \end{array} \right\}
 \begin{array}{c}
 a \quad b \quad c \\
 \diagdown \quad \diagup \quad / \\
 \quad \quad \quad \quad \quad \backslash \\
 \quad \quad \quad \quad \quad f \\
 \quad \quad \quad \quad \quad \quad \quad \backslash \\
 \quad \quad \quad \quad \quad \quad \quad \quad d
 \end{array}$$

Figure 35: Associativity of fusion involves the quantum $6j$ symbol.

- There is a distinguished object 0 that plays the role of *identity*, so that every object fusing with it leaves the object unchanged.
- For every simple object a one can also define the dual object \bar{a} so that $0 \in a \otimes \bar{a}$.

The fusion product is associative in a *weak* sense. Rather than imposing that $(a \otimes b) \otimes c$ is directly equal to $a \otimes (b \otimes c)$, these two sets of fusion maps are only required to be linearly dependent. Denote the basis of the fusion maps from $(a \otimes b)$ to c by $V_{ab}^c(\alpha)$ where $1 \leq \alpha \leq N_{ab}^c \neq 0$. For simplicity, in the following we will focus on the cases where $N_{ab}^c \leq 1$, in which case we can omit the labels α, β for each fusion channel. The associativity is then expressed through the $6j$ symbols as

$$V_{ab}^e V_{ec}^d = \sum_{f \in \mathcal{C}} \sqrt{d_e d_f} \left\{ \begin{array}{ccc} a & b & e \\ c & d & f \end{array} \right\} V_{af}^d V_{bc}^f. \quad (\text{A.21})$$

There is a very convenient diagrammatic representation of the above associativity relation, as depicted in Fig. 35.

The coefficient d_j is the quantum dimension of the simple object $j \in \mathcal{C}$. Note that $d_0 = 1$ and $d_a = d_{\bar{a}}$. These quantum dimensions also satisfy the identity

$$d_a d_b = \sum_c N_{ab}^c d_c. \quad (\text{A.22})$$

Quantum dimension is thus analogous to the dimension of a representation in the Chern-Simons theories discussed above. The unit object 0 corresponds to the “trivial representation” in a gauge theory.

The coefficient in curly bracket is precisely the analogue of the quantum $6j$ symbol that we introduced in the context of the Chern-Simons theories. This is part of the input data that define a fusion category, and the Pentagon relation expressed in (A.11) is satisfied. The Pentagon relation expresses the consistency under different orders of fusions of 4 objects, as illustrated in Fig. 36.

It should be clear that the representations of a group form a fusion category. Each representation corresponds to an object in the category, and the fusion of representations corresponds to the fusion morphisms discussed above, whose associativity is indeed controlled by the $6j$ symbols.

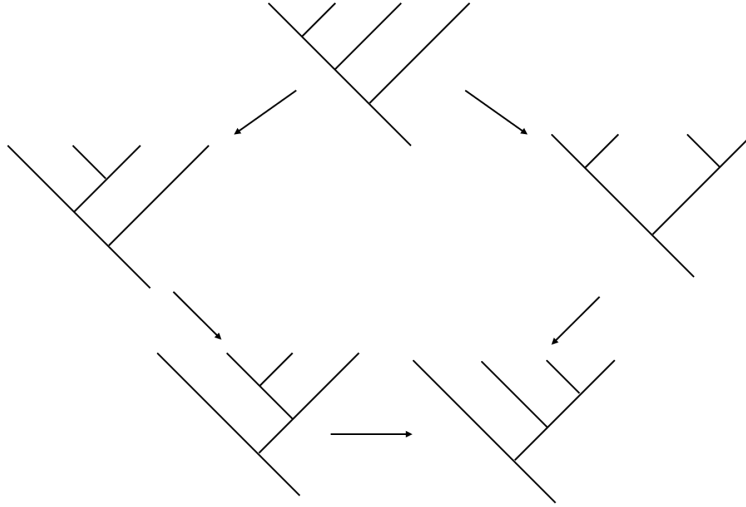


Figure 36: Pentagon identity for the quantum $6j$ symbols.

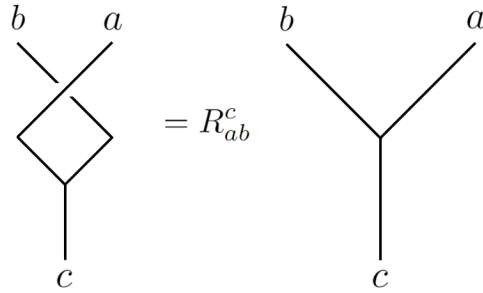


Figure 37: The braided structure is encoded in the R -matrix.

Given a fusion category \mathcal{C} , it is sufficient to define a Turaev-Viro path integral on any manifold \mathcal{M} [23] exactly as in (A.14).

Generically, it is possible to endow a fusion category with more structures. An important structure is the braided structure that exchanges two objects. This structure is encoded in the so-called R -matrix, with components R_{ab}^c which are phases, that connects $a \otimes b$ to $b \otimes a$. This is illustrated in Fig. 37. Note that there is a distinction between an “over-crossing” and “under-crossing”. The factor that appears in an “under-crossing” is related to the “over-crossing” by a complex conjugate of R_{ab}^c . The R -matrix satisfies some consistency conditions, so that the action of braiding is consistent with the associativity relations from fusion. These consistency conditions are given by the Hexagon relations [48].

One can define an S -matrix for a braided tensor category. The components of the S -matrix are given by

$$S_{ab} = \sum_c N_{ab}^c \frac{\theta_c}{\theta_a \theta_b} d_c, \quad (\text{A.23})$$

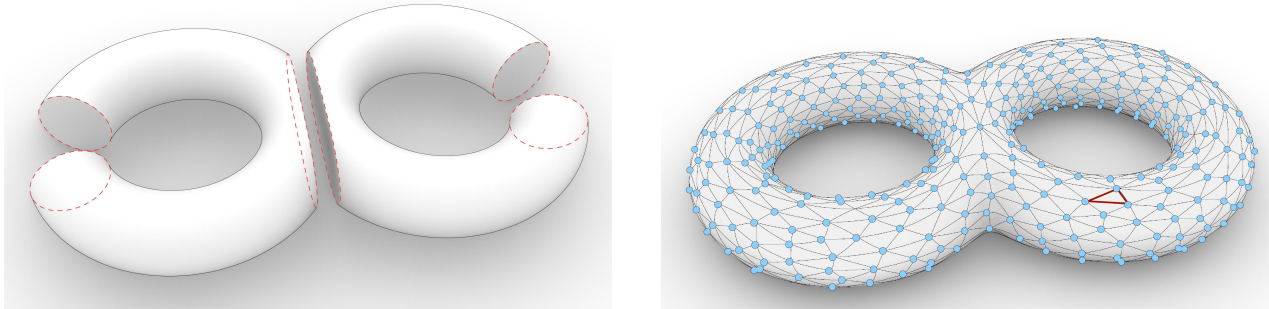


Figure 38: Two different cutting and gluing procedures for the computation of genus two CFT partition functions. The conventional method on the left involves the closed pair-of-pants decomposition. In contrast, we cut the manifold open into chipped triangles, which means the building blocks are open pairs of pants.

where θ_c is the “topological spin” of the object type c . It is related to the conformal dimension h_i of the primary by

$$\theta_c = e^{2\pi i h_c} . \quad (\text{A.24})$$

The square of the R matrix is also related to the h_c by

$$(R_{ab}^c)^2 = e^{2\pi i (h_a + h_b - h_c)} . \quad (\text{A.25})$$

We note that when the S -matrix is a unitary matrix, the braided tensor category is modular. It reduces to pairs of Chern-Simons theories described previously when \mathcal{C} is a *modular* tensor category.

B Tensor network state sum representation of 2D CFT path integrals

In this appendix, we review in great detail the tensor network state sum representation of 2D CFT path integrals [1, 29–31].

Instead of employing the more conventional decomposition of the CFT path integral on 2D manifolds into closed pairs of pants in the closed channels defined on circles, we decompose the path integral into small triangular regions and define Hilbert spaces along the lines connecting their endpoints. For example, the distinction between these approaches in computing the genus-two partition function is illustrated in Fig. 38. The tiny blue holes have radius R^{51} , and they are introduced in [1, 29–31] for regularization purposes, which are taken to zero at the end of the computation to recover the original CFT. However, in this paper, we demonstrate that these holes

⁵¹In [1], we mostly used the symbol ϵ to parameterise the size of the holes. As explained in the footnote 6 of that paper, when the length of the lattice site is Λ , then $\frac{\pi}{\epsilon} = \ln(\frac{\Lambda}{R})$.

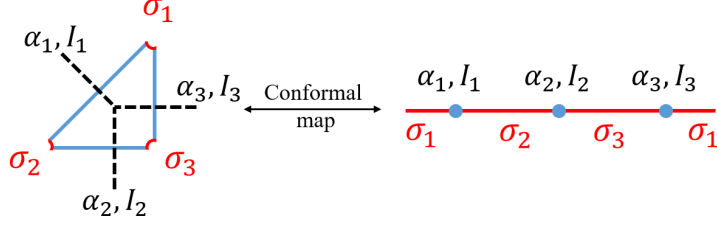


Figure 39: Conformal map from a chipped triangle (open pair of pants) to the upper half plane with three boundary-changing operators on the real line.

serve a more significant role: By allowing R to vary, they introduce a continuous family of topological symmetry-preserving deformations away from the original CFT. These deformations are analogous to the $T\bar{T}$ deformations discussed in Sec. 3, and similarly arise from gluing 3D gravitational path integrals -represented here by quantum $6j$ symbols - onto the 2D theories.

For the computation of the total CFT partition \mathcal{Z}_{CFT} function, the basic building block is the CFT path integral on the chipped triangles, as shown in Fig. 9⁵². These represent open pairs of pants, in contrast to the more conventional closed pairs of pants commonly found in the CFT literature. The Hilbert spaces in the computation are associated with the edges of the triangles, which are lines between the two endpoints where boundary conditions must be specified.

We first impose and fix some conformal boundary conditions, labeled by σ_i , as illustrated in Fig. 39. Once the boundary conditions are fixed, we insert a complete basis of states on the lines, compatible with the boundary conditions at the two endpoints. Through the state-operator correspondence in the open channel, these states correspond to boundary condition-changing operators such as $\Phi_{\alpha_i, I_i}^{\sigma_1 \sigma_2}$. These operators are classified by their primary label α_i and descendant label I_i under a single copy of the Virasoro algebra. The value of the open pairs of pants involving descendant fields is entirely determined by the Virasoro symmetry from those involving only primary fields. Therefore, we will focus solely on those associated with the primary fields in the following.

More concretely, we can use a conformal map to map the chipped triangles to the upper half-plane⁵³, where the BCFT primary three-point function takes the familiar form,

$$\langle \Phi_{\alpha_1}^{\sigma_1 \sigma_2}(x_1) \Phi_{\alpha_2}^{\sigma_2 \sigma_3}(x_2) \Phi_{\alpha_3}^{\sigma_3 \sigma_1}(x_3) \rangle = \frac{C_{\alpha_1, \alpha_2, \alpha_3}^{\sigma_3, \sigma_1, \sigma_2}}{|x_{21}|^{\Delta_1 + \Delta_2 - \Delta_3} |x_{32}|^{\Delta_2 + \Delta_3 - \Delta_1} |x_{31}|^{\Delta_3 + \Delta_1 - \Delta_2}}, \quad (\text{B.1})$$

When we consider the quantities associated with descendant fields, the numerator will remain unchanged, while the denominator will acquire dependence on the descendant labels, determined by the Virasoro symmetry. When we pull the three-point function from the upper half-plane back to

⁵²We will focus on 2D CFT defined on flat background δ_{ij} for simplicity here. The formalism can be easily generalized to general fixed curved backgrounds h_{ij} .

⁵³The explicit function realizing the conformal map for the flat background δ_{ij} can be found in [30, 85]. For more general background metrics, a more complicated conformal transformation will be applied

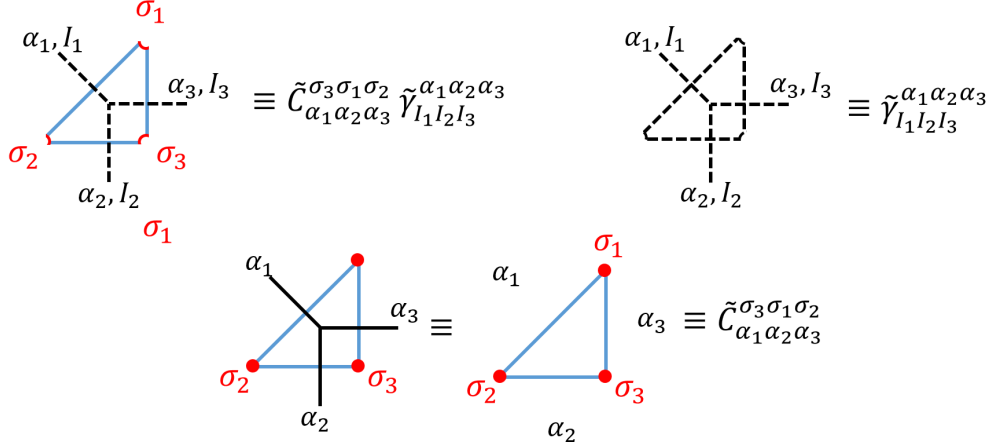


Figure 40: Diagrammatic notation for $\tilde{C}_{\alpha_1 \alpha_2 \alpha_3}^{\sigma_3 \sigma_1 \sigma_2}$ and $\tilde{\gamma}_{I_1 I_2 I_3}^{\alpha_1 \alpha_2 \alpha_3}(R)$.

the original chipped triangles, we obtain,

$$\mathcal{T}_{(\alpha_1, I_1)(\alpha_2, I_2)(\alpha_3, I_3)}^{\sigma_1 \sigma_2 \sigma_3}(\Delta, R) = C_{\alpha_1 \alpha_2 \alpha_3}^{\sigma_3 \sigma_1 \sigma_2} \gamma_{I_1 I_2 I_3}^{\alpha_1 \alpha_2 \alpha_3}(R), \quad (\text{B.2})$$

This normalization is what we call the ‘‘Block gauge’’. For later convenience, we also introduce the ‘‘Racah gauge’’ [1, 29–31, 225], where

$$\begin{aligned} \mathcal{T}_{(\alpha_1, I_1)(\alpha_2, I_2)(\alpha_3, I_3)}^{\sigma_1 \sigma_2 \sigma_3}(\Delta, R) &\equiv \tilde{C}_{\alpha_1 \alpha_2 \alpha_3}^{\sigma_3 \sigma_1 \sigma_2} \tilde{\gamma}_{I_1 I_2 I_3}^{\alpha_1 \alpha_2 \alpha_3}(R) \\ &= (C_{\alpha_1 \alpha_2 \alpha_3}^{\sigma_3 \sigma_1 \sigma_2} \mathcal{N}_{\alpha_1 \alpha_2 \alpha_3}) \frac{\gamma_{I_1 I_2 I_3}^{\alpha_1 \alpha_2 \alpha_3}(R)}{\mathcal{N}_{\alpha_1 \alpha_2 \alpha_3}} \end{aligned} \quad (\text{B.3})$$

$\mathcal{N}_{\alpha_1 \alpha_2 \alpha_3}$ is a function chosen such that the crossing kernels for these rescaled conformal blocks are proportional to the Racah coefficients or the quantum $6j$ symbols, and the explicit form of these functions can be found in [1, 29–31, 225]. A diagrammatic representation is introduced in Fig. 40.

For diagonal CFTs, the label set of conformal boundary conditions coincides with the set of primary fields (this is referred to as the Cardy case [89] in the literature), and the rescaled BCFT OPE coefficients are directly proportional to the quantum $6j$ symbols, as first discovered by Runkel [86], as

$$\tilde{C}_{\alpha_1 \alpha_2 \alpha_3}^{\sigma_3 \sigma_1 \sigma_2} = (d_{\alpha_1} d_{\alpha_2} d_{\alpha_3})^{1/4} \begin{Bmatrix} \alpha_1 & \alpha_2 & \alpha_3 \\ \sigma_3 & \sigma_1 & \sigma_2 \end{Bmatrix}, \quad (\text{B.4})$$

where d_{α_i} is the quantum dimension associated with α_i , as introduced above. For theories with a continuous spectrum, such as the Liouville theory, this corresponds to the Plancherel measure [1, 126]. In the diagonal case, the $6j$ symbol enjoys the tetrahedron symmetry, and we associate it with a tetrahedron, which serves as the fundamental building block of the Turaev-Viro TQFT, as reviewed above.

$$\begin{array}{c} \alpha_1 \\ \alpha_2 \\ \alpha_3 \\ \sigma_1 \\ \sigma_2 \\ \sigma_3 \end{array} \equiv \begin{Bmatrix} \alpha_1 & \alpha_2 & \alpha_3 \\ \sigma_3 & \sigma_1 & \sigma_2 \end{Bmatrix} \begin{array}{c} \sigma_1 \\ \alpha_1 \\ \alpha_3 \\ \alpha_2 \\ \sigma_2 \\ \sigma_3 \end{array} = (d_{\alpha_1} d_{\alpha_2} d_{\alpha_3})^{1/4} \begin{array}{c} \alpha_1 \\ \alpha_2 \\ \alpha_3 \\ \sigma_1 \\ \sigma_2 \\ \sigma_3 \end{array}$$

For more general non-diagonal CFTs, a formula similar to (B.4) holds. The boundary conditions now take values in the “module category”, which we explain in Sec. 6.2. For now, it suffices to understand that this is a different label set from the primary labels, and the curly brackets denote the generalized $6j$ symbols with mixed indices. These generalized symbols can also be expressed in terms of the standard $6j$ symbols, where the standard $6j$ symbols are “dressed” with quantities associated with these boundary conditions [32, 87]. Diagrammatically, we introduce the following representation:

$$\begin{array}{c} \alpha_1 \\ \alpha_2 \\ \alpha_3 \\ \sigma_1 \\ \sigma_2 \\ \sigma_3 \end{array} \equiv \begin{Bmatrix} \alpha_1 & \alpha_2 & \alpha_3 \\ \sigma_3 & \sigma_1 & \sigma_2 \end{Bmatrix} \begin{array}{c} \sigma_1 \\ \alpha_1 \\ \alpha_3 \\ \alpha_2 \\ \sigma_2 \\ \sigma_3 \end{array} = (d_{\alpha_1} d_{\alpha_2} d_{\alpha_3})^{1/4} \begin{array}{c} \alpha_1 \\ \alpha_2 \\ \alpha_3 \\ \sigma_1 \\ \sigma_2 \\ \sigma_3 \end{array}$$

After summing over all intermediate primaries and descendants, we get a partition function that depends on the fixed boundary conditions $\{\sigma_a\}$

$$\mathcal{Z}(\{\sigma_a\}, R) = \sum_{\{\alpha_i\}} \sum_{\{I_i\}} \prod_{\Delta} \mathcal{T}_{(\alpha_i, I_i)(\alpha_j, I_j)(\alpha_k, I_k)}^{\sigma_a \sigma_b \sigma_c}(\Delta, R), \tag{B.5}$$

As we explain in the main text, to ensure that we get the correct IR fixed point and reveal the connection to topological symmetries, we sum over the boundary conditions with a specific weight, proportional to the quantum dimension $\omega_{\sigma_a} \propto d_{\sigma_a}$, following [1, 29–31, 85, 88]

$$\mathcal{Z}(R) = \sum_{\{\sigma_a\}} \prod_v \omega_{\sigma_a} \sum_{\{\alpha_i\}} \sum_{\{I_i\}} \prod_{\Delta} \mathcal{T}_{(\alpha_i, I_i)(\alpha_j, I_j)(\alpha_k, I_k)}^{\sigma_a \sigma_b \sigma_c}(\Delta, R). \tag{B.6}$$

This weighted sum brings the Turaev-Viro TQFT and the string-net model into the game, and we can explicitly write the expression above as an overlap (2.5) of the PEPS tensor network states, in the Hilbert space of the string-net model, as shown in (4.9).

To recover the CFT partition function, we simply take

$$\mathcal{Z}_{\text{CFT}} = \lim_{R \rightarrow 0} (\prod_v e^{-\frac{c}{6} \ln(R)})_{\Lambda} \langle \Omega^R | \Psi \rangle_{\Lambda}. \tag{B.7}$$

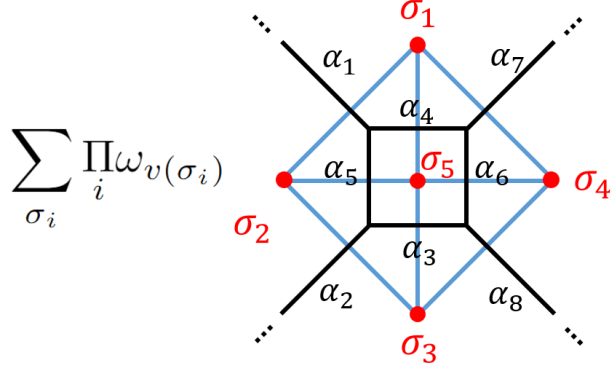


Figure 41: A local representation with five vertices and eight edges of the ground state $|\Psi\rangle_\Lambda$.

C Tensor network SymQRG

In this appendix, we explain in more detail the tensor network SymQRG algorithm introduced in [1, 13, 29–31]. We start with a local configuration of $|\Psi\rangle_\Lambda$ as in Fig. 41. Explicitly in formula as in (4.10), this state is locally expressed as

$$|\Psi\rangle_{\Lambda, \text{local}} = \sum_{\sigma_i} \sum_{\alpha_i} \omega_{\sigma_1} \omega_{\sigma_2} \omega_{\sigma_3} \omega_{\sigma_4} \omega_{\sigma_5} \tilde{C}_{\alpha_1 \alpha_5 \alpha_4}^{\sigma_5 \sigma_1 \sigma_2} \tilde{C}_{\alpha_2 \alpha_3 \alpha_5}^{\sigma_5 \sigma_2 \sigma_3} \tilde{C}_{\alpha_8 \alpha_6 \alpha_3}^{\sigma_5 \sigma_3 \sigma_4} \tilde{C}_{\alpha_7 \alpha_4 \alpha_6}^{\sigma_5 \sigma_4 \sigma_2} |\{\alpha_{i=1\dots 8}\}\rangle_\Lambda. \quad (\text{C.1})$$

Alternatively, for a specific basis state labeled by the coloring $\{\alpha_{i=1\dots 8}\}$, the wavefunction is locally

$$\Psi^\Lambda(\{\alpha_{i=1\dots 8}\}) = \sum_{\sigma_i} \omega_{\sigma_1} \omega_{\sigma_2} \omega_{\sigma_3} \omega_{\sigma_4} \omega_{\sigma_5} \tilde{C}_{\alpha_1 \alpha_5 \alpha_4}^{\sigma_5 \sigma_1 \sigma_2} \tilde{C}_{\alpha_2 \alpha_3 \alpha_5}^{\sigma_5 \sigma_2 \sigma_3} \tilde{C}_{\alpha_8 \alpha_6 \alpha_3}^{\sigma_5 \sigma_3 \sigma_4} \tilde{C}_{\alpha_7 \alpha_4 \alpha_6}^{\sigma_5 \sigma_4 \sigma_2}. \quad (\text{C.2})$$

The BCFT OPE coefficients solve the conformal bootstrap equations. In particular, for the BCFT four point functions, it is illustrated in Figure 42.

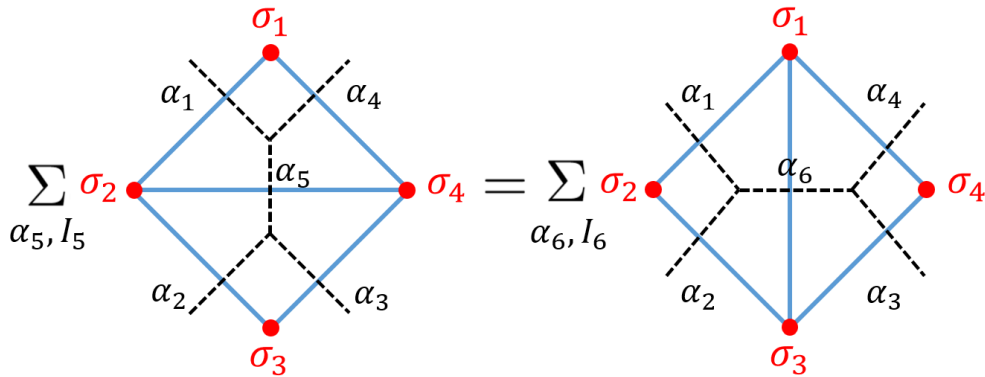


Figure 42: Crossing equation of the BCFT four point functions.

As an algebraic equation, it gives

$$\sum_{\alpha_5} \tilde{C}_{\alpha_1 \alpha_5 \alpha_4}^{\sigma_4 \sigma_1 \sigma_2} \tilde{C}_{\alpha_3 \alpha_5 \alpha_2}^{\sigma_2 \sigma_3 \sigma_4} \tilde{\mathcal{F}}^t(\alpha_5; \alpha_{i=1,4}, x_{i=1,4}) = \sum_{\alpha_6} \tilde{C}_{\alpha_1 \alpha_2 \alpha_6}^{\sigma_3 \sigma_1 \sigma_2} \tilde{C}_{\alpha_3 \alpha_4 \alpha_6}^{\sigma_1 \sigma_3 \sigma_4} \tilde{\mathcal{F}}^s(\alpha_6; \alpha_{i=1,4}, x_{i=1,4}), \quad (\text{C.3})$$

where $\tilde{\mathcal{F}}^t$ and $\tilde{\mathcal{F}}^s$ are the conformal blocks in the t and s channel respectively in Racah gauge, and they are related via the crossing kernel:

$$\tilde{\mathcal{F}}^t(\alpha_5; \alpha_{i=1,4}, x_{i=1,4}) = \sum_{\alpha_6} F_{\alpha_6, \alpha_5}^{\text{Racah}} \begin{pmatrix} \alpha_1 & \alpha_4 \\ \alpha_2 & \alpha_3 \end{pmatrix} \tilde{\mathcal{F}}^s(\alpha_6; \alpha_{i=1,4}, x_{i=1,4}). \quad (\text{C.4})$$

Thus the BCFT OPE coefficients are related by,

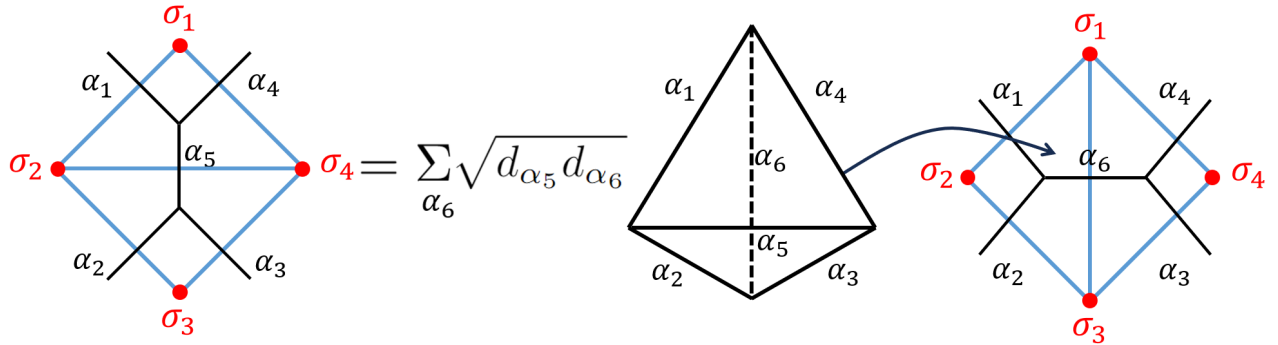
$$\tilde{C}_{\alpha_1 \alpha_5 \alpha_4}^{\sigma_4 \sigma_1 \sigma_2} \tilde{C}_{\alpha_3 \alpha_5 \alpha_2}^{\sigma_2 \sigma_3 \sigma_4} = \sum_{\alpha_6} \tilde{C}_{\alpha_1 \alpha_2 \alpha_6}^{\sigma_3 \sigma_1 \sigma_2} \tilde{C}_{\alpha_3 \alpha_4 \alpha_6}^{\sigma_1 \sigma_3 \sigma_4} F_{\alpha_6, \alpha_5}^{\text{Racah}} \begin{pmatrix} \alpha_1 & \alpha_4 \\ \alpha_2 & \alpha_3 \end{pmatrix}. \quad (\text{C.5})$$

The crossing kernel in Racah gauge is related to the $6j$ symbols via,

$$F_{\alpha_6, \alpha_5}^{\text{Racah}} \begin{pmatrix} \alpha_1 & \alpha_4 \\ \alpha_2 & \alpha_3 \end{pmatrix} = \sqrt{d_{\alpha_5} d_{\alpha_6}} \left\{ \begin{matrix} \alpha_1 & \alpha_4 & \alpha_5 \\ \alpha_3 & \alpha_2 & \alpha_6 \end{matrix} \right\}. \quad (\text{C.6})$$

Notice that the $6j$ symbol above depends solely on the primary labels and not on the boundary conditions. Therefore, it is entirely determined by SymTFT in the bulk, rather than by the specific choice of $|\Psi\rangle_\Lambda$ or the topological boundary condition.

Diagrammatically, we have the following,



Since the wavefunctions for the string-net ground states are represented by the BCFT structure coefficients, this equation establishes a relationship between the states in two different triangulations. In the 3D perspective, this corresponds to modifying the 2D triangulation by gluing an additional layer of 3D tetrahedra, which is related to the 3-2 Pachner move.

Applying this equation twice, to both the left and right parts of Fig. 41, we obtain:

$$\sum_{\sigma_5} \omega_{\sigma_5} \sigma_2 \sigma_4 = \sum_{\sigma_5} \omega_{\sigma_5} \sum_{\alpha_9, \alpha_{10}} F_{\alpha_9, \alpha_5}^{\text{Racah}} \begin{pmatrix} \alpha_1 & \alpha_4 \\ \alpha_2 & \alpha_3 \end{pmatrix} F_{\alpha_{10}, \alpha_6}^{\text{Racah}} \begin{pmatrix} \alpha_4 & \alpha_7 \\ \alpha_3 & \alpha_8 \end{pmatrix}$$

The orthogonality condition of the (generalized) $6j$ symbols is [32, 87],

$$\sum_{\sigma_5} d_{\sigma_5} \begin{Bmatrix} \alpha_3 & \alpha_4 & \alpha_9 \\ \sigma_1 & \sigma_3 & \sigma_5 \end{Bmatrix} \begin{Bmatrix} \alpha_3 & \alpha_4 & \alpha_{10} \\ \sigma_1 & \sigma_3 & \sigma_5 \end{Bmatrix} = \frac{\delta_{\alpha_9, \alpha_{10}}}{d_{\alpha_9}} N_{\alpha_3 \alpha_4}^{\alpha_9} N_{\sigma_1 \sigma_3}^{\alpha_9}, \quad (\text{C.7})$$

where $N_{\alpha_3 \alpha_4}^{\alpha_9}$ and $N_{\sigma_1 \sigma_3}^{\alpha_9}$ take values of either 0 or 1, indicating whether the configuration is admissible.

We can use it to get,

$$\sum_{\sigma_5} \omega_{\sigma_5} \sigma_2 \sigma_4 = \sum_{\alpha_9} \sqrt{\frac{d_{\alpha_3} d_{\alpha_4}}{d_{\alpha_9}}} F_{\alpha_9, \alpha_5}^{\text{Racah}} \begin{pmatrix} \alpha_1 & \alpha_4 \\ \alpha_2 & \alpha_3 \end{pmatrix} F_{\alpha_9, \alpha_6}^{\text{Racah}} \begin{pmatrix} \alpha_4 & \alpha_7 \\ \alpha_3 & \alpha_8 \end{pmatrix}$$

$$= \sum_{\alpha_9} \sqrt{d_{\alpha_3} d_{\alpha_4} d_{\alpha_5} d_{\alpha_6} d_{\alpha_9}} \begin{array}{c} \alpha_1 \quad \alpha_4 \quad \alpha_7 \\ \alpha_5 \quad \alpha_9 \quad \alpha_6 \\ \alpha_2 \quad \alpha_3 \quad \alpha_8 \end{array}$$

Figure 43: Coarse-graining equation of the Levin-Wen ground state $|\Psi\rangle_{\Lambda}$.

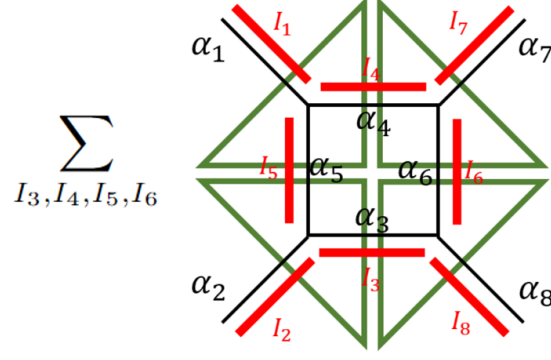


Figure 44: A local representation of a general PEPS state ${}_{\Lambda}\langle\Omega|$ to be coarse-grained.

We get the transformation rule relating a ground state at scale Λ and another larger scale $\Lambda' = \sqrt{2}\Lambda$,

$$|\Psi\rangle_{\Lambda} = \hat{U}_{\text{RG}}^{\Lambda, \Lambda'} |\Psi\rangle_{\Lambda'} . \quad (\text{C.8})$$

As outlined in Sec. 2.3, this procedure can also be used to define the coarse-graining map for ${}_{\Lambda}\langle\Omega^R|$, as follows:

$${}_{\Lambda'}\langle\Omega'^R| = {}_{\Lambda}\langle\Omega^R| \hat{U}_{\text{RG}}^{\Lambda, \Lambda'} . \quad (\text{C.9})$$

We can also incorporate the rescaling step to deform the theory from the overlap.

Now we illustrate the general procedure involving singular value decompositions for arbitrary seed states. We start with a general PEPS state ${}_{\Lambda}\langle\Omega|$. For example, using a direct product seed state ${}_{\Lambda}\langle\Omega|$ and taking its overlap with $|\Psi\rangle_{\Lambda}$ reproduces the Ising lattice model [13, 84]. By applying the RG procedure described below, the critical temperature can be determined numerically with high accuracy [29].

For general initial PEPS states ${}_{\Lambda}\langle\Omega|$, locally shown in Fig. 44 and written as,

$${}_{\Lambda}\langle\Omega| = \sum_{\alpha_i} {}_{\Lambda}\langle\{\alpha_{i=1,8}\}| \sum_{I_3, I_4, I_5, I_6} \Omega_{I_1 I_5 I_4}^{\alpha_1 \alpha_5 \alpha_4} \Omega_{I_2 I_3 I_5}^{\alpha_2 \alpha_3 \alpha_5} \Omega_{I_8 I_6 I_3}^{\alpha_8 \alpha_6 \alpha_3} \Omega_{I_7 I_4 I_6}^{\alpha_7 \alpha_4 \alpha_6} . \quad (\text{C.10})$$

The RG operator maps the state to

$${}_{\Lambda'}\langle\Omega'| = {}_{\Lambda}\langle\Omega| \hat{U}_{\text{RG}}^{\Lambda, \Lambda'} = \sum_{\alpha_{i=1,2,7,8,9}} {}_{\Lambda'}\langle\{\alpha_{i=1,2,7,8,9}\}| \sum_{\alpha_{i=3,4,5,6}} \sqrt{\frac{d_{\alpha_3} d_{\alpha_4}}{d_{\alpha_9}}} F_{\alpha_9, \alpha_5}^{\text{Racah}} \begin{pmatrix} \alpha_1 & \alpha_4 \\ \alpha_2 & \alpha_3 \end{pmatrix} F_{\alpha_9, \alpha_6}^{\text{Racah}} \begin{pmatrix} \alpha_4 & \alpha_7 \\ \alpha_3 & \alpha_8 \end{pmatrix} \sum_{I_3, I_4, I_5, I_6} \Omega_{I_1 I_5 I_4}^{\alpha_1 \alpha_5 \alpha_4} \Omega_{I_2 I_3 I_5}^{\alpha_2 \alpha_3 \alpha_5} \Omega_{I_8 I_6 I_3}^{\alpha_8 \alpha_6 \alpha_3} \Omega_{I_7 I_4 I_6}^{\alpha_7 \alpha_4 \alpha_6} \quad (\text{C.11})$$

The next step is to express the wavefunctions as contractions of local tensors defined on the

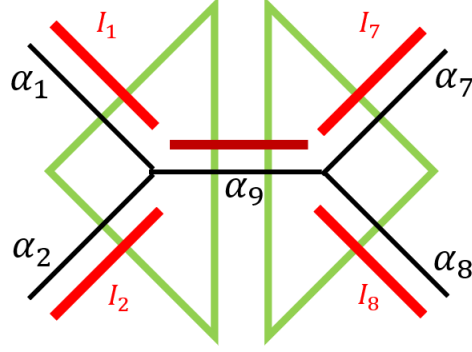


Figure 45: The singular value decomposition turns the result with four dangling physical legs into a contraction of contributions from two triangles.

triangles as in Fig. 45, using singular value decomposition [29, 93], as follows:

$$\Omega'^{\Lambda'}(\alpha_{i=1,2,7,8,9}) = \sum_{I_9} \Omega'_{I_1 I_2 I_9}{}^{\alpha_1 \alpha_2 \alpha_9} \Omega'_{I_8 I_7 I_9}{}^{\alpha_8 \alpha_7 \alpha_9}. \quad (\text{C.12})$$

In numerical computations, truncation is typically performed at this step. The bond dimensions in tensor networks are related to the amount of entanglement required to glue different pieces together. In the coarse-graining procedure towards the CFT fixed point, quantum entanglement is recursively generated until the bond dimension becomes infinite, reflecting long range correlation which is captured by the presence of infinitely many descendant states.

For the family of theories proposed in (4.9), the coarse-grained wavefunction is given by:

$$\begin{aligned} \Omega'^{\Lambda'}(\alpha_{i=1,2,7,8,9}) = & \sum_{\alpha_i=3,4,5,6} \sqrt{\frac{d_{\alpha_3} d_{\alpha_4}}{d_{\alpha_9}}} F_{\alpha_9, \alpha_5}^{\text{Racah}} \begin{pmatrix} \alpha_1 & \alpha_4 \\ \alpha_2 & \alpha_3 \end{pmatrix} F_{\alpha_9, \alpha_6}^{\text{Racah}} \begin{pmatrix} \alpha_4 & \alpha_7 \\ \alpha_3 & \alpha_8 \end{pmatrix} \\ & \sum_{I_3, I_4, I_5, I_6} \tilde{\gamma}_{I_1 I_5 I_4}^{\alpha_1 \alpha_5 \alpha_4} \tilde{\gamma}_{I_2 I_3 I_5}^{\alpha_2 \alpha_3 \alpha_5} \tilde{\gamma}_{I_8 I_6 I_3}^{\alpha_8 \alpha_6 \alpha_3} \tilde{\gamma}_{I_7 I_4 I_6}^{\alpha_7 \alpha_4 \alpha_6}. \end{aligned} \quad (\text{C.13})$$

Diagrammatically,

$$\sum_{\alpha_i=3,4,5,6} \sum_{I_3, I_4, I_5, I_6} \sqrt{\frac{d_{\alpha_3} d_{\alpha_4}}{d_{\alpha_9}}} F_{\alpha_9, \alpha_5}^{\text{Racah}} \begin{pmatrix} \alpha_1 & \alpha_4 \\ \alpha_2 & \alpha_3 \end{pmatrix} F_{\alpha_9, \alpha_6}^{\text{Racah}} \begin{pmatrix} \alpha_4 & \alpha_7 \\ \alpha_3 & \alpha_8 \end{pmatrix}$$

We first use the definition of crossing kernel to turn the conformal blocks on the left and right

to the crossed channel.

$$\sum_{\alpha_3, \alpha_4} \sum_{I_3, I_4, I_9, I_9'} \sqrt{\frac{d_{\alpha_3} d_{\alpha_4}}{d_{\alpha_9}}} \text{Diagram}$$

Next, we use the identity in Racah gauge:

$$F_{\mathbb{1}, \alpha_4}^{\text{Racah}} \begin{pmatrix} \alpha_9 & \alpha_3 \\ \alpha_9 & \alpha_3 \end{pmatrix} = \sqrt{\frac{d_{\alpha_4}}{d_{\alpha_3} d_{\alpha_9}}}, \quad (\text{C.14})$$

to turn this into

$$\sum_{\alpha_3} d_{\alpha_3} \sum_{I_3, I_4', I_9, I_9'} \text{Diagram}$$

Finally, we use the fact that $d_3 \propto S_{\mathbb{1}\alpha_3}$, to get,

$$\sum_{I_3', I_4', I_9, I_9'} \text{Diagram}$$

and we turn this into contribution of two triangles as we explain in the main text.

Away from the $R \rightarrow 0$ fixed point, singular value decomposition need to be performed to update the tensor values assigned to the triangles after each RG step. It would be fascinating to explore in

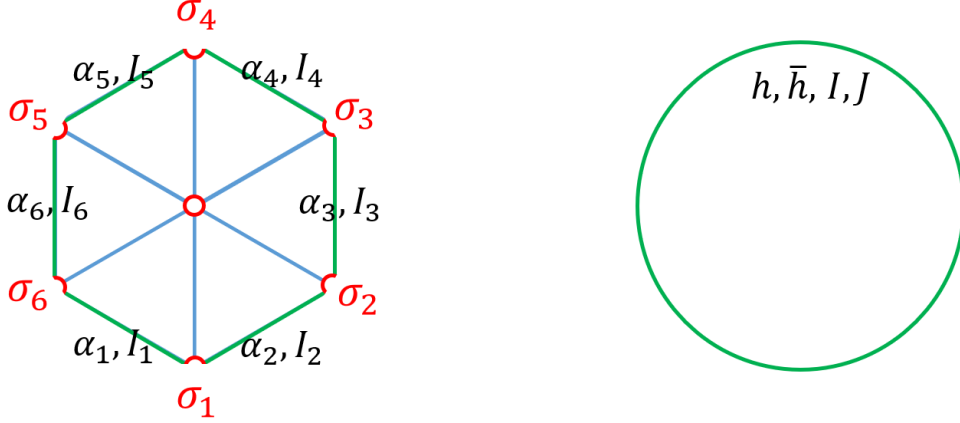


Figure 46: Two different ways of obtaining a state living on a circle by Euclidean path integral. The open CFT triangulation method provides a state with 18 labels on the left, and the closed CFT method provides a state with 4 labels on the right.

greater detail the properties of this non-perturbatively defined family of theories and their connection to continuum field theories.

D Tensor network for CFT wavefunctions from Euclidean path integrals, perfect tensors and random tensors

In this appendix, we explain exact tensor network construction for CFT wavefunctions from Euclidean path integrals. We also discuss the connection to perfect tensors and random tensors.

The initial motivation for connecting tensor networks to gravity did not originate from constructing a spacetime tensor network to represent the local dictionary for partition functions, as we have done above. Instead, Swingle observed that the Ryu-Takayanagi formula, used to compute the entanglement entropy of holographic CFT quantum states on codimension-one surfaces, exhibited a striking resemblance to the entanglement structure in ground states represented by tensor networks [35, 36]. Swingle’s analogy suggested that tensor networks could encode the spatial entanglement patterns within a CFT in a manner that mirrors the holographic entanglement entropy calculation in the AdS/CFT correspondence.

On the other hand, as discussed in [1], our approach extends the application of tensor networks by constructing a representation for codimension-one quantum states prepared through a Euclidean CFT path integral. This construction directly links to conventional studies of spatial entanglement in quantum states. In the following, we first review this construction and then demonstrate how it aligns with previously proposed “perfect tensor network” and “random tensor network” models for holography [105, 226]. Notably, our approach encodes dynamical information for both the AdS and

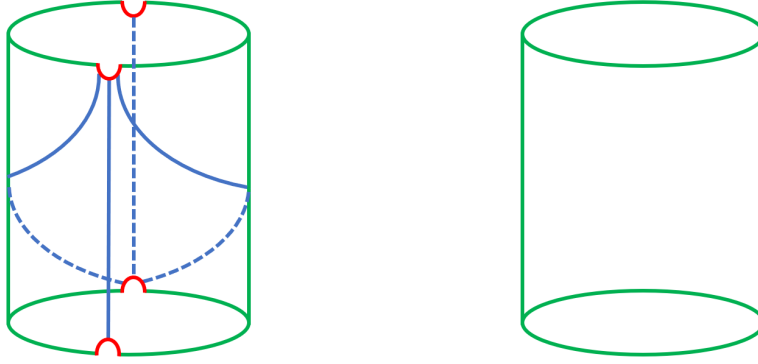


Figure 47: Two different ways of computing the CFT propagator represented by a cylinder. The closed CFT spectrum can be extracted from the open CFT computation on the left.

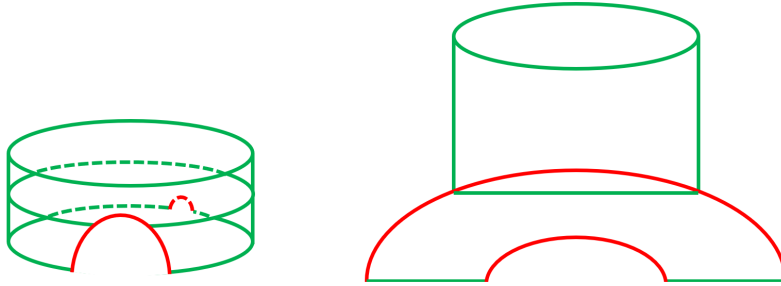


Figure 48: The map between the open and closed bases is gotten from gluing the “whistle diagram” (the open-closed one-point function) to the open pair of pants.

the CFT, providing a refined exact framework for holographic tensor networks that goes beyond toy models.

The idea here is to consider CFT path integrals defined on manifolds with boundaries rather than on closed manifolds, which yield partition functions. We will still triangulate these path integrals. For example, the CFT ground state defined on a circle can be prepared using the Euclidean path integral on a disk, as shown in Fig. 46. The primary distinction from the partition function case is that some auxiliary legs, which would otherwise be contracted, now become dangling physical legs.

In Fig. 46, for instance, the Hilbert space consists of 18 labels corresponding to the basis states $|\alpha_i, I_i, \sigma_i\rangle, i = 1 \dots 6$. Here, α_i represents the primary fields, I_i the descendants, and σ_i the boundary conditions. Typically, CFT techniques assign a Hilbert space on the circle labeled by closed CFT operators $|h, \bar{h}, I, J\rangle$, where h and \bar{h} are the chiral and anti-chiral conformal dimensions of the closed CFT primaries, and I, J are the descendant labels. These two Hilbert spaces are, in fact, equivalent.

To check this equivalence, consider the path integral on a cylinder, as illustrated in Fig. 47. In

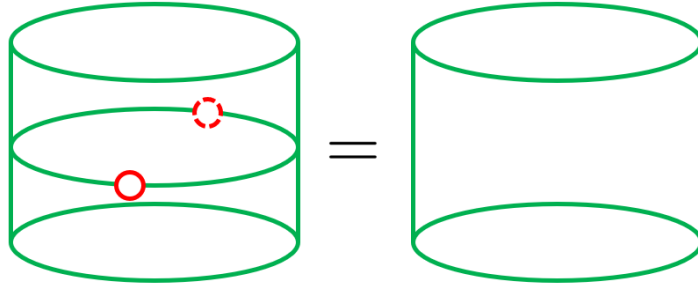


Figure 49: The equivalence of the open and closed Hilbert spaces can be seen from the fact that the tiny red holes are contractable as we showed in appendix C.

the closed CFT picture (right side), this computation corresponds to the matrix element of $e^{-\beta\hat{H}}$, where the indices are labeled by $\{h, \bar{h}, I, J\}$, and the eigenvalues of the transfer matrix are given by the closed CFT spectrum. On the left side, we compute the matrix element of this transfer matrix using triangulation, where the matrix indices are labeled with a different set, $\{\alpha_i, I_i, \sigma_i, i = 1 \dots 4\}$. However, upon diagonalizing this matrix, we find that the spectrum matches exactly with the closed CFT results! This equivalence has been checked numerically for several minimal models. Remarkably, it was observed that even when truncating the number of descendants to a very small number (e.g. 2 or 3) for each edge of a triangle, the resultant glued cylinder can still capture the lowest ~ 20 states (including closed CFT primaries and descendants) with high accuracy [30].

The map between these two bases is represented in Fig. 48, involving the gluing of the “whistle diagram” (the open-closed one-point function) to the open pair of pants. The equivalence of these two Hilbert spaces follows from the ability to shrink the holes in Fig. 49 in the $R \rightarrow 0$ limit, as detailed in appendix C.

We can also separate the BCFT OPE piece and the conformal block piece, as we did for the partition function. This decomposition is illustrated in Fig. 50.

The surface at the top, denoted by the red lines, represents a Cauchy slice in the bulk. Additional layers of the tensor network can be constructed using the crossing move shown in Fig. 42. For example, the next layer corresponds to the purple lines in the diagram above.

Since the tensor network reproduces the exact CFT results, it inherently incorporates the correct kinematics and dynamics of the CFT, which are both long-standing difficulties. This is achieved because one part of the tensors encodes the OPE coefficients, which captures the dynamical information of the CFT, while the other part arises from the conformal blocks, providing the correct scaling laws in the CFT⁵⁴.

⁵⁴In the literature, there is another suggested method to produce a tensor network related to a Cauchy slice from QFT path integrals using “Cauchy slice holography” [68, 227, 228]. It will be interesting to understand the connection with our formalism. We thank Ronak Soni for pointing this to us.

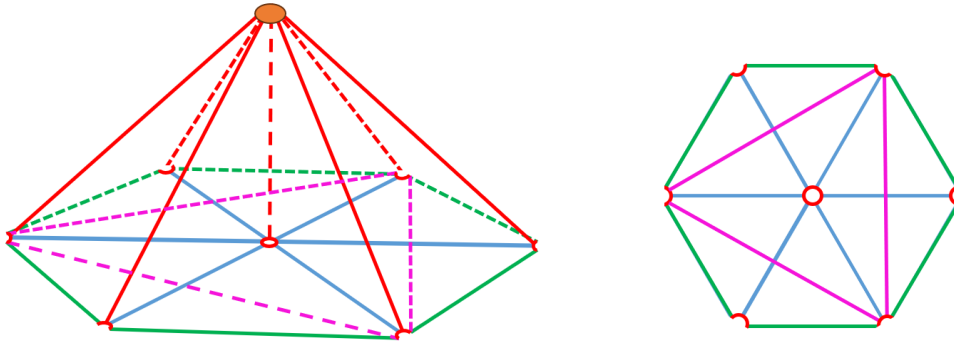


Figure 50: We can separate the OPE coefficients and the conformal blocks, as we did for the partition functions above, leading to an emergent 3D interpretation. Using the crossing move, we can also transition from the blue edges to the purple edges. The Cauchy slice in the bulk correspond to the surface on the top with red edges.

Next, we will demonstrate how our wavefunction tensor network relates to and generalizes the best existing tensor network models proposed to describe holography—namely, the perfect tensor network [105] and the random tensor network [226]. Our construction incorporates the intrinsic CFT data into the tensor network, which are necessary to describe both AdS and CFT, thereby establishing a connection between tensor networks and gravity that goes beyond mere analogy.

Quasi-Perfect tensor network

The first model constructed to exactly saturate the Ryu-Takayanagi formula is the HaPPY code introduced in [105], which uses perfect tensors for the tensor network. The model is constructed explicitly to recover wavefunctions of 2D models that live on a line. The holographic network that prepares the wavefunction covers a two-dimensional space in a way very similar to the MERA tensor network [35]. The idea is to consider placing a tensor network over the dual graph of a given (regular) tiling over hyperbolic planes. The polygons chosen in the tiling carry an even number of edges, and each host a perfect tensor with even number of legs. The property of a perfect tensor $U^{i_1 \dots i_{2N}}$ is such that when one treats any of the N indices as input indices and the other N indices as output indices, the matrix remains unitary. The dangling indices in the tensor network can then be identified with the Hilbert space in which the wavefunction lives.

Consider the computation of the entanglement entropy of a simply connected interval A for the tensor network wavefunction. When the indices belonging to the complement \bar{A} are contracted with the complex conjugate of the wavefunction, the property of a hyperbolic tiling is such that each contracted tensor living at the boundary would have more than half of their indices contracted. As a perfect tensor, this produces the identity operator, and the contraction of indices thus propagates

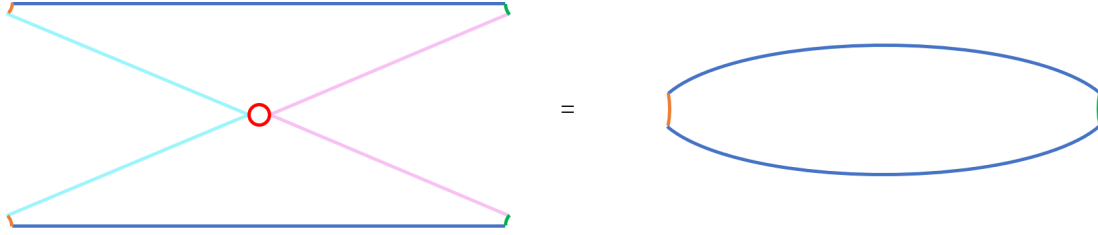


Figure 51: The “quasi-perfect-isometric” condition of tensor network for CFT states from Euclidean path integral.

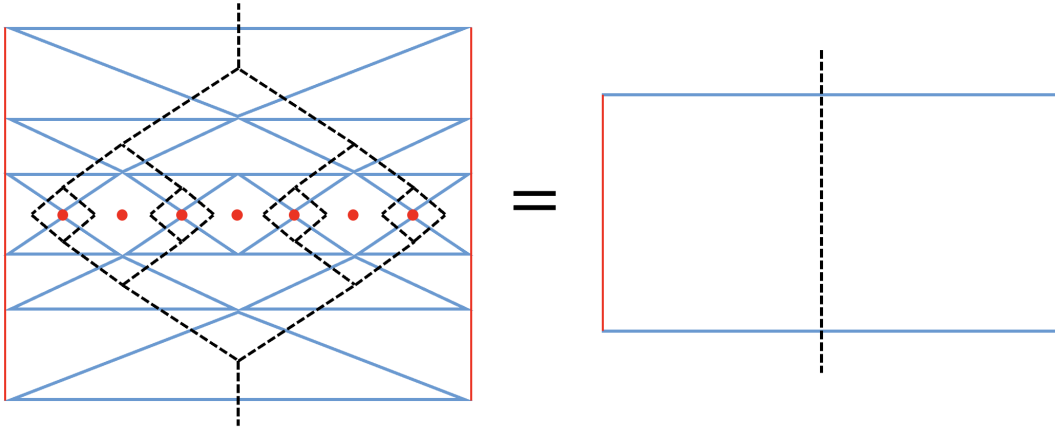


Figure 52: The “quasi-perfect-isometric” condition in our CFT wavefunction tensor network allows us to simplify the single-interval reduced density matrix to an open CFT propagator.

into the bulk of the hyperbolic plane. In [105] it was shown that this process ends precisely when one reaches a minimal cut that separates A and \bar{A} . The entanglement spectrum of the resultant reduced density matrix is flat, and its rank is given precisely by the number of links cut by the minimal cut across the tiling. The entanglement entropy is thus proportional to $L \ln D$, where D is the bond dimension of each index and L is the number of links cut by the minimal cut. This thus reproduces the Ryu-Takayanagi formula. In our construction of the CFT wavefunction as discussed above and illustrated in Fig. 46, a structure emerges that partly resembles the perfect tensor. Take any two triangles and contract any of the two edges and the corner index between the two chosen edges, resulting in the “propagator” of the remaining edge, as illustrated in Fig. 51. This is referred to as the “quasi-perfect-isometric” condition in [1].

When we construct the wavefunction with a canonical choice of triangulation as in Fig. 46, it is not immediately clear how to compute the reduced density matrix. To make use of the “quasi-perfect-isometric” condition, we can convert the triangulation using crossing relations, as illustrated

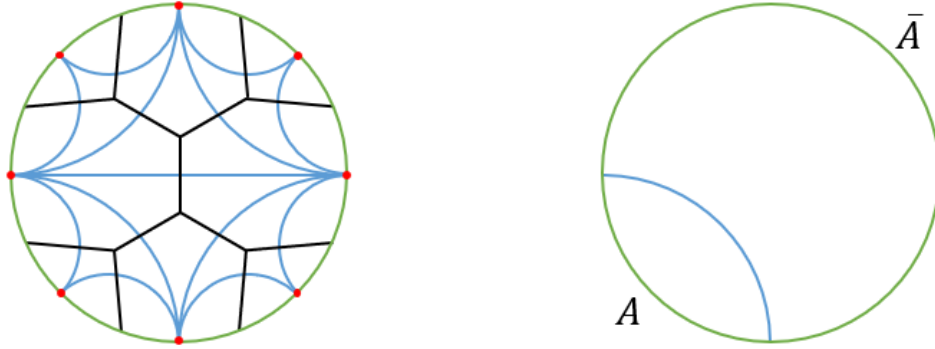


Figure 53: On the left, we repeatedly use the crossing relation to convert the tensor network to take the form of a MERA like tensor network. On the right, we illustrate the fact that the cancellation in the computation of the reduced density matrix using the quasi-perfect-isometric property ends at the Ryu-Takayanagi surface.

in Fig. 50, in which the crossing relation allows one to replace the blue lines by the purple lines. By repeated use of the crossing relation, one can convert the tensor network to take the form of a MERA-like tensor network, as illustrated in the left figure of Fig. 53. When we compute the reduced density matrix, the quasi-perfect isometric condition would play a similar role as the perfect condition, as illustrated in Fig. 52. The cancellation ends at the Ryu-Takayanagi surface illustrated in the right figure of Fig. 53.

The edges of the triangles correspond to geodesics in the 3D hyperbolic space, with the geodesic lengths associated with the Virasoro representation labels propagating along these edges, as illustrated in Fig. 54, turning it into a geodesic tensor network. This connection is the primary focus of Sec. 5.

As an exact reconstruction of the CFT wavefunction, the entanglement spectrum is not flat but reproduces exactly that of the CFT.

Random tensor network

In the discussion so far, we have been working with a given CFT, where its structure coefficients exactly solve all the consistency relations of the CFT. Alternatively, one can consider an ensemble average of CFTs by invoking the eigenstate thermalization hypothesis (ETH). (A further discussion of the connection between gravity and ETH is presented in Sec. 5.5.) This approach involves treating the OPE coefficients as (pseudo)random variables [140, 145].

In the context of 3D gravity, the idea of seeing the emergence of gravity by treating closed OPE coefficients in the pair-of-pants decomposition as random tensors was introduced in [229], and later

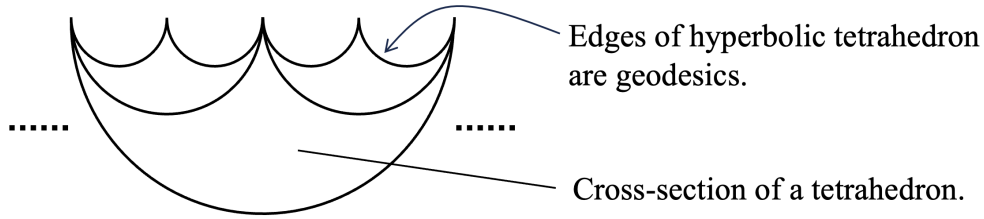


Figure 54: The edges in our tensor networks have the physical meaning of hyperbolic geodesic lengths, and this will be explained in Sec. 5.

adapted into a tensor network framework in [230]. For example, a simple MPS tensor network, constructed with random closed OPE coefficients in a 2D CFT as tensors, can be interpreted as discretizing the radial direction in the bulk dual in the semi-classical approximation, and approximately reproduces the location of the horizon [229, 230]. In our framework, which recovers the full CFT path integral, it is also natural to consider an ensemble average of the structure coefficients for boundary-changing operators. The ensemble average of the structure coefficients for the boundary-changing operators in the large central charge limit has been studied in [146, 147]. Applied to our formalism, this results in a random tensor network that represents the ensemble-averaged CFT path integral as outlined in [1], and will appear soon in [149]. A crucial distinction in our tensor network construction is worth emphasizing: We used the *open* structure coefficients of the CFT, rather than the *closed* ones, to build the CFT tensor network. From our perspective, the open structure coefficients are more directly connected to the emergence of bulk geometry and allow for discretizing both the CFT and AdS spaces arbitrarily, not only along the radial direction or having to come with external operator insertions.

Although the resulting random tensor network contains some ingredients similar to those in [226], there is a key difference: Tensors at different locations in our construction are not treated as independent random variables.

E Quantum Teichmuller theory and its connection to $U_q(SL(2, \mathbb{R}))$ $6j$ symbols

This appendix first provides a review of quantum Teichmuller theory and the Teichmuller TQFT, then we show how the tetrahedron operator in quantum Teichmuller theory is related to $U_q(SL(2, \mathbb{R}))$ $6j$ symbols we used in our main text.

E.1 Reviewing quantum Teichmuller theory and Teichmuller TQFT

The central idea of quantum Teichmuller theory and Teichmuller TQFT follows from constructing explicit representations of the mapping class group on a hyperbolic Riemann surface.

In [231], it is shown that the quantum $6j$ symbols in $U_q(SL(2, \mathbb{R}))$ are related to the tetrahedra operator T introduced by Kashaev in quantum Teichmuller theory [52, 137].

To appreciate the relation given in [231], we provide a brief review of quantum Teichmuller theory and the T operator introduced in [137]. To ensure convergence within the discrete formulation of Teichmuller TQFT, these T operators were later extended to their charged counterparts, as developed in [21].

The first step is to construct representations of the mapping class group on a hyperbolic Riemann surface [52]. A hyperbolic Riemann surface satisfies

$$M \equiv 2g + n - 2 > 0 , \tag{E.1}$$

where g is the genus and n is the number of punctures. (In general, we could consider n finite boundary components instead, but in the following we will illustrate the main ideas when these boundary components have infinitesimal sizes, and thus punctures.)

Consider the space of deformations of complex structures on the surface Σ . This is called the Teichmuller space $\mathcal{T}(\Sigma)$. For a chosen complex structure on the given Riemann surface, there is a unique metric with constant negative curvature. The metric can be represented as $ds^2 = e^{2\phi} dz d\bar{z}$, where ϕ satisfies the Liouville equation

$$\partial\bar{\partial}\phi = \frac{1}{4}e^{2\phi} . \tag{E.2}$$

The Teichmuller space can be identified with the space of deformations of these constant-curvature metrics. The idea of Penner coordinates for the Teichmuller space is to use geodesic lengths to parameterize the space of metrics [232]. Consider, thus, this specific hyperbolic conformal frame. The punctures are mapped to cusps. In the following, we would be using these two terms interchangeably.

Consider triangulating the surface. The surface of genus g with cusps n can be triangulated with triangles whose vertices are given by the puncture, and the edges are geodesics that run between the punctures. This triangulation τ is called an “ideal triangulation”. Since these edges connect the punctures, they have infinite geodesic lengths. To regulate these edge lengths, pick a “horocycle”, which is a closed geodesic surrounding each puncture. Each edge e intersects each horocycle once. The regulated geodesic length l_e for the edge e is given by the segment between the intersections with the horocycles. See Fig. 55 for an illustration. The regulated edge lengths $\{l_e\}$ can be taken as a coordinate of the Teichmuller space.

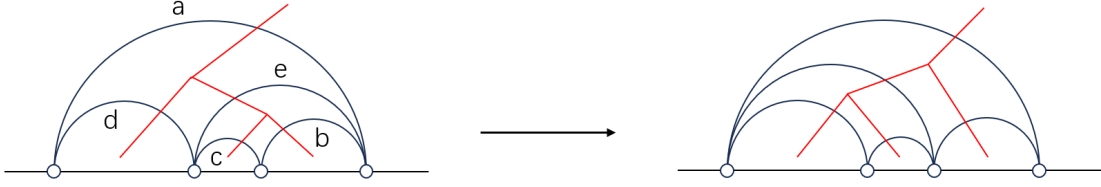


Figure 56: Change of an ideal triangulation.

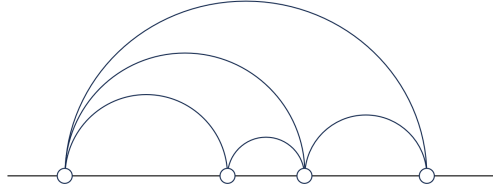


Figure 55: An ideal triangulation with four punctures.

The mapping class group of the surface corresponds to (orientation-preserving) diffeomorphisms not isotopic to the identity. i.e.

$$\text{MCG}(\Sigma) = \text{Diff}^+(\Sigma)/\text{Diff}_0^+(\Sigma) , \quad (\text{E.3})$$

where Diff^+ are orientation-preserving diffeomorphisms.

The triangulation of a surface can be changed. In particular, one can consider two neighboring triangles that share an edge. One can remove the shared edge and replace it by another edge connecting the other two vertices. Considering the dual graph of the triangles (the dual graph is called the “fat graph” in this context), this change in triangulation is, in fact, the crossing transformation. Under a change of triangulation, the tuples of edge lengths would change. This change can be considered as a change of coordinates of the Teichmuller space. These transformations generate the “Ptolemy groupoid”.

This transformation admits a simple expression if we introduce another set of coordinates called Fock coordinates $\{z_e\}$ [233], which is also attached to every edge e in triangulation τ . Each edge e is shared between two triangles. Suppose that one of the triangles has two other edges a, d and the other triangle has two other edges b, c . This is shown in Fig. 56.

Then z_e is related to the geodesic lengths of a, b, c, d as

$$z_e = l_a + l_c - l_b - l_d. \quad (\text{E.4})$$

In the Fock coordinates, the “crossing” transformation between two triangles correspond to the

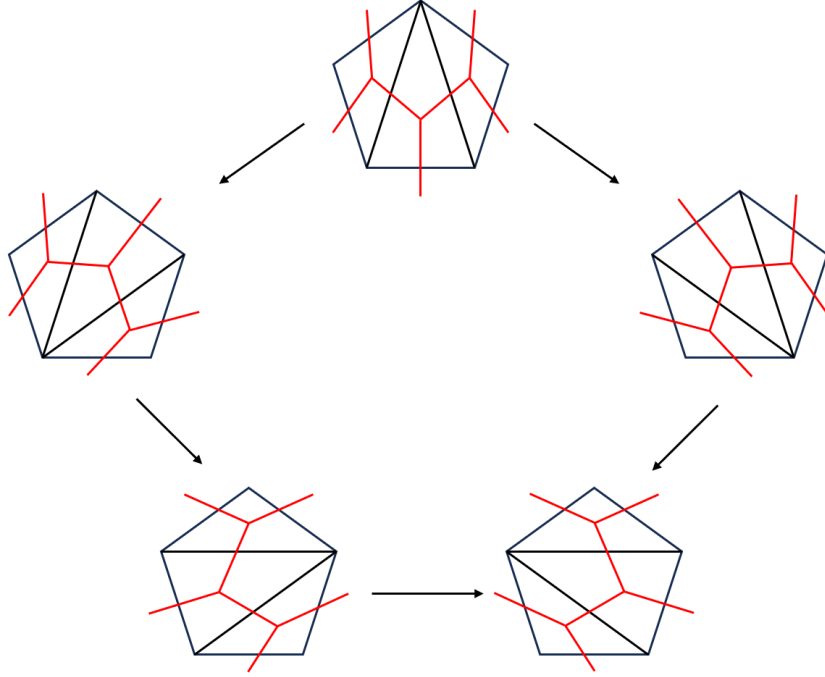


Figure 57: Consistency condition for re-triangulation.

following change of coordinates

$$\begin{aligned}
 z'_e &= -z_e, & \phi(x) &= \ln(1 + e^x), \\
 z'_a &= z_a - \phi(-z_e), & z'_b &= z_b + \phi(z_e), \\
 z'_d &= z_d + \phi(z_e), & z'_c &= z_c - \phi(-z_e).
 \end{aligned}
 \tag{E.5}$$

Since this is essentially a crossing relation from the perspective of the dual graph, these transformations should satisfy a consistency condition analogous to the Pentagon relation. This is depicted in Fig. 57.

Under the action of the mapping class group $\text{MCG}(\Sigma)$, a triangulation τ is mapped to another triangulation τ' . Similarly, repeated application of the “crossing transformation” can relate one triangulation to another. This parallel suggests that representations of the mapping class group can be constructed leveraging these transformations.

The ultimate goal, however, is to obtain a quantized Teichmüller space and quantum actions of the mapping class group.

To do so, one needs to make use of the symplectic structure naturally defined in the Teichmüller space. It is called the Weil-Petersson symplectic form. In terms of the Penner coordinate with a

choice of triangulation τ , it is given by

$$\omega = - \sum_{\Delta \in \tau} dl_{e_1(\Delta)} \wedge dl_{e_2(\Delta)} + dl_{e_2(\Delta)} \wedge dl_{e_3(\Delta)} + dl_{e_3(\Delta)} \wedge dl_{e_1(\Delta)} , \quad (\text{E.6})$$

where Δ denotes triangles in τ and $e_{1,2,3}(\Delta)$ are the three edges of the triangle Δ with labels ordered counter-clockwise around the triangle. The symplectic form can, of course, also be expressed in terms of the Fock coordinates, which we shall not reproduce here.

The quantization of the Teichmüller space is achieved by upgrading the Poisson bracket to a commutator. i.e.

$$[z_e, z'_e] = 2\pi i b^2 \{z_e, z'_e\} , \quad (\text{E.7})$$

where one introduces a “Planck constant” b . Ultimately, the parameter b would coincide with the quantum group deformation parameter b in the Liouville theory introduced in (5.13).

Then one needs to construct the action of the mapping class group on the quantized variables and also on the Hilbert space that follows from quantization. Such a transformation should preserve the Poisson bracket, while satisfying the same consistency condition of the flip, including the relation depicted in Fig. 57, now as an operator relation.

This is in fact possible, if the operator transformation under “crossing” is given precisely by (E.5), with $\phi(x)$ upgraded to the special function $\phi_b(x)$ given by

$$\phi_b(x) = \frac{\pi b^2}{2} \int_{i0-\infty}^{i0+\infty} dw \frac{e^{-ixw}}{\sinh(\pi w) \sinh(\pi b^2 w)} . \quad (\text{E.8})$$

that reduces to $\phi(x)$ in the limit $b \rightarrow 0$. With the explicit form of transformation, one needs to construct the operator that in fact has the correct commutation with the variables z_e to generate these transformations. That would produce explicit quantum representations of the crossing relations, and subsequently the mapping class group.

The main idea of such a construction by Kashaev in [137] follows from expressing the Fock variables in terms of canonical variables p, q that satisfy the usual commutation relation $[q, p] = 1$.

This relation with canonical variables is constructed as follows. For every triangle Δ in the triangulation, Kashaev assigns a canonical pair q_Δ, p_Δ . To connect them with the edge lengths, an extra structure is needed on the triangle. One particular vertex is singled out, and we will mark the vertex with a star, and this is called a decorated triangle. We label the edges of the decorated triangle l_1, l_2, l_3 with a particular anti-clockwise order as shown in Fig. 58.

Then

$$(q_\Delta, p_\Delta) = (l_3 - l_2, l_1 - l_2) . \quad (\text{E.9})$$

There are $3M$ edges in the triangulation, but we have introduced $4M$ variables for $2M$ triangles, more than the original set. For that matter, there is a set of constraints [52, 137].

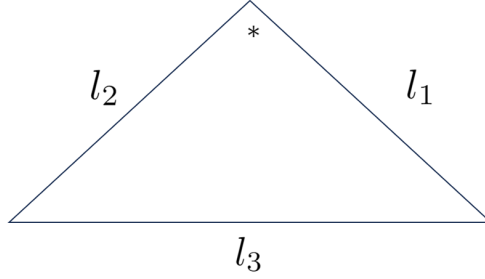


Figure 58: A decorated triangle in Kashaev's construction of quantum Teichmuller theory.

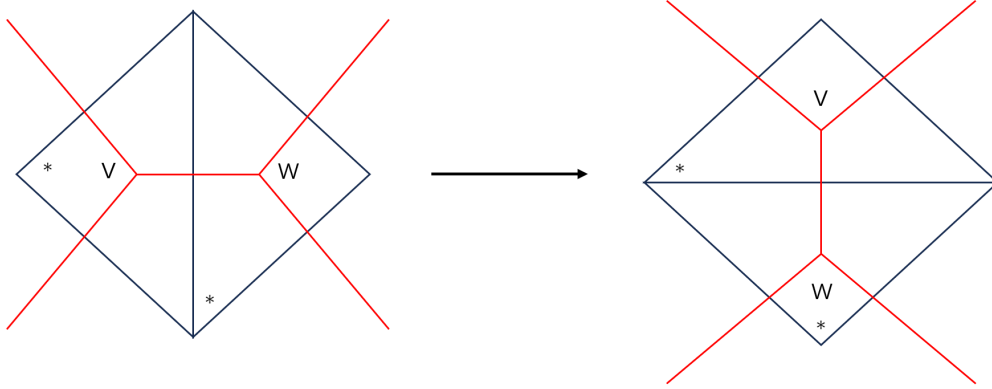


Figure 59: Crossing move in Kashaev's construction with decorations explicitly labeled.

The crossing relation can now be translated to a transformation T_{vw} in the Kashaev variables. It is given by

$$\begin{aligned} (U_v, V_v) &\rightarrow (U_v U_w, U_v V_w + V_v) , \\ (U_w, V_w) &\rightarrow (U_w V_v (U_v V_w + V_v)^{-1}, V_w (U_v V_w + V_v)^{-1}) , \end{aligned} \quad (\text{E.10})$$

where v, w label the decorated triangles, and they are sharing an edge to be transformed into the crossed triangulation. In addition, the variables in capitals are related to the Kashaev canonical variables in each triangle via

$$U_{v,w} = \exp(q_{v,w}) , \quad V_{v,w} = \exp(p_{v,w}) . \quad (\text{E.11})$$

The above crossing relation is depicted in Fig. 59, with the decorations shown explicitly.

Now that the triangles are decorated, one also needs to construct transformations A_v that correspond to moving the marked vertex inside a given decorated triangle v . They correspond to

$$(q_v, p_v) \rightarrow (p_v - q_v, -q_v) . \quad (\text{E.12})$$

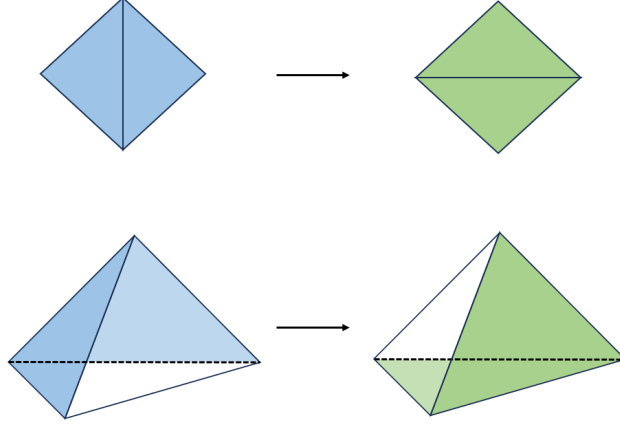


Figure 60: The change of triangulation is given by an operator T , and takes the role of a tetrahedron.

The important point is that A_v and T_{vw} are the basic building blocks in constructing the representations of the mapping class group. Moreover, Kashev’s discrete version of the Teichmuller TQFT is also built from them. The T_{vw} operator basically takes the role of a tetrahedra. Explicitly in terms of the canonical variables, it is given by

$$T_{vw} = e_b(q_v + p_w - q_w)e^{-2\pi i p_v q_w} , \quad (\text{E.13})$$

where

$$e_b = \exp \left(\frac{1}{4} \int_{i0-\infty}^{i0+\infty} \frac{dw}{w} \frac{e^{-2izw}}{\sinh(bw) \sinh(w/b)} \right) , \quad (\text{E.14})$$

which is the renowned Fadeev’s quantum dilogarithm that played an important role in integrable models.

The TQFT on a 3-manifold is basically defined as the product of these tetrahedra that triangulates the 3 manifolds, with the caveat that not all 3-manifolds can admit a finite answer and that there could be issues with divergence. Moreover, since the Hilbert space constructed from the canonical variables is infinite-dimensional and in fact continuous, to ensure convergence, the operator T is further regulated by two positive variables α, γ satisfying $1/2 - \alpha - \gamma > 0$. These are called “charged” tetrahedral operators

$$T_{vw}(\alpha, \gamma) = e^{+\pi i Q^2((\alpha-\gamma+1)/6)} e^{-2\pi Q(\alpha p_w - \gamma q_w)} T_{vw} e^{2\pi Q(\alpha p_w + \gamma q_w)} , \quad (\text{E.15})$$

which reduce to the original tetrahedral operator when these twist parameters approach 0.

One can check out explicit examples in [21] where the (charged) tetrahedral operator builds up the 3 manifold.

There is another operation that plays an important role. Namely the operator A that moves the

marked point in the triangle from one corner to its neighbour. This operator is given by

$$A_v = e^{-i\pi/3} e^{i3\pi q_v^2} e^{i\pi(p_v+q_v)^2} . \quad (\text{E.16})$$

E.2 $U_q(SL(2, \mathbb{R}))$ $6j$ -symbols and quantum Teichmüller theory

Now we give an overly simplified review of the connection of these tetrahedral operator T_{vw} and the $U_q(SL(2, \mathbb{R}))$ quantum $6j$ symbols [231]. The purpose is to translate the convoluted mathematical construction into an intuitive physical picture and to appreciate the relation between the quantum $6j$ symbols and Kashev's tetrahedra in his formulation of the Teichmüller TQFT. Readers should consult [21, 52, 137, 231, 234] for complete details.

The connection follows from two ways of parameterising the Riemann surface Σ . In Kashaev's discussion, one discretizes the Riemann surface into triangles. This is quite different from what field theorists, particularly string theorists are familiar with. For field/string theorists, it is customary to consider cutting the Riemann surface along closed curves, and decomposing the surface into closed pairs of pants. There is a natural way to construct coordinates of the moduli space based on the pair-of-pants decomposition, and construct representations of the mapping class group associated to this set of coordinates. The latter construction is shown to be related to the $U_q(SL(2, \mathbb{R}))$ $6j$ -symbols.

To appreciate some more of the details, the set of coordinates on the Teichmüller space that are natural to the closed pair-of-pants decomposition is called the Fenchel–Nielsen coordinates.

The decomposition of the Riemann surface is achieved by a collection of cuts along non-intersecting closed curves $\{C_i\}$, which is called a cut system, where

$$1 \leq i \leq 3g + n - 3 \equiv \kappa . \quad (\text{E.17})$$

For each pair of pants in which the boundary components are geodesics, one can go to the unique conformal frame with constant curvature -1 and label the surface by the geodesic lengths of the boundary components (L_1, L_2, L_3) . We use capital L_i 's to distinguish them from the Penner coordinates. In addition, to specify the original Riemann surface, one has to describe how the pair of pants are glued back together along the cuts $\{C_i\}$. In general, one could twist one of the boundary component of a trinion sharing a given cut by an angle ϕ_i before gluing. A Dehn twist in particular would shift these twist angles by 2π . Every cut is also assigned this twist label ϕ_i . Together, there are 2κ variables $\{L_1, \dots, L_\kappa; \phi_1, \dots, \phi_\kappa\}$. The Weil-Petersson form takes the form

$$\omega = \sum_i^\kappa d(L_i \frac{\phi_i}{2\pi}) \wedge dL_i . \quad (\text{E.18})$$

Note that the associated Poisson bracket $\{L_i, L_j\}$ vanishes.

There is a simple conversion between the closed geodesic lengths L_i and the Fock coordinates.

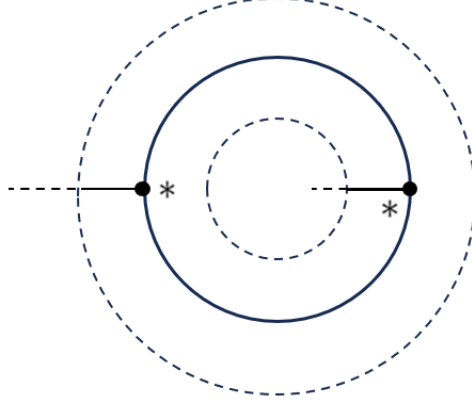


Figure 61: The connection between the Fenchel–Nielsen coordinate and the Fock coordinate can be understood by examining the triangulation of an annulus region surrounding closed geodesics.

Recall that the Fock coordinates are defined based on an (ideal) triangulation of the Riemann surface. Consider the dual graph of the triangulation, and pick up a closed path γ_i that is homotopic to a closed cut C_i in the cut system chosen for the Fenchel–Nielsen coordinates. Then the relation between the geodesic length L_i and the Fock coordinates of the ordered collection of edges $\{z_{e_m}\}_{\gamma_i}$ along the path γ_i is given by [233]

$$2 \cosh\left(\frac{L_i}{2}\right) = |\text{Tr}(X_{\gamma_i})|, \quad (\text{E.19})$$

where X_i is

$$X_{\gamma_i} = V^{\sigma_r} E(z_{e_r}) \dots V^{\sigma_1} E(z_{e_1}), \quad e_i \in \gamma_i. \quad (\text{E.20})$$

Here

$$E(z) = \begin{pmatrix} 0 & e^{z/2} \\ -e^{-z/2} & 0 \end{pmatrix}, \quad V = \begin{pmatrix} 1 & 1 \\ -1 & 0 \end{pmatrix}, \quad (\text{E.21})$$

and $\sigma_m = \pm 1$, depending on whether the segment e_m is turning right (+1) when it connects to e_{m+1} or left (−1). This is a classical relation. When one quantizes the Teichmüller space, the conversion between the Fenchel–Nielsen length operators and the Fock operators would be a nontrivial transformation. This transformation is constructed by considering an annular region which admits a canonical ideal triangulation with two triangles that would be naturally assigned two pairs of Kashaev’s canonical variables. The closed geodesics at the boundary of the annulus can then be expressed in terms of these Kashaev variables. See Fig. 61 for an illustration. These have been constructed in detail in [52]. The mapping class group representations can thus alternatively be constructed with the L_i ’s eigenstates serving as eigenbasis.

Now it comes to the emergence of the quantum $6j$ symbol. Consider two pairs of pants joining at

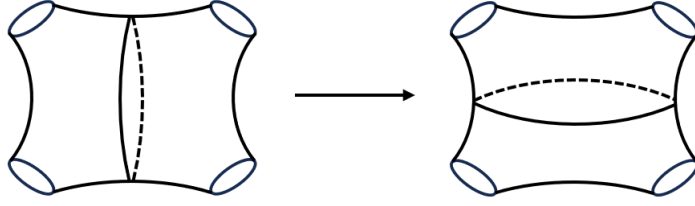


Figure 62: Crossing move for two closed pairs of pants decomposition of the four punctured sphere.

one circle. This is conformally related to a sphere with four punctures. It is possible to decompose this surface differently into two other pairs of pants, where each pair of pants contains one boundary component, each of the previous decomposition. This is depicted in Fig. 62. This is essentially the crossing transformation of the four punctures/incoming closed strings. The two decompositions were shown to be related precisely by the quantum $6j$ symbol of $U_q(SL(2, \mathbb{R}))$ introduced in (5.17). Recall that each of the parameters α_i, β_i in the $6j$ symbol is parametrized by (5.15)

$$\alpha = \frac{Q}{2} + iP_\alpha, \quad P_\alpha \in \mathbb{R}_{>0}. \quad (\text{E.22})$$

Here, they are related to the geodesic length of each boundary cycle and the intermediate cycles that propagate between the two pairs of pants by

$$P_i = \frac{L_i}{2\pi b}. \quad (\text{E.23})$$

Finally, one needs to connect the “crossing transformation” for the closed pairs of pants with the flipping of the triangulation in the Fock/Penner coordinates.

Intuitively, in order to make explicit the intermediate propagating cycle between two pairs of pants from the Fock coordinates, the triangulation should contain paths homotopic to the intermediate cycle. It is not surprising therefore to perform crossing in this picture of closed curve decomposition (i.e. Fenchel–Nielsen coordinates) one has to change the triangulation in the Fock/Penner picture. These considerations produce the final relation between the quantum $6j$ symbols and Kashaev’s tetrahedral operators, which is given as follows:

$$\begin{aligned} & \left\{ \begin{array}{ccc} Q/2 + iP_1 & Q/2 + iP_2 & Q/2 + iP_{12} \\ Q/2 + iP_3 & Q/2 + iP_4 & Q/2 + iP_{23} \end{array} \right\} \\ & = \langle \{P_i, P_{12}\} | C_2(s_3, s_{12}) C_1(s_2, s_1) T_{23}^{-1} T_{12}^{-1} T_{23} T_{13} C_2^{-1}(s_3, s_2) C_1^{-1}(s_{23}, s_1) | \{P_i, P_{23}\} \rangle. \quad (\text{E.24}) \end{aligned}$$

where C is the Clebsh-Gordan map and is detailed in [231]. The labels of the tetrahedral operator are related to a canonical ideal triangulation tiling the pairs of pants. Rather than explaining that

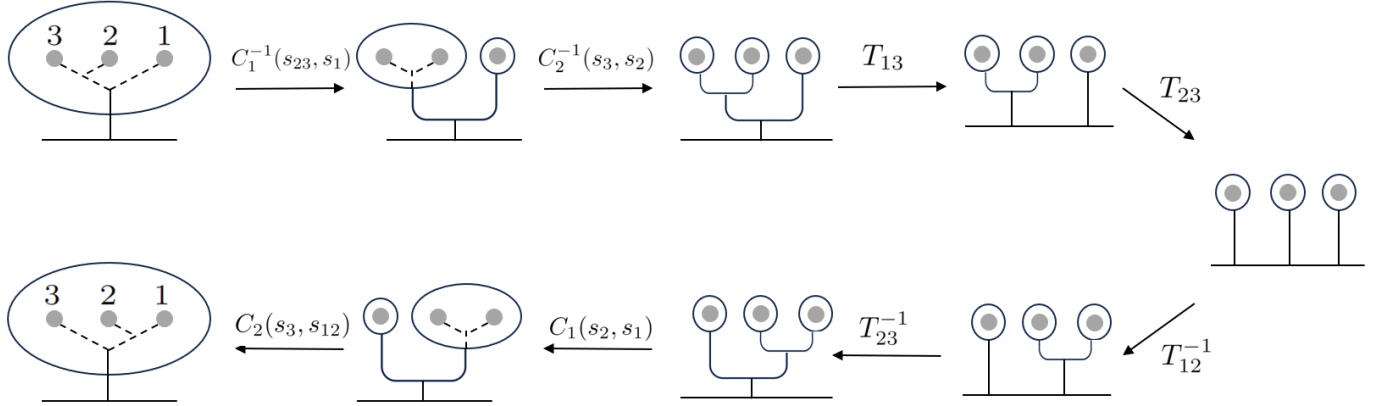


Figure 63: The computation of the $U_q(SL(2, \mathbb{R}))$ $u6j$ symbol is performed by first applying the (inverse of) Clebesh–Gordan map, such that we can apply the tetrahedron flip operator T on triangles, and then converting back to eigenstates of the Fenchel–Nielsen coordinates.

triangulation, it is much more instructive to depict the whole procedure as in Fig. 63.

This shows that a single quantum $6j$ symbol of $U_q(SL(2, \mathbb{R}))$ can be decomposed into four tetrahedra in Kashaev’s Tecihtmuller TQFT (with the twist operators already sent to zero, which is acceptable since this combination is finite anyway).

References

- [1] L. Chen, L.-Y. Hung, Y. Jiang and B.-X. Lao, Quantum 2D Liouville Path-Integral Is a Sum over Geometries in AdS₃ Einstein Gravity, 2024, [arXiv:2403.03179 [hep-th]].
- [2] J. M. Maldacena, The Large N limit of superconformal field theories and supergravity, *Adv. Theor. Math. Phys.* **2**, 231–252, 1998, [arXiv:hep-th/9711200].
- [3] S. S. Gubser, I. R. Klebanov and A. M. Polyakov, Gauge theory correlators from noncritical string theory, *Phys. Lett. B* **428**, 105–114, 1998, [arXiv:hep-th/9802109].
- [4] E. Witten, Anti-de Sitter space and holography, *Adv. Theor. Math. Phys.* **2**, 253–291, 1998, [arXiv:hep-th/9802150].
- [5] D. Gaiotto and J. Kulp, Orbifold groupoids, *JHEP* **02**, 132, 2021, [arXiv:2008.05960 [hep-th]].
- [6] D. S. Freed, G. W. Moore and C. Teleman, Topological symmetry in quantum field theory, 2022, [arXiv:2209.07471 [hep-th]].
- [7] W. Ji and X.-G. Wen, Categorical symmetry and noninvertible anomaly in symmetry-breaking and topological phase transitions, *Phys. Rev. Res.* **2**, 033417, 2020, [arXiv:1912.13492 [cond-mat.str-el]].
L. Kong, T. Lan, X.-G. Wen, Z.-H. Zhang and H. Zheng, Algebraic higher symmetry and categorical symmetry – a holographic and entanglement view of symmetry, *Phys. Rev. Res.* **2**, 043086, 2020, [arXiv:2005.14178 [cond-mat.str-el]].

- L. Kong, T. Lan, X.-G. Wen, Z.-H. Zhang and H. Zheng, Classification of topological phases with finite internal symmetries in all dimensions, *JHEP* **09**, 093, 2020, [[arXiv:2003.08898 \[math-ph\]](#)].
- A. Chatterjee and X.-G. Wen, Symmetry as a shadow of topological order and a derivation of topological holographic principle, *Phys. Rev. B* **107**, 155136, 2023, [[arXiv:2203.03596 \[cond-mat.str-el\]](#)].
- [8] F. Apruzzi, F. Bonetti, I. n. García Etxebarria, S. S. Hosseini and S. Schafer-Nameki, Symmetry TFTs from String Theory, *Commun. Math. Phys.* **402**, 895–949, 2023, [[arXiv:2112.02092 \[hep-th\]](#)].
- [9] D. S. Freed and C. Teleman, Topological dualities in the Ising model, *Geom. Topol.* **26**, 1907–1984, 2022, [[arXiv:1806.00008 \[math.AT\]](#)].
- [10] L. Kong and H. Zheng, A mathematical theory of gapless edges of 2d topological orders. Part I, *JHEP* **02**, 150, 2020, [[arXiv:1905.04924 \[cond-mat.str-el\]](#)].
- [11] L. Bhardwaj and Y. Tachikawa, On finite symmetries and their gauging in two dimensions, *JHEP* **03**, 189, 2018, [[arXiv:1704.02330 \[hep-th\]](#)].
- [12] V. V. Albert, D. Aasen, W. Xu, W. Ji, J. Alicea and J. Preskill, Spin chains, defects, and quantum wires for the quantum-double edge, 2021, [[arXiv:2111.12096 \[cond-mat.str-el\]](#)].
- [13] R. Vanhove, M. Bal, D. J. Williamson, N. Bultinck, J. Haegeman and F. Verstraete, Mapping topological to conformal field theories through strange correlators, *Phys. Rev. Lett.* **121**, 177203, 2018, [[arXiv:1801.05959 \[quant-ph\]](#)].
- [14] D. Aasen, P. Fendley and R. S. K. Mong, Topological Defects on the Lattice: Dualities and Degeneracies, 2020, [[arXiv:2008.08598 \[cond-mat.stat-mech\]](#)].
- [15] D. Gaiotto, A. Kapustin, N. Seiberg and B. Willett, Generalized Global Symmetries, *JHEP* **02**, 172, 2015, [[arXiv:1412.5148 \[hep-th\]](#)].
- [16] L. Kong, T. Lan, X.-G. Wen, Z.-H. Zhang and H. Zheng, Algebraic higher symmetry and categorical symmetry: A holographic and entanglement view of symmetry, *Phys. Rev. Res.* **2**, 043086, 2020.
- [17] L. Susskind and E. Witten, The Holographic bound in anti-de Sitter space, 1998, [[arXiv:hep-th/9805114](#)].
- [18] J. de Boer, E. P. Verlinde and H. L. Verlinde, On the holographic renormalization group, *JHEP* **08**, 003, 2000, [[arXiv:hep-th/9912012](#)].
- [19] K. Skenderis, Lecture notes on holographic renormalization, *Class. Quant. Grav.* **19**, 5849–5876, 2002, [[arXiv:hep-th/0209067](#)].
- [20] E. P. Verlinde, Fusion Rules and Modular Transformations in 2D Conformal Field Theory, *Nucl. Phys. B* **300**, 360–376, 1988.
- [21] J. Ellegaard Andersen and R. Kashaev, A TQFT from Quantum Teichmüller Theory, *Commun. Math. Phys.* **330**, 887–934, 2014, [[arXiv:1109.6295 \[math.QA\]](#)].
- [22] S. Collier, L. Eberhardt and M. Zhang, Solving 3d gravity with Virasoro TQFT, *SciPost Phys.* **15**, 151, 2023, [[arXiv:2304.13650 \[hep-th\]](#)].

- [23] V. G. Turaev and O. Y. Viro, State sum invariants of 3 manifolds and quantum 6j symbols, *Topology* **31**, 865–902, 1992.
- [24] M. A. Levin and X.-G. Wen, String net condensation: A Physical mechanism for topological phases, *Phys. Rev. B* **71**, 045110, 2005, [arXiv:cond-mat/0404617].
- [25] X. Chen, Z. C. Gu and X. G. Wen, Local unitary transformation, long-range quantum entanglement, wave function renormalization, and topological order, *Phys. Rev. B* **82**, 155138, 2010, [arXiv:1004.3835 [cond-mat.str-el]].
- [26] A. Kitaev and J. Preskill, Topological entanglement entropy, *Phys. Rev. Lett.* **96**, 110404, 2006, [arXiv:hep-th/0510092].
M. Levin and X.-G. Wen, Detecting topological order in a ground state wave function, *Phys. Rev. Lett.* **96**, 110405, 2006.
- [27] A. B. Zamolodchikov, Expectation value of composite field T anti- T in two-dimensional quantum field theory, 2004, [arXiv:hep-th/0401146].
- [28] L. McGough, M. Mezei and H. Verlinde, Moving the CFT into the bulk with $T\bar{T}$, *JHEP* **04**, 010, 2018, [arXiv:1611.03470 [hep-th]].
- [29] L. Chen, H. Zhang, K. Ji, C. Shen, R. Wang, X. Zeng and L.-Y. Hung, CFT_D from $TQFT_{D+1}$ via Holographic Tensor Network, and Precision Discretisation of CFT_2 , 2022, [arXiv:2210.12127 [hep-th]].
- [30] G. Cheng, L. Chen, Z.-C. Gu and L.-Y. Hung, Exact fixed-point tensor network construction for rational conformal field theory, 2023, [arXiv:2311.18005 [cond-mat.str-el]].
- [31] L.-Y. Hung and Y. Jiang, Building up quantum spacetimes with BCFT Legos, 2024, [arXiv:2404.00877 [hep-th]].
- [32] J. Fuchs, I. Runkel and C. Schweigert, TFT construction of RCFT correlators 1. Partition functions, *Nucl. Phys. B* **646**, 353–497, 2002, [arXiv:hep-th/0204148].
J. Fuchs, I. Runkel and C. Schweigert, TFT construction of RCFT correlators. 2. Unoriented world sheets, *Nucl. Phys. B* **678**, 511–637, 2004, [arXiv:hep-th/0306164].
J. Fuchs, I. Runkel and C. Schweigert, TFT construction of RCFT correlators. 3. Simple currents, *Nucl. Phys. B* **694**, 277–353, 2004, [arXiv:hep-th/0403157].
J. Fuchs, I. Runkel and C. Schweigert, TFT construction of RCFT correlators IV: Structure constants and correlation functions, *Nucl. Phys. B* **715**, 539–638, 2005, [arXiv:hep-th/0412290].
J. Fjelstad, J. Fuchs, I. Runkel and C. Schweigert, TFT construction of RCFT correlators. V. Proof of modular invariance and factorisation, *Theor. Appl. Categor.* **16**, 342–433, 2006, [arXiv:hep-th/0503194].
J. Frohlich, J. Fuchs, I. Runkel and C. Schweigert, Duality and defects in rational conformal field theory, *Nucl. Phys. B* **763**, 354–430, 2007, [arXiv:hep-th/0607247].
J. Fjelstad, J. Fuchs, I. Runkel and C. Schweigert, Uniqueness of open / closed rational CFT with given algebra of open states, *Adv. Theor. Math. Phys.* **12**, 1283–1375, 2008, [arXiv:hep-th/0612306].
- [33] H. L. Verlinde, Conformal Field Theory, 2- D Quantum Gravity and Quantization of Teichmuller Space, *Nucl. Phys. B* **337**, 652–680, 1990.

- [34] L. Freidel, Reconstructing AdS/CFT, 2008, [[arXiv:0804.0632 \[hep-th\]](#)].
- [35] G. Vidal, Class of Quantum Many-Body States That Can Be Efficiently Simulated, *Phys. Rev. Lett.* **101**, 110501, 2008, [[arXiv:quant-ph/0610099](#)].
- [36] B. Swingle, Entanglement Renormalization and Holography, *Phys. Rev. D* **86**, 065007, 2012, [[arXiv:0905.1317 \[cond-mat.str-el\]](#)].
- [37] F. Apruzzi, F. Bedogna and N. Dondi, SymTh for non-finite symmetries, 2024, [[arXiv:2402.14813 \[hep-th\]](#)].
- [38] S.-S. Lee, Quantum Renormalization Group and Holography, *JHEP* **01**, 076, 2014, [[arXiv:1305.3908 \[hep-th\]](#)].
- [39] S.-S. Lee, Horizon as Critical Phenomenon, *JHEP* **09**, 044, 2016, [[arXiv:1603.08509 \[hep-th\]](#)].
- [40] L. D. Faddeev and L. A. Takhtajan, Liouville model on the lattice, *Lect. Notes Phys.* **246**, 166–179, 1986.
- [41] M. Banados, C. Teitelboim and J. Zanelli, The Black hole in three-dimensional space-time, *Phys. Rev. Lett.* **69**, 1849–1851, 1992, [[arXiv:hep-th/9204099](#)].
- [42] G. W. Moore and N. Seiberg, Classical and Quantum Conformal Field Theory, *Commun. Math. Phys.* **123**, 177, 1989.
G. W. Moore and N. Seiberg, LECTURES ON RCFT, in 1989 Banff NATO ASI: Physics, Geometry and Topology, 1989.
- [43] K. G. Wilson, The renormalization group and critical phenomena, *Rev. Mod. Phys.* **55**, 583–600, 1983.
- [44] L. P. Kadanoff, Scaling laws for ising models near T_c , *Physics Physique Fizika* **2**, 263–272, 1966.
- [45] J. Polchinski, Renormalization and Effective Lagrangians, *Nucl. Phys. B* **231**, 269–295, 1984.
- [46] I. Heemskerck and J. Polchinski, Holographic and Wilsonian Renormalization Groups, *JHEP* **06**, 031, 2011, [[arXiv:1010.1264 \[hep-th\]](#)].
T. Faulkner, H. Liu and M. Rangamani, Integrating out geometry: Holographic Wilsonian RG and the membrane paradigm, *JHEP* **08**, 051, 2011, [[arXiv:1010.4036 \[hep-th\]](#)].
- [47] S.-S. Lee, Background independent holographic description : From matrix field theory to quantum gravity, *JHEP* **10**, 160, 2012, [[arXiv:1204.1780 \[hep-th\]](#)].
- [48] G. W. Moore and N. Seiberg, Polynomial Equations for Rational Conformal Field Theories, *Phys. Lett. B* **212**, 451–460, 1988.
- [49] V. B. Petkova and J. B. Zuber, Generalized twisted partition functions, *Phys. Lett. B* **504**, 157–164, 2001, [[arXiv:hep-th/0011021](#)].
- [50] C.-M. Chang, Y.-H. Lin, S.-H. Shao, Y. Wang and X. Yin, Topological Defect Lines and Renormalization Group Flows in Two Dimensions, *JHEP* **01**, 026, 2019, [[arXiv:1802.04445 \[hep-th\]](#)].
- [51] S. Jackson, L. McGough and H. Verlinde, Conformal Bootstrap, Universality and Gravitational Scattering, *Nucl. Phys. B* **901**, 382–429, 2015, [[arXiv:1412.5205 \[hep-th\]](#)].

- [52] J. Teschner, An Analog of a modular functor from quantized teichmuller theory, 2005, [[arXiv:math/0510174](#)].
- [53] D. Friedan and S. H. Shenker, The Analytic Geometry of Two-Dimensional Conformal Field Theory, *Nucl. Phys. B* **281**, 509–545, 1987.
- [54] R. Dijkgraaf, E. P. Verlinde and H. L. Verlinde, $C = 1$ Conformal Field Theories on Riemann Surfaces, *Commun. Math. Phys.* **115**, 649–690, 1988.
- [55] Y.-H. Lin, M. Okada, S. Seifnashri and Y. Tachikawa, Asymptotic density of states in 2d CFTs with non-invertible symmetries, *JHEP* **03**, 094, 2023, [[arXiv:2208.05495 \[hep-th\]](#)].
- [56] B. S. DeWitt, Quantum theory of gravity. i. the canonical theory, *Phys. Rev.* **160**, 1113–1148, 1967.
J. B. Hartle and S. W. Hawking, Wave function of the universe, *Phys. Rev. D* **28**, 2960–2975, 1983.
- [57] I. R. Klebanov and E. Witten, AdS / CFT correspondence and symmetry breaking, *Nucl. Phys. B* **556**, 89–114, 1999, [[arXiv:hep-th/9905104](#)].
- [58] E. Witten, Multitrace operators, boundary conditions, and AdS / CFT correspondence, 2001, [[arXiv:hep-th/0112258](#)].
- [59] M. Guica and R. Monten, $T\bar{T}$ and the mirage of a bulk cutoff, *SciPost Phys.* **10**, 024, 2021, [[arXiv:1906.11251 \[hep-th\]](#)].
- [60] M. Guica, $J\bar{T}$ -deformed CFTs as non-local CFTs, 2021, [[arXiv:2110.07614 \[hep-th\]](#)].
M. Guica, R. Monten and I. Tsiaras, Classical and quantum symmetries of $T\bar{T}$ -deformed CFTs, 2022, [[arXiv:2212.14014 \[hep-th\]](#)].
- [61] E. Llabrés, General solutions in Chern-Simons gravity and $T\bar{T}$ -deformations, *JHEP* **01**, 039, 2021, [[arXiv:1912.13330 \[hep-th\]](#)].
S. Ebert, C. Ferko, H.-Y. Sun and Z. Sun, $T\bar{T}$ in JT Gravity and BF Gauge Theory, *SciPost Phys.* **13**, 096, 2022, [[arXiv:2205.07817 \[hep-th\]](#)].
- [62] H. Ma and S.-S. Lee, Constraints on beta functions in field theories, *SciPost Phys.* **12**, 046, 2022, [[arXiv:2009.11880 \[hep-th\]](#)].
- [63] F. A. Smirnov and A. B. Zamolodchikov, On space of integrable quantum field theories, *Nucl. Phys. B* **915**, 363–383, 2017, [[arXiv:1608.05499 \[hep-th\]](#)].
- [64] E. A. Mazenc, V. Shyam and R. M. Soni, A $T\bar{T}$ Deformation for Curved Spacetimes from 3d Gravity, 2019, [[arXiv:1912.09179 \[hep-th\]](#)].
- [65] A. J. Tolley, $T\bar{T}$ deformations, massive gravity and non-critical strings, *JHEP* **06**, 050, 2020, [[arXiv:1911.06142 \[hep-th\]](#)].
- [66] A. Belin, A. Lewkowycz and G. Sarosi, Gravitational path integral from the T^2 deformation, *JHEP* **09**, 156, 2020, [[arXiv:2006.01835 \[hep-th\]](#)].
- [67] K.-S. Kim, S. Ryu and K. Lee, Emergent dual holographic description as a nonperturbative generalization of the Wilsonian renormalization group, *Phys. Rev. D* **105**, 086019, 2022, [[arXiv:2112.06237 \[hep-th\]](#)].

- [68] G. Araujo-Regado, R. Khan and A. C. Wall, Cauchy slice holography: a new AdS/CFT dictionary, *JHEP* **03**, 026, 2023, [[arXiv:2204.00591 \[hep-th\]](#)].
- [69] V. Shyam, General Covariance from the Quantum Renormalization Group, *Phys. Rev. D* **95**, 066003, 2017, [[arXiv:1611.05315 \[gr-qc\]](#)].
- [70] J. Cardy, Quantum Quenches to a Critical Point in One Dimension: some further results, *J. Stat. Mech.* **1602**, 023103, 2016, [[arXiv:1507.07266 \[cond-mat.stat-mech\]](#)].
J. Cardy, The $T\bar{T}$ deformation of quantum field theory as random geometry, *JHEP* **10**, 186, 2018, [[arXiv:1801.06895 \[hep-th\]](#)].
- [71] T. Hartman, J. Kruthoff, E. Shaghoulian and A. Tajdini, Holography at finite cutoff with a T^2 deformation, *JHEP* **03**, 004, 2019, [[arXiv:1807.11401 \[hep-th\]](#)].
- [72] A. Cavaglià, S. Negro, I. M. Szécsényi and R. Tateo, $T\bar{T}$ -deformed 2D Quantum Field Theories, *JHEP* **10**, 112, 2016, [[arXiv:1608.05534 \[hep-th\]](#)].
- [73] M. Han, Canonical Path-Integral Measures for Holst and Plebanski Gravity. II. Gauge Invariance and Physical Inner Product, *Class. Quant. Grav.* **27**, 245015, 2010, [[arXiv:0911.3436 \[gr-qc\]](#)].
- [74] V. Balasubramanian and P. Kraus, A Stress tensor for Anti-de Sitter gravity, *Commun. Math. Phys.* **208**, 413–428, 1999, [[arXiv:hep-th/9902121](#)].
- [75] E. Witten, A note on the canonical formalism for gravity, *Adv. Theor. Math. Phys.* **27**, 311–380, 2023, [[arXiv:2212.08270 \[hep-th\]](#)].
- [76] J. D. Brown and M. Henneaux, Central Charges in the Canonical Realization of Asymptotic Symmetries: An Example from Three-Dimensional Gravity, *Commun. Math. Phys.* **104**, 207–226, 1986.
- [77] E. Witten, (2+1)-Dimensional Gravity as an Exactly Soluble System, *Nucl. Phys. B* **311**, 46, 1988.
- [78] E. Witten, Quantum Field Theory and the Jones Polynomial, *Commun. Math. Phys.* **121**, 351–399, 1989.
- [79] S. Elitzur, G. W. Moore, A. Schwimmer and N. Seiberg, Remarks on the Canonical Quantization of the Chern-Simons-Witten Theory, *Nucl. Phys. B* **326**, 108–134, 1989.
- [80] A. Kirillov, Jr, String-net model of Turaev-Viro invariants, 2011, [[arXiv:1106.6033 \[math.AT\]](#)].
- [81] A. Y. Kitaev, Fault tolerant quantum computation by anyons, *Annals Phys.* **303**, 2–30, 2003, [[arXiv:quant-ph/9707021](#)].
- [82] R. König, B. W. Reichardt and G. Vidal, Exact entanglement renormalization for string-net models, *Physical Review B—Condensed Matter and Materials Physics* **79**, 195123, 2009.
- [83] Y. Hu, N. Geer and Y.-S. Wu, Full dyon excitation spectrum in extended Levin-Wen models, *Phys. Rev. B* **97**, 195154, 2018, [[arXiv:1502.03433 \[cond-mat.str-el\]](#)].
- [84] D. Aasen, R. S. K. Mong and P. Fendley, Topological Defects on the Lattice I: The Ising model, *J. Phys. A* **49**, 354001, 2016, [[arXiv:1601.07185 \[cond-mat.stat-mech\]](#)].

- [85] E. M. Brehm and I. Runkel, Lattice models from CFT on surfaces with holes: I. Torus partition function via two lattice cells, *J. Phys. A* **55**, 235001, 2022, [[arXiv:2112.01563 \[cond-mat.stat-mech\]](#)].
E. M. Brehm and I. Runkel, Lattice models from CFT on surfaces with holes II: Cloaking boundary conditions and loop models, 2024, [[arXiv:2410.19938 \[math-ph\]](#)].
- [86] I. Runkel, Boundary structure constants for the A series Virasoro minimal models, *Nucl. Phys. B* **549**, 563–578, 1999, [[arXiv:hep-th/9811178](#)].
I. Runkel, Structure constants for the D series Virasoro minimal models, *Nucl. Phys. B* **579**, 561–589, 2000, [[arXiv:hep-th/9908046](#)].
- [87] L. Lootens, J. Fuchs, J. Haegeman, C. Schweigert and F. Verstraete, Matrix product operator symmetries and intertwiners in string-nets with domain walls, *SciPost Phys.* **10**, 053, 2021, [[arXiv:2008.11187 \[quant-ph\]](#)].
- [88] L. Y. Hung and G. Wong, Entanglement branes and factorization in conformal field theory, *Phys. Rev. D* **104**, 026012, 2021, [[arXiv:1912.11201 \[hep-th\]](#)].
- [89] J. L. Cardy, Boundary conformal field theory, 2004, [[arXiv:hep-th/0411189](#)].
- [90] D. Perez-Garcia, F. Verstraete, M. M. Wolf and J. I. Cirac, Matrix product state representations, *Quant. Inf. Comput.* **7**, 401–430, 2007, [[arXiv:quant-ph/0608197](#)].
Verstraete, Frank and Murg, V and Cirac, JI, Matrix product states, projected entangled pair states, and variational renormalization group methods for quantum spin systems, *ADVANCES IN PHYSICS* **57**, 143–224, 2008.
- [91] F. Verstraete and J. I. Cirac, Valence-bond states for quantum computation, *Phys. Rev. A* **70**, 060302, 2004.
F. Verstraete and J. I. Cirac, Renormalization algorithms for quantum-many body systems in two and higher dimensions, 2004, [[arXiv:cond-mat/0407066](#)].
- [92] Y.-Z. You, Z. Bi, A. Rasmussen, K. Slagle and C. Xu, Wave function and strange correlator of short-range entangled states, *Phys. Rev. Lett.* **112**, 247202, 2014.
- [93] M. Levin and C. P. Nave, Tensor renormalization group approach to two-dimensional classical lattice models, *Phys. Rev. Lett.* **99**, 120601, 2007.
G. Evenbly and G. Vidal, Tensor network renormalization, *Phys. Rev. Lett.* **115**, 180405, 2015.
S. Yang, Z.-C. Gu and X.-G. Wen, Loop optimization for tensor network renormalization, *Phys. Rev. Lett.* **118**, 110504, 2017.
M. Bal, M. Mariën, J. Haegeman and F. Verstraete, Renormalization group flows of hamiltonians using tensor networks, *Phys. Rev. Lett.* **118**, 250602, 2017.
- [94] R. König, B. W. Reichardt and G. Vidal, Exact entanglement renormalization for string-net models, *Phys. Rev. B* **79**, 195123, 2009.
R. Koenig, G. Kuperberg and B. W. Reichardt, Quantum computation with turaev–viro codes, *Annals of Physics* **325**, 2707–2749, 2010.

- [95] M. Van Raamsdonk, Building up spacetime with quantum entanglement II: It from BC-bit, 2018, [[arXiv:1809.01197 \[hep-th\]](#)].
- [96] Z.-X. Luo, E. Lake and Y.-S. Wu, The structure of fixed-point tensor network states characterizes the patterns of long-range entanglement, *Phys. Rev. B* **96**, 035101, 2017, [[arXiv:1611.01140 \[cond-mat.str-el\]](#)].
- [97] L. Chen, L.-Y. Hung, H. Geng and Y. Jiang, “Tensor network representation of JT gravity.” In preparation.
- [98] Y. Jiang, $T\bar{T}$ Deformation: A Lattice Approach, *Symmetry* **15**, 2212, 2023, [[arXiv:2312.12078 \[hep-th\]](#)].
- [99] V. Bonzom, E. R. Livine and S. Speziale, Recurrence relations for spin foam vertices, *Class. Quant. Grav.* **27**, 125002, 2010, [[arXiv:0911.2204 \[gr-qc\]](#)].
V. Bonzom and L. Freidel, The Hamiltonian constraint in 3d Riemannian loop quantum gravity, *Class. Quant. Grav.* **28**, 195006, 2011, [[arXiv:1101.3524 \[gr-qc\]](#)].
- [100] S. Ryu and T. Takayanagi, Holographic derivation of entanglement entropy from AdS/CFT, *Phys. Rev. Lett.* **96**, 181602, 2006, [[arXiv:hep-th/0603001](#)].
- [101] A. Hamilton, D. N. Kabat, G. Lifschytz and D. A. Lowe, Local bulk operators in AdS/CFT: A Boundary view of horizons and locality, *Phys. Rev. D* **73**, 086003, 2006, [[arXiv:hep-th/0506118](#)].
A. Hamilton, D. N. Kabat, G. Lifschytz and D. A. Lowe, Holographic representation of local bulk operators, *Phys. Rev. D* **74**, 066009, 2006, [[arXiv:hep-th/0606141](#)].
- [102] B. Czech, J. L. Karczmarek, F. Nogueira and M. Van Raamsdonk, The Gravity Dual of a Density Matrix, *Class. Quant. Grav.* **29**, 155009, 2012, [[arXiv:1204.1330 \[hep-th\]](#)].
- [103] D. L. Jafferis, A. Lewkowycz, J. Maldacena and S. J. Suh, Relative entropy equals bulk relative entropy, *JHEP* **06**, 004, 2016, [[arXiv:1512.06431 \[hep-th\]](#)].
- [104] A. Almheiri, X. Dong and D. Harlow, Bulk Locality and Quantum Error Correction in AdS/CFT, *JHEP* **04**, 163, 2015, [[arXiv:1411.7041 \[hep-th\]](#)].
X. Dong, D. Harlow and A. C. Wall, Reconstruction of Bulk Operators within the Entanglement Wedge in Gauge-Gravity Duality, *Phys. Rev. Lett.* **117**, 021601, 2016, [[arXiv:1601.05416 \[hep-th\]](#)].
- [105] F. Pastawski, B. Yoshida, D. Harlow and J. Preskill, Holographic quantum error-correcting codes: Toy models for the bulk/boundary correspondence, *JHEP* **06**, 149, 2015, [[arXiv:1503.06237 \[hep-th\]](#)].
- [106] W. Donnelly, B. Michel, D. Marolf and J. Wien, Living on the Edge: A Toy Model for Holographic Reconstruction of Algebras with Centers, *JHEP* **04**, 093, 2017, [[arXiv:1611.05841 \[hep-th\]](#)].
X.-L. Qi, Emergent bulk gauge field in random tensor networks, 2022, [[arXiv:2209.02940 \[hep-th\]](#)].
X. Dong, S. McBride and W. W. Weng, Holographic tensor networks with bulk gauge symmetries, *JHEP* **02**, 222, 2024, [[arXiv:2309.06436 \[hep-th\]](#)].
C. Akers and A. Y. Wei, Background independent tensor networks, *SciPost Phys.* **17**, 090, 2024, [[arXiv:2402.05910 \[hep-th\]](#)].

- [107] C. Akers, R. M. Soni and A. Y. Wei, Multipartite edge modes and tensor networks, *SciPost Phys. Core* **7**, 070, 2024, [[arXiv:2404.03651 \[hep-th\]](#)].
- [108] S. Singh and G. Vidal, Symmetry protected entanglement renormalization, *Phys. Rev. B* **88**, 121108, 2013, [[arXiv:1303.6716 \[cond-mat.str-el\]](#)].
S. Singh and G. Vidal, Tensor network states and algorithms in the presence of a global SU(2) symmetry, *Phys. Rev. B* **86**, 195114, 2012, [[arXiv:1208.3919 \[cond-mat.str-el\]](#)].
- [109] E. Verlinde and H. Verlinde, Black Hole Entanglement and Quantum Error Correction, *JHEP* **10**, 107, 2013, [[arXiv:1211.6913 \[hep-th\]](#)].
- [110] E. Verlinde and H. Verlinde, Black Hole Information as Topological Qubits, 2013, [[arXiv:1306.0516 \[hep-th\]](#)].
- [111] N. Bao, Y. Jiang and J. Naskar, Subregion duality, wedge classification and no global symmetries in AdS/CFT, 2024, [[arXiv:2408.04016 \[hep-th\]](#)].
- [112] H. Verlinde, Poking Holes in AdS/CFT: Bulk Fields from Boundary States, 2015, [[arXiv:1505.05069 \[hep-th\]](#)].
K. Goto, M. Miyaji and T. Takayanagi, Causal Evolutions of Bulk Local Excitations from CFT, *JHEP* **09**, 130, 2016, [[arXiv:1605.02835 \[hep-th\]](#)].
A. Lewkowycz, G. J. Turiaci and H. Verlinde, A CFT Perspective on Gravitational Dressing and Bulk Locality, *JHEP* **01**, 004, 2017, [[arXiv:1608.08977 \[hep-th\]](#)].
K. Goto and T. Takayanagi, CFT descriptions of bulk local states in the AdS black holes, *JHEP* **10**, 153, 2017, [[arXiv:1704.00053 \[hep-th\]](#)].
- [113] F. Bonetti, M. Del Zotto and R. Minasian, SymTFTs for Continuous non-Abelian Symmetries, 2024, [[arXiv:2402.12347 \[hep-th\]](#)].
- [114] T. D. Brennan and Z. Sun, A SymTFT for Continuous Symmetries, 2024, [[arXiv:2401.06128 \[hep-th\]](#)].
- [115] A. Antinucci and F. Benini, Anomalies and gauging of U(1) symmetries, 2024, [[arXiv:2401.10165 \[hep-th\]](#)].
- [116] A. Achucarro and P. K. Townsend, A Chern-Simons Action for Three-Dimensional anti-De Sitter Supergravity Theories, *Phys. Lett. B* **180**, 89, 1986.
- [117] J. Cotler and K. Jensen, AdS₃ gravity and random CFT, *JHEP* **04**, 033, 2021, [[arXiv:2006.08648 \[hep-th\]](#)].
- [118] E. Witten, Three-Dimensional Gravity Revisited, 2007, [[arXiv:0706.3359 \[hep-th\]](#)].
- [119] F. Benini, C. Copetti and L. Di Pietro, Factorization and global symmetries in holography, *SciPost Phys.* **14**, 019, 2023, [[arXiv:2203.09537 \[hep-th\]](#)].
- [120] V. Fateev, A. B. Zamolodchikov and A. B. Zamolodchikov, Boundary Liouville field theory. 1. Boundary state and boundary two point function, 2000, [[arXiv:hep-th/0001012](#)].
- [121] J. Teschner, Remarks on Liouville theory with boundary, *PoS tmr2000*, 041, 2000, [[arXiv:hep-th/0009138](#)].

- [122] B. Ponsot and J. Teschner, Boundary Liouville field theory: Boundary three point function, *Nucl. Phys. B* **622**, 309–327, 2002, [[arXiv:hep-th/0110244](#)].
- [123] D. Kazhdan and G. Lusztig, “Tensor structures arising from affine lie algebras..” iv, *Journal of the American Mathematical Society* 7 (1994), no. 2 383–453.
- [124] J. Teschner and G. Vartanov, 6j symbols for the modular double, quantum hyperbolic geometry, and supersymmetric gauge theories, *Lett. Math. Phys.* **104**, 527–551, 2014, [[arXiv:1202.4698 \[hep-th\]](#)].
- [125] L. D. Faddeev, Modular double of quantum group, in *Conference Moshe Flato*, pp. 149–156, 2000. [[arXiv:math/9912078](#)].
- [126] B. Ponsot and J. Teschner, Liouville bootstrap via harmonic analysis on a noncompact quantum group, 1999, [[arXiv:hep-th/9911110](#)].
B. Ponsot and J. Teschner, Clebsch-Gordan and Racah-Wigner coefficients for a continuous series of representations of $U(\mathfrak{q})(\mathfrak{sl}(2, \mathbb{R}))$, *Commun. Math. Phys.* **224**, 613–655, 2001, [[arXiv:math/0007097](#)].
- [127] J. L. Cardy, Operator Content of Two-Dimensional Conformally Invariant Theories, *Nucl. Phys. B* **270**, 186–204, 1986.
- [128] L. McGough and H. Verlinde, Bekenstein-Hawking Entropy as Topological Entanglement Entropy, *JHEP* **11**, 208, 2013, [[arXiv:1308.2342 \[hep-th\]](#)].
- [129] G. Hayward, Gravitational action for spacetimes with nonsmooth boundaries, *Phys. Rev. D* **47**, 3275–3280, 1993.
- [130] T. Takayanagi and K. Tamaoka, Gravity Edges Modes and Hayward Term, *JHEP* **02**, 167, 2020, [[arXiv:1912.01636 \[hep-th\]](#)].
- [131] T. Regge, GENERAL RELATIVITY WITHOUT COORDINATES, *Nuovo Cim.* **19**, 558–571, 1961.
T. Regge and G. Ponzano, “Semiclassical limit of racah coefficients.” p1-58, in: *Spectroscopic and group theoretical methods in physics*, ed. F. Bloch, North-Holland Publ. Co., Amsterdam, 1968.
- [132] W. Z. Chua and Y. Jiang, Hartle-Hawking state and its factorization in 3d gravity, *JHEP* **03**, 135, 2024, [[arXiv:2309.05126 \[hep-th\]](#)].
- [133] T. G. Mertens, J. Simón and G. Wong, A proposal for 3d quantum gravity and its bulk factorization, *JHEP* **06**, 134, 2023, [[arXiv:2210.14196 \[hep-th\]](#)].
G. Wong, A note on the bulk interpretation of the quantum extremal surface formula, *JHEP* **04**, 024, 2024, [[arXiv:2212.03193 \[hep-th\]](#)].
- [134] D. L. Jafferis and D. K. Kolchmeyer, Entanglement Entropy in Jackiw-Teitelboim Gravity, 2019, [[arXiv:1911.10663 \[hep-th\]](#)].
- [135] W. Donnelly, Y. Jiang, M. Kim and G. Wong, Entanglement entropy and edge modes in topological string theory. Part I. Generalized entropy for closed strings, *JHEP* **10**, 201, 2021, [[arXiv:2010.15737 \[hep-th\]](#)].
Y. Jiang, M. Kim and G. Wong, Entanglement entropy and edge modes in topological string theory. Part II. The dual gauge theory story, *JHEP* **10**, 202, 2021, [[arXiv:2012.13397 \[hep-th\]](#)].

- [136] A. B. Zamolodchikov and A. B. Zamolodchikov, Liouville field theory on a pseudosphere, 2001, [[arXiv:hep-th/0101152](#)].
 L. D. Faddeev, R. M. Kashaev and A. Y. Volkov, Strongly coupled quantum discrete Liouville theory. 1. Algebraic approach and duality, *Commun. Math. Phys.* **219**, 199–219, 2001, [[arXiv:hep-th/0006156](#)].
 L. D. Faddeev and R. M. Kashaev, Strongly coupled quantum discrete Liouville theory. 2. Geometric interpretation of the evolution operator, *J. Phys. A* **35**, 4043–4048, 2002, [[arXiv:hep-th/0201049](#)].
 R. M. Kashaev, Discrete Liouville equation and Teichmüller theory, *arXiv e-prints arXiv:0810.4352*, 2008, [[arXiv:0810.4352 \[math.QA\]](#)].
- [137] R. M. Kashaev, Quantization of Teichmüller spaces and the quantum dilogarithm, *eprint arXiv:q-alg/9705021 q-alg/9705021*, 1997, [[arXiv:q-alg/9705021 \[math.QA\]](#)].
 R. M. Kashaev, On the spectrum of Dehn twists in quantum Teichmüller theory, 2000, [[arXiv:math/0008148](#)].
- [138] R. M. Kashaev, Discrete liouville equation and teichmüller theory, 2008, [[arXiv:0810.4352 \[math.QA\]](#)].
- [139] M. Srednicki, Chaos and Quantum Thermalization, **50**, *Phys. Rev. E*, 1994, [[arXiv:cond-mat/9403051](#)].
 J. M. Deutsch, Quantum statistical mechanics in a closed system, *Phys. Rev. A* **43**, 2046–2049, 1991.
- [140] A. Belin and J. de Boer, Random statistics of OPE coefficients and Euclidean wormholes, *Class. Quant. Grav.* **38**, 164001, 2021, [[arXiv:2006.05499 \[hep-th\]](#)].
- [141] P. Saad, Late Time Correlation Functions, Baby Universes, and ETH in JT Gravity, 2019, [[arXiv:1910.10311 \[hep-th\]](#)].
 D. Stanford, More quantum noise from wormholes, 2020, [[arXiv:2008.08570 \[hep-th\]](#)].
 J. Pollack, M. Rozali, J. Sully and D. Wakeham, Eigenstate Thermalization and Disorder Averaging in Gravity, *Phys. Rev. Lett.* **125**, 021601, 2020, [[arXiv:2002.02971 \[hep-th\]](#)].
- [142] A. Belin, J. de Boer, D. L. Jafferis, P. Nayak and J. Sonner, Approximate CFTs and random tensor models, *JHEP* **09**, 163, 2024, [[arXiv:2308.03829 \[hep-th\]](#)].
- [143] D. L. Jafferis, L. Rozenberg and G. Wong, 3d Gravity as a random ensemble, 2024, [[arXiv:2407.02649 \[hep-th\]](#)].
- [144] J. Chandra, S. Collier, T. Hartman and A. Maloney, Semiclassical 3D gravity as an average of large-c CFTs, *JHEP* **12**, 069, 2022, [[arXiv:2203.06511 \[hep-th\]](#)].
- [145] S. Collier, A. Maloney, H. Maxfield and I. Tsiaras, Universal dynamics of heavy operators in CFT_2 , *JHEP* **07**, 074, 2020, [[arXiv:1912.00222 \[hep-th\]](#)].
- [146] Y. Kusuki, Analytic bootstrap in 2D boundary conformal field theory: towards braneworld holography, *JHEP* **03**, 161, 2022, [[arXiv:2112.10984 \[hep-th\]](#)].
 Y. Kusuki, Semiclassical gravity from averaged boundaries in two-dimensional boundary conformal field theories, *Phys. Rev. D* **106**, 066020, 2022, [[arXiv:2206.03035 \[hep-th\]](#)].
- [147] T. Numasawa and I. Tsiaras, Universal dynamics of heavy operators in boundary CFT_2 , *JHEP* **08**, 156, 2022, [[arXiv:2202.01633 \[hep-th\]](#)].

- [148] T. Hartman, C. A. Keller and B. Stoica, Universal Spectrum of 2d Conformal Field Theory in the Large c Limit, *JHEP* **09**, 118, 2014, [[arXiv:1405.5137 \[hep-th\]](#)].
- [149] L. Chen, L.-Y. Hung, Y. Jiang and B.-X. Lao, “Ensemble averaged CFT - gravity correspondence from random BCFT tensor network.” In preparation.
- [150] J. Chandra, S. Collier, T. Hartman and A. Maloney, Semiclassical 3D gravity as an average of large- c CFTs, *JHEP* **12**, 069, 2022, [[arXiv:2203.06511 \[hep-th\]](#)].
- [151] O. Coussaert, M. Henneaux and P. van Driel, The Asymptotic dynamics of three-dimensional Einstein gravity with a negative cosmological constant, *Class. Quant. Grav.* **12**, 2961–2966, 1995, [[arXiv:gr-qc/9506019](#)].
M. Henneaux, W. Merbis and A. Ranjbar, Asymptotic dynamics of AdS_3 gravity with two asymptotic regions, *JHEP* **03**, 064, 2020, [[arXiv:1912.09465 \[hep-th\]](#)].
- [152] A. Kitaev and L. Kong, Models for Gapped Boundaries and Domain Walls, *Communications in Mathematical Physics* **313**, 351–373, 2012, [[arXiv:1104.5047 \[cond-mat.str-el\]](#)].
- [153] J. Fuchs, C. Schweigert and A. Valentino, Bicategories for boundary conditions and for surface defects in 3-d TFT, *Commun. Math. Phys.* **321**, 543–575, 2013, [[arXiv:1203.4568 \[hep-th\]](#)].
- [154] A. Kitaev and L. Kong, Models for Gapped Boundaries and Domain Walls, *Commun. Math. Phys.* **313**, 351–373, 2012, [[arXiv:1104.5047 \[cond-mat.str-el\]](#)].
- [155] L. Kong and X.-G. Wen, Braided fusion categories, gravitational anomalies, and the mathematical framework for topological orders in any dimensions, 2014, [[arXiv:1405.5858 \[cond-mat.str-el\]](#)].
- [156] L. Kong, X.-G. Wen and H. Zheng, Boundary-bulk relation in topological orders, *Nucl. Phys. B* **922**, 62–76, 2017, [[arXiv:1702.00673 \[cond-mat.str-el\]](#)].
- [157] P. Etingof and V. Ostrik, Finite tensor categories, 2003, [[arXiv:math/0301027 \[math.QA\]](#)].
- [158] I. Heemskerck, J. Penedones, J. Polchinski and J. Sully, Holography from Conformal Field Theory, *JHEP* **10**, 079, 2009, [[arXiv:0907.0151 \[hep-th\]](#)].
- [159] J. Lou, C. Shen, C. Chen and L.-Y. Hung, A (dummy’s) guide to working with gapped boundaries via (fermion) condensation, *JHEP* **02**, 171, 2021, [[arXiv:2007.10562 \[hep-th\]](#)].
- [160] F. A. Bais, B. J. Schroers and J. K. Slingerland, Broken quantum symmetry and confinement phases in planar physics, *Phys. Rev. Lett.* **89**, 181601, 2002, [[arXiv:hep-th/0205117](#)].
- [161] F. A. Bais and J. K. Slingerland, Condensate induced transitions between topologically ordered phases, *Phys. Rev. B* **79**, 045316, 2009, [[arXiv:0808.0627 \[cond-mat.mes-hall\]](#)].
- [162] F. A. Bais, J. K. Slingerland and S. M. Haaker, A Theory of topological edges and domain walls, *Phys. Rev. Lett.* **102**, 220403, 2009, [[arXiv:0812.4596 \[cond-mat.mes-hall\]](#)].
- [163] L. Kong, Anyon condensation and tensor categories, *Nucl. Phys. B* **886**, 436–482, 2014, [[arXiv:1307.8244 \[cond-mat.str-el\]](#)].
- [164] Z. Komargodski, K. Ohmori, K. Roumpedakis and S. Seifnashri, Symmetries and strings of adjoint QCD_2 , *JHEP* **03**, 103, 2021, [[arXiv:2008.07567 \[hep-th\]](#)].

- [165] L. Kong and I. Runkel, Cardy algebras and sewing constraints. I., *Commun. Math. Phys.* **292**, 871–912, 2009, [[arXiv:0807.3356 \[math.QA\]](#)].
- [166] A. Kapustin and N. Saulina, Surface operators in 3d Topological Field Theory and 2d Rational Conformal Field Theory, 2010, [[arXiv:1012.0911 \[hep-th\]](#)].
- [167] J. M. Maldacena and A. Strominger, AdS(3) black holes and a stringy exclusion principle, *JHEP* **12**, 005, 1998, [[arXiv:hep-th/9804085](#)].
- [168] A. Maloney and E. Witten, Quantum Gravity Partition Functions in Three Dimensions, *JHEP* **02**, 029, 2010, [[arXiv:0712.0155 \[hep-th\]](#)].
- [169] E. Witten, Analytic Continuation Of Chern-Simons Theory, *AMS/IP Stud. Adv. Math.* **50**, 347–446, 2011, [[arXiv:1001.2933 \[hep-th\]](#)].
- [170] D. Harlow, J. Maltz and E. Witten, Analytic Continuation of Liouville Theory, *JHEP* **12**, 071, 2011, [[arXiv:1108.4417 \[hep-th\]](#)].
- [171] J. McNamara and C. Vafa, Baby Universes, Holography, and the Swampland, 2020, [[arXiv:2004.06738 \[hep-th\]](#)].
- [172] A. Almheiri, T. Hartman, J. Maldacena, E. Shaghoulian and A. Tajdini, Replica Wormholes and the Entropy of Hawking Radiation, *JHEP* **05**, 013, 2020, [[arXiv:1911.12333 \[hep-th\]](#)].
- [173] G. Penington, S. H. Shenker, D. Stanford and Z. Yang, Replica wormholes and the black hole interior, *JHEP* **03**, 205, 2022, [[arXiv:1911.11977 \[hep-th\]](#)].
- [174] S. W. Hawking, Breakdown of predictability in gravitational collapse, *Phys. Rev. D* **14**, 2460–2473, 1976.
D. N. Page, Information in black hole radiation, *Phys. Rev. Lett.* **71**, 3743–3746, 1993, [[arXiv:hep-th/9306083](#)].
D. N. Page, Average entropy of a subsystem, *Phys. Rev. Lett.* **71**, 1291–1294, 1993, [[arXiv:gr-qc/9305007](#)].
- [175] J. M. Maldacena and L. Maoz, Wormholes in AdS, *JHEP* **02**, 053, 2004, [[arXiv:hep-th/0401024](#)].
X. Yin, On Non-handlebody Instantons in 3D Gravity, *JHEP* **09**, 120, 2008, [[arXiv:0711.2803 \[hep-th\]](#)].
N. Arkani-Hamed, J. Orgera and J. Polchinski, Euclidean wormholes in string theory, *JHEP* **12**, 018, 2007, [[arXiv:0705.2768 \[hep-th\]](#)].
- [176] P. Saad, S. H. Shenker and D. Stanford, JT gravity as a matrix integral, 2019, [[arXiv:1903.11115 \[hep-th\]](#)].
- [177] D. Marolf and H. Maxfield, Transcending the ensemble: baby universes, spacetime wormholes, and the order and disorder of black hole information, *JHEP* **08**, 044, 2020, [[arXiv:2002.08950 \[hep-th\]](#)].
- [178] J. D. Bekenstein, Black holes and entropy, *Phys. Rev. D* **7**, 2333–2346, 1973.
S. W. Hawking, Particle Creation by Black Holes, *Commun. Math. Phys.* **43**, 199–220, 1975. [Erratum: *Commun.Math.Phys.* 46, 206 (1976)].

- [179] V. Balasubramanian, A. Lawrence, J. M. Magan and M. Sasieta, Microscopic Origin of the Entropy of Black Holes in General Relativity, *Phys. Rev. X* **14**, 011024, 2024, [arXiv:2212.02447 [hep-th]].
V. Balasubramanian, A. Lawrence, J. M. Magan and M. Sasieta, Microscopic Origin of the Entropy of Astrophysical Black Holes, *Phys. Rev. Lett.* **132**, 141501, 2024, [arXiv:2212.08623 [hep-th]].
A. Climent, R. Emparan, J. M. Magan, M. Sasieta and A. Vilar López, Universal construction of black hole microstates, *Phys. Rev. D* **109**, 086024, 2024, [arXiv:2401.08775 [hep-th]].
H. Geng and Y. Jiang, Microscopic Origin of the Entropy of Single-sided Black Holes, 2024, [arXiv:2409.12219 [hep-th]].
- [180] D. L. Jafferis, Bulk reconstruction and the Hartle-Hawking wavefunction, 2017, [arXiv:1703.01519 [hep-th]].
- [181] D. Marolf and A. C. Wall, Eternal Black Holes and Superselection in AdS/CFT, *Class. Quant. Grav.* **30**, 025001, 2013, [arXiv:1210.3590 [hep-th]].
N. Bao, J. Pollack and G. N. Remmen, Wormhole and Entanglement (Non-)Detection in the ER=EPR Correspondence, *JHEP* **11**, 126, 2015, [arXiv:1509.05426 [hep-th]].
D. Berenstein and A. Miller, Can Topology and Geometry be Measured by an Operator Measurement in Quantum Gravity?, *Phys. Rev. Lett.* **118**, 261601, 2017, [arXiv:1605.06166 [hep-th]].
D. Berenstein and A. Miller, Superposition induced topology changes in quantum gravity, *JHEP* **11**, 121, 2017, [arXiv:1702.03011 [hep-th]].
- [182] G. Di Ubaldo and E. Perlmutter, AdS₃/RMT₂ duality, *JHEP* **12**, 179, 2023, [arXiv:2307.03707 [hep-th]].
- [183] S. R. Coleman, Black holes as red herrings: Topological fluctuations and the loss of quantum coherence, *Nucl. Phys. B* **307**, 867–882, 1988.
S. B. Giddings and A. Strominger, Loss of incoherence and determination of coupling constants in quantum gravity, *Nuclear Physics B* **307**, 854–866, 1988.
- [184] A. Blommaert, T. G. Mertens and H. Verschelde, Eigenbranes in Jackiw-Teitelboim gravity, *JHEP* **02**, 168, 2021, [arXiv:1911.11603 [hep-th]].
A. Blommaert, L. V. Iliesiu and J. Kruthoff, Gravity factorized, *JHEP* **09**, 080, 2022, [arXiv:2111.07863 [hep-th]].
- [185] P. Saad, S. H. Shenker, D. Stanford and S. Yao, Wormholes without averaging, *JHEP* **09**, 133, 2024, [arXiv:2103.16754 [hep-th]].
P. Saad, S. H. Shenker and S. Yao, Comments on wormholes and factorization, *JHEP* **10**, 076, 2024, [arXiv:2107.13130 [hep-th]].
- [186] L. Eberhardt, Summing over Geometries in String Theory, *JHEP* **05**, 233, 2021, [arXiv:2102.12355 [hep-th]].
L. Eberhardt, Partition functions of the tensionless string, *JHEP* **03**, 176, 2021, [arXiv:2008.07533 [hep-th]].
- [187] E. Gesteau, M. Marcolli and J. McNamara, Wormhole Renormalization: The gravitational path integral, holography, and a gauge group for topology change, 2024, [arXiv:2407.20324 [hep-th]].

- [188] J. McNamara. “The Structure of Gravitational Hidden Sectors.”. Talk given at KITP High Energy and Gravity Seminars, Sep. 26, 2024.
- [189] S. H. Shenker and D. Stanford, Black holes and the butterfly effect, *JHEP* **03**, 067, 2014, [[arXiv:1306.0622 \[hep-th\]](#)].
- [190] A. Kitaev. “Hidden correlations in the hawking radiation and thermal noise.”. Talk given at the Fundamental Physics Prize Symposium, Nov. 10, 2014.
- [191] A. I. Larkin and Y. N. Ovchinnikov, Quasiclassical Method in the Theory of Superconductivity, Soviet Journal of Experimental and Theoretical Physics **28**, 1200, 1969.
- [192] D. Simmons-Duffin. TASI Lectures on Conformal Field Theory in Lorentzian Signature.
- [193] L. Cornalba, M. S. Costa, J. Penedones and R. Schiappa, Eikonal Approximation in AdS/CFT: From Shock Waves to Four-Point Functions, *JHEP* **08**, 019, 2007, [[arXiv:hep-th/0611122](#)].
L. Cornalba, M. S. Costa, J. Penedones and R. Schiappa, Eikonal Approximation in AdS/CFT: Conformal Partial Waves and Finite N Four-Point Functions, *Nucl. Phys. B* **767**, 327–351, 2007, [[arXiv:hep-th/0611123](#)].
L. Cornalba, M. S. Costa and J. Penedones, Eikonal approximation in AdS/CFT: Resumming the gravitational loop expansion, *JHEP* **09**, 037, 2007, [[arXiv:0707.0120 \[hep-th\]](#)].
L. Cornalba, Eikonal methods in AdS/CFT: Regge theory and multi-reggeon exchange, 2007, [[arXiv:0710.5480 \[hep-th\]](#)].
- [194] T. Hartman, D. Mazac, D. Simmons-Duffin and A. Zhiboedov, Snowmass White Paper: The Analytic Conformal Bootstrap, in *Snowmass 2021*, 2022. [[arXiv:2202.11012 \[hep-th\]](#)].
- [195] T. Hartman, S. Jain and S. Kundu, Causality Constraints in Conformal Field Theory, *JHEP* **05**, 099, 2016, [[arXiv:1509.00014 \[hep-th\]](#)].
- [196] S. Caron-Huot, Analyticity in Spin in Conformal Theories, *JHEP* **09**, 078, 2017, [[arXiv:1703.00278 \[hep-th\]](#)].
- [197] M. S. Costa, V. Goncalves and J. Penedones, Conformal Regge theory, *JHEP* **12**, 091, 2012, [[arXiv:1209.4355 \[hep-th\]](#)].
- [198] D. A. Roberts and D. Stanford, Two-dimensional conformal field theory and the butterfly effect, *Phys. Rev. Lett.* **115**, 131603, 2015, [[arXiv:1412.5123 \[hep-th\]](#)].
- [199] A. L. Fitzpatrick, J. Kaplan and M. T. Walters, Universality of Long-Distance AdS Physics from the CFT Bootstrap, *JHEP* **08**, 145, 2014, [[arXiv:1403.6829 \[hep-th\]](#)].
- [200] P. Caputa, T. Numasawa and A. Veliz-Osorio, Out-of-time-ordered correlators and purity in rational conformal field theories, *PTEP* **2016**, 113B06, 2016, [[arXiv:1602.06542 \[hep-th\]](#)].
Y. Gu and X.-L. Qi, Fractional Statistics and the Butterfly Effect, *JHEP* **08**, 129, 2016, [[arXiv:1602.06543 \[hep-th\]](#)].
- [201] G. Turiaci and H. Verlinde, On CFT and Quantum Chaos, *JHEP* **12**, 110, 2016, [[arXiv:1603.03020 \[hep-th\]](#)].

- [202] Y. Kusuki and M. Miyaji, Entanglement Entropy, OTOC and Bootstrap in 2D CFTs from Regge and Light Cone Limits of Multi-point Conformal Block, *JHEP* **08**, 063, 2019, [[arXiv:1905.02191 \[hep-th\]](#)].
- [203] K. Schoutens, H. L. Verlinde and E. P. Verlinde, Quantum black hole evaporation, *Phys. Rev. D* **48**, 2670–2685, 1993, [[arXiv:hep-th/9304128](#)].
Y. Kiem, H. L. Verlinde and E. P. Verlinde, Black hole horizons and complementarity, *Phys. Rev. D* **52**, 7053–7065, 1995, [[arXiv:hep-th/9502074](#)].
- [204] T. Dray and G. 't Hooft, The gravitational shock wave of a massless particle, *Nuclear Physics B* **253**, 173–188, 1985.
- [205] L. Kong, “An ongoing revolution in quantum many-body theory.” Video for the talk available at <https://www.koushare.com/live/details/37923>.
- [206] S. Leutheusser and H. Liu, Causal connectability between quantum systems and the black hole interior in holographic duality, *Phys. Rev. D* **108**, 086019, 2023, [[arXiv:2110.05497 \[hep-th\]](#)].
S. A. W. Leutheusser and H. Liu, Emergent Times in Holographic Duality, *Phys. Rev. D* **108**, 086020, 2023, [[arXiv:2112.12156 \[hep-th\]](#)].
- [207] S. Carpi, Y. Kawahigashi, R. Longo and M. Weiner, From vertex operator algebras to conformal nets and back, 2015, [[arXiv:1503.01260 \[math.OA\]](#)].
- [208] V. F. R. Jones, Index for subfactors, *Invent. Math.* **72**, 1–25, 1983.
R. Longo, Index of subfactors and statistics of quantum fields. I, *Commun. Math. Phys.* **126**, 217–247, 1989.
- [209] E. Witten, Gravity and the crossed product, *JHEP* **10**, 008, 2022, [[arXiv:2112.12828 \[hep-th\]](#)].
- [210] V. Chandrasekaran, G. Penington and E. Witten, Large N algebras and generalized entropy, *JHEP* **04**, 009, 2023, [[arXiv:2209.10454 \[hep-th\]](#)].
V. Chandrasekaran, R. Longo, G. Penington and E. Witten, An algebra of observables for de Sitter space, *JHEP* **02**, 082, 2023, [[arXiv:2206.10780 \[hep-th\]](#)].
- [211] J. van der Heijden and E. Verlinde, An Operator Algebraic Approach To Black Hole Information, 2024, [[arXiv:2408.00071 \[hep-th\]](#)].
- [212] G. Penington and E. Witten, Algebras and States in JT Gravity, 2023, [[arXiv:2301.07257 \[hep-th\]](#)].
D. K. Kolchmeyer, von Neumann algebras in JT gravity, *JHEP* **06**, 067, 2023, [[arXiv:2303.04701 \[hep-th\]](#)].
- [213] P. W. Anderson, More is different, *Science* **177**, 393–396, 1972, [<https://www.science.org/doi/pdf/10.1126/science.177.4047.393>].
- [214] E. Witten, APS Medal for Exceptional Achievement in Research: Invited article on entanglement properties of quantum field theory, *Rev. Mod. Phys.* **90**, 045003, 2018, [[arXiv:1803.04993 \[hep-th\]](#)].
- [215] L. Eberhardt, M. R. Gaberdiel and R. Gopakumar, The Worldsheet Dual of the Symmetric Product CFT, *JHEP* **04**, 103, 2019, [[arXiv:1812.01007 \[hep-th\]](#)].
L. Eberhardt, M. R. Gaberdiel and R. Gopakumar, Deriving the AdS₃/CFT₂ correspondence, *JHEP* **02**, 136, 2020, [[arXiv:1911.00378 \[hep-th\]](#)].

- [216] L. Susskind, Computational Complexity and Black Hole Horizons, *Fortsch. Phys.* **64**, 24–43, 2016, [[arXiv:1403.5695 \[hep-th\]](#)]. [Addendum: *Fortsch.Phys.* 64, 44–48 (2016)].
 D. Stanford and L. Susskind, Complexity and Shock Wave Geometries, *Phys. Rev. D* **90**, 126007, 2014, [[arXiv:1406.2678 \[hep-th\]](#)].
 A. R. Brown, D. A. Roberts, L. Susskind, B. Swingle and Y. Zhao, Holographic Complexity Equals Bulk Action?, *Phys. Rev. Lett.* **116**, 191301, 2016, [[arXiv:1509.07876 \[hep-th\]](#)].
- [217] A. Belin, R. C. Myers, S.-M. Ruan, G. Sárosi and A. J. Speranza, Does Complexity Equal Anything?, *Phys. Rev. Lett.* **128**, 081602, 2022, [[arXiv:2111.02429 \[hep-th\]](#)].
 A. Belin, R. C. Myers, S.-M. Ruan, G. Sárosi and A. J. Speranza, Complexity equals anything II, *JHEP* **01**, 154, 2023, [[arXiv:2210.09647 \[hep-th\]](#)].
 R. C. Myers and S.-M. Ruan, Complexity Equals (Almost) Anything, 2024. [[arXiv:2403.17475 \[hep-th\]](#)].
- [218] P. Caputa, N. Kundu, M. Miyaji, T. Takayanagi and K. Watanabe, Anti-de Sitter Space from Optimization of Path Integrals in Conformal Field Theories, *Phys. Rev. Lett.* **119**, 071602, 2017, [[arXiv:1703.00456 \[hep-th\]](#)].
 P. Caputa, N. Kundu, M. Miyaji, T. Takayanagi and K. Watanabe, Liouville Action as Path-Integral Complexity: From Continuous Tensor Networks to AdS/CFT, *JHEP* **11**, 097, 2017, [[arXiv:1706.07056 \[hep-th\]](#)].
- [219] J. Roberts, Skein theory and turaev-viro invariants, *Topology* **34**, 771–787, 1995.
- [220] J. W. Alexander, The combinatorial theory of complexes, *Annals of Mathematics* **31**, 292–320, 1930.
- [221] F. J. Burnell and S. H. Simon, Space-Time Geometry of Topological phases, *Annals Phys.* **325**, 2550–2593, 2010, [[arXiv:1004.5586 \[cond-mat.str-el\]](#)].
 F. J. Burnell and S. H. Simon, A Wilson line picture of the Levin-Wen partition functions, *New Journal of Physics* **13**, 065001, 2011, [[arXiv:1004.5147 \[cond-mat.str-el\]](#)].
- [222] N. Reshetikhin and V. G. Turaev, Invariants of three manifolds via link polynomials and quantum groups, *Invent. Math.* **103**, 547–597, 1991.
- [223] A. Kitaev, Anyons in an exactly solved model and beyond, *Annals Phys.* **321**, 2–111, 2006, [[arXiv:cond-mat/0506438](#)].
- [224] P. Etingof, S. Gelaki, D. Nikshych and V. Ostrik, *Tensor Categories*. AMS, 2015.
- [225] T. Kojita, C. Maccaferri, T. Masuda and M. Schnabl, Topological defects in open string field theory, *JHEP* **04**, 057, 2018, [[arXiv:1612.01997 \[hep-th\]](#)].
- [226] P. Hayden, S. Nezami, X.-L. Qi, N. Thomas, M. Walter and Z. Yang, Holographic duality from random tensor networks, *JHEP* **11**, 009, 2016, [[arXiv:1601.01694 \[hep-th\]](#)].
- [227] R. M. Soni and A. C. Wall, A New Covariant Entropy Bound from Cauchy Slice Holography, 2024, [[arXiv:2407.16769 \[hep-th\]](#)].
- [228] R. Soni, “Topological gravity, tensor networks and tt..” video for the talk available at <https://www.youtube.com/watch?v=gjkLRmSWccI>.

- [229] H. Verlinde, “Ope and the black hole information paradox.” talk at the conference *Gravitational Emergence in AdS/CFT*, BIRS, October 2021. Video available at <https://www.birs.ca>.
A.Almheiri, R.Ding, H.Lin, B.Liu and H.Verlinde. in preparation.
- [230] J. Chandra and T. Hartman, Toward random tensor networks and holographic codes in CFT, *JHEP* **05**, 109, 2023, [[arXiv:2302.02446](https://arxiv.org/abs/2302.02446) [hep-th]].
- [231] I. Nidaiev and J. Teschner, On the relation between the modular double of $U_q(sl(2, R))$ and the quantum Teichmueller theory, 2013, [[arXiv:1302.3454](https://arxiv.org/abs/1302.3454) [math-ph]].
- [232] R. C. Penner, The decorated Teichmüller space of punctured surfaces, *Communications in Mathematical Physics* **113**, 299–339, 1987.
R. C. Penner, Weil-Petersson volumes, *Journal of Differential Geometry* **35**, 559 – 608, 1992.
- [233] V. V. Fock, Dual Teichmüller spaces, eprint [arXiv:dg-ga/9702018](https://arxiv.org/abs/dg-ga/9702018) dg-ga/9702018, 1997, [[arXiv:dg-ga/9702018](https://arxiv.org/abs/dg-ga/9702018) [math.DG]].
- [234] J. Teschner, On the relation between quantum Liouville theory and the quantized Teichmuller spaces, *Int. J. Mod. Phys. A* **19S2**, 459–477, 2004, [[arXiv:hep-th/0303149](https://arxiv.org/abs/hep-th/0303149)].